DOCTOR OF PHILOSOPHY

Regulation of transcription factors NRF2 and HSF1 in mediating cellular stress responses

Dayalan Naidu, Sharadha

Award date:
2016

Regulation of transcription factors NRF2 and HSF1 in mediating cellular stress responses

Sharadha Dayalan Naidu

A thesis submitted for the degree of Doctor of Philosophy, August 2016

Table of Contents

DECLARATIONS ..... **i**
TABLE OF CONTENTS ..... **ii**
LIST OF FIGURES AND TABLES ..... **vi**
ACKNOWLEDGEMENTS **1**
ABSTRACT **4**
Section 1: Introduction
Chapter A: NRF2, KEAP1 and their interaction **7**
1.A.1 Introduction 7
1.A.2 The NRF2/KEAP1/ARE pathway 8
1.A.3 Cytoprotective response of the NRF2/KEAP1/ARE pathway 11
1.A.4 KEAP1: The main negative NRF2 regulator 13
1.A.4.1 KEAP1 structure and its cysteine sensors 15
1.A.4.2 KEAP1-Cullin3 interaction 23
1.A.5 Concluding remarks 24
Chapter B: The cytoprotective role of the mammalian heat shock factor 1 ..... **26**
1.B.1 Introduction 26
1.B.2 HSF family members 27
1.B.3 HSF1: Structure, Function and Regulation 30
1.B.4 Small molecule activators of HSF1 38
1.B.4.1 Endogenous metabolites 38
1.B.4.2 Phytochemicals 43
1.B.4.3 Synthetic compounds 48
1.B.5 HSF1 activates cytoprotective responses 52
1.B.6 Crosstalk between HSF1- and NRF2-regulated cytoprotective responses 53
1.B.7 HSF1 and neurodegenerative diseases 55
1.B.8 HSF1 and cardiovascular disease 61
1.B.9 HSF1 and cancer 66
1.B.10.1 HSF1 and chemoresistance 69
1.B.10 HSF1 and cell division 70
1.B.11 HSF1 turnover: Stability and degradation 76
1.B.12 Concluding remarks 80
Chapter C: p38 mitogen-activated protein kinases **82**
1.C.1 Introduction 82
1.C.2 p38 MAPKs 83
1.C.3 Structure of p38 MAPKs 85
1.C.4 p38 MAPK signalling 86
1.C.4.1 p38 MAPK signalling cascade 90
1.C.5 Some of the pathophysiological impacts of p38 MAPK signalling 92
1.C.5.1 Specific roles and functional redundancies 92
1.C.6 Conclusions 95
Section 2: Materials and Methods **97**
2.1 Materials 97
2.2 Cell culture 97

2.3 Western blotting sample preparation 98
2.4 Western Blot Analysis 98
2.4.1 SDS-PAGE gel electrophoresis 98
2.4.2 NuPAGE gel electrophoresis 99
2.4.3 Wet transfer 99
2.4.4 Immunoblotting 100
2.5 Primary antibodies 101
2.6 Nuclear-cytoplasmic separation 101
2.7 Quantitative real-time PCR 102
2.8 Luciferase assay 103
2.9 ATP-binding assay 103
2.10 Detection of HSF1 trimerization 104
2.11 Co-immunoprecipitation 105
2.12 Generation of p38δ and p38ɣ stable knockdown cell lines 106
2.13 Expression and purification of recombinant hexahistidine-tagged HSF1 107
2.14 High content microscopy and analysis 108
2.15 Kinase assays 108
2.16 Generation of HSF1-knockout HeLa cell line 110
2.17 Cell viability assay 111
2.18 Mitotic wash-off 112
2.19 Immunofluorescence 113
2.20 Generation of stable Keap1-knockout Keap1-rescued cell lines 114
2.21 Generation of Keap1 knock-in mice 115
2.22 Peritoneal macrophage isolation 116
2.23 In-cell western (ICW) 116
2.24 Statistical analysis 117
Section 3: Results, Discussion and Conclusions
Chapter 1: Cyanoenone class of compounds are sensed by a specific cysteine residue in KEAP1 118
3.1.1 Introduction 118
3.1.2 RTA-408 121
3.1.2.1 KEAP1 cysteine 151 is a sensor for RTA-408 in vitro and ex vivo 124
3.1.3 TBE-31 127
3.A.3.1 KEAP1 cysteine 151 is the primary sensor for TBE-31 in vitro and ex vivo 130
3.A.3.2 TBE-31 is a potent anti-inflammatory agent 132
3.A.3.3 TBE-31-mediated suppression of inflammation is potentially dependent on KEAP1 C151 134
3.1.3.4 KEAP1$^{C151S/C151S}$ knock-in mice are more susceptible to LPS-induced inflammation than KEAP1 wild-type animals 136
3.1.4 MCE-23 138
3.1.4.1 KEAP1 cysteine 151 is the primary sensor for MCE-23 138
3.1.5 MCE-1 140
3.1.5.1 KEAP1 cysteine 151 is the primary sensor for

MCE-1 in vitro and ex vivo 140
3.1.6 Conclusions 142
Chapter 2: Heat Shock Factor 1 is a substrate for p38 MAPKs 145
3.2.1 Phenethyl isothiocyanate (PEITC) 145
3.2.2 PEITC causes stabilisation of NRF2 through reacting with cysteine 151 of KEAP1 147
3.2.3 Cysteine-reactive PEITC induces the heat shock response 150
3.2.4 PEITC requires HSF1 for the induction of Hsp70 152
3.2.5 Loss of HSF1 enhances the cytotoxicity of PEITC 154
3.2.6 PEITC causes nuclear accumulation of HSF1 and its trimerization 156
3.2.7 PEITC causes an increase in Hsp70.1 promoter activity as well as Hsp70 mRNA levels 158
3.2.8 PEITC inhibits Hsp90 158
3.2.9 PEITC causes phosphorylation of HSF1 at S326 160
3.2.10 PEITC activates p38 MAPK 166
3.2.11 p38 MAPK phosphorylate HSF1 at S326 in vitro 168
3.2.12 Deletion or inhibition of p38γ decreases the phosphorylation of HSF1 at S326 in cells 177
3.2.13 HSF1 S326A, S326D and S326E mutants do not affect the binding at the Hsp70.1 promoter under basal conditions 182
3.2.14 siRNA-mediated knockdown of ASK1 in HeLa-HSE-luc cells greatly reduces the basal and PEITC-mediated phosphorylation of HSF1 at S326 186
3.2.15 siRNA-mediated knockdown of ASK1 in HeLa-HSE-luc cells increases the Hsp70.1 promoter activity during PEITC-mediated heat shock response activation 188
3.2.16 siRNA-mediated knockdown of ASK1 and exposure to the ASK1 inhibitor (NDQI-1) in MDA-MB-231 cells does not affect phosphorylation of HSF1 at S326. 190
3.2.17 HSF1 S326E phospho-mimetic mutant is unable to bind to Hsp90 193
3.2.18 Discussion 194
3.2.19 Conclusions 198
Chapter 3: Physiological significance of HSF1 phosphorylation at S326 201
3.3.1 Introduction 201
3.3.2 HSF1 pS326 and HSF1 differ in their sub-cellular localisation 202
3.3.3 The levels of HSF1 pS326 are significantly higher in mitotic cells compared to interphase cells 205
3.3.4 The localisation of HSF1 pS326 and α-tubulin are mutually exclusive in interphase cells 211
3.3.5 HSF1 pS326 localisation is diffused throughout the mitotic cell and is not present at the chromosomes 214
3.3.6 HSF1 pS326 concentrates at the midbody during telophase 214
3.3.7 The HSF1 pS326 levels are significantly higher in taxol-arrested mitotic cells

compared to interphase cells 223
3.3.8 The total HSF1 levels decrease in taxol-arrested mitotic cells and interphase cells 227
3.3.9 HSF1 pS303 and pS121 levels are decreased in U2OS cells arrested in mitosis with taxol compared to interphase cells 228
3.3.10 p38α and p38β are active in interphase cells whereas, p38β is predominantly active in taxol -arrested mitotic cells 230
3.3.10 Discussion 230
3.3.11 Future Perspectives 234
Concluding remarks 235
Section 4: References 237
Section 5: Appendix 265

List of Figures and Tables

FIGURE	DESCRIPTION	PAGE
A1	Schematic diagram of NRF2 and KEAP1 domains	9
A2	The KEAP1/NRF2 pathway	10
A3	Amino acid sequence alignment of various mammalian KEAP1	14
A4	Structure of the human KEAP1 BTB domain	18
A5	Modelled structure of the human KEAP1 IVR domain	20
A6	Structure of the KEAP1 Kelch domain	22
B1	The heat shock response	31
B2	Schematic diagram of the structure and posttranslational modifications of HSF1	34
B3	Structure of the DNA-binding domain (DBD) of human HSF1 (amino acids 10-123)	37
B4	Endogenous small-molecule activators of HSF1	39
B5	Phytochemical activators of HSF1	44
B6	Synthetic small-molecule activators of HSF1	50
B7	Control of cell cycle progression by cyclin-CDK complexes	71
B8	Different phases during mitosis	73
C1	p38 MAPK isoforms	84
C2	Schematic diagram of the p38α structure	87
C3	p38 MAPK signalling cascade showing the substrate specificities for the individual isoforms.	89
C4	The physiological roles and pathological implications of p38 MAPKs.	96
1.1	KEAP1 C151 is the primary sensor for RTA-408	125
1.2	KEAP1 C151 is the primary sensor for TBE-31	131
1.3	TBE-31 suppresses LPS-induced inflammation in WT mouse peritoneal macrophage cells	133
1.4	NRF2 activation of TBE-31 in mouse peritoneal macrophage cells is primarily through KEAP1 C151	135

1.5	KEAP1$^{C151S/C151S}$ mouse peritoneal macrophages are much more sensitive to LPS-induced inflammation than their WT counterparts.	137
1.6	KEAP1 C151 is the primary sensor for MCE-23	139
1.7	KEAP1 C151 is the primary sensor for MCE-1	141
1.8	Structure of CDDO and its complex with KEAP1 BTB domain	143
2.1	KEAP1 C151 is the primary sensor for PEITC.	149
2.2	PEITC is a robust inducer of the heat shock response	149
2.3	PEITC requires HSF1 for the induction of Hsp70	153
2.4	Loss of HSF1 enhances cytotoxicity of PEITC	155
2.5	PEITC causes nuclear accumulation of HSF1 and its trimerization	157
2.6	PEITC causes an increase in Hsp70.1 promoter activity as well as Hsp70 mRNA levels	159
2.7	PEITC inhibits Hsp90	161
2.8	PEITC causes phosphorylation of HSF1 at S326	163
2.9	Predicted proline-directed phosphorylation sites on HSF1	164
2.10	PEITC activates p38 MAPK. PEITC activates p38 and inhibits mTOR	167
2.11	The MEK inhibitor U0126 reduces the levels of heat-shock induced phosphorylation of HSF1 at S326 after a 24 h pre-treatment, but 1 h pre-treatment has no effect	169
2.12	p38 MAPK phosphorylate HSF1 in vitro	170
2.13	p38 MAPK phosphorylate HSF1 in vitro	172
2.14	Deletion or inhibition of p38γ MAPK reduces the levels of pS326 HSF1 in cells	178
2.15	Deletion or inhibition of p38γ MAPK reduces the levels of pS326 HSF1 in cells	179
2.16	Deletion or inhibition of p38γ MAPK reduces the levels of pS326 HSF1 in cells	181
2.17	S326A/E mutation does not influence the nucleo-cytoplasmic distribution of ectopically expressed HSF1-GFP	183
2.18	HSF1 S326A, S326D and S326E mutants do not affect the Hsp70.1 promoter activity under basal conditions	185
2.19	Knockdown of ASK1 in HSE-HeLa-luc cells greatly	187

	reduces the phosphorylation of HSF1 at S326	
2.20	siRNA-mediated knockdown of ASK1 in HSE-HeLa-luc cells increases the Hsp70.1 promoter activity during PEITC-mediated heat shock response activation	189
2.21	Knockdown of ASK1 and exposure to the ASK1 inhibitor (NDQI-1) in MDA-MB-231 cells does not affect phosphorylation of HSF1 at S326	191
2.22	siRNA for ASK1 efficiently reduces ASK1 mRNA levels	192
2.23	p38 MAPKs are able to phosphorylate the Neh6 domain of NRF2	199
3.1	Localisation of HSF1 phosphorylated at S326 in interphase or resting cells is almost mutually exclusive to total HSF1 localisation	203
3.2	Localisation of HSF1 phosphorylated at S326 in interphase or resting cells is almost mutually exclusive to total HSF1 localisation	204
3.3	Phosphorylation of HSF1 at S326 is significantly higher in mitotic cells compared to interphase cells	206
3.4	Phosphorylation of HSF1 at S326 is significantly higher in mitotic cells compared to interphase cells and colocalises with total HSF1	207
3.5	Total HSF1 and HSF1 pS326 co-localise in an U2OS cell undergoing prophase	208
3.6	Total HSF1 and HSF1 pS326 co-localise in an U2OS cell undergoing telophase	209
3.7	Total HSF1 and HSF1 pS326 co-localise in an U2OS cell undergoing telophase and are present at the midbody	210
3.8	HSF1 pS326 shows a filamentous localisation that does not co-localise with in an U2OS cell in interphase	212
3.9	HSF1 pS326 shows a filamentous localisation that does not co-localise with in an U2OS cell in interphase	213
3.10	HSF1 pS326 is ubiquitously expressed in an U2OS cell undergoing mitosis with lower expression at the chromosomes	215
3.11	HSF1 pS326 is ubiquitously expressed in an U2OS cell undergoing at metaphase with lower expression at the chromosomes	216
3.12	HSF1 pS326 is ubiquitously expressed in an U2OS	217

	cell in late anaphase with lower expression at the chromosomes	
3.13	HSF1 pS326 is ubiquitously expressed in an U2OS cell in late anaphase with lower expression at the chromosomes	218
3.14	HSF1 pS326 is highly expressed at the midbody of an U2OS cell undergoing telophase	219
3.15	HSF1 pS326 is highly expressed at the midbody of an U2OS cell undergoing telophase	220
3.16	HSF1 pS326 is highly expressed at the midbody of an U2OS cell undergoing telophase	221
3.17	Ponceau S staining of a western blot membrane	224
3.18	HSF1 pS326 levels are significantly higher in taxol-arrested mitotic cells compared to interphase cells	225
3.19	Total HSF1 is degraded, whereas, HSF1 pS326 levels are significantly higher in taxol-arrested mitotic cells than in interphase	226
3.20	HSF1 pS303 and HSF1 pS121 levels are lower in taxol-arrested mitotic cells compared to interphase cells	229
3.21	Different p38 isoforms are phosphorylated during taxol-arrested mitosis compared to interphase cells	231
3.22	CDK9 Inhibitor reduces HSF1 pS326 in MCF7 cells	233
5.1A	In-cell western kinase inhibitor screen	265
5.1B	In-cell western kinase inhibitor screen	266
5.1C	In-cell western kinase inhibitor screen	267
5.2	PEITC activates p38 and JNK1/2 MAPK	268
TABLE	**DESCRIPTION**	**PAGE**
2.1	Phosphopeptides of recombinant human HSF1 identified by liquid chromatography tandem mass spectrometry	175

ACKNOWLEDGEMENTS

I would like to express my deepest gratitude to my supervisor Dr. Albena T. Dinkova-Kostova for her utmost support, guidiance and patience. You have given me numerous opportunities during the course of my PhD which as enriched my experience and allowed me to develop as a scientist. You are an excellent researcher, role model and mentor, and without your hardwork and guidance I would not have been able to attain many of the achievements I have today.

I would like to express my profound gratitude towards my mother, Ms Kalavathi Ramdass who has made many sacrifices for her children and without whom I will not be where I am today. You have been a pillar of strength and your unwavering belief in my capabilities has pushed me to achieve my dreams.

I would like to express my deepest appreciation to my husband, Kristaps Bezbailis for his unwavering love, loyalty, support and belief. You have been endlessly patient, caring and understanding and words cannot express how instrumental you have been in this journey.

I would like to thank my second supervisor Professor John D. Hayes for imparting his valuable thoughts and useful comments throughout the course of my PhD and for always trying to uplift the spirits of everyone around him. I would like to offer my sincerest thanks to Dr. Ying Zhang, Dr. Elena Knatko, Ms. Maureen Higgins, Dr. Ritu Sharma, Dr. Dina Dikovskaya, Mr. Kevin Roth and Ms. Kimi Ebisine for creating a great and enjoyable environment to learn and work in. I will miss the funny/crazy conversations we've had in the reading room. Before I proceed, I would like to apologise for using the word "thank" repeatedly, as I am unable to find other words that deem fit.

I would like to thank Dr. Calum D. Sutherland for taking the time to impart his knowledge on kinases and also for teaching and helping me with my experiments. I would like to thank Dr. Laureano de la Vega for taking the time to teach me and help me with the design of my experiments. I would like to thank Dr. Rumen Kostov for his help in generating several figures. I would like to thank Ying for proving me with a great foundation when I first came into the lab and for always giving me scientific advice and help whenever I needed. I would like to thank Lena for teaching me the immunofluorescence technique, giving me a tour of the animal unit as well as giving me loads of scientific and non-scientific advice.

I would like to thank Maureen for helping me look after my precious cells whenever I was not around to do so as well as giving me tips on where to travel in Scotland. I would also like to thank Ritu for her guidance on molecular cloning (especially whenever I hit a road-block) as well as being a supportive friend throughout. I would like to thank Dina for taking the time to be involved during my theis writing. Though I have known you for a short amount of time, I have learnt immensely from you. Thank you for helping me delve into the world of mitosis and also taking the time be involved with teaching and helping me with new techniques and experiments. I would like to thank Kevin for helping me whenever he could in the lab and for the very important coffee breaks.

I would like to thank Ms. Laura Torrente for being a wonderful friend and constant support and encouragement in the past three years. I have enjoyed our scientific and mostly non-science related conversations and the PhD would have been a really boring experience without you there. Thank you for taking the time to help me with some experiments. I would like to also thank you for being my library buddy – I don't think I would be able to sit continuously for periods of 4 hours or more to write the thesis without you. I would like to thank Ms. Bianca Ihrig for being a great friend and for showering me with her unwavering support and encouragement from the moment we began our Master's course together. I would like to thank Ms. Suelynn Tan-Stroud for her encouragement and being a great listening ear. I would like to thank my childhood friends Ms Kumari Shanker and Ms Shanthini Sandramohan who have been cheering me on from the other side of the world ever since I came to the UK. I would like to thank my father and brother for supporting me throughout and giving me great memories. I would like to thank Mr. Oleg Kiricenko and Mr. Marcis Jirgensons for providing laughter and great memories.

I would like to thank my students, Ms. Egle Gaurilcikaite, Mr. Glenn Koh, Mr. Axel Laurell, Mr. Chang Lee Rui, Ms Macha Aldigeri and Mr. Calum Saunders for making my PhD experience a great one. I have learnt a lot from the experiences I've had with all of you. I would like to thank Mr. Glenn Koh for always going extra mile to help me during the times when I was really busy in the lab.

I am extremely grateful to my supervisor Albena and Professor Masayuki (Masi) Yamamoto for giving me to opportunity to experience life as a research student in Japan. I spent approximately two months at Tohoku University in Sendai, Japan in Professor Masayuki Yamamoto's Lab and gained a highly enriching and unforgettable experience. The data shown in Chapter 1 of Section 2 was obtained during the course of my stay in Japan. I would like to thank Assistant Professor Takafumi Suzuki for taking care of my well-being during my stay. I would like to thank Dr. Keiko Taguchi for being a great friend and bringing me around Sendai. I would like to thank Dr. Yoko Yagishita for taking time out of her busy schedule to ensure that my experiments were working. I would like to thank Dr. Ryota Saito for helping me settle in, ensuring that my experiments were going well and most importantly, making me feel welcome. I would like to thank Mr. Soichiro Asami for helping me with mice experiments as well as being my lunch/dinner buddy and most importantly being a great friend.

I would like to thank my thesis monitoring committee advisors Dr. Mark Saville, Dr. Adrian Saurin, Dr. Gareth Inman, Dr. Gillian Smith and Dr. Sara Brown for their helpful advice and comments during the course of the PhD.

I am extremely grateful to the Medical Research Institute of the University of Dundee, the BBSRC (BB/J007498/1) for financial support.

I would like to thank my Professor Carol Mackintosh and Dr. Patricija van Oosten-Hawle for agreeing to be my examiners for the PhD *viva voce* examination.

This thesis is dedicated to Kris (a.k.a the husband and the best friend)

Abstract

The KEAP1/NRF2/ARE pathway is at the forefront of cellular defense. Induction of this pathway is protective against various conditions of stress such as oxidative stress and exposure to electrophiles. Conversely, failure to upregulate the pathway leads to increased disease susceptibility and accelerated pathogenesis. Under basal conditions, transcription factor nuclear factor erythroid 2 p45-related factor 2 (NRF2) is targeted for ubiquitination and proteasomal degradation by a repressor protein Kelch-like (ECH)-associated protein (KEAP1), a substrate adaptor for Cullin 3-based E3 ubiquitin ligase. Inducers of the pathway chemically modify specific cysteines within KEAP1, leading to loss of repressor function, NRF2 accumulation and enhanced transcription of genes encoding a large network of cytoprotective proteins.

The cyanoenones are the most potent NRF2 activators known. Cyanoenones bind to KEAP1 covalently and reversibly, and are suitable for chronic *in vivo* administration. However, the cysteine sensor for these compounds is unknown. Among the cysteine sensors of KEAP1, C151 in the BTB domain and C273 and C288 in the intervening region, are best characterized. In this study using KEAP1-knockout mouse embryonic fibroblasts (MEFs) rescued with wild-type (WT) KEAP1 or cysteine mutants, we tested a series of cyanoenones for their ability to modify specific cysteine sensors in KEAP1. We discovered that remarkably, all compounds of this class specifically target C151 regardless of their molecular shape or size. In addition, primary peritoneal macrophages (PMφ) derived from KEAP1$^{C151S/C151S}$ knock-in mice

generated using the CRISPR/Cas9 technology, had higher LPS-induced inflammatory responses than cells from WT animals. Furthermore, at nanomolar concentrations, the tricyclic cyanoenone TBE-31 strongly suppresses LPS-induced inflammatory responses in primary PMφ cells, suggesting the potential for therapeutic use in inflammatory diseases.

Another cytoprotective response is the heat shock response (HSR) which is activated when cells are exposed to stressors such as elevated temperatures, heavy metals and cytotoxic compounds. The HSR, mainly mediated by Heat Shock Factor 1 (HSF1), protects the integrity of the cellular proteome through the upregulation of a battery of genes involved in ameliorating proteotoxicity. Several small molecule activators of the KEAP1/NRF2/ARE pathway have been shown to activate HSR through the activation of HSF1. Work in this thesis focused on one such dual activator, the dietary agent phenethyl isothiocyanate (PEITC). We found that PEITC reacts with KEAP1 C151 to stabilize NRF2, and that it is able to activate the HSR by activating HSF1 through the inhibition of heat shock protein 90, the main negative regulator of HSF1. We further showed that PEITC activates p38 mitogen-activated protein kinases (MAPKs). *In vitro*, all members of the p38 MAPK family rapidly and stoichiometrically catalyze the phosphorylation of HSF1 on S326, a hallmark of HSF1 activation. The use of stable knockdown cell lines and inhibitors indicated that among the p38 MAPK, p38γ is the principal isoform responsible for the phosphorylation of HSF1 at S326 in cells. A protease-mass spectrometry approach confirmed S326 phosphorylation, and unexpectedly, revealed that p38 MAPKs also catalyze the phosphorylation of HSF1 at S303/307, previously known repressive post-

translational modifications. Thus, we identified p38 MAPKs as highly efficient catalysts for the phosphorylation of HSF1. Furthermore, our findings suggest that the magnitude and persistence of activation of p38 MAPKs are important determinants of the extent and duration of the HSR.

In order to investigate the physiological significance of HSF1 phosphorylation at S326, we used immunofluorescence and western blotting techniques. We found that mitotic cells have high levels of HSF1 pS326 compared to interphase cells. Interestingly, our studies revealed that phosphorylated HSF1 at S326 is concentrated at the midbody of telophase cells, suggesting a potential role for HSF1 during the late-stage of cell division. Further studies are needed to define the role(s) of the HSF1 pS326 during the cell cycle.

Section 1: Introduction

Chapter A

NRF2, KEAP1 and their interaction

1.A.1 Introduction

Oxidation-reduction reactions, also known as redox reactions play a central role in numerous biological processes. Living organisms are constantly exposed to reactive oxygen species (ROS) (e.g. superoxide anion, peroxide, hydrogen peroxide, hydroxyl anion and singlet oxygen) or reactive nitrogen species (RNS) (e.g. nitroxyl anion, peroxyl nitrate, nitric oxide and nitrosyl cation) produced by both endogenous and exogenous sources. Oxidative stress is defined as the imbalance between the amount of oxidants and antioxidants, where the former is in excess, leading to the disturbance of the intracellular redox-homeostasis and subsequent damage (Sies, 2015). Examples of exogenous oxidative stressors are electrophilic molecules, carcinogens such as DNA-damaging agents, heavy metals and UV radiation. Endogenous stressors are usually produced by intracellular metabolic reactions during processes such as respiration and inflammation. Exposure to ROS/RNS or other chemically reactive species has been reported to damage cellular macromolecules such as DNA, proteins and cytoskeletal structures. As a consequence, chronic oxidative stress has been implicated in cancer (Mahalingaiah et al., 2015, Mehlman, 1992), diabetes (Ceriello, 2006, Bravi et al., 2006), neurodegenerative (Praprotnik et al., 1996, Castellani et al., 1996), respiratory (Hector et al., 2014, Bast et al., 2010), cardiovascular (Bast et al., 2010, Costa et al., 2016) and inflammatory (Muntane

et al., 1995) diseases as well as aging (Fukagawa, 1999, Joseph and Roth, 1992). In order to protect themselves from such insults, eukaryotic cells have developed several complex mechanisms to restore cellular redox homeostasis. One such mechanism is by inducing the production of anti-oxidant and cytoprotective proteins. This cytoprotective response is orchestrated by the transcription factor nuclear factor erythroid 2 p45-related factor 2 (NRF2) (**Fig. A1**).

1.A.2 The NRF2/KEAP1/ARE pathway

At basal conditions, NRF2 is negatively regulated by interaction with Kelch-like (ECH)-associated protein (KEAP1) (**Fig. A1**) (Itoh et al., 1999), a substrate adaptor protein for Cullin 3–RING (really interesting new gene)-box protein (Rbx)1-based E3 ubiquitin ligase, which uses a cyclical mechanism to continuously target NRF2 for ubiquitination and proteasomal degradation (**Fig. A2A**) (Baird et al., 2013, Kensler et al., 2007, Suzuki et al., 2013, Hayes and Dinkova-Kostova, 2014). Small molecules which activate NRF2 (termed inducers) block this cycle by modifying reactive cysteine sensors of KEAP1 (Dinkova-Kostova et al., 2002, McMahon et al., 2010) or disrupting the KEAP1 : NRF2 binding interface (**Fig. A2B**) (Hu et al., 2013, Marcotte et al., 2013). Consequently, NRF2 is not degraded and free KEAP1 is not regenerated. The newly synthesized NRF2 accumulates, translocates to the nucleus and binds (as a heterodimer with a small Maf protein) to antioxidant response elements (ARE, 5'-TGACnnnGC-3') in the upstream regulatory regions of its target genes (Suzuki et al., 2013, Kensler et al., 2007, Hayes and Dinkova-Kostova, 2014). In addition

FIGURE A1

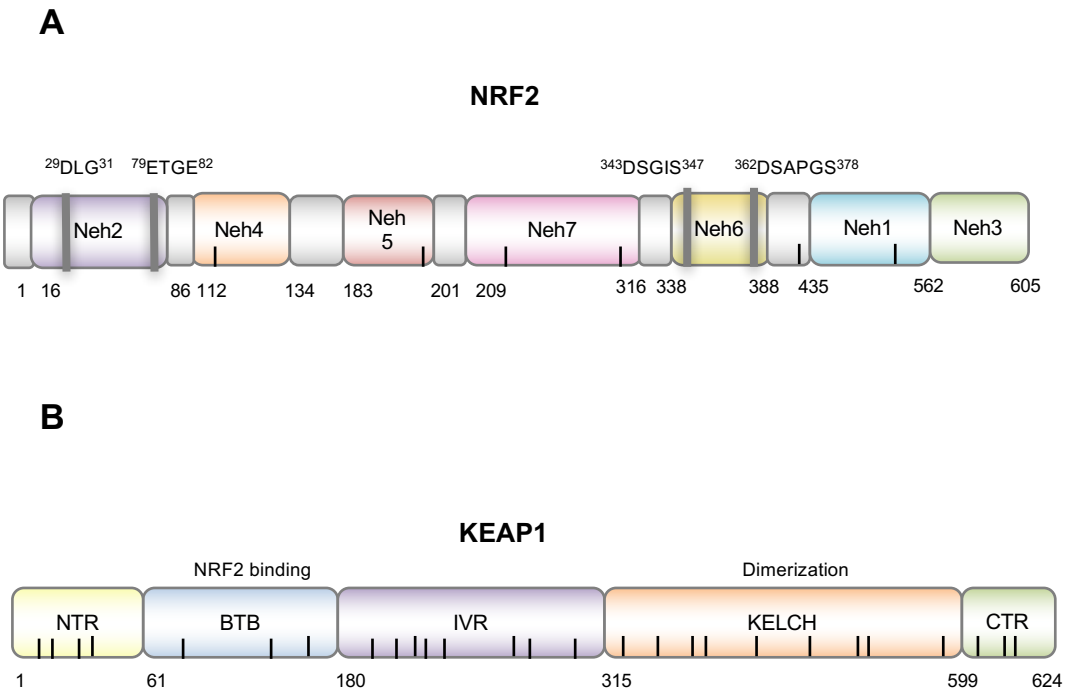

Figure A1. Schematic diagram of NRF2 and KEAP1 domains **A) Schematic diagram of NRF2 domains.** NRF2 has seven functional domains, termed NRF2-ECH homology (Neh)1–7 domains. The low-affinity "DLG" and the high affinity "ETGE" motifs that bind KEAP1-Kelch domain are shown. Neh4 and Neh5 are transactivation domains that recruit cAMP response element-binding (CREB)-binding protein (CBP) and/or receptor-associated coactivator (RAC)3. NRF2 is also negatively regulated by binding to retinoid X receptor alpha (RXRα), through the Neh7 domain of the transcription factor. The Neh6 domain mediates interaction with another negative regulator, the β-transducin repeat-containing protein (β-TrCP1), a substrate adaptor for the S-phase kinase-associated protein 1 (Skp1)–Cul1–Rbx1 ubiquitin ligase complex. The "DSGIS" and "DSAPGS" motifs that bind β-TrCP1 are shown. Neh1 contains the heterodimerisation domain which is responsible for binding with small musculoaponeurotic fibrosarcoma (Maf) proteins, and is the site of binding to antioxidant/electrophile response element (ARE/EpRE) sequences in DNA. The C-terminal Neh3 region of NRF2 is a transactivation domain that recruits chromo-ATPase/helicase DNA-binding protein (CHD)6. **B) Schematic diagram of KEAP1 domains.** KEAP1 is a member of the BTB-Kelch family of proteins. Members of this family are able to bind to Cullin 3 through their BTB domain. KEAP1 is a multidomain homodimeric protein which has five distinct domains: N-terminal region (NTR) (amino acids 1−60), broad complex, Tramtrack, Bric-á-brac (BTB) (amino acids 61−179), intervening region (IVR) (amino acids 180−314), Kelch domain (KELCH) (amino acids 315−598), and the C-terminal region (CTR) (amino acids 599−624). The black bars represent cysteine residues present in each of the proteins.

FIGURE A2

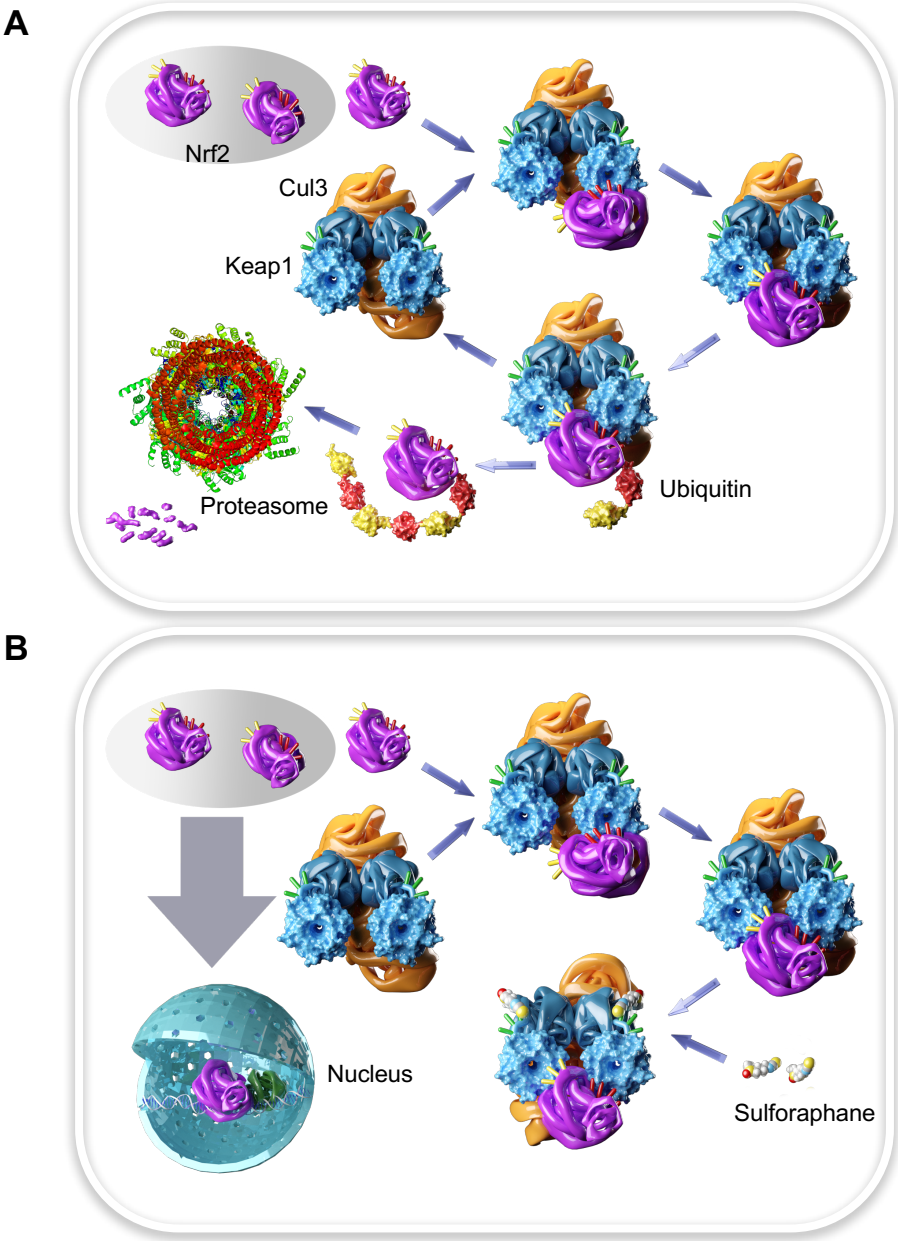

Figure A2. The KEAP1/NRF2 pathway. (A) Monomeric NRF2 (purple) binds sequentially to a free KEAP1 dimer (blue), a substrate adaptor protein for Cul3-based E3 ubiquitin ligase (orange): first through the high-affinity "ETGE" motif (red sticks) to form the open conformation of the KEAP1 : NRF2 protein complex, and then through the low-affinity "DLG" motif (yellow sticks) to form the closed conformation of the complex. In the closed conformation, NRF2 is targeted for ubiquitination and degradation by the proteasome. Ubiquitinated NRF2 is released from KEAP1 and degraded, free KEAP1 is regenerated and able to bind to newly-translated NRF2, and the cycle of KEAP1-mediated degradation of NRF2 begins again. **(B)** Electrophiles and oxidants (termed inducers and exemplified by the isothiocyanate sulforaphane) activate NRF2 by reacting with cysteine sensors (green sticks) of KEAP1 and disrupt the cycle by causing accumulation of the KEAP1 : NRF2 protein complex in the "closed" conformation, without release of NRF2. Consequently, free KEAP1 is not regenerated, and newly-synthesized NRF2 is stabilized. The transcription factor then enters the nucleus, where it forms a heterodimer with a small Maf protein (green) to drive transcription of downstream target genes [image drawn by Dr. Rumen Kostov and taken from (Dayalan Naidu et al., 2015)].

to KEAP1, the activity of NRF2 is also negatively regulated through glycogen synthase kinase (GSK)3/ β-transducin repeat-containing protein (β-TrCP)1-mediated degradation (Chowdhry et al., 2013) or by interaction with retinoid X receptor (RXR)α (Wang et al., 2013a).

1.A.3 Cytoprotective response of the NRF2/KEAP1/ARE pathway

NRF2-dependent genes encode a large network of cytoprotective proteins, including those that are involved in the metabolism and transport of a wide array of endo- and xenobiotics, proteins that have antioxidant functions, as well as those that participate in the synthesis, utilization, and regeneration of glutathione and NAD(P)H (Dayalan Naidu et al., 2015). The number of genes that are under the transcriptional control of NRF2 is fascinatingly large: a recent study integrating chromatin-immunoprecipitation with parallel sequencing (ChIP-Seq) and global transcription profiling identified 645 basal and 654 inducible direct targets of NRF2, with 244 genes at the intersection (Malhotra et al., 2010). Moreover, the functional diversity of the NRF2-dependent cytoprotective proteins is extraordinary and provides the cell with multiple layers of protection (Dayalan Naidu et al., 2015). Examples of NRF2-dependent proteins include: (i) antioxidant enzymes (e.g., heme oxygenase 1 (HO-1), NAD(P)H:quinone oxidoreductase 1 (NQO1), thioredoxin reductase); (ii) conjugating enzymes (e.g. glutathione *S*-transferases (GSTs) and UDP-glucuronosyltransferases); (iii) proteins that facilitate the export of xenobiotics and/or their metabolites (e.g., solute carrier- and ATP-binding cassette transporters); (iv) anti-inflammatory enzymes (e.g., leukotriene B_4 dehydrogenase); (v) enzymes that participate in

the synthesis and regeneration of glutathione (e.g., x-CT, the core subunit of the cystine/glutamate membrane transporter, ɣ-glutamate cysteine ligase catalytic (GCLC) and modulatory (GCLM) subunits, glutathione reductase); (vi) enzymes that are responsible for the synthesis of reducing equivalents (e.g., glucose 6-phosphate dehydrogenase (G6PD), 6-phosphogluconate dehydrogenase (PGD), malic enzyme (ME)1); (vii) proteins that protect against metal overload (e.g., ferritin and metallothioneins); and (viii) proteins that participate in the repair and removal of damaged proteins (e.g., subunits of the 26S proteasome) (Dayalan Naidu et al., 2015).

NRF2 activity profoundly affects the levels of the main intracellular small molecule antioxidant, reduced glutathione (GSH). NRF2 controls the gene expression of the two subunits GCLC and GCLM, the enzyme catalyzing the rate-limiting step in the GSH biosynthesis (Wild and Mulcahy, 2000) as well as of the cystine/glutamate antiporter (SLC7A11, system x_c^-) (Sasaki et al., 2002) that is responsible for the import of cystine, which in turn is converted to cysteine, a GSH precursor. Enhanced flux of glutamine into anabolic pathways under conditions of NRF2 activation (Mitsuishi et al., 2012) provides glutamate, the second GSH precursor; glutamate is also necessary for the import of cystine by system x_c^-. Provision of the third GSH precursor, glycine, is facilitated by the transporter SLC6A9, another NRF2-regulated gene (Hirotsu et al., 2012). In addition to the biosynthesis, NRF2 also regulates the regeneration of GSH. The transcription factor controls the expression of glutathione peroxidase (GPX), which during detoxification of peroxides oxidizes GSH to oxidized glutathione (GSSG). Subsequently, glutathione reductase (GSR), another NRF2 target, regenerates

GSH from GSSG using NADPH as a cofactor. The requirement for NADPH is provided by NRF2, which regulates the gene expression of the four principal NADPH-generating enzymes, i.e. G6PD, PGD, isocitrate dehydrogenase (IDH)1, and ME1 (Mitsuishi et al., 2012, Singh et al., 2013).

1.A.4 KEAP1: The main negative NRF2 regulator

In mammals, KEAP1 is a highly conserved 624-amino acid protein sharing approximately 90% sequence homology between species (**Fig. A3**). KEAP1 is mainly found in the cytoplasm as it is sequestered there due to its interaction with cytoskeletal actin filaments which prevent it from entering the nucleus (Kang et al., 2004). KEAP1 is also highly cysteine rich and the cysteines are highly conserved across the mammalian species. In humans there are 27 cysteine residues in KEAP1, whereas, in mouse there are 25 (**Fig. A3**), 9 of which (i.e., C23, C38, C151, C241, C273, C288, C297, C319, and C613) are flanked by basic amino acids. The presence of neighboring basic amino acids is known to lower the pK_a value of cysteine, favoring the formation of the thiolate anion at neutral pH, and thus increasing the cysteine reactivity (Snyder et al., 1981). Due to the presence of multiple cysteine residues, KEAP1 is able to function as an oxidative and electrophilic stress sensor and this is supported by experiments conducted by Dinkova-Kostova and colleagues where the authors discovered that several inducers of the KEAP1/NRF2/ARE pathway react with cysteine thiols in KEAP1 to disrupt its binding to the Neh2 domain of NRF2 (Dinkova-Kostova et al., 2002).

FIGURE A3

Amino acid sequence alignment of mammalian Keap1 using Clustal Omega Program

```
SP|Q14145|KEAP1_HUMAN   MQPDPRPSGAGACCRFLPLQSQCPEGAGDAVMYASTECKAEVTPSQHGNRTFSYTLEDHT 60
SP|Q9Z2X8|KEAP1_MOUSE   MQPEPKLSGAPRSSQFLPLWSKCPEGAGDAVMYASTECKAEVTPSQDGNRTFSYTLEDHT 60
SP|P57790|KEAP1_RAT     MQPEPKPSGAPRSSQFLPLWSKCPEGAGDAVMYASTECKAEVTPSQDGNRTFSYTLEDHT 60
SP|Q684M4|KEAP1_PIG     MQPEPRPSGAGAHTQFLPLRSQRPEGAGDTVMYASTECKAEVTPSQHGNRTFSYTLEDHT 60
SP|Q5R774|KEAP1_PONAB   MQPDPRPSGAGACSRFLPLRSQCPEGAGDAVMYASTECKAEVTPSQHGNRTFSYTLEDHT 60
TR|H2QFB9|H2QFB9_PANTR  MQPDPRPSGAGACCRFLPLQSQCPEGAGDAVMYASTECKAEVTPSQHGNRTFSYTLEDHT 60
                        ***:*: ***    :**** *: ******:****************.*************

SP|Q14145|KEAP1_HUMAN   KQAFGIMNELRLSQQLCDVTLQVKYQDAPAAQFMAHKVVLASSSPVFKAMFTNGLREQGM 120
SP|Q9Z2X8|KEAP1_MOUSE   KQAFGVMNELRLSQQLCDVTLQVKYEDIPAAQFMAHKVVLASSSPVFKAMFTNGLREQGM 120
SP|P57790|KEAP1_RAT     KQAFGIMNELRLSQQLCDVTLQVKYEDIPAAQFMAHKVVLASSSPVFKAMFTNGLREQGM 120
SP|Q684M4|KEAP1_PIG     KQAFGIMNELRLSQQLCDVTLQVKYEDAPAAQFMAHKVVLASSSPVFKAMFTNGLREQGM 120
SP|Q5R774|KEAP1_PONAB   KQAFGIMNELRLSQQLCDVTLQVKYQDAPAAQFMAHKVVLASSSPVFKAMFTNGLREQGM 120
TR|H2QFB9|H2QFB9_PANTR  KQAFGIMNELRLSQQLCDVTLQVKYQDAPAAQFMAHKVVLASSSPVFKAMFTNGLREQGM 120
                        *****:******************:* ********************************

SP|Q14145|KEAP1_HUMAN   EVVSIEGIHPKVMERLIEFAYTASISMGEKCVLHVMNGAVMYQIDSVVRACSDFLVQQLD 180
SP|Q9Z2X8|KEAP1_MOUSE   EVVSIEGIHPKVMERLIEFAYTASISVGEKCVLHVMNGAVMYQIDSVVRACSDFLVQQLD 180
SP|P57790|KEAP1_RAT     EVVSIEGIHPKVMERLIEFAYTASISVGEKCVLHVMNGAVMYQIDSVVRACSDFLVQQLD 180
SP|Q684M4|KEAP1_PIG     EVVSIEGIHPKVMERLIEFAYTASISMGEKCVLHVMNGAVMYQIDSVVRACSDFLVQQLD 180
SP|Q5R774|KEAP1_PONAB   EVVSIEGIHPKVMERLIEFAYTASISMGEKCVLHVMNGAVMYQIDSVVRACSDFLVQQLD 180
TR|H2QFB9|H2QFB9_PANTR  EVVSIEGIHPKVMERLIEFAYTASISMGEKCVLHVMNGAVMYQIDSVVRACSDFLVQQLD 180
                        **************************:********************************

SP|Q14145|KEAP1_HUMAN   PSNAIGIANFAEQIGCVELHQRAREYIYMHFGEVAKQEEFFNLSHCQLVTLISRDDLNVR 240
SP|Q9Z2X8|KEAP1_MOUSE   PSNAIGIANFAEQIGCTELHQRAREYIYMHFGEVAKQEEFFNLSHCQLATLISRDDLNVR 240
SP|P57790|KEAP1_RAT     PSNAIGIANFAEQIGCTELHQRAREYIYMHFGEVAKQEEFFNLSHCQLATLISRDDLNVR 240
SP|Q684M4|KEAP1_PIG     PSNAIGIANFAEQIGCAELHQRAREYIYMHFGEVAKQEEFFNLSHCQLVTLISRDDLNVR 240
SP|Q5R774|KEAP1_PONAB   PSNAIGIANFAEQIGCVELHQRAREYIYMHFGEVTKQEEFFNLSHCQLVTLISRDDLNVR 240
TR|H2QFB9|H2QFB9_PANTR  PSNAIGIANFAEQIGCVELHQRAREYIYMHFGEVAKQEEFFNLSHCQLVTLISRDDLNVR 240
                        ****************.*****************:*************.************

SP|Q14145|KEAP1_HUMAN   CESEVFHACINWVKYDCEQRRFYVQALLRAVRCHSLTPNFLQMQLQKCEILQSDSRCKDY 300
SP|Q9Z2X8|KEAP1_MOUSE   CESEVFHACIDWVKYDCPQRRFYVQALLRAVRCHALTPRFLQTQLQKCEILQADARCKDY 300
SP|P57790|KEAP1_RAT     CESEVFHACIDWVKYDCPQRRFYVQALLRAVRCHALTPRFLQTQLQKCEILQADARCKDY 300
SP|Q684M4|KEAP1_PIG     CESEVFHACINWVKYDCEQRRFYVQALLRAVRCHSLTPHFLQMQLQKCEILQSDSRCKDY 300
SP|Q5R774|KEAP1_PONAB   CESEVFHACINWVKYDCEQRRFYVQALLRAVRCHSLTPNFLQMQLQKCEILQSDSRCKDY 300
TR|H2QFB9|H2QFB9_PANTR  CESEVFHACINWVKYDCEQRRFYVQALLRAVRCHSLTPNFLQMQLQKCEILQSDSRCKDY 300
                        **********:****** ****************:***.*** *********:*:*****

SP|Q14145|KEAP1_HUMAN   LVKIFEELTLHKPTQVMPCRAPKVGRLIYTAGGYFRQSLSYLEAYNPSDGTWLRLADLQV 360
SP|Q9Z2X8|KEAP1_MOUSE   LVQIFQELTLHKPTQAVPCRAPKVGRLIYTAGGYFRQSLSYLEAYNPSNGSWLRLADLQV 360
SP|P57790|KEAP1_RAT     LVQIFQELTLHKPTQAVPCRAPKVGRLIYTAGGYFRQSLSYLEAYNPSNGSWLRLADLQV 360
SP|Q684M4|KEAP1_PIG     LVKIFQELTLHKPTQVMPCRAPKVGRLIYTAGGYFRQSLSYLEAYNPSDGTWLRLADLQV 360
SP|Q5R774|KEAP1_PONAB   LVKIFEELTLHKPTQVMPCRAPKVGRLIYTAGGYFRQSLSYLEAYNPSDGTWLRLADLQV 360
TR|H2QFB9|H2QFB9_PANTR  LVKIFEELTLHKPTQVMPCRAPKVGRLIYTAGGYFRQSLSYLEAYNPSDGTWLRLADLQV 360
                        **:**:*********.:*********************************:*:*********

SP|Q14145|KEAP1_HUMAN   PRSGLAGCVVGGLLYAVGGRNNSPDGNTDSSALDCYNPMTNQWSPCAPMSVPRNRIGVGV 420
SP|Q9Z2X8|KEAP1_MOUSE   PRSGLAGCVVGGLLYAVGGRNNSPDGNTDSSALDCYNPMTNQWSPCASMSVPRNRIGVGV 420
SP|P57790|KEAP1_RAT     PRSGLAGCVVGGLLYAVGGRNNSPDGNTDSSALDCYNPMTNQWSPCASLSVPRNRSGGGV 420
SP|Q684M4|KEAP1_PIG     PRSGLAGCVVGGLLYAVGGRNNSPDGNTDSSALDCYNPMTNQWSPCAPMSVPRNRIGVGV 420
SP|Q5R774|KEAP1_PONAB   PRSGLAGCVVGGLLYAVGGRNNSPDGNTDSSALDCYNPMTNQWSPCAPMSVPRNRIGVGV 420
TR|H2QFB9|H2QFB9_PANTR  PRSGLAGCVVGGLLYAVGGRNNSPDGNTDSSALDCYNPMTNQWSPCAPMSVPRNRIGVGV 420
                        ********************************************** :****** * **

SP|Q14145|KEAP1_HUMAN   IDGHIYAVGGSHGCIHHNSVERYEPERDEWHLVAPMLTRRIGVGVAVLNRLLYAVGGFDG 480
SP|Q9Z2X8|KEAP1_MOUSE   IDGHIYAVGGSHGCIHHSSVERYEPERDEWHLVAPMLTRRIGVGVAVLNRLLYAVGGFDG 480
SP|P57790|KEAP1_RAT     IDGHIYAVGGSHGCIHHSSVERYEPDRDEWHLVAPMLTRRIGVGVAVLNRLLYAVGGFDG 480
SP|Q684M4|KEAP1_PIG     IDGHIYAVGGSHGCIHHNSVERYEPERDEWHLVAPMLTRRIGVGVAVLNRLLYAVGGFDG 480
SP|Q5R774|KEAP1_PONAB   IDGHIYAVGGSHGCIHHNSVERYEPERDEWHLVAPMLTRRIGVGVAVLNRLLYAVGGFDG 480
TR|H2QFB9|H2QFB9_PANTR  IDGHIYAVGGSHGCIHHNSVERYEPERDEWHLVAPMLTRRIGVGVAVLNRLLYAVGGFDG 480
                        ****************.*******:********************************** 

SP|Q14145|KEAP1_HUMAN   TNRLNSAECYYPERNEWRMITAMNTIRSGAGVCVLHNCIYAAGGYDGQDQLNSVERYDVE 540
SP|Q9Z2X8|KEAP1_MOUSE   TNRLNSAECYYPERNEWRMITPMNTIRSGAGVCVLHNCIYAAGGYDGQDQLNSVERYDVE 540
SP|P57790|KEAP1_RAT     TNRLNSAECYYPERNEWRMITPMNTIRSGAGVCVLHSCIYAAGGYDGQDQLNSVERYDVE 540
SP|Q684M4|KEAP1_PIG     TNRLNSAECYYPERNEWRMITPMNTIRSGAGVCVLHNCIYAAGGYDGQDQLNSVERYDVE 540
SP|Q5R774|KEAP1_PONAB   TNRLNSAECYYPERNEWRMITAMNTIRSGAGVCVLHNCIYAAGGYDGQDQLNSVERYDVE 540
TR|H2QFB9|H2QFB9_PANTR  TNRLNSAECYYPERNEWRMITAMNTIRSGAGVCVLHNCIYAAGGYDGQDQLNSVERYDVE 540
                        ********************* **************.********************** 

SP|Q14145|KEAP1_HUMAN   TETWTFVAPMKHRRSALGITVHQGRIYVLGGYDGHTFLDSVECYDPDTDTWSEVTRMTSG 600
SP|Q9Z2X8|KEAP1_MOUSE   TETWTFVAPMRHHRSALGITVHQGKIYVLGGYDGHTFLDSVECYDPDSDTWSEVTRMTSG 600
SP|P57790|KEAP1_RAT     TETWTFVASMKHRRSALGIAVHQGRIYVLGGYDGHTFLDSVECYDPDTDTWSEVTRLTSG 600
SP|Q684M4|KEAP1_PIG     TETWTFVAPMKHRRSALGITVHQGRIYVLGGYDGHTFLDSVECYDPDTDTWSEVTRMTSG 600
SP|Q5R774|KEAP1_PONAB   TETWTFVAPMKHRRSALGITVHQGRIYVLGGYDGHTFLDSVECYDPDTDTWSEVTRMTSG 600
TR|H2QFB9|H2QFB9_PANTR  TETWTFVAPMKHRRSALGITVHQGRIYVLGGYDGHTFLDSVECYDPDTDTWSEVTRMTSG 600
                        ******** *:*:******:****:**********************:********:*** 

SP|Q14145|KEAP1_HUMAN   RSGVGVAVTMEPCRKQIDQQNCTC 624
SP|Q9Z2X8|KEAP1_MOUSE   RSGVGVAVTMEPCRKQIDQQNCTC 624
SP|P57790|KEAP1_RAT     RSGVGVAVTMEPCRKQIDQQNCTC 624
SP|Q684M4|KEAP1_PIG     RSGVGVAVTMEPCRKQIDQQNCTC 624
SP|Q5R774|KEAP1_PONAB   RSGVGVAVTMEPCRKQIDQQNCTC 624
TR|H2QFB9|H2QFB9_PANTR  RSGVGVAVTMEPCRKQIDQQNCTC 624
                        ************************
```

Amino acid sequence identity amongst these species is 92%

Figure A3. Amino acid sequence alignment of various mammalian KEAP1. Alignment performed using the web-based Clustal Omega program found within www.uniprot.org. The uniprot IDs are listed. Q14145 (Human), Q9Z2X8 (Mouse), P57790 (Rat), Q684M4 (Pig), Q5R774 (Orangutan), H2QFB9 (Chimpanzee). The highly conserved cysteine residues are highlighted in yellow.

1.A.4.1 *KEAP1 structure and its cysteine sensors*

KEAP1 is a member of the BTB-Kelch family of proteins which are named Kelch-like 1 to 42 (KLHL1-42). All members of this family are able to bind to Cullin 3 through their BTB domain. KEAP1 is a multidomain homodimeric protein which has five distinct domains (**Fig. A1B**): N-terminal region (NTR) (amino acids 1−60), broad complex, Tramtrack, Bric-á-brac (BTB) (amino acids 61−179), intervening region (IVR) (amino acids 180−314), Kelch domain (KELCH) (amino acids 315−598), and the C-terminal region (CTR) (amino acids 599−624).

The BTB domain is required for KEAP1 dimerisation, and it has been reported that mutation of S104 to an alanine residue prevents its homodimerisation and causes NRF2 accumulation in the nucleus (Zipper and Mulcahy, 2002). There are three cysteines present in the KEAP1 BTB domain, C77, C151 and C171. Single mutants of each of the cysteines in the BTB domain to a serine behave like the wild-type (WT) KEAP1 in terms of the ability to repress NRF2-dependent gene expression (Zhang and Hannink, 2003). The KEAP1 C151 is the most well-characterised in the literature. The KEAP1 C151S mutant under basal conditions is also able to mediate the degradation of NRF2, similarly to the WT protein (McMahon et al., 2010, Zhang and Hannink, 2003, Saito et al., 2015). Zhang et al. found that the BTB domain of KEAP1 protected KEAP1 from ubiquitin-mediated degradation (Zhang et al., 2005). Interestingly, it has been shown by several groups that under basal conditions, when subjected to SDS-PAGE, WT KEAP1 migrates as two distinct species, one at approximately 65 kDa and the other at 130 kDa and that the slow migrating species does not appear

with in the C151S mutant (Fourquet et al., 2010, Zhang and Hannink, 2003). Zhang and colleagues suggested that the slow migrating species of KEAP1 is due to the posttranslational modifications occurring on the protein, as the mutation of C151S prevents its occurrence. However, Fourquet et al. showed that the slower migrating KEAP1 species is non-inducible and redox insensitive and upon exposure to electrophiles, the intensity of the slower migrating species increased. The authors subsequently exposed induced samples to the reducing agent β-mercaptoethanol and observed a complete reduction in the intensified slower migrating species of KEAP1 hence suggesting that this species mainly comprises of the oxidized form of KEAP1 (Fourquet et al., 2010).

Some of the well-known NRF2 inducers that modify C151 are the isothiocyanate sulforaphane (SFN), iodoacetamide (IAA), *tert*-butyl hydroquinone (tBHQ) and diethylmaleate (DEM) (McMahon et al., 2010, Takaya et al., 2012, Saito et al., 2015, Bryan et al., 2013). In 2010, using molecular modeling McMahon et al. postulated that the cysteine reactivity of C151 in KEAP1 was due to the presence of five proximate basic amino acid residues (His 129, Lys 131, Arg 135, Lys 150 and His 154) (McMahon et al., 2010), which have the ability to deprotonate the sulfhydryl group of C151 thus lowering its pK_a. This results in the thiol group of C151 to exist as an anion under physiological pH conditions. Indeed, the authors discovered that KEAP1 bearing the triple mutations at K131M, R135M and K150M lost the ability to sense electrophiles that specifically targeted C151.

The crystal structure of the BTB domain of KEAP1 with the triterpenoid CDDO was solved in 2014 and deposited in the Protein Database Bank (pdb.org) with the accession number 4CXI using the Pymol software (**Fig.A4A**) (Cleasby et al., 2014). We measured the distances of the 5 positively charged amino acids mentioned that were adjacent to C151 and found that R135 had the closest proximity to C151 with a distance of 3.6Å (**Fig. A4B**), which further supports the findings reported by McMahon and colleagues (McMahon et al., 2010).

To date, there is no crystal structure of the IVR domain of KEAP1 (aa 180 to 315). The KEAP1 IVR domain, flanked by the N-terminal BTB domain and the Kelch domain at the C-terminus, contains 8 cysteine residues (cysteines 196, 226, 241, 249, 257, 273, 288 and 297), of which, C273 and C288 are the most well characterised. Exposure to electrophiles or alkylating agents targeting the cysteines within the IVR domain, predominantly C273 and C288, leads to the inactivation of KEAP1 and subsequent activation of NRF2 (Dinkova-Kostova et al., 2002, Kobayashi et al., 2004, Wu et al., 2010). Single or double mutations of C273 or C288 to serine or alanine render KEAP1 inactive with respect to its repression and degradation of NRF2 (McMahon et al., 2010, Zhang and Hannink, 2003, Kobayashi et al., 2004, Levonen et al., 2004), Wakabayashi et al. 2004). Since these C273S/A and C288S/A mutants inactivated KEAP1, they presented a difficulty to study the electrophiles that could potentially target these cysteines. Recently, Saito and colleagues showed that single or double mutation of C273 and C288 to tryptophan or glutamic acid did not impede the KEAP1-mediated repression and degradation of NRF2 hence allowing to precisely identify electrophiles that are sensed by either or both of these residues (Saito et al.,

FIGURE A4

A

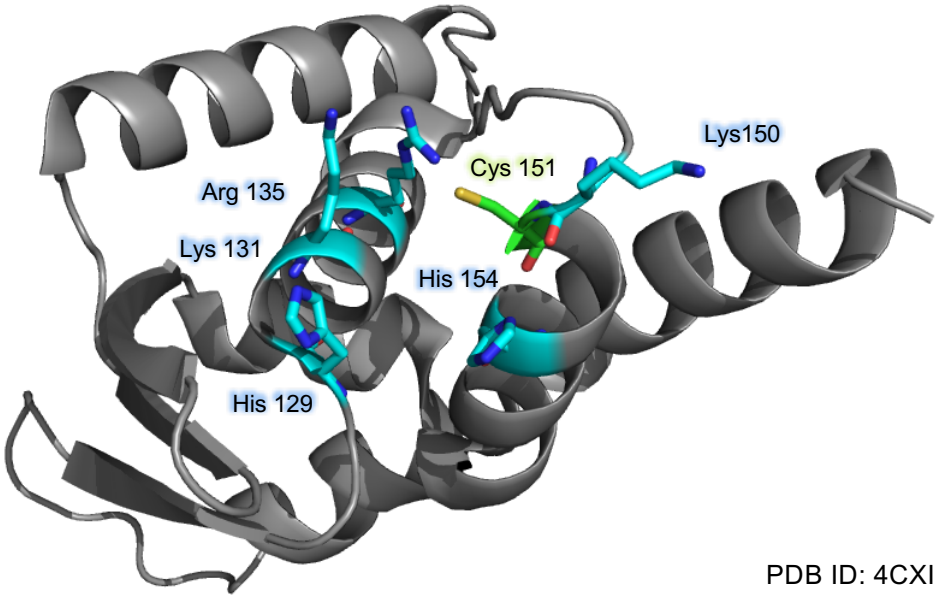

B

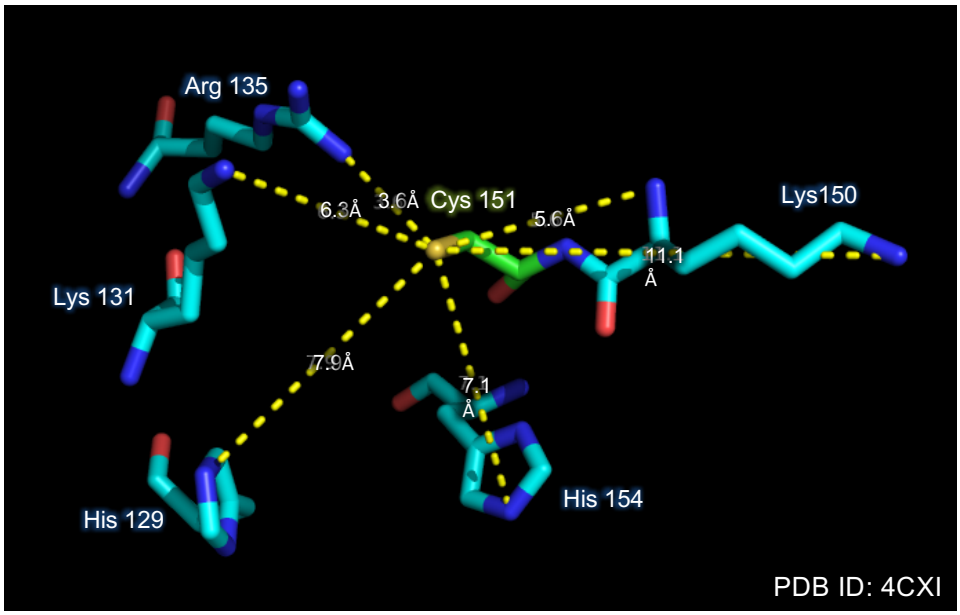

Figure A4. Structure of the human KEAP1 BTB domain. A) Cartoon representation of the human KEAP1 BTB domain (grey). The basic amino acids (His 129, Lys 131, Arg 135, Lys 150 and His 154) adjacent to the Cys 151 residue (green sticks) are represented with cyan coloured stick drawings. Structure drawn using Pymol using the PDB accession 4CXI. **B**) The distances calculated in angstroms (Å) between basic residues (His 129, Lys 131, Arg 135, Lys 150 and His 154) and Cys 151.

2015). In the report published by Saito et al. the authors showed that 15-deoxy-$\Delta^{12,14}$-prostaglandin J_2 (15d-PGJ_2) is sensed specifically by C288. We performed molecular modeling of the amino acid residues comprising the IVR domain using the I-TASSER platform (**Fig. A5**), and found that it is comprised of 8 α-helices and that basic amino acids are found adjacent to C273 (i.e. R272 and H274) and C288 (i.e. K287), which could cause the deprotonation of the thiol groups, hence increasing their reactivity.

The Kelch domain of KEAP1 is evolutionarily conserved and contains nine cysteine residues at amino acids 319, 368, 395, 406, 434, 489, 513, 518 and 583. The first crystal structure of the KEAP1 Kelch domain was solved at a resolution of 1.85Å in 2004 by Li and colleagues (Li et al., 2004). Several crystal structures of both the human and murine KEAP1 Kelch domains with different resolutions and in combination with compounds or short peptide sequences of the Neh2 domain of NRF2 have since been reported (Lo et al., 2006, Tong et al., 2007, Komatsu et al., 2010, Fukutomi et al., 2014, Winkel et al., 2015, Davies et al., 2016, Saito et al., 2016). The Kelch domain in KEAP1 contains six Kelch repeats that assembles into a six-bladed β-propeller structure (blades I-VI), where the C-terminal residues form the first strand in the first blade. Four-stranded antiparallel β sheets (A-D) form one blade, where the shortest β sheet A is found at the central core (Canning et al., 2015, Li et al., 2004). The Kelch domain also contains double glycine repeats (DGR), which are located at the terminal end of the β sheets. In several reports within the literature, the Kelch domain and the CTR are collectively called the DGR.

FIGURE A5

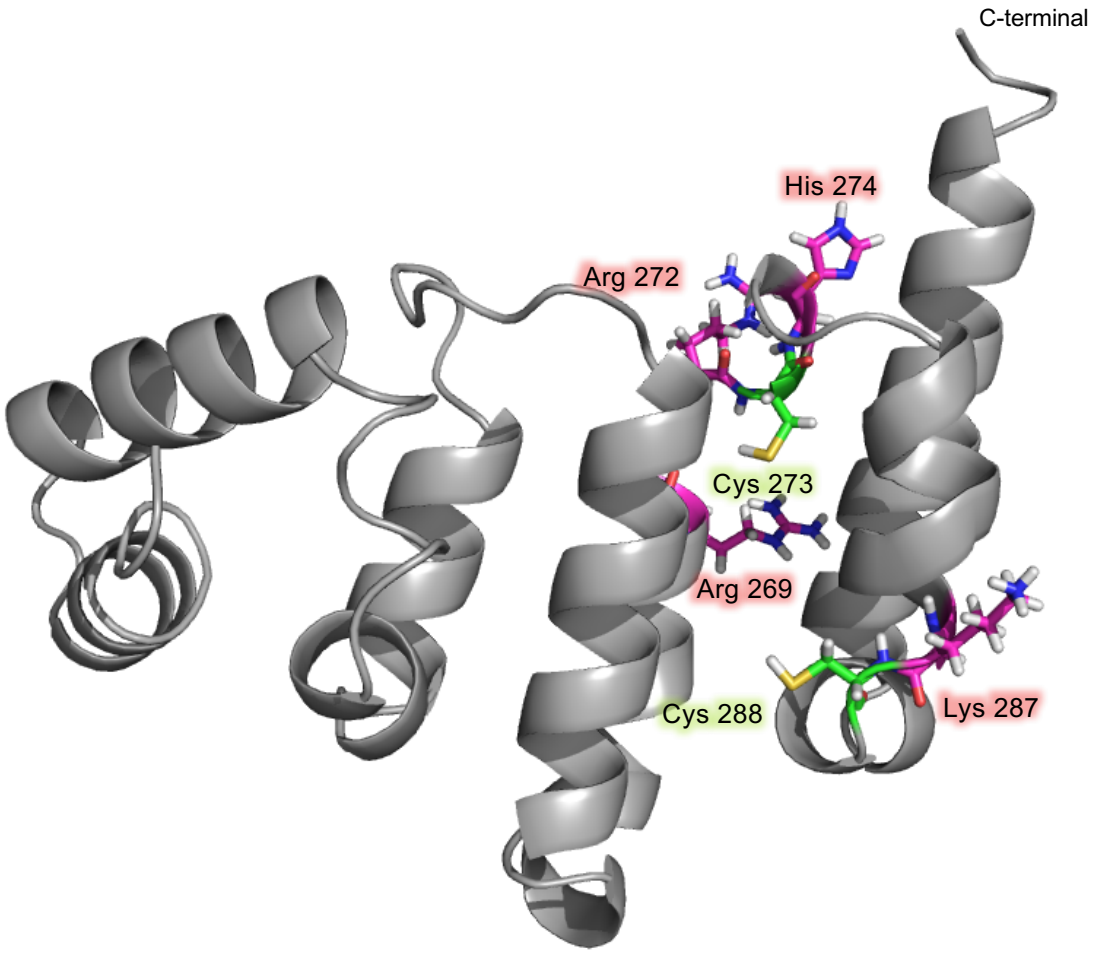

Figure A5. Modelled structure of the human KEAP1 IVR domain. Cartoon representation of the I-TASSER program modelled human KEAP1 IVR domain displaying 8 α-helices, amino acids 180 to 315 (grey). The basic amino acids (Arg 272 and His 274, pink) found adjacent to the Cys 273 residue (green) as well as the hydrophobic Lys 287 (pink) residue found adjacent to Cys 288 (green) are represented with coloured stick drawings.

First discovered in 1999 by Itoh and colleagues, the N-terminal Neh2 domain within NRF2 has been since reported by various groups to bind to the KEAP1 Kelch domain (Itoh et al., 1999). Using nuclear magnetic resonance spectroscopy, Tong et al. discovered that the Neh2 domain was intrinsically disordered (Tong et al., 2006). It was subsequently found that the evolutionarily conserved DLG (McMahon et al., 2004) and ETGE (Itoh et al., 1999) motifs within the NRF2-Neh2 domain (**Fig. A1A**) were responsible for binding to the KEAP1 Kelch domains (McMahon et al., 2006, Tong et al., 2006). The DLG motif has a 200-fold lower affinity binding constant to the Kelch domain of KEAP1 compared to the ETGE motif (Tong et al., 2007). When we compared the independently X-ray crystallographically-resolved complexes of ETGE containing peptide-Kelch KEAP1 with the DLG containing peptide-Kelch KEAP1 by superimposing the two using the Pymol software, we discovered that that both the DLG and ETGE motifs occupy the Kelch domain pocket in a similar fashion (**Fig.A6A and B**). The most striking difference observed between the occupancy of the DLG containing peptide compared to the ETGE-containing peptide was that the N-terminus of the DLG peptide adopted an α-helical secondary structure (**Fig. A6**). The DLG and ETGE motifs flank a lysine-rich α-helix to allow for the conjugation of ubiquitin molecules by the activated E2-ubiquitin conjugating enzyme. To summarize, the dimer of KEAP1 binds to NRF2 through its Neh2 domain where one KEAP1 monomer binds to the ETGE motif and the other binds to the DLG motif to serve as a substrate adaptor to mediate the proteasomal degradation of NRF2 through Cullin 3, a scaffolding protein for the E3 ubiquitin ligase complex.

FIGURE A6

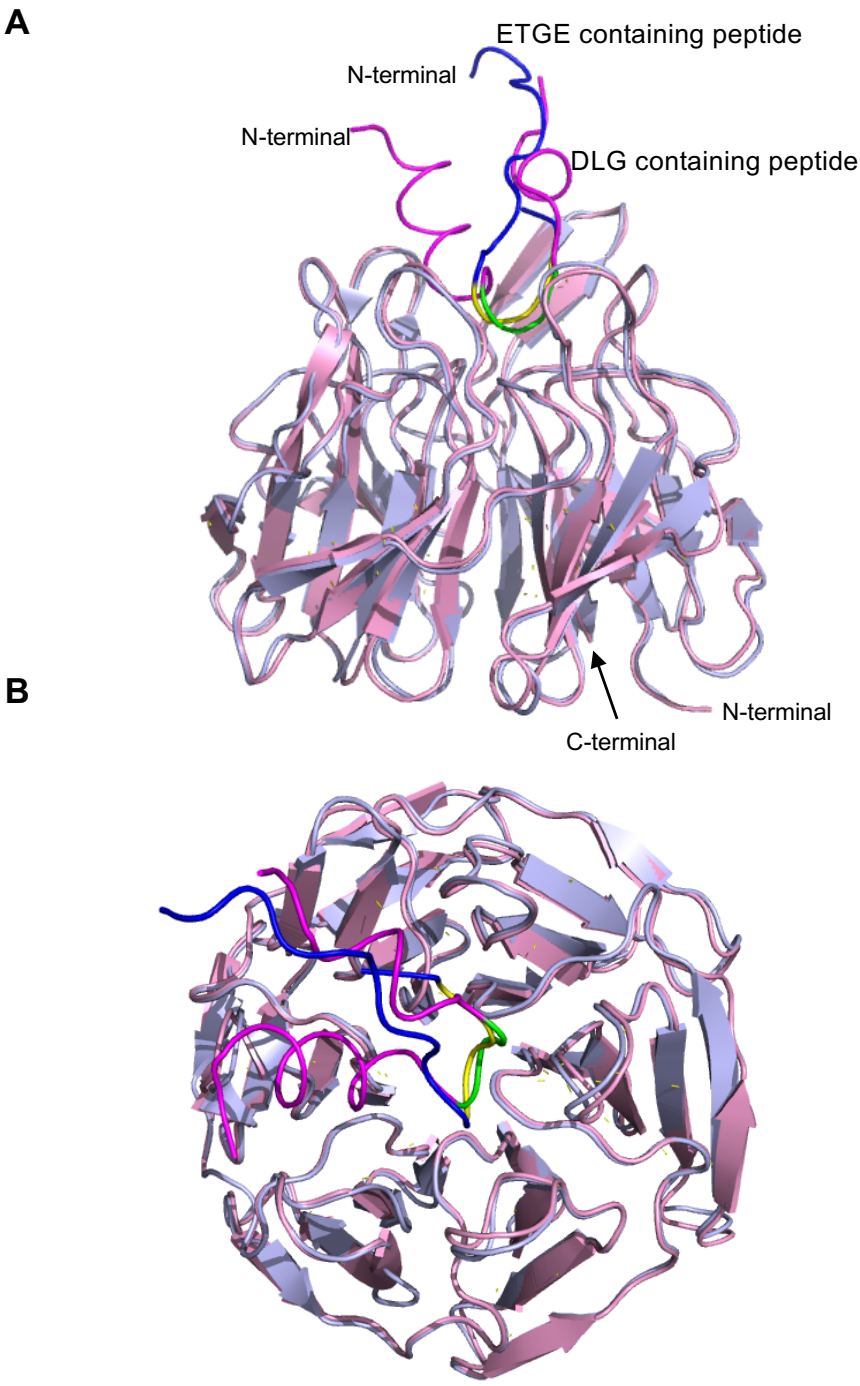

Figure A6. Structure of the KEAP1 Kelch domain. Cartoon representation of superimposed human KEAP1-Kelch domain (pale blue) complexed with the ETGE (yellow) containing human NRF2 peptide sequence (amino acids 69 to 84) (blue) (PDB ID: 2FLU) and the murine KEAP1-Kelch domain (pale pink) complexed with the murine NRF2 peptide (amino acids 17-40) (pink) containing the DLG motif (green) (PDB ID: 3WN7). A) shows the side view and B) shows the top view of the Kelch domains of KEAP1.

1.A.4.2 *KEAP1-Cullin3 interaction*

The primary system for protein degradation in the cell is the ubiquitin-proteasome system, where E3 ubiquitin ligases are essential components. Cullins are a family of hydrophobic proteins that confer substrate specificity by acting as scaffolds for E3 ubiquitin ligase complexes (Sarikas et al., 2011, Anderica-Romero et al., 2013). Thus far, in mammals, there have been seven Cullins (1, 2, 3, 4A, 4B, 5 and 7) identified. Cullin 3 is the only member of its family that is able to recognize BTB domains-containing proteins (Anderica-Romero et al., 2013). Since KEAP1 contains the BTB domain, in 2004, Kobayashi and colleagues hypothesized that under basal conditions, Cullin 3 could be mediating the degradation of NRF2 through binding of the substrate adaptor KEAP1 due to its ability to bind to proteins containing the BTB domain (Kobayashi et al., 2004). Indeed, they discovered that, *in vivo*, Cullin 3 was able to bind to KEAP1, however, it was surprising that the interaction between the two proteins was between the IVR domain of KEAP1 and the N-terminal domain of Cullin 3 instead of the BTB domain of KEAP1 (Kobayashi et al., 2004). Subsequently, at the beginning of 2005, in the same journal, Furukawa and Xiong, reported that KEAP1 and Cullin 3 binding occurs between the BTB-domain of the former and the N-terminal domain of the latter. Subsequently, it was discovered that Cullin 3 homodimerisation requires the presence of its N-terminal domain and is dependent on its interaction with BTB domain containing substrates (i.e. KEAP1) which also are able to homodimerise at their BTB domains (Choo and Hagen, 2012).

Using a quantitative fluorescence recovery after photobleaching (FRAP)-based approach, Baird and Dinkova-Kostova, found that NRF2 inducers such as the semisynthetic triterpernoid CDDO, the isothiocyante sulforaphane and hydrogen peroxide do not affect the binding between ectopically expressed fluorophore-tagged KEAP1-EGFP and mCherry-Cullin 3, and suggested that conformational changes could inactivate their repressive functions, ultimately leading to activation of NRF2 (Baird and Dinkova-Kostova, 2013). Under basal conditions, the KEAP1-E3 ubiquitin ligase complex binds to one NRF2 molecule. A small protein, Nedd8 is covalently attached to a highly conserved lysine residue at the C-terminus region of Cullin 3. This leads to the reconfiguration of the KEAP1-Cullin 3-E3 ubiquitinating complex and allows for the association E2 enzymes to come into contact with NRF2, leading to its polyubiquitination and subsequent degradation by the proteasome (Canning et al., 2013, Duda et al., 2008, Saha and Deshaies, 2008). It could be envisioned that when this complex is exposed to electrophiles or reactive oxygen species, the polyubiquitination of NRF2 ceases due to chemical modification of the reactive 'sensor' cysteine residues in KEAP1, which disables its NRF2-repressor function.

1.A.5 Concluding remarks

More than 20 years of research conducted on the KEAP1/NRF2 pathway by various independent groups have highlighted the exceptional importance of these two proteins. The extraordinary ability of KEAP1 to sense a multitude of inducers that vary in shape, size and order of reactivity has led to an intricately complex 'cysteine code', which guarantees a finely tuned and tightly regulated

antioxidant response pathway. The induction of this pathway is the purpose of the small molecule NRF2 activators, which are currently in clinical trials. It is vital that further research is conducted to achieve a greater understanding of the detailed consequences of activating NRF2 by targeting of KEAP1 for the treatment and prevention of various diseases.

Section 1: Introduction

Chapter B

The cytoprotective role of the mammalian heat shock factor 1

1.B.1 Introduction

In the early 1960s, the Italian researcher Ferruccio Rittosa was studying the type(s) of nucleic acid that was being transcribed at the puffs in the chromosomes of the *Drosophila* salivary glands (Ritossa and Vonborstel, 1964), where these chromosome puffs were found to be transcriptionally active regions. By accident, one of his colleagues had increased the temperature of the incubator where he had kept his *Drosophila* larvae and during this time (Ritossa, 1996), Ritossa noticed a unique puffing pattern in the *Drosophila* polytene chromosomes (Ritossa, 1964) when they were exposed to heat, sodium salicylate or di-nitrophenol. Subsequently, independent groups observed this phenomenon in other *Drosophila* tissues, and this ultimately led to the discovery of the heat shock proteins when the researchers Tissieres and Mitchell found these proteins to be upregulated during the chromosomal puffing that occurred upon heat stress (Tissieres et al., 1974).

In all living organisms known to man, the cellular response to elevated temperatures is universal, and is triggered by a temperature increase of just a few degrees above the optimal temperature. All organisms are adapted to a precise range of temperatures for optimal function. Cells within these organisms possess intricate mechanisms that allow for adaptation and survival during

elevated temperatures. In humans, the core body temperature is normally around 37 degrees Celsius (^{o}C). However, temperatures above 41 ^{o}C induce the heat shock response (HSR), which is characterized by the activation of transcription of *heat shock protein (Hsp)* genes orchestrated by a family of transcription factors, within which heat shock factor 1 (HSF1) is most prominent. The HSR causes the elevation of the Hsps such as Hsp24, Hsp40, Hsp70 and Hsp90 most of which are molecular chaperones that function to prevent protein misfolding and aggregation within the cell. The HSR is a cytoprotective mechanism that is also stimulated upon cellular stresses such as hypoxia (Benjamin et al., 1990), fluctuations in intracellular pH (Jolly and Morimoto, 2000), proteotoxicity and exposure to heavy metals (Lee et al., 2002a, Saydam et al., 2003). Critically, in addition to providing an adaptive response to thermal stress resulting in thermotolerance, the HSR orchestrated by HSF1 has protective effects in numerous pathophysiological conditions, including ageing and neurodegenerative diseases (Aridon et al., 2011, Hoshino et al., 2011, Anckar and Sistonen, 2011, Morley and Morimoto, 2004).

1.B.2 HSF family members

To date, there are four known members belonging to the HSF protein family, of which HSF1, HSF2 and HSF4 (Schuetz et al., 1991, Nakai et al., 1997) have been identified and characterized in mammals, and HSF3 was initially identified in the avian species (Nakai et al., 1995). In unstressed cells, HSF1 is a monomer and in contrast, HSF2 exists as a dimer. Upon stress, HSF2 can either form a homotrimer or it can heterotrimerize with HSF1 in the nucleus and induce

the transcription of both the classical heat shock genes as well as non-classical heat shock genes such as the tandem satellite III DNA repeats (Sandqvist et al., 2009, Ostling et al., 2007). A recent study has discovered that HSF1 and HSF2 interact with each other through their coiled-coil domains adjacent to their DNA binding domains (Jaeger et al., 2016). Unlike HSF1, HSF2 expression is tissue- and cell-specific (Akerfelt et al., 2010). In the mouse, HSF2 plays a vital role in spermatogenesis, female fertility and early development (Wang et al., 2004a, Kallio et al., 2002). Kallio *et al.* discovered that HSF2-null (HSF2-/-) mice, although embryonically viable, display brain abnormalities, which are characterized by a reduced striatum and hippocampus; furthermore, HSF2-/- female mice produce eggs with meiotic defects (Kallio et al., 2002). Although much of the early research on HSF2 was focused on its role in development, a more recent study highlighted the link between HSF2 and neurodegeneration (Shinkawa et al., 2011). The researchers found that the loss of HSF2 in the R6/2 Huntington's disease mouse model exacerbates the aggregation of the polyglutamine protein leading to a decreased lifespan.

HSF4 lacks the LZ4 domain that is required for the suppression of trimerization of HSF1, is localized mainly in the nucleus, and is ubiquitously expressed in cells. HSF4 plays an important role in development and its expression is increased during lens development (Fujimoto et al., 2004). Many studies have shown that HSF4 is crucial for the development and maintenance of the lens as mutations in HSF4 (Fujimoto et al., 2008), particularly in the DNA-binding domain are correlated with the development of cataracts in humans (Ke et al., 2006, Forshew et al., 2005, Smaoui et al., 2004, Bu et al., 2002). One of

the isoforms of HSF4, HSF4a, has been shown to negatively regulate HSF2 by downregulating the expression and inhibiting the transcriptional activity of HSF2 at the *hsp70* promoter via directly binding to HSF2 (Kim et al., 2012b). Loss of the ATP-dependent chromatin remodelling enzyme Snf2h is vital for lens development in mice. Interestingly, depletion of Snf2h dramatically reduces HSF4 transcript levels suggesting that the transcription factor is regulated by chromatin remodelling, and that the importance of Snf2h in lens development might be in part mediated by HSF4 (He et al., 2016).

The mammalian HSF1 orthologue in avian cells is functionally redundant, however, in chickens, HSF3 is the major heat shock transcription factor (Kawazoe et al., 1999). Furthermore, human HSF1 is able to rescue the induction of the classical heat shock responsive genes in the absence of chicken HSF3, although chicken HSF1 confers cellular cytoprotection when cells are exposed to stressors such as UV irradiation (Inouye et al., 2003) and is able to do so without inducing the classical heat shock genes, suggesting that chicken HSF1 also plays a vital role in other pro-survival pathways. In the chicken, HSF3 exists as a dimer in unstressed cells and is able to form homotrimers upon heat shock(Nakai et al., 1995, Nakai and Ishikawa, 2000). The mouse HSF3 discovered in 2010 by Fujimoto et al. (Fujimoto et al., 2010) can activate the transcription of non-classical heat shock genes, and its isoform mHSF3a, has the ability of protect cells from heat shock and proteotoxicity. Of note, although HSF3 is considered to be the avian ortholog of the mammalian HSF1, a recent study suggests that its involvement in the regulation of a number of febrile response mediators, such as

the interleukins IL-6. IL-1β, and activating transcription factor 3 (ATF3), have evolutionally diverged in mammalian and avian species (Prakasam et al., 2013).

1.B.3 HSF1: Structure, Function and Regulation

HSF1 is the most well studied member of the HSF family. During unstressed conditions, the mammalian HSF1 exists as a monomer more abundantly in cytoplasm relative to the nucleus (**Fig. B1**). The DNA-binding and transcriptional capacity of the transcription factor is suppressed at both the intramolecular level as well as the intermolecular level, where in the latter, molecular chaperones such as Hsp70 (Shi et al., 1998) and Hsp90 (Ali et al., 1998) interact with HSF1 to inhibit its activation. Upon cellular tress, HSF1 undergoes several activating post-translational modifications and also forms a transcriptionally active trimer that accumulates in the nucleus and binds to heat shock elements (HSE) which contain the inverted repeats of the deoxyribonucleotides TTCnGAAnTTC that are found in the upstream regulatory regions of the *hsp* genes (Trinklein et al., 2004).

Nuclear stress bodies (nSBs) are relatively large distinct structures (0.3 to 3 μm in diameter) that are formed in the nucleus when the cell is exposed to stresses such as heat shock or heavy metals (Biamonti and Vourc'h, 2010). The formation of nSBs requires the transcriptionally active HSF1 to interact with pericentrometric tandem repeats of satellite III (sat II) sequences within the 9q12 chromosomal locus leading to the transcription of non-coding single-stranded RNA molecules. Also, HSF1 binds to the histone acetyl transferase (HAT) CREB

Figure B1

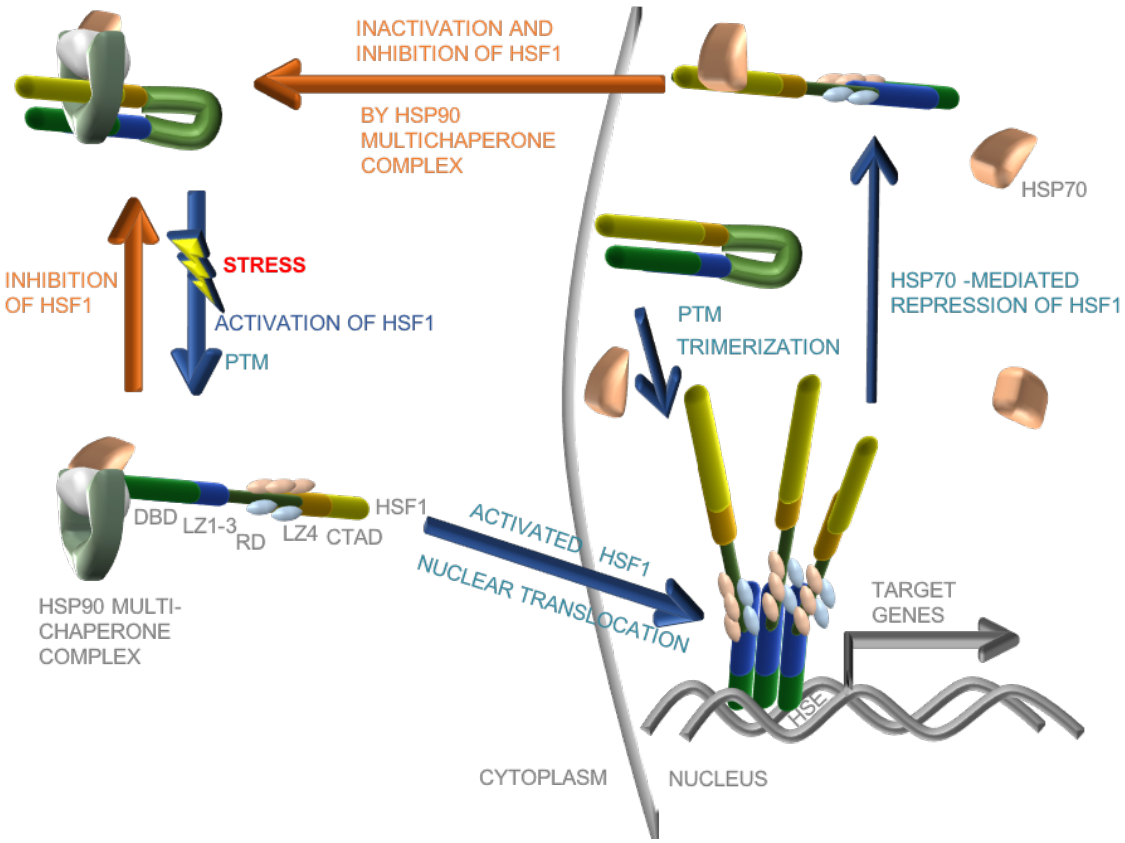

Figure B1. The heat shock response. Various types of cellular stressors such as heat and proteotoxicity can activate the heat shock response by causing the release of the transcription factor HSF1 which is basally sequestered by the Hsp90 multi-chaperone complex that also includes the co-chaperone Hsp70. In addition, the binding between the leucine zipper (LZ) domains LZ1-3 and LZ4 is disrupted and the regulatory domain of HSF1 becomes hyperphosphorylated at several serine residues within its regulatory domain (RD), leading to HSF1 activation. The transcriptionally active HSF1 is then able to enter the nucleus, homotrimerize and bind to the heat shock elements to induce the transcription of its target genes. HSF1 that is basally present in the nucleus also becomes activated upon stress and is able to homotrimerize to elicit the heat shock response. In the attenuation phase of the heat shock response, nuclear Hsp70 binds to the C-terminal transactivation domain (CTAD) of HSF1 to inhibit its function. During this time HSF1 is also dephosphorylated and shuttles out of the nucleus, resumes its inactivated form and is once again bound to the Hsp90- multichaperone complex.

and causes the hyperacetylation of nucleosomes at the satellite III repeats, allowing RNA polymerase as well as several RNA-binding proteins to transcribe sat III mRNA transcripts. The mRNA and RNA-binding protein complexes generated are known as the perichromatin granules (PGs) and are generated in large clusters during stress forming mature distinct nSBs (Biamonti, 2004). Interestingly, at the nSBs, HSF1 and HSF2 form transcriptionally active heterocomplexes (Alastalo et al., 2003) and the formation of nSBs coincides with the nucleolar accumulation of Hsp70. Although, the function of the nSBs is currently quite unclear, it is interesting that upon stimulation, nSBs are formed as early as 5 minutes and they are able to last for several hours after the initial stimulation. During the heat shock response, Hsp70 levels are increased, and the HSF1 trimers that exit the nSBs are dissociated into inactive HSF1 monomers by the binding of Hsp70 (Biamonti, 2004).

The generation of HSF1-knockout mice ($HSF1^{-/-}$) provided new insights into the functional significance of HSF1(Yan et al., 2002). $HSF1^{-/-}$ mice have altered redox homeostasis in the cardiac cells, and their mitochondria are highly susceptible to oxidative damage. By use of mouse embryonic fibroblasts (MEFs), it was found that HSF1 is essential for induction of the classical heat shock genes, and $HSF1^{-/-}$ MEFs are more sensitive to apoptosis during heat stress compared to their wild-type counterparts (Yan et al., 2002) showing the importance of HSF1 for cell survival. Female $HSF1^{-/-}$ mice display placental insufficiency, which contributes to the partial fetal lethality of the absence of the transcription factor. Male $HSF1^{-/-}$ mice are fertile, however the females with this genotype are sterile. HSF1 plays a vital role in oogenesis: HSF1 is highly abundant in the nucleus of

immature oocytes and plays an important role in the initial cleavage stages, hence explaining the infertility described in the HSF1$^{-/-}$ females (Christians et al., 2000).

HSF1 is constitutively expressed in most tissues and cell types and is regulated by multiple post-translational modifications (PTMs) such as sumoylation, acetylation and phosphorylation throughout its activation and attenuation cycle (**Fig. B2**). In an unstressed system, HSF1 is a monomeric phosphoprotein where it is phosphorylated on multiple serine residues (Sarge et al., 1993, Baler et al., 1993, Holmberg et al., 2001, Cotto et al., 1996), and is also negatively regulated at the intramolecular level due to the binding of the LZ1-3 domain and the LZ4 domain. The LZ1-3 domain, or the oligomerization domain, due to its coiled-coil structure has the ability to form homotrimers (Rabindran et al., 1993, Farkas et al., 1998, Liu and Thiele, 1999). Upon stress, the intramolecular coiled-coil interaction is lost and an intermolecular coiled-coil interaction is established. The regulatory domain (RD) of HSF1 lies between the LZ1-3 and LZ4 domains. Its absence causes HSF1 to become transcriptionally active even in unstressed conditions, which highlights the role of the RD as a repressor of HSF1 activity and also as a stress sensor (Yoshima et al., 1998, Newton et al., 1996, Budzynski et al., 2015).

During exposure to stress such as heat shock, HSF1 is hyperphosphorylated and this hyperphosphorylation of HSF1 increases the half-life of the HSF1 trimers and prolongs its transactivating capabilities (Xia and Voellmy, 1997). The RD is subjected to many PTMs such as acetylation,

Figure B2

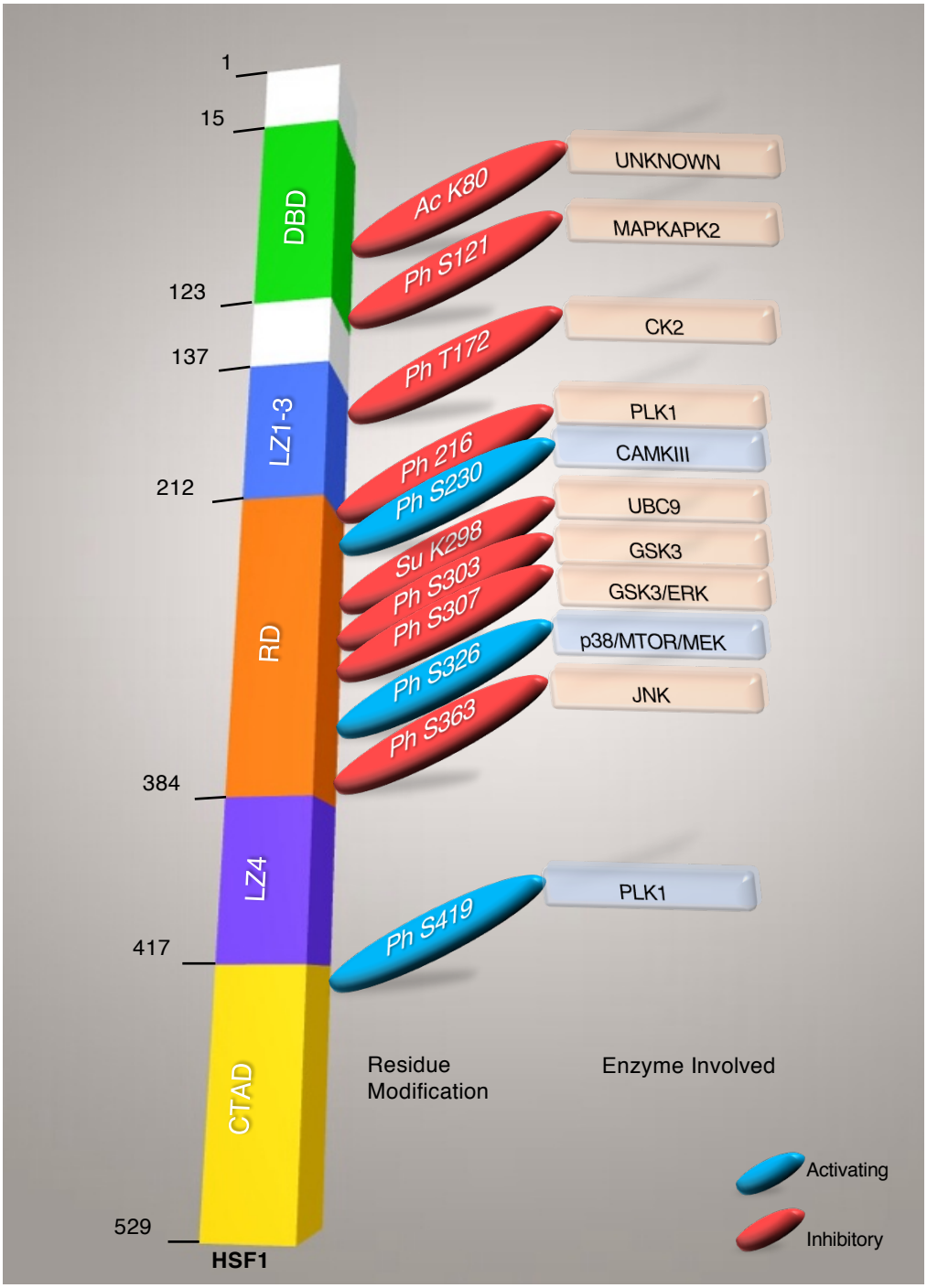

Figure B2. Schematic diagram of the structure and posttranslational modifications of HSF1. HSF1 is posttranslationally modified by various enzymes and these modifications can confer HSF1 to be either transcriptionally active or inactive. The activating modifications (blue) are phosphorylation (Ph) modifications on Ser residues 230, 326, and 419. The repressive modifications (red) on HSF1 are acetylation (Ac) on Lys 80, phosphorylation on Ser residues 121, 172, 303, 307 and 363 and sumoylation (Su) on Lys 298. The enzymes that catalyze these modifications are listed beside the respective residue modifications; DBD: N-terminal DNA-binding domain, LZ: Leucine zippers LZ1-3 and LZ4, RD: Regulatory domain, and CTAD: C-terminal transactivation domain. Trimerization of HSF1 occurs at the LZ1-3 region, whereas at basal conditions, it is negatively regulated by LZ4. Also, in unstressed systems the CTAD is negatively regulated by the RD.

phosphorylation and sumoylation. In 2005, Guettouche and colleagues performed an extensive study on the phosphorylation sites on human HSF1 and identified that HSF1 was phosphorylated on at least 12 serine residues, and interestingly, they did not detect phosphorylation on threonine or tyrosine residues (Guettouche et al., 2005); however, other groups have identified phosphorylation events occurring on such residues (Soncin et al., 2003, Olsen et al., 2006). Although most of the phosphorylations that occur within the RD are inhibitory, phosphorylations on serine 230 (Holmberg et al., 2001) and serine 326 (Guettouche et al., 2005, Boellmann et al., 2004) are activating. Thus, the calcium/calmodulin-dependent kinase CAMKII phosphorylates HSF1 at serine 230 during stress conditions, and mutation of this residue reduces the transcriptional capacity of HSF1(Holmberg et al., 2001). The phosphorylation of serine 326 of HSF1 allows DAXX to bind to HSF1 to enhance its transcription (Boellmann et al., 2004), and mutations of serine 326 have been shown to reduce the transcriptional activity of HSF1 by more than 70% (Guettouche et al., 2005, Boellmann et al., 2004).

The kinases that phosphorylate HSF1 at S326 were proposed to be MEK (Tang et al., 2015) and mTOR (Chou et al., 2012). Experiments described in this thesis showed that all members of the p38 MAPK family have the ability to phosphorylate HSF1 at S326 *in vitro* and in cells, p38ɣ was identified to be the primary kinase that phosphorylates HSF1 at this site (Dayalan Naidu et al., 2016). In addition, phosphorylation on serine 303 that lies within the regulatory domain of HSF1 is required for sumoylation (conjugation of small ubiquitin modifiers (SUMO) 2/3) at lysine 298 (Hietakangas et al., 2003), and this mechanism was

first discovered in HSF1 where phosphorylation-dependent sumoylation motif (PDSM) characterized by the consensus sequence ΨKxExxSP (where Ψ is a branched hydrophobic amino acid and x is any amino acid) was identified (Hietakangas et al., 2006). Sumoylation at lysine 298 renders HSF1 transcriptionally incompetent (Hilgarth et al., 2003). Brunet Simioni et al. found that the phosphorylation of serine 303 and 307 itself does not affect the transcriptional activity of HSF1; however, the phospho-S303-dependent sumoylation on lysine 298 blocks its transactivation capacity (Brunet Simioni et al., 2009).

The DNA-binding domain (DBD) located at the N-terminal region of HSF1 is highly conserved across species (Anckar and Sistonen, 2011) (**Fig. B3**). Within the HSF1 trimers, each of the DBD of the monomers recognizes the nGAAn sequence in the major groove (Cicero et al., 2001, Littlefield and Nelson, 1999). Phosphorylation of serine 121 by MAPK-activated protein kinase 2 (MAPKAPK2) at the DBD causes HSF1 to lose its transcriptional activity and promotes its binding to Hsp90, a negative regulator of HSF1 (Wang et al., 2006). In addition, acetylation on lysine 80 hinders the transcriptional capacity of HSF1, as mutagenesis studies in yeast have revealed a loss-of-function phenotype when lysine 80 was mutated (Hubl et al., 1994, Torres et al., 1995). Activation of the SIRT1 deacetylase prolonged the transcriptional competency of HSF1, whereas the decrease in SIRT1 accelerated the attenuation phase of HSF1.

The available literature on the functional characterization of the HSF1 C-terminal transactivation domain (CTAD) is limited compared to the other domains described above. The CTAD consists of two transactivation domains, TAD1 and

Figure B3

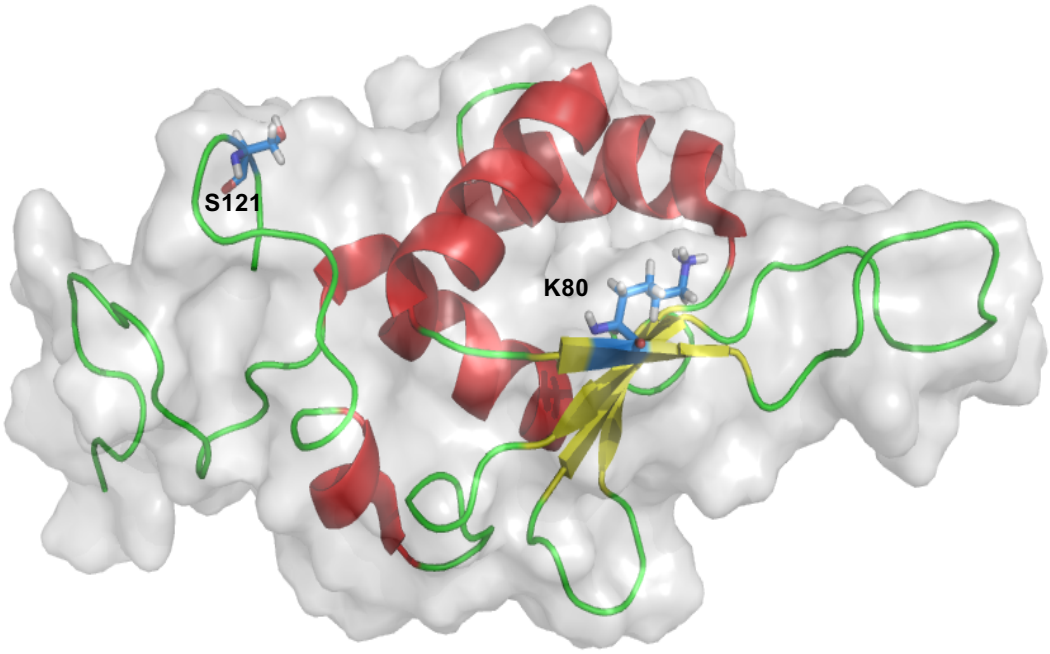

Figure B3. Structure of the DNA-binding domain (DBD) of human HSF1 (amino acids 10-123). The domain is coloured according to the secondary structure of the protein where the alpha helices and beta-sheets are represented by red and yellow respectively. Amino acid residues Lysine 80 (K80) and Serine 121 (S121) are represented as blue sticks. Figure drawn using Pymol using the PDB entry 2LDU.

TAD2 (Newton et al., 1996). TAD1 (amino acids 401-420) is rich in hydrophobic amino acids and interacts with TATA-box binding protein associated factor TAF9 *in vitro,* and mutations within the hydrophobic patch of TAD1 prevent HSF1 transactivating capability (Choi et al., 2000). TAD2 contains both acidic and hydrophobic residues and is proline-rich. BRG1 belonging to chromatin remodeler SWI/SNF complex binds to HSF1 at the CTAD (Sullivan et al., 2001). It is likely that the CTAD could be the hub for interaction of transcriptional co-factors and HSF1. Interestingly, Hsp70 binds to the CTAD of HSF1 (Abravaya et al., 1992), therefore, it could potentially negatively regulate HSF1 by disrupting the association of HSF1 with its transcriptional co-activators such as p300/CBP (Xu et al., 2008). Although it is clear from the literature that HSF1 and Hsp90 interact (Zou et al., 1998, Ali et al., 1998, Shi et al., 1998), to our knowledge, the precise interaction site has not been mapped.

1.B.4 Small molecule activators of HSF1

1.B.4.1 *Endogenous metabolites*

HSF1-mediated transcription can be induced by endogenously produced electrophilic oxidized and nitrated lipids as well as α,β-unsaturated aldehydes. Examples include 4-hydroxy-2-nonenal, acrolein, 10-nitro-octadecenoic acid (nitro-oleic acid), and 15-deoxy-$\Delta^{12,14}$-prostaglandin J_2 (15d-PGJ_2) (**Fig. B4**). Nuclear accumulation of HSF1 and induction of Hsp70 and Hsp40, as well as of HSE-dependent luciferase reporter, have been observed when human colon cancer cells were exposed to 4-hydroxy-2-nonenal, and siRNA-mediated

Figure B4

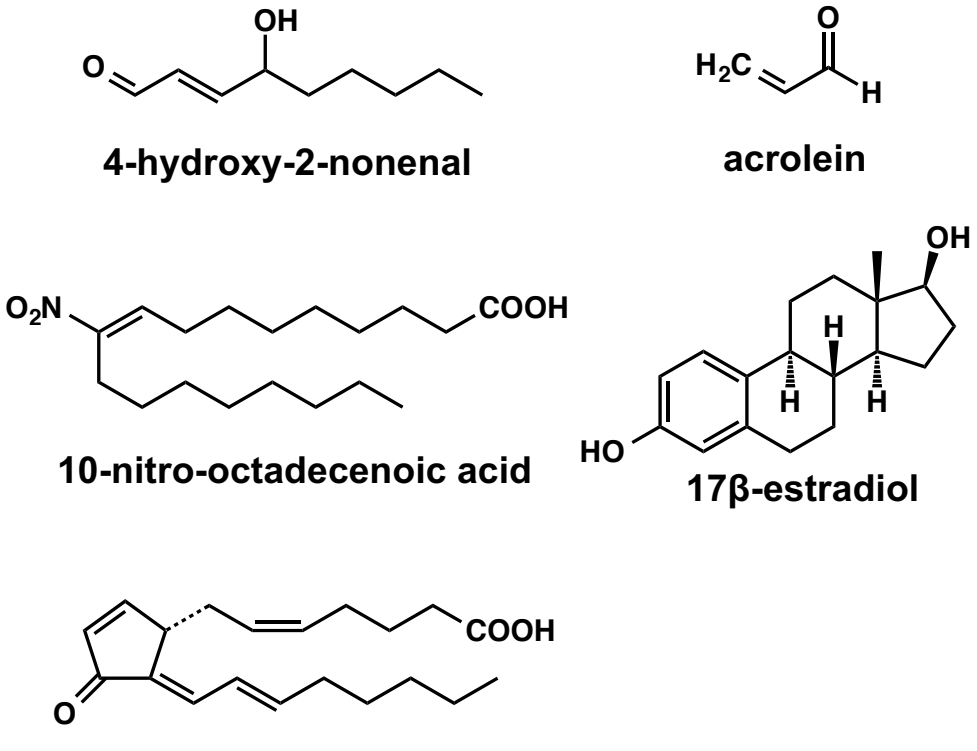

Figure B4. Endogenous small-molecule activators of HSF1.

silencing of HSF1 abolished this induction (Jacobs and Marnett, 2007). Treatment of human endothelial cells with 10-nitro-octadecenoic (nitro-oleic) acid, a nitrated product of oleic acid with cytoprotective activities, led to activation of the heat shock response (Kansanen et al., 2009). Induction of Hsp70 and Hsp40 also occurred when A549 human lung cancer cells were exposed to the electrophilic lipid peroxidation product acrolein (Thompson and Burcham, 2008). The DNA binding activity of HSF1 was increased and the expression of Hsp70 was robustly upregulated by 15d-PGJ_2 in the heart of male Wistar rats undergoing ischemia-reperfusion injury (Zingarelli et al., 2004). In addition, high concentrations of 17 β-estradiol have been shown to activate HSF1 and induce Hsp70 (Knowlton and Sun, 2001, Hamilton et al., 2004). Unlike the other endogenous HSF1 activators mentioned above, 17 β-estradiol is not electrophilic; however, it can be metabolically converted to the electrophilic quinone derivatives 2-hydroxy- and 4-hydroxy-estradiol (Zhu and Conney, 1998), which might be the ultimate inducers.

A striking common feature of these endogenous inducers is their electrophilicity. The role of this chemical property for inducer activity has been tested by use of structurally-related analogues. In contrast to the active electrophilic cyclopentenone 15d-PGJ_2, which contain an α,β-unsaturated carbonyl moiety in its cyclopentane ring, other arachidonic acid metabolites which lack this electrophilic functional group, are inactive (Rossi et al., 1996, Elia et al., 1999). Similarly, the non-electrophilic oleic acid is devoid of inducer activity, in sharp contrast to its electrophilic counterpart, nitro-oleic acid (Kansanen et al., 2009). The importance of electrophilicity for inducer activity strongly suggests that

the primary protein targets contain reactive nucleophilic amino acids which act as sensors for inducers.

As Hsp90 and Hsp70 are the major negative regulators of HSF1, it is possible that inducer binding to one or both of them interferes with their ability to form a complex with HSF1. Indeed, covalent modification at cysteine 572 of Hsp90 by 4-hydroxy-2-nonenal has been detected in purified recombinant human Hsp90 (Carbone et al., 2005). Endogenous Hsp90 and Hsp70 were also modified upon exposure of cells to 4-hydroxy-2-nonenal (Jacobs and Marnett, 2007, Jacobs and Marnett, 2010), and to its azido- and alkynyl-tagged derivatives, as identified by click chemistry and *ex vivo* biotinylation (Vila et al., 2008). By use of noncovalent affinity capture with a biotinyl-geldanamycin probe, both Hsp90α and Hsp90β were isolated from human colorectal cancer cells, and histidine adducts that were endogenously formed by treatment with 4-hydroxy-2-nonenal were detected (Connor et al., 2011). Furthermore, modifications in Hsp90 and Hsp70 by 4-hydroxy-2-nonenal have been reported to occur in rat liver in a model of alcoholic liver disease (Smathers et al., 2011). The same compound was also found to disrupt the interaction of ectopically expressed c-Myc-tagged Hsp70 with HSF1 and induce the HSR (Jacobs and Marnett, 2007). Interestingly, the yeast Hsp90 does not contain any cysteine residues, and C264 and C303 of the Hsp70 chaperone Ssa1 serve as the sensors for electrophilic HSF1 activators, as demonstrated by mutagenesis analysis and click chemistry approach after treatment with an alkynyl-tagged derivative of 4-hydroxy-2-nonenal (Wang et al., 2012). Together, these findings strongly suggest that modifications of the

negative regulators Hsp90 and/or Hsp70 may cause release of HSF1 and activation of HSF1-dependent transcription.

In addition to endogenous electrophiles, the HSF1-mediated HSR is directly activated by the oxidant hydrogen peroxide (H_2O_2). Interestingly, in this case, HSF1 itself is the protein sensor as activation of murine HSF1 by H_2O_2 is dependent on cysteine 35 and cysteine 105, which form a disulfide bridge (Ahn and Thiele, 2003). The corresponding pair of cysteines (i.e., cysteine 36 and cysteine 103) in human HSF1 form an intermolecular disulfide bridge, promoting HSF1 trimerization and binding to the HSE (Lu et al., 2008). A subsequent study has shown that an intermolecular interaction between the aromatic residues tryptophan 37 and phenylalanine 104 supports the approach of cysteine 36 and cysteine 103 (Lu et al., 2009). In contrast, an intramolecular disulfide bridge formation (in which cysteine 153, cysteine 373 and cysteine 378 participate) inhibits trimerization and DNA binding of HSF1 (Lu et al., 2008).

The signalling molecule nitric oxide has been reported to activate HSF1 and induce Hsp70 in vascular smooth muscle cells (Xu et al., 1997). Interestingly, *S*-nitrosation at cysteine 597 of human Hsp90α inhibits the ATPase activity of the chaperone(Martinez-Ruiz et al., 2005), and substituting cysteine 597 with *S*-nitrosation-mimicking residues, such as asparagine and aspartic acid, shifts the conformational equilibrium of the chaperone, decreasing its activity (Retzlaff et al., 2009). It is therefore possible that HSF1 activation by nitric oxide is due to inactivation of Hsp90.

Activation of HSF1 can also be stimulated by electrophilic and reactive oxygen species which are formed during physiological and pathophysiological processes. Thus, HSF1 is activated in atherosclerotic lesions, and cytokine stimulation and mechanical stretching of smooth muscle cells result in HSF1 hyperphosphorylation, nuclear translocation, and enhanced Hsp70 expression (Metzler et al., 2003). In addition, HSF1 activation has been implicated in the production of plasminogen activator inhibitor-1 after stimulation by glycated low density lipoproteins as well as by oxidized very low density lipoproteins in cultured vascular endothelial cells (Zhao and Shen, 2007, Zhao et al., 2008). Subsequent studies have shown that in this case, activation of HSF1 is mediated by induction of NADPH oxidase (Zhao et al., 2009, Sangle et al., 2010, Zhao et al., 2011).

1.B.4.2 *Phytochemicals*

A screen of bioactive small molecules in the human HeLa cell line hsp70.1pr-luc (stably transfected with a luciferase-encoding construct under the transcriptional control of the *hsp70* promoter) identified the phytochemical celastrol as inducer of the HSR (Westerheide et al., 2004b). Celastrol is a quinone methide triterpenoid (**Fig. B5**) found in the Chinese plant *Tripterygium wilfordii*. In addition to the cervical cancer HeLa reporter cell line, celastrol activates the *hsp70* promoter reporter in the breast cancer cell lines MCF7 and BT474, the nonsmall cell lung carcinoma cell line H157, and the neuroblastoma cell line SH-SY5Y), and importantly, the magnitude of activation is comparable to that induced by heat shock (42 °C) (Westerheide et al., 2004b). In agreement, exposure to celastrol is protective against lethal heat stress, and to a similar extent as a 42

Figure B5

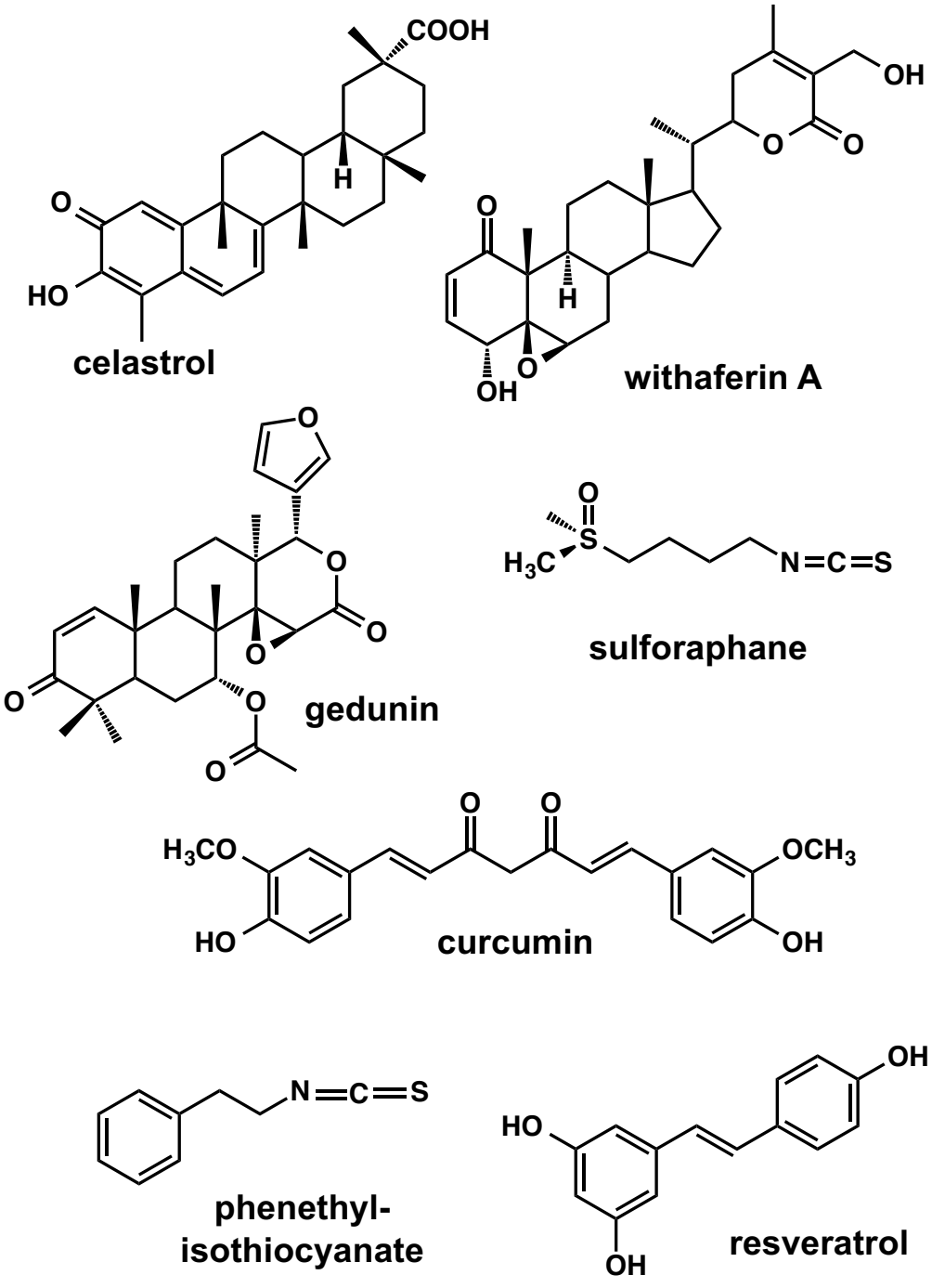

Figure B5. Phytochemical activators of HSF1.

°C heat shock. Treatment with celastrol leads to hyperphosphorylation of HSF1, enhanced binding of HSF1 to the HSE, and transcriptional activation of endogenous heat shock genes (Westerheide et al., 2004b). Transcriptional profiling and biochemical studies suggest that inhibition of Hsp90 by celastrol may be the initial event that triggers dissociation of HSF1 from the protein complex (Hieronymus et al., 2006, Zhang et al., 2008, Chadli et al., 2010, Matts et al., 2011). This possibility is further supported by mechanistic studies showing that celastrol reacts with Hsp90 and inhibits the ATPase activity of the chaperone without affecting ATP binding (Zhang et al., 2009b).

The tetranortriterpenoid gedunin (**Fig. B5**) from the Indian neem tree *Azadirachta indica* is another activator of HSF1. Compared to celastrol, gedunin is less potent, but appears to use similar mechanisms by which it activates HSF1, i.e. inhibition of the function of the negative regulator Hsp90(Hieronymus et al., 2006, Matts et al., 2011, Brandt et al., 2008). The use of a high content screening platform, an image-based, multiparametric assay which monitors the formation of HSF1/Hsp70 stress granules in heat-shocked HeLa cells (Au et al., 2008), identified four compounds closely related to gedunin, i.e., deoxygedunin, deacetoxy-7-oxogedunin, deacetylgedunin, and sappanone A, which were subsequently confirmed to activate HSF1 and induce Hsp70 in an HSF-dependent manner(Zhang et al., 2009a).

Withaferin A (**Fig. B5**), a withanolide found in the Indian plant *Withania somnifera*, was identified in a screen of a library of more than 80,000 natural and synthetic compounds using a reporter cell line which expresses enhanced green

fluorescent protein (EGFP) under the transcriptional control of a minimal consensus HSE-containing promoter(Santagata et al., 2012). Like celastrol and gedunin, withaferin A also inhibits the function of Hsp90, and this inhibition may be responsible for activation of HSF1 (Yu et al., 2010, Grover et al., 2011). The same high-throughput screen confirmed that celastrol, withaferin A, gedunin are all inducers of the HSR, and identified several other natural products, such as the limonoids anthothecol, cedrelone, and the gedunin derivative 7-desacetoxy-6,7-dehydrogedunin, as well as a fungal product, the macrocyclic lactone dehydrocurvularin among the active compounds (Santagata et al., 2012). Notably, all of these compounds have an α,β-unsaturated carbonyl functional group, emphasizing the importance of electrophilicity for inducer activity.

Curcumin [1,7-bis(4-hydroxy 3-methoxy phenyl)-1,6-heptadiene-3,5-dione, diferuloylmethane, **Fig. B5**], a polyphenol from the East Indian plant *Curcuma longa*, has been shown to induce heat shock proteins in numerous cell culture and animal models (Kato et al., 1998, Chen et al., 2004, Shen et al., 2007, Kanitkar and Bhonde, 2008, Khan and Heikkila, 2011). The observed disruption of the binding of the Hsp90-p23 complex to its client protein p210 BCR/ABL, and the consequent degradation of the kinase in chronic myelogenous leukemia cells upon exposure to curcumin (Wu et al., 2006) suggests that, for this compound too, induction of heat shock proteins could be a consequence of inhibition of Hsp90 function. Notably, curcumin has been present in the human diet for centuries, and there is a wealth of information regarding its safety and efficacy in both animals and humans (Surh and Chun, 2007, Hatcher et al., 2008, Lao et al., 2006). To date, there have been 91 different clinical trials registered evaluating

this polyphenol in a number of conditions, including mild cognitive impairment, Alzheimer's disease, multiple myeloma, pancreatic cancer, colorectal cancer, and myelodysplastic syndrome (www.clinicaltrials.gov).

Sulforaphane [1-isothiocyanato-(4*R*)-(methylsulfinyl)butane, **Fig. B5**] is an isothiocyante which is formed from a glucosinolate precursor (glucoraphanin) upon plant tissue injury. Cruciferous vegetables, such as broccoli (*Brassica oleracea*), are rich dietary sources of this phytochemical. Nuclear accumulation of HSF1 and induction of heat shock proteins by sulforaphane has been demonstrated in several cell culture models, including human cell lines, as well as in animals after a single oral dose of the isothiocyanate (Hu et al., 2006a, Gan et al., 2010, Sharma et al., 2010). Another isothiocyanate, phenethyl isothiocyanate which occurs in watercress, has also been shown to induce expression of heat shock proteins in cultured cells and animals(Hu et al., 2006b, Moon et al., 2011). Again, the available experimental evidence points to Hsp90 as the target of sulforaphane which mediates HSF1 activation: (i) co-treatment with sulforaphane enhances the anti-tumor effect of the Hsp90 inhibitor 17-allylamino 17-demethoxygeldanamycin (17-AAG); (ii) sulforaphane disrupts the interaction of Hsp90 with its co-chaperone Cdc37; (iii) synergistically with 17-AAG, the isothiocyanate downregulates several Hsp90 client proteins, such as mutant p53, Raf-1, and Cdk4 (Li et al., 2011), (iv) Hsp90 is covalently modified by a sulfoxythiocarbamate derivative of sulforaphane both *in vitro* and in cells (Zhang et al., 2011, Zhang et al., 2014), and (v) the ability of sulforaphane to downregulate the activity of histone deacetylase (HDAC) (Myzak et al., 2004, Myzak et al., 2006b, Myzak et al., 2006a, Pledgie-Tracy et al., 2007, Gibbs et al.,

2009) may further inhibit the activity of Hsp90 through altering acetylation of the chaperone. Indeed, inhibition or knock-down of HDAC6 leads to acetylation of Hsp90 and disruption of its chaperone function (Bali et al., 2005), and treatment with sulforaphane downregulates the activity of HDAC6, resulting in hyperacetylation of Hsp90 (Gibbs et al., 2009).

In contrast to the electrophilic phytochemicals, the stilbene resveratrol (**Fig. B5**) appears to activate HSF1 by promoting the persistent DNA binding of the transcription factor and suppressing the attenuation phase of the HSR (Westerheide et al., 2009). In this case, the phytochemical functions by activating the predominantly nuclear NAD^+-dependent deacetylase sirtuin-1 (SIRT1) and maintaining HSF1 in a deacetylated, DNA-binding competent state. Resveratrol directly activates SIRT1 through an allosteric mechanism resulting in the lowering of the K_m for both the acetylated protein substrate and for the NAD^+ cofactor (Howitz et al., 2003). Most small-molecule SIRT1 activators known to date are planar compounds comprised of multiple phenyl rings bearing hydroxyl groups (Howitz et al., 2003, Hubbard and Sinclair, 2014). Whether other phytochemicals which activate SIRT1, such as the flavonoid quercetin and the chalcone butein, have the same effect on HSF1 is presently unknown.

1.B.4.3 *Synthetic compounds*

The possibility of developing small molecule activators of the HSR as pharmacological agents for protection against human diseases, especially protein conformational diseases, has led to the development of several high-

throughput screening strategies. Neef et al. reported the development of a humanized yeast-based high-throughput screen, which is insensitive to proteotoxic stress and Hsp90 inhibition, and identified two potent small-molecule activators of human HSF1 within a chemical library of over 10,000 compounds (Neef et al., 2010). These HSF1 activators (named HSF1A and HSF1C) are benzyl pyrazole derivatives (**Fig. B6**). The more potent compound, HSF1A, was then shown to activate HSF1 and induce Hsp70 in wild-type, but not HSF1-deficient mouse embryonic fibroblast, as well as in HeLa cells. In contrast to the electrophilic HSF1 activators, pre-incubation with DTT had no effect on the inducer activity of HSF1A. HSF1A has been found to inhibit T-complex-protein-1 (TCP1)-ring-complex/ chaperonin-containing TCP1 (TRiC/CCT)-HSF1-binding (Neef et al., 2014).

Calamini et al. have developed a mammalian cell-based high-throughput screen (Calamini et al., 2012). It measures the activation of the HSR by cell-permeable small molecules in HeLa cells stably transfected with a luciferase reporter gene under the transcriptional control of the proximal human *HSP70.1* promoter sequence. Approximately 900,000 compounds were screened, and ~200 small molecule activators of the HSR were found. Electrophilicity is a common feature among many, although not all, active compounds. A cyclohexanone derivative (named compound A1) containing the electrophilic α,β-unsaturated carbonyl groups is closely related to bis(benzylidene)acetone and bis(2-hydroxybenzylidene)acetone (**Fig. B6**), two structurally similar Hsp70 inducers, which however differ substantially in inducer potency (Zhang et al., 2011a). Inducer potency correlates with sulfhydryl reactivity: compared to the

Figure B6

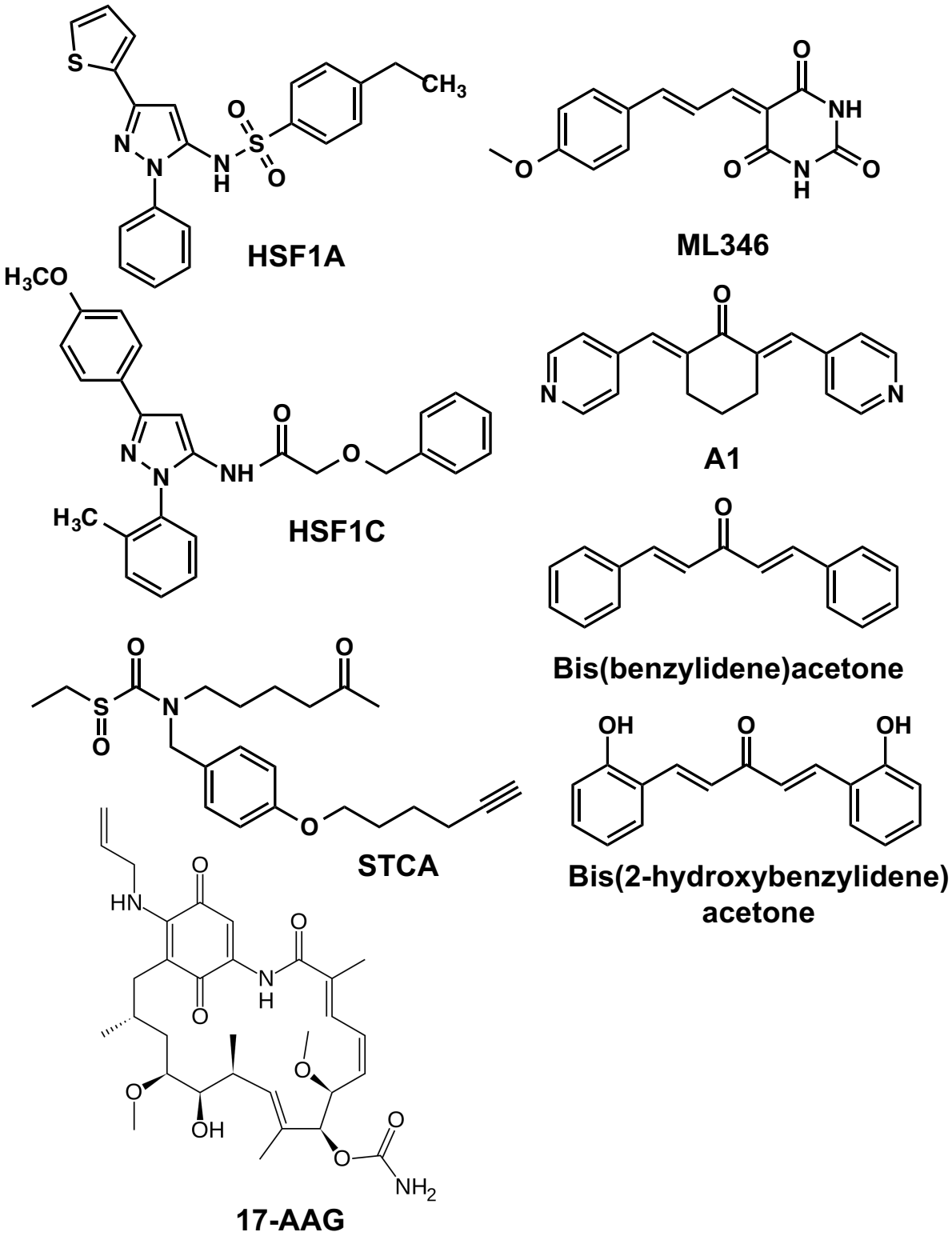

Figure B6. Synthetic small-molecule activators of HSF1.

hydroxylated analogue, bis(2-hydroxybenzylidene)acetone, the parent compound bis(benzylidene)acetone reacts more slowly with the sulfhydryl groups of glutathione and DTT (Dinkova-Kostova et al., 2001), and has lower potency in inducing Hsp70 (Zhang et al., 2011).

The mildly-electrophilic sulfoxythiocarbamate analogues of the isothiocynate sulforaphane constitute another class of synthetic HSF1 activators. Sulfoxythiocarbamate alkyne (STCA) (**Fig. B6**), which forms stable adducts with sulfhydryl groups (Ahn et al., 2010), reacts with C412, C564, and C589/590 of recombinant Hsp90, and activates HSF1-mediated transcription of a luciferase reporter as well as of the endogenous Hsp70 in mammalian cells of many different types, including MEFs, HeLa, and MCF-7 cells (Zhang et al., 2011, Zhang et al., 2014). Pyrrolidinedithiocarbamate and 1,2-dithiole-3-thione are two other activators of HSF1-mediated induction of Hsp70 (Stuhlmeier, 2000, Kwak et al., 2004), which have the ability to react with sulfhydryl groups (Zhang et al., 1996). Activation of HSF1 and induction of the HSR has also been reported to occur upon exposure of cells to pro-electrophilic oxidizable diphenols; in this case, the corresponding oxidized electrophilic metabolites are the ultimate inducers (Satoh et al., 2011).

Notably, global transcriptional profiling and protein expression/proteomics analyses have consistently shown that, in addition to activating HSF1, most of the inducers discussed above, both naturally occurring as well as synthetic, also activate transcription factor nuclear factor-erythroid 2 p45-related factor 2 (NRF2) which controls the gene expression of numerous cytoprotective antioxidant, drug-

metabolizing, anti-inflammatory, and metabolic proteins, providing an interface between redox and intermediary metabolism (Hayes and Dinkova-Kostova). In MEFs, induction of Hsp70 is dependent on HSF1, but independent of NRF2; conversely, transcriptional upregulation of the NRF2-dependnet enzyme NQO1 occurs in the absence of HSF1, but requires functional NRF2 (Zhang et al., 2011). It is thus very likely that together, both HSF1- and NRF2-dependent responses mediate the overall cytoprotective effects (see below) of these compounds.

1.B.5 HSF1 activates cytoprotective responses

Transcriptional activation of HSF1 by heat shock results in enhanced expression of a large number of genes encoding proteins with versatile cytoprotective functions. Global transcriptional profiling, differential display, and proteomic approaches have revealed that, in different organisms, approximately 50–200 genes are induced (Eisen et al, 1998, Hasch et al. 2000). These include the classical molecular chaperones that prevent unspecific aggregation of non-native or partially misfolded proteins, proteolytic proteins that can eliminate or recycle irreversibly-damaged proteins which cannot be refolded by the chaperones, RNA- and DNA-modifying enzymes which participate in DNA damage repair, proteins involved in sustaining cellular structures such as the cytoskeleton and membranes, and proteins which participate in transport and detoxification. In addition, heat shock upregulates a number of metabolic enzymes ([e.g., ACAT2 (acetyl-CoA acetyltransferase), ALAS1 (aminolevulinate synthase), ChGn (chondroitin β-1,4-N-acetylgalactosaminyltransferase)] that are

needed to reorganize and maintain the energy supply of the cell. Induction of other transcription factors, kinases and phosphatases [e.g., RHOH (Ras homolog), PTPG1 (tyrosine phosphatase), RGS2 (regulator of G-protein signaling), IER5 (regulator of immediate early response)] also occurs following heat shock, and may further activate other stress response pathways, thus amplifying the initial signal.

Notably, not all genes are induced at the same time and with the same duration: some, such as those responsible for the correct protein folding, are immediate responders (within minutes), whereas others, such as those involved in DNA damage repair and cell metabolism, are somewhat slower (within hours) (Richter et al., 2010). Overall, induction of the HSR provides broad protection against stress of various different types, including and extending beyond heat shock. Furthermore, a recent study in *C. elegans* has also shown that HSF1-mediated activation of Hsp90 in response to an imbalance in proteostasis in one tissue functions in a non-autonomous fashion to initiate a protective response in adjacent tissues and to restore the balance within the whole organism (van Oosten-Hawle et al., 2013).

1.B.6 Crosstalk between HSF1- and NRF2-regulated cytoprotective responses

A number of studies suggest the existence of crosstalk between NRF2- and HSF1-regulated cytoprotective responses (reviewed in Dayalan Naidu et al., 2015). The participation of both transcription factors has been implicated in the

regulation of gene expression of the rodent heme oxygenase 1 (HO-1, also known as Hsp32) (Prestera et al., 1995, Maines and Ewing, 1996), the murine and zebrafish Hsp70 (Almeida et al., 2010), and in the autophagy cargo protein sequestosome 1 (p62/SQSTM1) (Komatsu et al., 2010, Jain et al., 2010, Lau et al., 2010, Copple et al., 2010, Zhang et al., 2008). HSF1-mediated induction of p62 may activate NRF2 as p62, especially upon phosphorylation, can displace NRF2 from KEAP1 and activate it (Komatsu et al., 2010, Ichimura et al., 2013), leading to NRF2-dependent upregulation of p62 expression. In addition, both HSF1 and NRF2 regulate the expression of activating transcription factor 3 (ATF3), a member of the mammalian activation transcription factor/cAMP responsive element-binding (CREB) protein family of transcription factors (Takii et al., 2010, Kim et al., 2010), and thus HSF1 and NRF2 have the ability to modulate gene expression indirectly. Finally, HSF1 and NRF2 affect the redox balance of the cell, promoting a more reduced environment. NRF2 controls the gene expression of both subunits (GCLC and GCLM) of γ-glutamylcysteine ligase, the enzyme that catalyzes the rate-limiting step in the biosynthesis of glutathione (Wild and Mulcahy, 2000). In addition, the levels of glucose-6-phosphate dehydrogenase (G6PDH), the rate-limiting enzyme in the pentose phosphate pathway, which is involved in the regeneration of NADPH that in turn is used by glutathione reductase to reduce oxidised glutathione (GSSG) to reduced glutathione (GSH), are increased by both activation of NRF2 (Mitsuishi et al., 2012, Lu and Wan, 2008) and upregulation of Hsp25/27 (Rajasekaran et al., 2007). Conversely, the enzyme activity of G6PDH and the GSH : GSSG ratio are decreased in the heart of HSF1-deficient mice compared to their wild-type counterparts (Yan et al., 2002).

Interestingly, methionine deprivation in HEK293 cells was recently shown to increase the expression of Hsp70 in an NRF2-dependent manner, but independently of HSF1 (Hensen et al., 2013a). Remarkably, in cells expressing an HSF1 mutant in which lysine 80 in the DNA binding domain is substituted with glutamine (HSF1 K80Q), thus impairing DNA binding, heat shock caused a delayed upregulation of Hsp70 and HO-1 at 24 h, when the primary transcriptional response to the heat shock in HSF1 wild-type expressing cells was largely attenuated; this delayed secondary response was found to be mediated by NRF2 (Hensen et al., 2013b), suggesting the possibility that upregulation of the NRF2-dependent antioxidant response may be partially compensating for HSF1 dysfunction. In agreement, the basal levels of HO-1 are higher (Zhang et al., 2011) and its induction is dramatically enhanced, from 12- to 130-fold (Calamini et al., 2012), in HSF1-knockout cells compared to their wild-type counterparts.

1.B.7 HSF1 and neurodegenerative diseases

Imbalances in protein homeostasis (termed proteostasis), oxidative stress and chronic inflammation are common features of many neurodegenerative diseases. Attenuation of HSF1 during ageing has been proposed to be an "upstream" event in the series of processes leading to synaptic dysfunction and cognitive impairment (Perez et al., 2014). Prominent among the protein conformational diseases are those which arise as a result of accumulation of misfolded polyglutamine expansion-containing proteins, such as the androgen receptor (AR), huntingtin (HTT), tau, α-synuclein, and Cu/Zn superoxide

dismutase (SOD1). These proteins adopt alternate folded states that have the propensity to self-associate and aggregate, leading to cytotoxicity.

Genetic or pharmacological induction of the HSR is an attractive strategy for restoring the cellular proteostasis as it results in enhanced expression of chaperones that are involved in ensuring the correct folding of proteins and in facilitating the degradation of abnormal proteins. Indeed, induction of the HSR, and especially Hsp70, is protective in numerous cell culture and animals models of protein conformational diseases (Morimoto, 2011). A recent study has reported an association between the expression levels of HSF1 and the accumulation of the pathogenic form of the AR in a mouse model of spinal and bulbar muscular atrophy, an adult-onset motor neuron disease caused by the expansion of a polyglutamine repeat in the AR (Kondo et al., 2013). In comparison with HSF1 wild-type animals expressing the human AR with 97 polyglutamine repeats (AR-97Q), their heterozygous HSF1-knockout counterparts accumulate high AR levels in both neuronal and non-neuronal tissues, and display exacerbated neuromuscular phenotype. Importantly, lentiviral-mediated delivery of HSF1 into the brain increases HSF1 expression and lowers the pathogenic AR accumulation and neuronal brain atrophy.

In *Drosophila* models of Huntington's and other polyglutamine protein conformational diseases, polyglutamine toxicity is synergistically suppressed by co-expression of Hsp70 and Hsp40 (Warrick et al., 1999, Kazemi-Esfarjani and Benzer, 2000, Chan et al., 2000). Protection can be also achieved by pharmacological induction of the HSR. Thus, in cells ectopically expressing a

fusion protein of polyglutamine and the yellow fluorescent protein (Q57-YFP), treatment with the HSF1 activator celastrol prevented the aggregation of the fusion protein and the associated cytotoxicity (Zhang and Sarge, 2007). Similarly, in a yeast model, curcumin inhibited the formation of Q72-GFP protein aggregates, and furthermore, this polyphenol was able to disrupt pre-formed Q72-GFP aggregates (Verma et al., 2012). Deoxygedunin, deacetoxy-7-oxogedunin, and deacetylgedunin, were all shown to activate HSF1, induce Hsp70, and improve cell survival in HeLa cells transiently transfected with a polyglutamine-expanded toxic isoform (Q103) of huntingtin as well as in an MG-132-induced protein misfolding neuronal cell culture model (Zhang et al., 2009a).

The synthetic cyclohexanone derivative compound A1 and a barbituric acid scaffold-containing compound, named ML346 (**Fig. B5**) (Calamini et al., 2010) were shown to be protective in two models of Huntington's disease. Thus, in PC12 cells conditionally expressing human huntingtin exon 1 containing an expansion of 74 glutamines fused to green fluorescent protein (HTTQ74-GFP), compound A1 and ML346 reduced the formation of HTTQ74-GFP protein aggregates, without altering the amounts of HTTQ74-GFP protein. Furthermore, in *C. elegans* expressing expanded polyglutamines (35 glutamines fused to yellow fluorescent protein, or polyQ35-YFP), the same compounds suppressed polyQ35-YFP aggregation and prevented polyQ35-mediated toxicity, almost completely restoring motility to that of wild-type animals. Similarly, the benzyl pyrazole HSF1A induced Hsp70 and reduced protein aggregation and cytotoxicity in HTTQ74-GFP expressing PC12 cells (Neef et al., 2010).

Using two mouse models of Huntington's disease, R6/2 exon 1 transgenic (Mangiarini et al., 1996) and *HdhQ150*-knockin (Lin et al., 2001, Woodman et al., 2007) mice, Labbadia et al. (Labbadia et al., 2011) reported that pharmacological activation of HSF1 with a brain-permeable Hsp90 inhibitor was beneficial and led to a significant phenotypic improvement. However the beneficial effects are transient, because alterations in chromatin architecture during disease progression leads to reduced binding of HSF1 to DNA, and impairing the HSR. It is tempting to speculate that similar chromatin alterations could be responsible, at least in part, for the observed decline in the HSR with ageing.

Curiously, a recent study has shown that although the HSR is triggered by genetic (overexpression) or pharmacological HSF1 activation, this results in a decrease, and not an increase, in the concentration threshold leading to protein aggregation of mutant polyglutamine-expanded fragments of the huntingtin protein (Bersuker et al., 2013). This finding suggests that rather than promoting refolding of the mutant protein, activation of the HSR may mediate its degradation or clearance, resulting in decreased aggregate formation or increased aggregate turnover. Whether this is indeed the case for mutant huntingtin (and possibly other polyglutamine-expanded mutant proteins) remains to be established.

In rodent models of Alzheimer's disease, genetic or pharmacological (by using the inducers celastrol or curcumin) upregulation of HSF1 is protective against the amyloid-β-associated pathologies, improving memory, learning, and psychomotor activity (Allison et al., 2001, Paris et al., 2010, Pierce et al., 2013). By inhibiting Hsp90, 17-(allylamino)geldanamycin (17-AAG) activates HSF1,

inducing transcription of heat shock and synaptic proteins in primary neurons, and attenuates amyloid-β-mediated synaptic toxicity as well as memory loss in mice (Chen et al., 2014). In a mouse model of Parkinson's disease, celastrol protected against the neurotoxicity of 1-methyl-4-phenyl-1,2,3,6-tetrahydropyridine (MPTP); the same study also found protection by celastrol against 3-nitropropionic acid-mediated neurotoxicity (Cleren et al., 2005). The protective effects of curcumin have been demonstrated in numerous models of both Alzheimer's disease and Parkinson's disease, and these, along with the limitations in translating the findings to human populations, have been extensively reviewed (Darvesh et al., 2012, Chin et al., 2013, Lee et al., 2013). The experimental evidence is further supported by epidemiological studies, such as the Indo-US Cross National Dementia Study, which have linked high curcumin consumption with lower prevalence of Alzheimer's disease and other types of dementia (Chandra et al., 1998). Although curcumin is able to cross the blood-brain barrier, it has low bioavailability; to overcome this limitation nanotechnology-based delivery systems are being developed. Thus, curcumin-encapsulated nanoparticles have recently been generated and shown to reverse learning and memory impairments in an amyloid-β-induced rat model of Alzheimer's disease (Tiwari et al., 2014).

Mutations in the Cu/Zn superoxide dismutase gene (SOD1) are responsible for 20% of the familial forms of amyotrophic lateral sclerosis (ALS). *In vitro*, the small heat shock proteins αB-crystallin and Hsp27 suppress SOD1 aggregation (Yerbury et al., 2013). In the G93A SOD1 transgenic mouse model of ALS, neuronal cell death, weight loss, and motor performance were all

improved by celastrol, and furthermore, disease onset was delayed (Kiaei et al., 2005). In the same mouse model, resveratrol decreased the acetylation of HSF1 and increased the levels of Hsp25 and Hsp70 in the spinal cord, and delayed the onset of disease and extended survival (Han et al., 2012). In the SOD1 H46R/H48Q transgenic ALS mice expressing mutant SOD1, over-expression of human HSF1 upregulated the expression of Hsp70 and αB-crystallin in spinal cord, and increased the solubility of mutant SOD1 (Lin et al., 2013). Furthermore, HSF1 over-expression was protective against weight loss, and led to a delay in disease onset and increased survival.

Of note, it was recently reported that HSF1 is a critical factor for neuronal cell survival and, furthermore, protects neurons against degeneration caused by non-proteotoxic as well as proteotoxic stress independently of its ability to trimerize and induce transcription of genes encoding heat shock proteins (Verma et al., 2014). Whilst the detailed mechanism remains to be established, it is interesting that the broad-spectrum HDAC inhibitor trichostatin A abolishes HSF1-mediated protection, whereas knockdown of HSF1 abrogates neuroptotection by SIRT1, suggesting that HSF1 and SIRT1 cooperate in neuronal protection. Another recent study has uncovered a role for HSF1 in increasing fetal cortical tolerance to prenatal environmental stressors, such as alcohol, maternal seizure, and methylmercury, and thus protecting against neuropsychiatric diseases (Hashimoto-Torii et al., 2014).

1.B.8 HSF1 and cardiovascular disease

The role of HSF1 in cardiovascular disease is both duration- and context-dependent. Whereas transient activation of HSF1 is beneficial in ischemic heart disease, constitutive excessive production of heat shock proteins, especially small heat shock proteins, and the associated redox imbalance may also be a causative factor for certain heart conditions, such as cardiomyopathy. HSF1-mediated induction of the HSR has been implicated in the protective effects of 17β-estradiol against ischemia/reperfusion injury (Knowlton and Korzick, 2014). Activation of HSF1 is observed after ischemia/reperfusion (Nishizawa et al., 1996). This activation, and the subsequent induction of Hsp70 and Hsp90, is mediated by reactive oxygen species (Nishizawa et al., 1999). Elevated heat shock protein levels in the heart are associated with reduction in infarct size and enhanced recovery after ischemia (Currie et al., 1988, Currie and Karmazyn, 1990, Currie et al., 1993, Donnelly et al., 1992, Karmazyn et al., 1990, Hutter et al., 1994, Locke et al., 1995). Part of the protective effect of HSF1 involves activation of Akt and inactivation of Jun N-terminal kinase and caspase 3 (Zou et al., 2003). Hsp70 itself has cardioprotective effects against myocardial dysfunction after ischemia/reperfusion by improving the mitochondrial function and preventing apoptosis (Marber et al., 1995, Trost et al., 1998, Suzuki et al., 2002). Cardiomyocyte apoptosis triggered by ischemia/reperfusion is also suppressed by overexpression of Ca^{2+}/calmodulin-dependent protein kinase (CaMK)II-deltaB which leads to phosphorylation of HSF1 and induction of Hsp70 (Peng et al., 2010). HSF1 and heat shock proteins are important for stabilization of the restored sinus rhythm after mitral valve surgery (Cao et al., 2011). The

cardioprotective effects of HSF1 are not solely due to induction of heat shock proteins, and HSF1 also protects the heart against ischemia as well as pressure overload by its ability to promote angiogenesis (Zou et al., 2011, Kubo et al., 2012). Overexpression of HSF1 attenuates cardiomyocyte cell death via inhibiting TNFα-mediated NFκB activation (Wu et al., 2013). Interestingly, transplantation of stem cells which had been subjected to heat shock was recently shown to have beneficial effects after myocardial infarction, attenuating cell death and fibrosis in the ischemic heart (Feng et al., 2014).

It is well established that the ability to mount the HSR decreases with age (Liu et al., 1989, Choi et al., 1990, Fargnoli et al., 1990, Blake et al., 1991, Heydari et al., 1993, Nitta et al., 1994). In comparison with hearts from adult mice, HSF1 activation and Hsp70 expression are reduced following heat stress in hearts from aged animals, even though the myocardial levels of the HSF1 protein are similar between aged and adult animals (Locke and Tanguay, 1996). A recent study has challenged these findings, and has shown that, compared to young mice, the protein levels of HSF1 in heart, but not in any other tissues, are dramatically reduced in old animals, although the HSF1 mRNA levels do not differ (Carnemolla et al. 2014). This is accompanied by lower levels of heat shock proteins, suggesting that if this is also the case in humans, the compromised expression of heat shock proteins in the heart may be a contributing factor for the cardiac amyloid deposits that are frequently observed in humans over 80 years old (Carnemolla et al., 2014, Dungu et al. 2012). Curiously, whereas the HSR decreased with age in hepatocytes from F344/Jcl rats, increased HSR was reported to occur in rats of the F344/DuCrj strain (Takahashi et al., 2002b), and

it is of interest that compared to F344/Jcl rats, F344/DuCrj animals have lower blood glucose levels and enhanced insulin secretion in an oral glucose tolerance test (Nagakura et al., 2001), suggesting a link between the HSR and glucose metabolism. Interestingly, following myocardial infarction, the induction of Hsp70 by heat stress is impaired in the failing heart, and it was found that the nuclear translocation of HSF1 was attenuated, whereas phosphorylation at Ser303 (Marunouchi et al., 2013b) and the amount of HSF1 bound to the Hsp90 chaperone complex were increased (Marunouchi et al., 2013a). Treatment with the Hsp90 inhibitor 17-AAG led to dissociation of HSF1 from Hsp90, induction of Hsp70, and preservation of cardiac function (Marunouchi et al., 2013a), suggesting the possibility of using Hsp90 inhibitors as therapeutic agents for heart failure following myocardial infarction.

The HSR also plays an important role in vascular health. In vascular smooth muscle cells, nitric oxide activates HSF1 and induces the expression of Hsp70 (Xu et al., 1997). In addition to heat shock proteins, exposure of endothelial cells to heat shock increases the expression of thrombomodulin (Conway et al., 1994). Thrombomodulin is expressed on the luminal surface of endothelial cells and forms a complex with thrombin, modifying its function to activate the anticoagulant protein C. Curiously, statins cause nitric oxide-dependent dissociation of HSF1 from Hsp90, nuclear translocation of HSF1, and binding to heat shock elements in the promoter of thrombomodulin (Fu et al., 2008, Uchiyama et al., 2007). These findings implicate HSF1 in the protective effects of statins in the vascular endothelium, beyond their cholesterol-lowering activity.

However, HSF1 activation and small heat shock protein induction can also have deleterious consequences for the cardiovascular system (Mehlen et al., 1995, Brewer et al., 2013). Paradoxically, the double knockout of *αB-crystallin* and *Hsp25* is protective against acute heart ischemia/reperfusion injury (Benjamin et al., 2007). Accumulation of Hsp27, but not Hsp70 or Hsp90, in the heart has been reported in humans with dilated cardiomyopathy and end-stage heart failure (Knowlton et al., 1998). An increase in the levels of Hsp27 also occurs during ischemic heart failure in rats (Tanonaka et al., 2003). In mice, overexpression of Hsp25 has been implicated in the cardiomyopathy and congestive heart failure caused by the chemotherapeutic agent doxorubicin: it was shown that doxorubicin treatment causes oxidative stress, activation of HSF1 and induction of Hsp25, followed by p53 activation and increase in the levels of the pro-apoptotic protein Bax, ultimately contributing to the death of cardiomyocytes in the failing heart (Vedam et al., 2010).

Transgenic mice overexpressing cardiac-specific loss-of-function mutant human αB-crystallin (hR120GCryAB) (Bova et al., 1999, Perng et al., 1999) have increased activity of glucose 6-phosphate dehydrogenase (G6PDH) and altered glutathione metabolism, and develop cardiomyopathy (Rajasekaran et al., 2007, Rajasekaran et al., 2008). Overexpression of R120G αB-crystallin triggers the HSR, inducing Hsp25 and antioxidant responses, including increased activity of G6PDH. In turn, the G6PDH-generated NADPH is used by glutathione reductase to reduce oxidised glutathione (GSSG), leading to increased levels of reduced glutathione (GSH). This is in agreement with earlier studies showing that the

levels of reactive oxygen species were decreased and GSH was elevated upon expression of the human and *Drosophila* Hsp27, and human αB-crystallin in murine fibroblasts (Mehlen et al., 1996), and that the presence of large aggregates of Hsp27 caused increase in the levels of G6PDH (Mehlen et al., 1997). Conversely, HSF1-knockout mice, which have lower cardiac expression of Hsp25 and αB-crystallin, have decreased GSH : GSSG ratio (Yan et al., 2002). The demonstration that G6PDH deficiency rescues the cardiomyopathic phenotype of the hR120GCryAB transgenic mouse established the central role of this enzyme in the disease pathogenesis (Rajasekaran et al., 2007). The development of a model of R120G αB-crystallin expression in *Drosophila* further revealed, that similar to G6PDH, mutants or RNAi-mediated knockdown of 6-phosphogluconate dehydrogenase, isocitrate dehydrogenase, and malic enzyme, the other major NADPH-generating enzymes, decreased the ratio of reduced to oxidized glutathione (GSH : GSSG) and suppressed the R120G αB-crystallin-mediated pathology, confirming the link with NADPH and glutathione metabolism (Xie et al., 2013).

Critically, increased NRF2 activity upregulates the gene expression of all of the four NADPH-generating enzymes (Thimmulappa et al., 2002, Lee et al., 2003, Wu et al., 2011, Mitsuishi et al., 2012, Lu and Wan, 2008) as well as of ɣ-glutamylcysteine ligase and glutathione reductase, the enzymes involved in the biosynthesis and regeneration of GSH (Wild and Mulcahy, 2000). Curiously, stable transfection of human Hsp27 in murine fibroblasts lowers the levels of iron (Arrigo et al., 2005). Although the underlying reasons for this are not understood at present, it is of interest that a microarray analysis of cardiac tissue of transgenic

mice overexpressing the human R120G αB-crystallin has revealed upregulation of expression of the iron-storage protein ferritin (Rajasekaran et al., 2008), another NRF2-dependent protein (Thimmulappa et al., 2002, Pietsch et al., 2003). It has been also shown that R120G αB-crystallin overexpression promotes formation of reactive oxygen species and sequesters KEAP1 in protein aggregates, thereby activating NRF2 (Rajasekaran et al., 2011). It is thus highly likely that activated NRF2 is ultimately responsible for the increased levels of NADPH and GSH. Together, these findings establish a tight connection between the HSR and the redox state of the cell, whereby increased expression of small heat shock proteins activates NRF2 and tilts the balance towards a more reduced state (i.e., increased GSH : GSSG ratio), a condition termed reductive stress (Rajasekaran et al., 2011, Brewer et al., 2013).

1.B.9 HSF1 and cancer

The HSR elicited by HSF1 in normal cells is a cytoprotective mechanism to ensure cell adaptation and survival during stressful conditions. On the other hand, in cancer, the HSF1 promotes malignant phenotypes as cells become addicted to the cytoprotective mechanisms it provides. Interestingly, using a chemical skin carcinogenesis mouse model, Dai and colleagues (Dai et al., 2007) found that HSF1-/- mice had a significantly lower tumour burden at 24 weeks compared to their wild-type counterparts; in addition, mice lacking HSF1 survived for a longer time. They also found that the lack of HSF1 in mice carrying the mutant p53 R172H allele were resistant to the tumourigenic effect of mutant p53 and survived much longer compared to the HSF1+/+ mice with the similar p53

background (Dai et al., 2007). When subjected to a variety of stresses, including the exposure to inhibitors of Hsp90, the activation of the heat shock response by HSF1 causes the elevation of the molecular chaperones such as Hsp27 (Schepers et al., 2005, Gorman et al., 2005) Hsp70 (Mosser et al., 2000, Garrido et al., 2003) which confer cytoprotection through their anti-apoptotic roles. On the other hand, small molecules that directly inhibit Hsp90 at its N-terminal ATP-binding pocket (Lesko et al., 2007, Nimmanapalli et al., 2001) (e.g. geldanamycin, 17-AAG, 17-DMAG) or possess the ability to modify its cysteine residues (Zhang et al., 2014) (e.g. the isothiocyanate analogue, sulfoxythiocarbamate alkyne) have been shown to cause apoptosis in cancer cells.

Inhibition of Hsp90 results in: 1) destabilisation and degradation of its oncogenic client proteins such as HER2 (Peng et al., 2005) and RAF1 (Schulte et al., 1995), 2) release of HSF1 from the Hsp90 protein complex, and 3) transcriptional activation of heat shock genes, and the subsequent elevation of the respective proteins. Cancer cells are intrinsically stressed, hence the requirement for the elevated expression and activation of HSF1 to provide them with anti-apoptotic proteins which are also molecular chaperones that help aid the stability of the mutated and aberrantly expressed oncogenic proteins within the cell that facilitates its survival. Many tumours have elevated expression of HSF1 and express high levels of Hsp90. As Hsp90 functions as a molecular chaperone to prevent protein misfolding and aggregation, cancer cells use the chaperone to stabilize multiple oncoproteins and prevent them from being degraded. Hence the elevation of Hsp90 by HSF1-mediated HSR allows for oncoprotein addiction. Thus, Hsp90, in recent years is actively being pursued as

a drug target in cancer. However, inhibition of Hsp90 often increases the stability of the HSF1 trimers and hence allows the heat shock response to continue. HSF1 is also a crucial transcriptional regulator of numerous genes that are essential for cell survival during conditions of stress by helping to coordinate fundamental cellular pathways such as glucose metabolism.

Recent research has allowed scientists to use HSF1 as a prognostic marker for breast cancer (Santagata et al., 2011). Increased nuclear HSF1 levels correlate with a poor prognosis in breast, colon and lung cancer (Mendillo et al., 2012, Dai et al., 2012). Furthermore, it is becoming increasingly clear that HSF1 is able to support malignant human cancers by orchestrating a transcriptional program beyond the HSR (Mendillo et al., 2012). It can be said that, HSF1, in cancer cells, is an essential promoter and regulator of oncogenesis. Hence, in addition to targeting Hsp90, inhibiting HSF1 could, in theory, improve the effectiveness of Hsp90 inhibitors. Several studies and clinical trials have shown synergistic effects when Hsp90 inhibitors are used in concert with conventional chemotherapeutic compounds that inhibit the transcriptional activation of HSF1. In a Phase I clinical trial, 17-AAG was given in combination with cisplatin and gemcitabine to patients with solid refractory tumours, and anti-tumour activity was observed (Hubbard et al., 2011).

Santagata and colleagues discovered that inhibition of protein translation in malignant cells reduced the activation of HSF1 (Santagata et al., 2013) providing an insight that a close relationship exists between the translational machinery and the transcriptional programme orchestrated by HSF1. The group

screened more than 300,000 compounds in search for HSF1 inhibitors, and successfully identified one compound, the naturally occurring rocaglamide A (Santagata et al., 2013). A series of natural and synthetic derivatives of rocaglamide A were then tested, and a very potent inhibitor of HSF1 was identified and named Rohinitib, which has an IC_{50} value of approximately 20 nM (Santagata et al., 2013). Recently, it was discovered that EP300/CREB, a histone acetyl transferase, was responsible for stabilization of HSF1 though acetylation of several of its lysine residues; knockdown of this enzyme by RNAi resulted in destabilisation of HSF1 (Raychaudhuri et al., 2014). This finding raises the possibility of targeting HSF1 by inhibiting the cellular processes that lead to stabilisation of HSF1 in cancer.

1.B.9.1 HSF1 and chemoresistance

Of late it has emerged that HSF1 plays a major role in maintaining chemoresistance. Desai et al. (Desai et al., 2013) found that when breast cancer cells were treated with the clinically approved chemotherapeutic drug carboplatin, which induces autophagy and inhibits cell proliferation, the administration of the drug was able to significantly increase these processes when HSF1 was knocked down. Autophagy is a cytoprotective process in response to stress such as starvation, hypoxia as well as exposure to chemotherapeutic agents. It is also a catabolic process by which cellular material such as organelles and several proteins are sequestered and degraded intracellularly within double-membrane structures known as autophagolysosomes to provide building blocks for protein synthesis and energy in the form of ATP. This process is orchestrated mainly by

the autophagy related genes (ATGs). Samples from breast cancer patients showed that higher expression levels of ATG7 correlated with poor prognosis. ATG7 is instrumental in autophagosome formation (Komatsu et al., 2005). HSF1 was found to be activated upon carboplatin exposure and to induce the transcription of ATG7 and furthermore, the knockdown of HSF1 prevented the induction of ATG7, suggesting a role of HSF1 in regulating cytoprotective autophagy which promotes cancer cell survival (Desai et al., 2013).

Local hyperthermia combined with administration of cisplatin has been used to treat patients with cervical cancer with positive outcomes (de Wit et al., 1999, Wust et al., 2002, Takahashi et al., 2002a). A study by Rossi et al. (Rossi et al., 2006) showed that loss of HSF1 in the human cervical cancer derived cells increased the sensitivity of cell death by apoptosis during a combined exposure to heat shock and cisplatin. These authors also found that when they co-expressed Hsp27, Hsp70 and Hsp90 in cells lacking HSF1, under similar conditions of combined exposure to heat shock and cisplatin, apoptosis was partially inhibited. Hence, this study further solidifies the role of HSF1 as a promoter of chemoresistance in cancer cells.

1.B.10 HSF1 and cell division

One of the most evolutionarily conserved processes is the cell division cycle. The cell cycle is characterised by four main phases: 1) cell growth, 2) DNA duplication 3) separation of duplicated DNA to the daughter cells, and 4) cell division. The cell division cycle itself can be divided into four main phases: Gap1

Figure B7

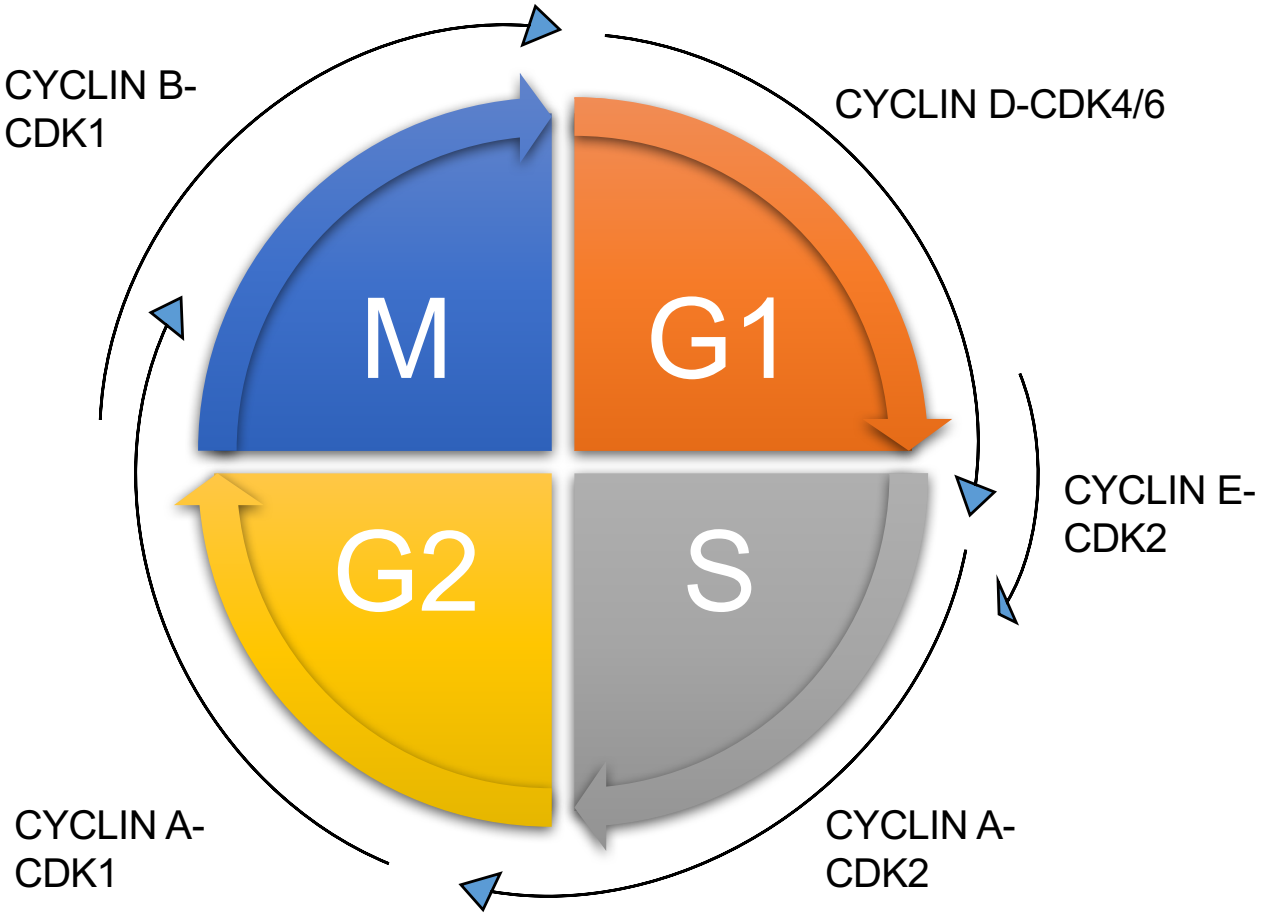

Figure B7. Control of cell cycle progression by cyclin-CDK complexes. The activation of these cyclin-CDK complexes are required during these stages of the cell cycle in order to act as a checkpoint and promote transition into the next stage.

(G1), Synthesis (S), Gap2 (G2) and Mitosis (M) (**Fig. B7**). It is during the G1 phase that cells commit to enter M phase, where the cell grows in size and is highly metabolically active, however, at this stage the DNA is not duplicated. During S phase, the DNA is replicated. The S phase is followed by the G2 phase where the cell continues to grow and prepare itself for transition into the M phase. The M phase is divided into four main stages, prophase, metaphase, anaphase and telophase, and it is followed by cytokinesis where two daughter cells are produced with identical genetic information (**Fig. B8**).

The cell cycle is tightly controlled. Cyclin-dependent kinases are serine-threonine kinases that exist as monomers, but form heterocomplexes with cyclins in order to be activated. CDK inhibitors (CDKi) are proteins that inhibit the function of the CDKs and are also essential regulators of the cell cycle. The activity of the CDKs fluctuate depending on the stages of the cell cycle. Cyclin-CDK complexes govern various stages of the cell cycle and function as important checkpoints to maintain the integrity of the cell division cycle (**Fig. B7**). Cancer cells differ greatly from normal cells in numerous ways (Hanahan and Weinberg, 2011), and one of the hallmarks of cancer is the presence of imbalanced chromosomes, known as aneuploidy. Overexpression of HSF1 inhibits mitotic exit, where cells are arrested in the G2/M phase due to the dysregulation of the metaphase-anaphase transition, ultimately increasing the chances of chromosomal abnormalities (Lee et al., 2008b). The authors show that the regulatory domain of HSF1 (amino acids 212-380) binds directly to Cdc20 and inhibits the anaphase-promoting complex (APC). HSF1 overexpression also caused increases in aneuploidy and multinucleation of mouse tumour (RIF) cells (Lee et al., 2008b). In support of this

Figure B8

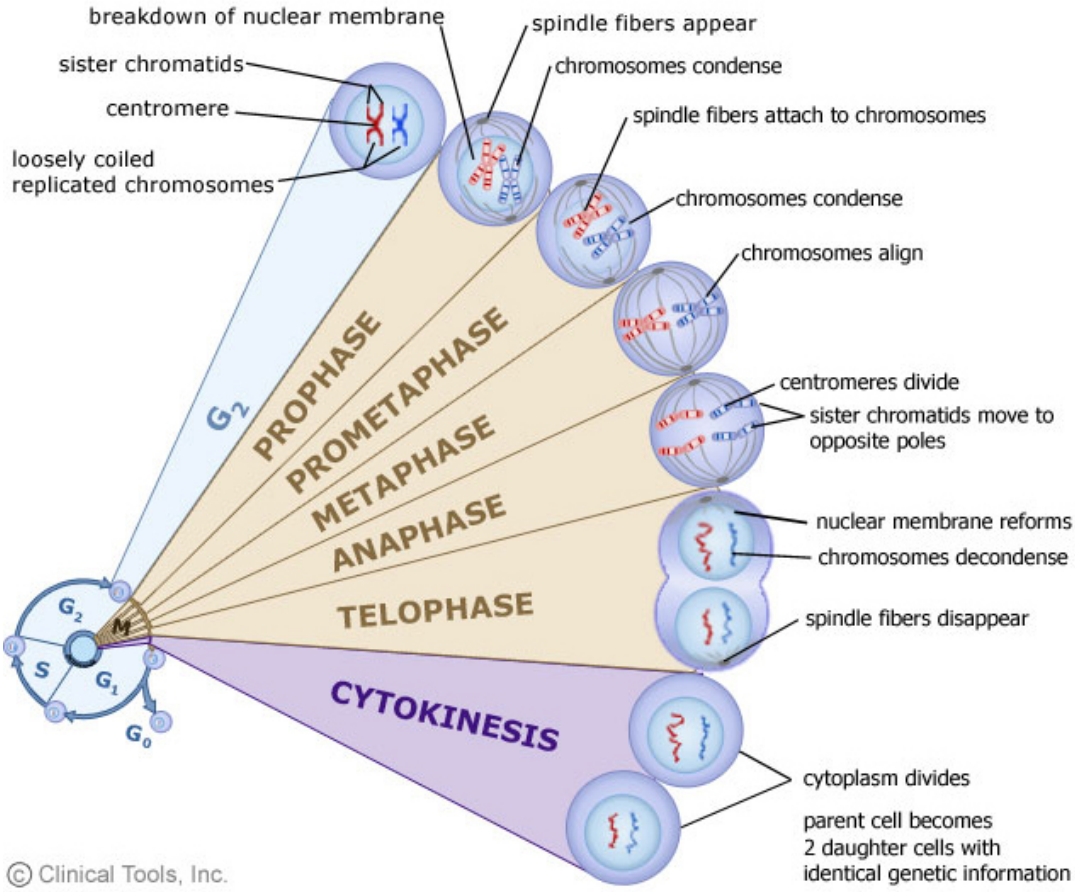

Figure B8. Different phases during mitosis. (Taken from the website http://www2.le.ac.uk/departments/genetics/vgec/schoolscolleges/topics/cellcycle-mitosis-meiosis. Accession date: 1st August 2016)

finding, overexpression of a dominant negative HSF1 (DN-HSF1), where LZ-4 of the C-terminal transactivation of HSF1 had been deleted, inhibits aneuploidy in prostate cancer (PC-3) cells. Overexpression of WT-HSF1 in PC-3 cells has been shown to regulate the degradation of Cyclin B1, where Cyclin B1/CDK1 complex promotes and regulates entry into mitosis (Wang et al., 2004b). DN-HSF1 overexpression prevents cyclin B1 degradation in cells undergoing mitosis, hence inhibiting mitotic exit, and could be one of the reasons why aneuploidy is decreased in cells overexpressing DN-HSF1 (Wang et al., 2004b).

HSF1 also plays a major role in gametogenesis (Le Masson et al., 2011, Nakai et al., 2000, Metchat et al., 2009, Wang et al., 2004a). Nakai and colleagues found that male mice expressing an active form of HSF1 in the testis were infertile due to the meiotic cells being arrested at the pachytene stage which ultimately resulted in apoptosis of the germ-line cells (Nakai et al., 2000). Le Masson and colleagues showed that oocytes from HSF1-deficient mice displayed chromosomal abnormalities. They also performed a comparative transcriptomic analysis on WT, $HSF1^{-/-}$ and $HSF2^{-/-}$ oocytes and identified that HSF1 and HSF2 regulated 1665 and 959 genes, respectively. Of these genes, 262 were regulated by both HSF1 and HSF2 suggesting their overlapping function or their roles as co-activators or co-repressors of these genes (Le Masson et al., 2011). Further analysis also showed that unlike HSF2, HSF1 was involved in the regulation of 75 genes that were involved in the cell cycle and the authors discovered that HSF1 regulated several meiotic genes (Le Masson et al., 2011). Intriguingly, in normally cycling cells exposed to heat stress, HSF1 was found to be bound to 1207 loci, however in mitotic cells exposed to heat stress, HSF1 was only able to

bind to 35 loci which mainly consisted of promoters of chaperones and proteins involved in mRNA translation (Vihervaara et al., 2013). Collectively, these data suggest that HSF1 plays a vital role in cell division, however it could have divergent roles in mitosis and meiosis.

Loss of HSF1 blocked meiosis, and it was shown that this was due to the persistent activation of the spindle assembly checkpoint (SAC) (Le Masson et al., 2011). The SAC is vital for monitoring the integrity of chromosomal segregation during mitosis or meiosis, where it controls the onset of anaphase until all the kinetochores on the chromosomes have been attached to the spindle fibres (Lara-Gonzalez et al., 2012). The effect of HSF1 on cell division has not only been observed in mammalian cells but also in yeast where it was discovered that the temperature sensitive HSF1 mutant displayed defects in spindle pole body duplication causing defects in cell division (Zarzov et al., 1997). Another study found that during mitosis, HSF1 was localised to the centrosome and also to the spindle poles during metaphase (Lee et al., 2008a), and the authors identified PLK1 as the kinase that mediated the phosphorylation of serine 216 at the DSGXXS motif of HSF1 during mitosis. This phosphorylated motif is recognised by the ubiquitin ligase complex SKP1-CUL1-F-BOX protein (SCF) bound to the E3 ubiquitin ligase β-TrCP ($SCF^{\beta\text{-}TrCP}$), which targets S216-phosphorylated HSF1 for degradation during mitosis. Interaction of HSF1 with Cdc20 prevents the recruitment of $SCF^{\beta\text{-}TrCP}$ and as a result, inhibits the transcription factor's degradation.

1.B.11 HSF1 turnover: Stability and degradation

Proteotoxic insults destabilise the cellular protein homeostasis by causing the misfolding and aggregation of proteins which deteriorates the overall health of the cell. Upon exposure to proteotoxic stress, HSF1 potentiates the transcription of a battery of molecular chaperone genes that aid in ameliorating the overall protein health and hence allowing the cells to adapt to the stress. The regulation of HSF1 with respect to its post-translational modifications has been well-studied in the field, however there is relatively less research done to uncover the mechanisms that govern the turnover of HSF1. The endogenous HSF1 protein has a relatively long half-life spanning from 13.6 h to 20 h (Kourtis et al., 2015, Yang et al., 2008, Seo et al., 2006). Unlike the long half-life of the protein, the half-life of HSF1 mRNA is approximately 100 mins (Kim et al., 2012a). It is highly likely that the reason for HSF1 being such a long-lived protein is to be readily available in the event of exposure to cytotoxic stress so that it is able to exert its cytoprotective effects immediately. The histone acetyltransferase E1A Binding Protein P300 (EP300) promotes the stability of endogenously expressed HSF1 through acetylation on several of its lysine residues (i.e., K208 and K298) hence preventing it from being targeted for proteasomal degradation (Raychaudhuri et al., 2014). Also, EP300 maintains HSF1 stability irrespective of its phosphorylation status (Raychaudhuri et al., 2014). One of the first insights regarding HSF1 turnover was provided by a study published in 2001 by Bonelli and colleagues who found that only under heat shock conditions, serum-starved late passage human fibroblast (HF) cells displayed reduced HSF1 levels

compared to early passage serum-starved HF cells (Bonelli et al., 2001). This finding is further supported by a recent publication showing that HSF1 degradation increases dramatically post-heat shock and furthermore, RNAi-mediated depletion of the proteasomal subunit PSMA7, prolonged the Hsp70 mRNA production by approximately 5 h under conditions of heat shock suggesting that the HSR is attenuated by the proteasome (Raychaudhuri et al., 2014). Interestingly, Riluzole which is the only FDA-approved drug for the treatment of the neurodegenerative disease Amyotropic Lateral Sclerosis (ALS), is able to dramatically increase the protein half-life of endogenous HSF1 from 13.6 h to 69.3 h (Yang et al., 2008), allowing greater activation of the HSR in cancer and neuronal cells (Yang et al., 2008, Liu et al., 2011). Furthermore, silencing LAMP2A using RNAi, curbed the turnover HSF1 in the presence of Riluzole which suggests that the compound could potentially block the clearance of HSF1 through chaperone-mediated autophagy (CMA) as LAMP2A is an essential potentiator of this process (Yang et al., 2008).

Until recently, not much was known about the mechanisms by which HSF1 is degraded, however, studies have emerged implicating several proteins that mediate the degradation of HSF1, namely, filamin interacting protein 1-like (FILIP-1L) and the E3 ligases, $SCF^{\beta\text{-}TrCP}$, F-Box and WD Repeat Domain Containing 7 (FBXW7) and neural precursor cell-expressed developmentally downregulated gene 4 (NEDD4). FILIP-1L was identified as a binding partner of HSF1 through a yeast-two-hybrid screen (Hu and Mivechi, 2011). The downregulation of FILIP-1L has been implicated in various human tumours and

has also been linked with hypermethylation at the FILIP-1L promoter and also global DNA methylation (Burton et al., 2011, Lu and Hallstrom, 2012). Hu and Mivechi discovered that overexpression of FILIP-1L leads to the decrease in HSF1 levels and as a consequence inhibits the transcription of HSF1 target genes. Also, they found that FILIP-1L acts as an adaptor protein for HSF1 to allow for binding to hHR23A, an ubiquitin receptor protein that functions to transfer ubiquitinated proteins to the 19S proteasomal subunit (Hu and Mivechi, 2011).

As described in the previous section, phosphorylation of HSF1 at S216 targets the protein for degradation by the E3 ubiquitin ligase SCF $^{\beta\text{-TrCP}}$ during mitosis, and mutation of this residue to arginine, dramatically increases its half-life (Lee et al., 2008a). FBXW7 is the substrate recognition component of the SCF ubiquitin ligase complex and in humans it functions as a tumour suppressor as it mediates the degradation of many proto-oncogenes such as MYC, NOTCH and JUN (Welcker and Clurman, 2008). FBXW7 binds to its substrates via their phosphodegron motifs which are called Cdc4 phosphodegrons (CPDs) where phosphorylation within the phosphodegrons has to occur in order for binding to take place (Welcker and Clurman, 2008). In most cases, FBXW7 substrates such as the ones mentioned above are phosphorylated by GSK3 within the phosphodegron. Interestingly, a recent article has linked the protein stability of HSF1 to FBXW7α; the authors reported that the SCF^{FBXW7} complex targets the degradation of HSF1 through direct binding at the phosphodegron motif spanning S303 and S307, where GSK3 and ERK1 phosphorylate these sites respectively (Kourtis et al., 2015). The phosphorylation of serine 303 and serine 307 is

required for the binding of FBXW7α to HSF1, and loss of FBXW7α causes persistent nuclear accumulation and activation of HSF1. In human melanoma cells, FBXW7α is downregulated, and Kourtis and colleagues showed that HSF1 accumulation and activation drives the metastatic potential (Kourtis et al., 2015). GSK3 is activated under low-serum or serum-starved conditions (Sutherland, 2011, Hetman et al., 2000, Sato et al., 2009). Taken together, the observations by Bonelli et al. and Kourtis et al. suggest that during serum-starvation heat shock could cause the activation of GSK3 and subsequent phosphorylation of HSF1 at the S303 and S307 phosphodegron to allow for SCF^{FBXW7}-mediated degradation of the transcription factor (Bonelli et al., 2001, Kourtis et al., 2015).

In contrast to cancer cell models, there have been numerous reports linking the loss of HSF1 to the promotion of neurodegenerative diseases (Jiang et al., 2013, Kondo et al., 2013). α-Synucleinopathies represent progressive neurodegenerative diseases such as Parkinson's Disease (PD), multiple system atrophy (MSA) and dementia with Lewy bodies (DLB) (Fellner and Stefanova, 2013, McCann et al., 2014) where there is accumulation of α-synuclein in the cytoplasm of a subset of neuronal and glial cells. A53T α-synuclein is able to form aggregates more readily that WT α-synuclein. In a recent study, Lim *et al*. found that overexpression of the mutant A53T α-synuclein in neuronal cells caused a decrease in HSF1 protein levels of more than 70% compared to WT α-synuclein whilst not affecting the *HSF1* mRNA levels (Kim et al., 2016). WT α-synuclein caused the decrease of HSF levels in the nucleus unlike the mutant A53T α-synuclein which decreased HSF1 levels in both the nucleus and cytoplasm (Kim

et al., 2016). A53T α-synuclein overexpression increased the amount of ubiquitinated HSF1, the authors had previously identified the E3 ligase NEDD4 levels to be elevated in brains from PD patients (Kwak et al., 2012), leading them to overexpress NEDD4 in neuronal cells where they observed a prominent decrease in HSF1 protein levels (Kim et al., 2016). The authors also found that loss of NEDD4 or the overexpression of HSF1 led to the display of a neuroprotective phenotype against α-synucleinophathy (Kim et al., 2016).

1.B.12 Concluding remarks

HSF1 orchestrates a comprehensive transcriptional program that includes genes encoding chaperones which prevent protein misfolding and aggregation to maintain cellular proteostasis, as well as proteins which take part in the repair and clearance of damaged macromolecules and maintain cellular metabolism. Together with transcription factor NRF2, activation of HSF1 allows adaptation and survival under conditions of electrophilic, oxidative, inflammatory, and thermal stress due to the extraordinary functional diversity of their downstream target genes. Small molecule activators of HSF1 and/or NRF2 have shown protective effects in numerous animal models of chronic disease, including neurodegenerative disease, cardiovascular disease, and cancer. However, although the functions of both HSF1 and NRF2 are undoubtedly broadly cytoprotective, the consequences of their activation are both context- and duration-dependent and may have not only beneficial, but also negative effects for the organism, such as promoting cardiomyopathy or accelerating tumour

growth. This dichotomy should be very carefully considered when these transcription factors are being targeted for disease prevention or treatment.

Section 1: Introduction

Chapter C

p38 mitogen-activated protein kinases

1.C.1 Introduction

Eukaryotic cells have evolved ways to be able to respond quickly to external or internal stimuli by being able to sense, transmit the signals and coordinate the appropriate responses. Examples of these stimuli are in the form of growth factors, nutrients, cytokines, toxins, and physical changes such as osmolarity and oxygen levels. The signal transduction occurs through a subset of proteins known as kinases, which control the functional properties of their substrates by catalysing phosphorylation reactions. In the human genome, there are more than 600 putative kinase genes (Cheng et al., 2014). To date, 518 human kinases have been described, and of these, only approximately 50% have been studied (Johnson and Hunter, 2005, Jacoby et al., 2015). Kinases belonging to the mitogen-activated protein kinase (MAPK) family are among the most well-studied protein kinases. MAPK signalling pathways play major roles in various cellular processes such as immunity, inflammation, development, cell differentiation and cancer. MAPKs operate through a three-tiered signalling cascade, where the top tier is comprised of a MAPK kinase kinase (MAP3K) which when activated by phosphorylation, usually by autophosphorylation, phosphorylates and activates the middle tier MAPK kinase (MAP2K) which ultimately phosphorylates the MAPK belonging to the final tier. Subsequently, the phosphorylation activated MAPK is then able to phosphorylate its substrate(s).

There are four main subfamilies belonging to the MAPK superfamily and they are c-JUN NH2-terminal kinases or stress-activated protein kinases (JNK/SAPK), extracellular signal regulated kinases (ERKs), ERK5/big MAP kinase 1(BMK1) and p38 MAPKs (Zarubin and Han, 2005, Manna and Stocco, 2011).

1.C.2 p38 MAPKs

To date, in mammalian cells, four main isoforms of p38 MAPKs encoded by different genes have been identified: p38α, p38β, p38ɣ and p38δ (**Fig. C1A**). p38α and p38 β are more closely related to each other sharing 75% of amino acid sequence identity, whereas p38ɣ and p38δ share 64% amino acid sequence homology. All four isoforms share approximately 45% amino acid sequence identity and their relative amino acid sequence identity is listed in **Fig. C1B.** p38α was the first out of the four isoforms to be isolated and most of the literature on the p38 MAPKs focuses on this particular isoform. p38α was initially isolated as a 38-kDa protein that was phosphorylated on its tyrosine residue when cells were exposed to lipopolysaccharide (LPS) or hyperosmolarity (Han et al., 1994). Also, in the same year, p38α was identified as a protein that was bound to pyridinyl imidazole class of compounds that were found to inhibit the production of the cytokines, interleukin 1 (IL-1) and tumour necrosis factor (TNF) in various cell types when exposed to inflammatory stimuli (Lee et al., 1994). This finding paved the way in the drug development field in search of p38αinhibitors for the treatment of inflammatory diseases, with SB203580, a compound belonging to the pyridinyl imidazole class, being one of the most widely studied p38α inhibitors (Lee et

FIGURE C1

A

Characteristic properties of the p38 MAPK isoforms

p38 MAPK isoform	Other names	No. of amino acids	Observed molecular wt (kDa)	Gene expression in tissues
p38α	MAPK14, SAPK2A	360	38	Most tissues
p38β	MAPK11, SAPK2B	364	39	Most tissues
p38ɣ	MAPK12, SAPK3	367	43	Skeletal
p38δ	MAPK13, SAPK4	365	40	Lung, Kidney, Testis, Pancreas & Small intestines

B

Sequence identity between the p38 MAPK isoforms (%)

	p38α	p38β	p38ɣ	p38δ
p38α	-	75.5	60.2	58.5
p38β		-	61	57.4
p38 ɣ			-	63.9
p38δ				-

Overall sequence identity between all four p38 MAPK isoforms is **45.1 %**

Figure C1. p38 MAPK isoforms. 1A) Characteristic properties of the p38 isoforms. **B)** Table showing the sequence homology between the different p38 MAPK isoforms, the percentages shown are derived from aligning the p38 isoform sequences in the uniprot.org website.

al.,1994). Structural and crystallographic studies have identified that pyridinyl imidazole compounds competitively bind the ATP-binding pocket of p38α.

Several years after the isolation of p38α, the other three isoforms were characterised. Due to the central role of p38 MAPKs in transducing inflammatory responses, there has been extensive research performed on them. Furthermore, since its discovery, efforts were made to develop and identify selective and potent p38 inhibitors. However, since it was discovered that p38 MAPKs have more than 100 substrates (Trempolec et al., 2013) which are involved in cellular pathways other than inflammation, it has become clear that inhibiting p38 inadvertently causes unwanted side effects, hence restricting the clinical application of this approach (Gurgis et al., 2014).

1.C.3 Structure of p38 MAPKs

The structures of human p38α (ter Haar et al., 2007), β (Roy et al., 2015) and δ (Patel et al., 2009) have been solved by X-ray crystallography. All isoforms of p38 contain a glycine-rich phosphate-anchoring domain containing the consensus sequence Gly-X-Gly-X-X-Gly at the N-terminus (aa 31-36) which is followed by the ATP-binding region (aa 42-52). The phosphorylation or activation lip of the protein contains the amino acids 170-185 (Wilson et al., 1996, Badrinarayan and Sastry, 2011). Within the activation lip, p38 is activated upon phosphorylation at T180 and Y182 at the highly conserved amino acid sequence Thr^{180}-Gly^{181}-Tyr^{182} (Wilson et al., 1996, Badrinarayan and Sastry, 2011). The linker consisting of the amino acids Asp^{168}-Phe^{169}-Gly^{170} also known as the DFG loop adopts two different conformations: 1) ‘DFG-in’ and 2) ‘DFG-out’. When p38

assumes the ‘DFG-in’ conformation, the ATP-binding pocket is exposed and phosphotransfer can be catalysed, whereas, when p38 adopts the ‘DFG-out’ conformation, the hydrophobic pocket that was previously occupied by Phe^{169} is revealed, rendering the kinase inactive (Young, 2013, Badrinarayan and Sastry, 2011) (**Fig. C2**). Unlike ATP-competitive inhibitors such as the pyridinyl imidazole class of inhibitors like SB202190, a compound belonging to the diaryl urea class, BIRB796, allosterically binds to and inhibits the function of all isoforms of p38 as it forces p38 to adopt the ‘DFG-out’ conformation (Cuenda and Rousseau, 2007, Cuadrado and Nebreda, 2010).

Interestingly, p38ɣ is the only isoform that at the end of its C-terminus contains a 5 amino acid sequence KETPL which is a PDZ (PSD-95, discs large, zona occludens 1) binding domain where the consensus sequence for this domain is KETXL where X can be any amino acid (Hasegawa et al., 1999). The PDZ binding domain on p38ɣ allows it to bind to substrates containing the PDZ domain and strikingly many of the p38ɣ-specific substrates such as α 1-syntrophin, myogenic differentiation 1 (MyoD1) and disks large homolog 1 (DLG1) contain the PDZ domain (Escos et al., 2016).

1.C.4 p38 MAPK signalling

The expression pattern of the p38 isoforms differs greatly in terms of tissue distribution. Although, p38α and p38β are ubiquitously expressed in most tissues, p38β has been found to be highly expressed in the brain (Lawson et al., 2013), whereas, p38ɣ is expressed mainly in skeletal muscle tissues and p38δ is mainly

FIGURE C2

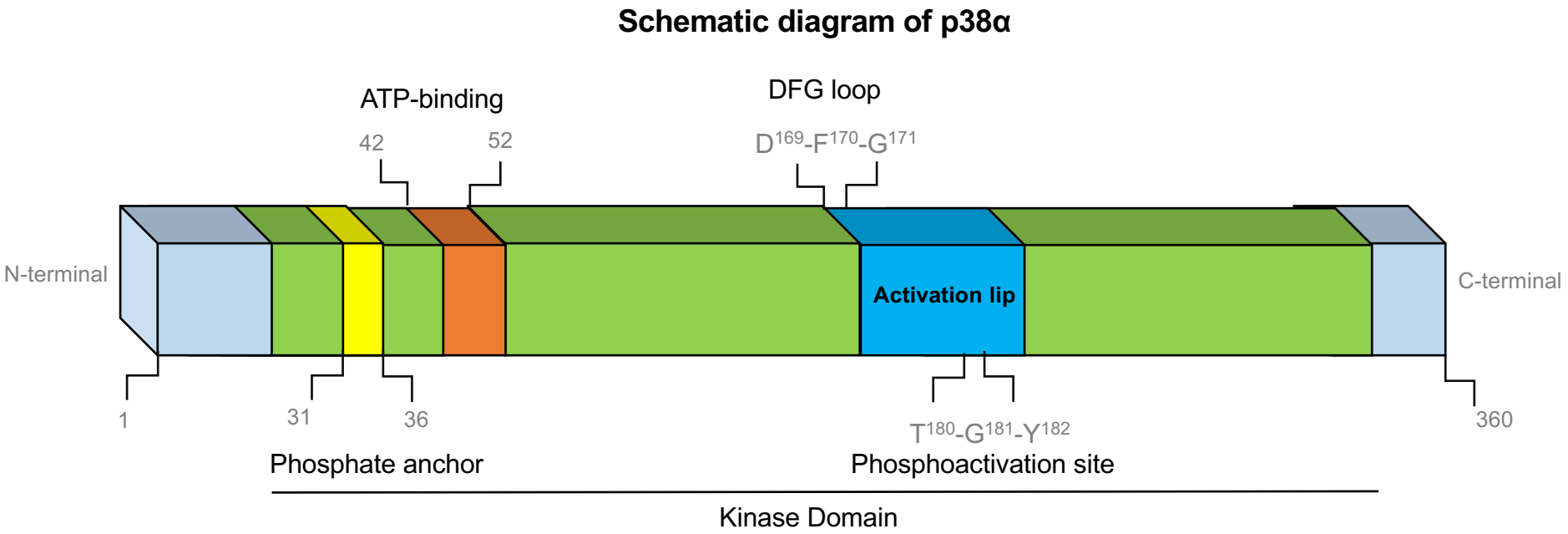

Figure C2. **Schematic diagram of the p38α structure.** The phosphate anchor (yellow), ATP-binding site (orange), flanking kinase domain (green) and the activation lip (blue) are labelled with the corresponding amino acid numbering.

expressed in the testis, pancreas, kidney and small intestine (**Fig. C1A**). The activation of the p38 signalling pathway through environmental stimuli has been observed in various species such as the budding yeast *Sacchromyces cerevisiae* (Hog1) (Posas et al., 1996), the round worm *Caenorhabditis elegans* (pmk1, pmk2 and pmk3) (Berman et al., 2001), the fruit fly *Drosophila melanogaster* (p38a, p38b and p38c) (Stronach and Perrimon, 1999) and in the African clawed frog *Xenopus laevi* (p38) (Keren and Bengal, 2010). In the yeast, HOG1 is a crucial regulator of adaptation and survival upon exposure to osmotic stress (Kim and Shah, 2007). Deletion of HOG1 in yeast exposed to high osmolarity confers lethality (Lee et al., 2002b). Also HOG1 is activated upon exposure to environmental stressors such as heat shock (Winkler et al., 2002). In mammalian systems, p38 has been found to be activated by osmotic shock, heat stress, ultraviolet (UV) radiation and exposure to endotoxins (e.g. LPS) as well as inflammatory cytokines (IL-1 and TNF-α) and growth factors (e.g. NGF and GM-CSF) (Lee and Young, 1996, ten Hove et al., 2007, Zhang et al., 2001, Seo et al., 2002, Xing et al., 1998, Winkler et al., 2002, Lee et al., 1994, Han et al., 1994). The ability of p38 MAPK pathway to sense and be activated by numerous forms of stimuli demonstrates that this pathway is highly sensitive and complex. The four p38 MAPK isoforms are differentially activated by their upstream kinases MAP2Ks which themselves are activated by their upstream kinases, the MAP3Ks (**Fig. C3**).

FIGURE C3

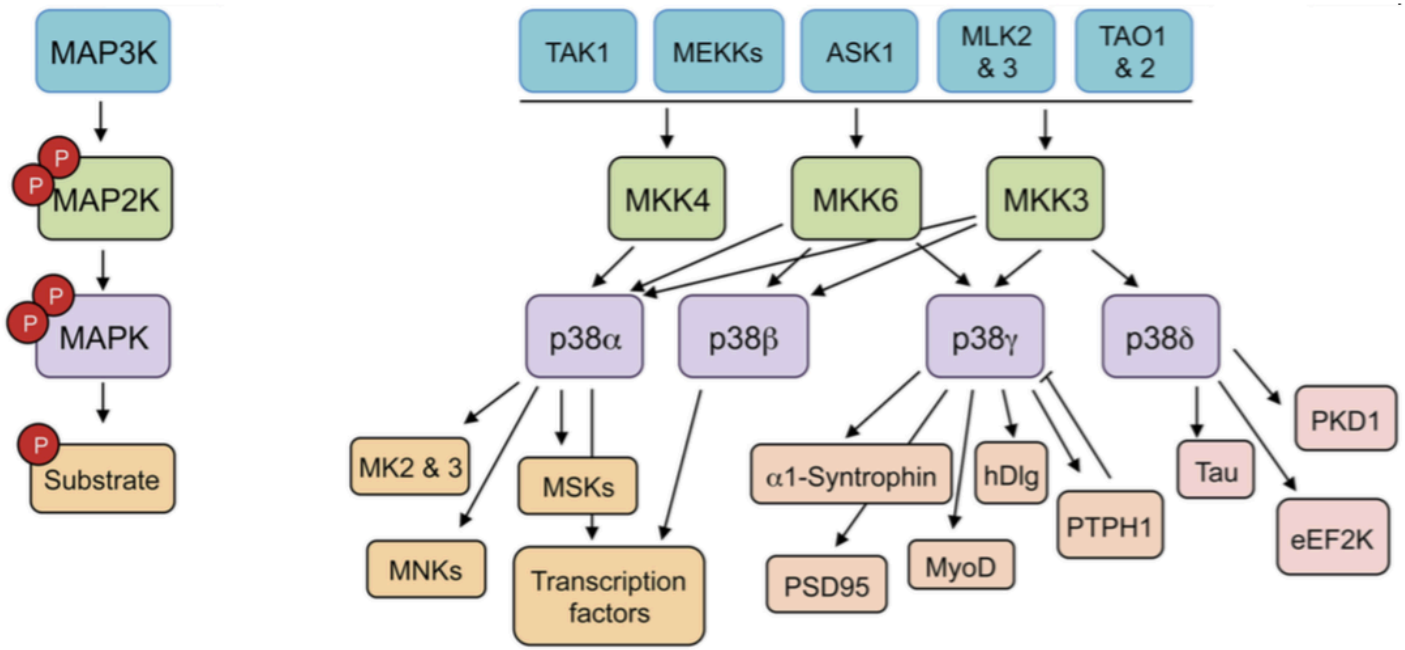

Figure C3. p38 MAPK signalling cascade showing the substrate specificities for the individual isoforms. Diagram taken from Escos et al. 2016.

1.C.4.1 *p38 MAPK signalling cascade*

The MAP3Ks bring about specificity for a stimulus-dependent triggering of the MAP2K-MAPK signalling cascade as well as have a role in determining cell fate (Craig et al., 2008, Escos et al., 2016). The main MAP3Ks that play a vital role in MKK3/4/6-p38 MAPK activation are Thousand-and-one amino acid kinase 1 and 2 (TAO1 and TAO 2), Apoptosis signal-regulating kinase 1 (MEKK5/ASK1), Mixed-lineage kinases 2 and 3 (MLK2 and MLK3), TGF-β activated kinase 1 (TAK1) and MAPK/ERK kinase kinases (MEKK) (Escos et al., 2016) (**Fig. C3**).

All the MAP2Ks or MAP kinase kinases (MKKs) upstream of p38 MAPKs phosphorylate p38 at the TGY motif found within the activation loop. MKKs contain a D-domain docking site for binding to various MAPKs such as JNK family and p38 MAPKs (Sharrocks et al., 2000). All isoforms of the p38 MAPKs have been reported to be activated by MKK3 and MKK6 *in vitro* and *in vivo*, however, the p38 isoforms are differentially activated by MKK3 and MKK6 in response to different stress stimuli (Brancho et al., 2003, Remy et al., 2010). Interestingly, MKK4 is able to activate all three isoforms of the JNK family of MAPKs as well as two isoforms of p38 MAPKs (α and β) (Deacon and Blank, 1997, Whitmarsh and Davis, 2007). These findings suggest that the MKKs are differentially regulated in order to provide an organised and synchronised p38 MAPK signalling cascade.

The scale and extent of p38 activation is vital in determining its effects on the cell. Within a few minutes upon stimulation, p38 MAPKs are rapidly activated, and depending on the cell type and stimulus, this activation could be transient or persistent, suggesting that p38 activation is tightly controlled under basal

conditions. p38 isoforms have various substrates that play an important role in cellular processes such as apoptosis, transcription, cell growth, cell division, protein transport and secretion, protein chaperoning, cytoskeletal organisation, protein degradation. The p38 MAPK isoforms have overlapping substrates as well as unique substrates (**Fig. C3**).

One of the first p38 MAPK substrates to be identified was MAPK-activated protein kinase 2 (MAPKAPK2 or MK2). MK2 when activated by p38, as able to activate various signals through the modulation of its substrates. MK2 is involved in cellular processes such as the inflammatory response, apoptosis and cell division. As mentioned earlier, since p38 inhibitors have failed in the clinical setting due to the presentation of high liver toxicity and unwarranted side-effects in patients, inhibitors targeting its downstream substrates are highly sought after. Activated MK2 is essential for the production of the pro-inflammatory cytokines TNFα, IL-1α, IL-1β, IL-6 (Castillo et al., 2016). $MK2^{-/-}$ mice have reduced production of pro-inflammatory cytokines and macrophages compared to their wild-type counterparts and are protected from developing neoplasms in a colorectal cancer model. MK2 phosphorylation by p38 allows for phosphorylation of heat shock protein 27 (Hsp27) which is found complexed to protein kinase B (AKT). Upon phosphorylation by MK2, Hsp27 dissociates from AKT. Hsp27 is known to be able to protect cells against oxidative damage caused by reactive oxygen species (ROS) which could be produced by environmental stimuli such as cytokines, heat stress and hypoxia (Zheng et al., 2006). Hsp27 decreases ROS levels by increasing intracellular glutathione levels and decreasing intracellular iron levels (Arrigo et al., 2005). Tristetrapolin (TTP), a protein that

functions to destabilise mRNA stability has been found to be inactivated through phosphorylation of the p38-MK2 signalling cascade suggesting a role in for the p38 MAPKs in mRNA processing. Other p38 MAPK substrates include transcription factors such as activating transcription factor 2 (ATF2), proto-oncogene c-Fos (FOS), transcription factor MafA (MafA) which are involved in pathways regulating DNA-damage response, cell proliferation and insulin regulation, respectively (Trempolec et al., 2013). Other substrates of the p38 MAPK pathway include the cell cycle regulator Cyclin D3 (Casanovas et al., 2004), the structural proteins Stathmin (Parker et al., 1998, Mizumura et al., 2006) and tau (Zhu et al., 2000, Reynolds et al., 1997) and RNA splicing factor 45 (SPF45) (Al-Ayoubi et al., 2012).

1.C.5 Some of the pathophysiological impacts of p38 MAPK signalling

1.C.5.1 *Specific roles and functional redundancies*

Each of the p38 isoforms have their unique substrates, and their substrate specificities are also cell and context dependent. However, the p38 isoforms share many substrates which suggests functional redundancies due to their high sequence homologies. *In vivo* knockout models have shed light on the functional redundancies of the p38 MAPKs. Thus far, only p38β, p38ɣ and p38δ-knockout mouse models have been generated and they all exhibit a normal phenotype. On the contrary, p38α-knockout mice display embryonic lethality at midgestation due to placental defects, suggesting a role for p38α in embryonic development. These

placental defects could not be rescued by a knock-in allele of p38β under the control of the p38α promoter, implying that these isoforms are not completely functionally redundant. Interestingly, tissue-specific p38α knockouts in mice have implicated the kinase in cardiomyocyte proliferation (Engel et al., 2005), liver gluconeogenesis (Jing et al., 2015) and hepatocyte proliferation (Tormos et al., 2013). Although, p38β-knockout mice are viable, several studies have emerged implicating the requirement of this isoform for bone mineralisation. Micro CT scans have shown that bones of four-week old p38β-knockout mice present with osteopenia (Greenblatt et al., 2010). Interestingly, p38β deficiency in osteoblasts showed defects in late stage of differentiation, whereas, p38α deficiency in the same system exhibits defects in both early and late stages of osteoblast differentiation (Greenblatt et al., 2010, Rodriguez-Carballo et al., 2016). Murine embryos deficient in both p38α and β displayed spina bifida, exencephaly and heart defects, and these phenotype were not observed in the single knockout embryos of either isoforms (del Barco Barrantes et al., 2011), suggesting that during embryonic development, p38α and β are functionally redundant.

The generation of single and double p38ɣ or/and p38δ knockout mice has provided answers regarding the functional roles and redundancies of these isoforms. It has been reported that p38ɣ/δ -double knockout mice-derived macrophage and dendritic cells have an impaired innate immune response when challenged with endotoxins such as LPS (Escos et al., 2016). In addition, the p38ɣ/δ-double knockout mouse displays cardiac hypertrophy (Gonzalez-Teran et al., 2016a). Since p38ɣ is mainly and highly expressed in skeletal tissues, and is induced during muscle differentiation, it is not surprising that the double

knockout of ɣ and δ isoforms display heart defects. Indeed, p38ɣ is an important factor for adult muscle differentiation and regeneration (Lassar, 2009). Studies conducted in p38δ-deficient mice have shown that this isoform, which is highly expressed in the lungs, is important for recruitment of neutrophils to sites of inflammation in the lung (Ittner et al., 2012).

There are publications showing that loss of p38ɣ or/and p38δ confers protection in several disease models. Sumara et. al. showed that the loss of p38δ promotes insulin secretion in pancreatic β cells and enhances glucose tolerance (Sumara et al., 2009). The authors found that pancreatic β cells from p38δ-null mice contain profoundly activated protein kinase D (PKD) which promotes insulin exocytosis in these cells (Sumara et al., 2009). Furthermore, mice lacking both p38ɣ and δ in their myeloid cells are resistant to the development of non-alcoholic fatty liver disease (NAFLD), glucose intolerance and triglyceride accumulation in the liver (Gonzalez-Teran et al., 2016b). The authors show that this protection is mediated by impaired recruitment of neutrophils to the liver, which as a consequence prevents inflammation and the development of liver steatosis (Gonzalez-Teran et al., 2016b). Using the two-stage 7,12-dimethylbenz(a)anthracene (DMBA)/12-O-tetradecanoylphorbol-13-acetate (TPA) skin carcinogenesis protocol, it was found that both p38δ-knockout and p38ɣ/δ-double knockout mice have a reduced susceptibility to tumour formation which could be due to defects in mounting inflammatory and proliferative responses (Schindler et al., 2009, Zur et al., 2015). Recently, Yin and colleagues showed that intestinal epithelial cell specific knockout of p38ɣ leads to inhibition of inflammation and tumouriginesis in a colitis-associated colon cancer model

(Yin et al., 2016). Global knockdown of both p38ɣ and p38δ is also protective in this model (Del Reino et al., 2014).

1.C.6 Conclusions

There have been a plethora of reports implicating the importance of p38 MAPKs in cellular pathways such as proliferation, differentiation, apoptosis, cell survival, development, senescence, inflammation and aging (**Fig. C4**). Notably, the p38 inhibitors that have been used in clinical trials primarily target the α and β isoforms, and such inhibitors have failed due to toxicities and importance of these pathways. Inhibiting their substrates such as MK2 as mentioned earlier seems to be a better option as it provides a more linear approach. Also, it is important to note that targeting p38ɣ and δ could be another possibility since in the last decade there has been significant progress in the understanding of the roles of these two isoforms. p38ɣ and δ have been shown to be vital regulators of inflammation, and the development of drugs that specifically target them might ameliorate inflammatory disease pathogenesis. Interestingly, it was recently found that the use of relatively specific p38δ inhibitors reduced the amount of mucus production in human bronchial epithelial cells (Escos et al., 2016). It will be fascinating to understand more about the mechanism behind how the ɣ and δ p38 MAPK isoforms govern innate immunity. This will ultimately lead to the search for highly selective inhibitors which could be of therapeutic use for the treatment of inflammatory diseases.

FIGURE C4

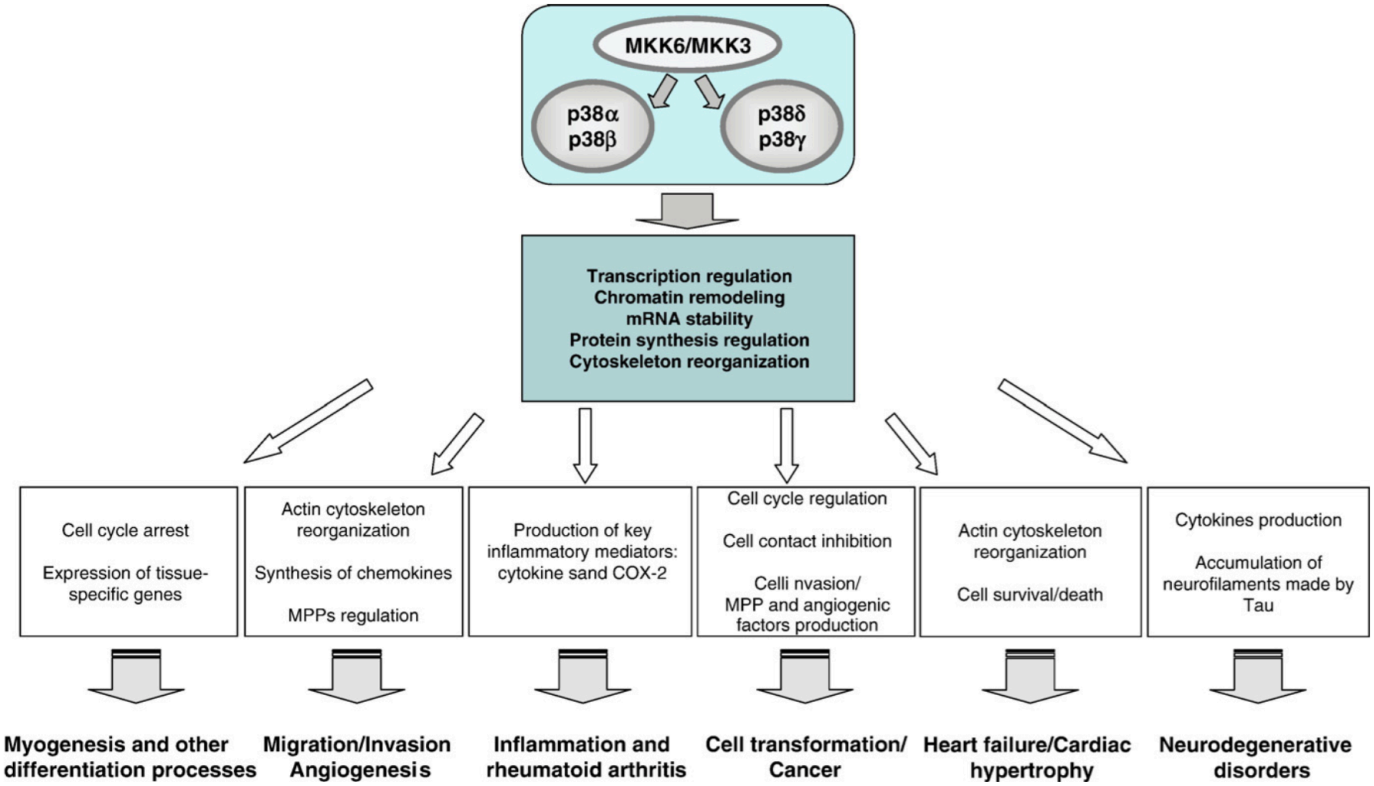

Figure C4. The physiological roles and pathological implications of p38 MAPKs. Diagram taken from Cuenda and Rousseau, 2007.

Section 2: Materials and Methods

2.1 Materials

All general chemicals and reagents were of analytical grade and obtained from either Sigma-Aldrich (Dorset, United Kingdom) or MERCK Millipore (Massachusetts, USA). PEITC was prepared as a stock solution in acetonitrile and diluted 1:1,000 in the cell culture medium before treatment. The concentration of the solvent was maintained at 0.1% (v/v) in all wells. The p38α/β MAPK inhibitor SB202190 was purchased from SYNkinase (Parkville, Australia). The pan p38 inhibitor BIRB0796 was purchased from Axon Medchem (Groningen, Netherlands). The JNK inhibitor JNK-In-8 was a kind gift from Dario Alessi (University of Dundee). The GST-tagged recombinant NRF2 NEH6+ protein was a kind gift from Professor. John D. Hayes.

2.2 Cell culture

MDA-MB-231 cells were from ATCC. HeLa-HSE-luc cells (Calamini et al., 2012) were a generous gift from Richard I. Morimoto (Northwestern University, USA). MCF7 cells were a kind gift from Dr. Mark Saville (University of Dundee, UK). HeLa cells were a generous gift from Dr. Sonia Rocha (University of Dundee, UK). Mouse embryonic fibroblasts (MEF) from wild-type or HSF1-knockout mice were isolated as described previously (Xiao et al., 1999). The human epidermoid cancer cell line A431 and the production and transduction of lentivirus short hairpin RNA to generate stable clones, which do not express p38ɣ or p38δ, have been described (Zur et al., 2015). All cell lines were maintained at 5% CO_2 in air at 37°C and were cultured in Dulbecco's Modified Eagle Medium (DMEM)

(Invitrogen) supplemented with 10% (v/v) heat-inactivated FBS (Invitrogen) unless specified. The medium in which HeLa-HSE-luc cells were grown also contained 100 µg/mL G418 (Invitrogen), whereas the medium for MEF cells was additionally supplemented with non-essential amino acids (Invitrogen) and 50 U/ml penicillin/streptomycin (Invitrogen).

2.3 Western blotting sample preparation

Cells grown in 6-well plates were washed twice with phosphate buffered saline (PBS) and lysed in 150 µl of either RIPA buffer [50 mM Tris-Cl pH 7.5, 150 mM NaCl, 0.5% (w/v) sodium deoxycholate, 1% IGEPAL (v/v), 0.1% SDS (w/v) and 1 mM EDTA), containing 1 protease inhibitor cocktail tablet (Roche) per 10 ml of buffer] or SDS-lysis buffer [50 mM Tris-Cl pH 6.8, 2% (w/v) SDS, 10% (v/v) glycerol and 0.005% bromophenol blue). The lysates derived from RIPA buffer were transferred into 1.5-ml Eppendorf tubes which were placed on a rotator at 4°C for 30 min. The cell debris was then removed by centrifugation at 16,300 x g for 10 min at 4°C, and the supernatant was transferred to a new tube. The lysates derived from the SDS-lysis buffer were subjected to sonication at 20% amplitude for 20 sec. The BCA assay (Thermo) was used to determine protein concentrations.

2.4 Western Blot Analysis

2.4.1 SDS-PAGE gel electrophoresis

For this technique, unless specified, equal amounts of sample lysates (5 µg – 20 µg protein) were incubated with sodium dioecyl sulphate (SDS) lysis buffer (13.3 mM Tris HCL pH 6.8, 6% (v/v) Glycerol, 1% (w/v) SDS, 1.2% (v/v) β-

Mercaptoethanol and 0.1% w/v Bromophenol Blue). The samples, along with a prestained standard protein marker (Invitrogen), were loaded onto SDS-polyacrylamide (ProtoGel 30%, National Diagnostics) gels prepared in the laboratory, and separated by electrophoresis (SDS-PAGE) using 80V for 30 minutes and 120V for 1 hour. The gel was run using the gel running buffer (25 mM Tris, 192 mM Glycine, 0.1% (w/v) SDS) and the system used was purchased from the manufacturer Biorad.

2.4.2 NuPAGE gel electrophoresis

For this technique, unless specified, equal amounts of sample lysates (5 µg – 20 µg protein) were incubated with SDS-lysis buffer. The samples along with a prestained standard protein marker (Pageruler, Invitrogen) were loaded onto precast 4-12% gradient or 10% NuPAGE gels and separated by electrophoresis using 80V for 15 minutes and 150V for 1 hour. The gel was run using the gel running buffer (1 X MOPS buffer, Invitrogen) and the gel-running system used was purchased from the manufacturer Invitrogen.

2.4.3 Wet transfer

The proteins from the gel were transferred onto 0.45 µm nitrocellulose membrane (NC) (Amersham Biosciences) using the wet transfer system following the manufactuer's instructions (Critereon, Biorad). The transfer buffer (25 mM Tris, 192 mM glycine and 20% (v/v) methanol) was used to transfer the proteins from the gel to the NC membrane at 100V for 30 or 45 minutes for 0.75 mm or 1.00 mm thick gels respectively. Once the proteins were transferred from the gel to the NC membrane, the latter was blocked using 10% w/v milk (Marvel) prepared

in 0.1% PBS containing 0.1% Tween 20 (PBS-T) for 30 min at a constant agitation of 70 rpm on a shaker (SSM1, Stuart).

2.4.4 Immunoblotting

All the antibodies were prepared in 10% (w/v) milk (Marvel) dissolved in PBS-T (0.1% (v/v) Tween 20 dissolved in PBS) and contained within a 50 ml centrifuge tubes. Next, the NC membrane was added to the preferred primary antibody contained in the falcon tube. The 50 m tubes containing the primary antibody and the NC membrane were placed on a rotator (SRT6, Stuart) for an overnight incubation (16-24 h) at 4^{o}C or 2 h at room temperature (RT).

After the incubation with the primary antibodies, the membrane was washed thrice every 15 minutes in PBS-T. The NC membrane is incubated with its respective secondary antibody (Section 2.3) for 45 minutes at RT. Next, the membrane was washed with PBS-T for three times every 15 minutes. Enhanced chemiluminescence (ECL) stock A (2.5 mM Luminol (Fluka), 100 mM Tris HCL pH 8.5, 0.4 mM p-coumaric acid) and B (0.0192% H_2O_2 and 100 mM Tris HCL pH 8.5) are mixed at a 1:1 ratio. 1 ml of ECL (A+B) was required for one membrane. The ECL solution was spread onto the NC membrane evenly. A developing cassette containing a transparent plastic film was used for the membranes to be placed beneath it. In the dark room, the membranes were exposed to an X-ray film, which were developed using the machine (Compact X4, Xograph).

2.5 Primary antibodies

Table displaying the specifications of the primary antibodies used.

Antibody Name	Species	Type	Dilution	Diluted in	Company	Country	APPLICATIONS
Hsp70	Mouse	Monoclonal	1:1,000	PBST-MILK	StressMarq	York, UK	WB
Hsp90	Mouse	Monoclonal	1:5,000	PBST-MILK	BD Biosciences	New Jersey, USA	WB
HER2	Rabbit	Polyclonal	1:500	PBST-MILK	Millipore	California, USA	WB
RAF1	Rabbit	Polyclonal	1:200	PBST-MILK	Santa Cruz	California, USA	WB
HSF1	Rabbit	Polyclonal	1:1,000	PBST-BSA	Enzo Life Sciences	Exeter, UK	WB
HSF1	Mouse	Monoclonal	1:1,000	PBST-BSA	Santa Cruz	California, USA	WB, IP, IF
HSF1 pS326	Rabbit	Monoclonal	1:10,000	PBST-BSA	Abcam	Cambridge, UK	WB
p38 MAPK	Rabbit	Polyclonal	1:1,000	PBST-BSA	Cell Signaling	Massachusetts, USA	WB
pp38 MAPK	Rabbit	Polyclonal	1:1,000	PBST-BSA	Cell Signaling	Massachusetts, USA	WB
p38α MAPK	Rabbit	Polyclonal	1:1,000	PBST-BSA	Cell Signaling	Massachusetts, USA	WB
p38β MAPK	Rabbit	Polyclonal	1:1,000	PBST-BSA	Cell Signaling	Massachusetts, USA	WB
p38γ MAPK	Rabbit	Polyclonal	1:1,000	PBST-BSA	DSTT	Dundee, UK	WB
p38δ MAPK	Rabbit	Polyclonal	1:1,000	PBST-BSA	Cell Signaling	Massachusetts, USA	WB
MK2 pT334	Rabbit	Polyclonal	1:1,000	PBST-BSA	Cell Signaling	Massachusetts, USA	WB
S6 pS235/236	Rabbit	Polyclonal	1:1,000	PBST-BSA	Cell Signaling	Massachusetts, USA	WB
ERK1/2	Rabbit	Monoclonal	1:800	PBS-NGS	Cell Signaling	Massachusetts, USA	IF
JNK1/2	Rabbit	Polyclonal	1:1,000	PBST-BSA	Cell Signaling	Massachusetts, USA	WB
pJNK1/2	Rabbit	Polyclonal	1:1,000	PBST-BSA	Cell Signaling	Massachusetts, USA	WB
pERK1/2	Rabbit	Polyclonal	1:1,000	PBST-BSA	Cell Signaling	Massachusetts, USA	WB
GAPDH	Rabbit	Polyclonal	1:5,000	PBST-MILK	Sigma	Dorset, UK	WB
β-actin	Mouse	Monoclonal	1:10,000	PBST-MILK	Sigma	Dorset, UK	WB
HRP-β-actin	Mouse	Monoclonal	1:40,000	PBST-MILK	Sigma	Dorset, UK	WB
α-tubulin	Mouse	Monoclonal	1:5,000	TBST-MILK	Cell Signaling	Massachusetts, USA	WB, IF
NRF2	Rat	Monoclonal	1:100	TBST	Yamamoto Lab	Sendai, Japan	WB
KEAP1	Rat	Monoclonal	1:100	TBST-MILK	Yamamoto Lab	Sendai, Japan	WB
HA	Rat	Monoclonal	1:1,000	TBST-MILK	Roche	California, USA	WB

Antibody dilution solutions are as follows:

PBST: 0.1% (v/v) Tween 20 dissolved in PBS

PBST-milk: 5% milk (Marvel) (w/v) dissolved in PBST

PBST-BSA: 1% bovine serum albumin (BSA) dissolved in PBST

PBS-NGS: 2.5% (v/v) normal goat serum (NGS) in PBS

TBST: 0.1% (v/v) Tween 20 dissolved in TBS

PBST-milk: 5% milk (Marvel) (w/v) dissolved in TBST

2.6 Nuclear-cytoplasmic separation

MDA-MB-231 cells (10^6 per dish) were plated in 6-cm dishes and treated for the indicated periods of time with 0.1% (v/v) acetonitrile or PEITC. The REAP method described by Suzuki et al. was used to obtain separate cytoplasmic and nuclear fractions (Suzuki et al., 2010). In short, cells were washed twice with ice-cold phosphate buffered saline (PBS, pH 7.5), collected in 500 µl of ice-cold PBS,

transferred to Eppendorf tubes, and subjected to centrifugation at 10,000 x g for 30 sec at room temperature. Next, the supernatant was discarded and the pellet was resuspended in 450 µl of ice-cold 0.1% IGEPAL (v/v) in PBS. The lysates were then subjected to a further centrifugation at 10,000 x g for 30 sec at room temperature. The supernatant was collected as the cytoplasmic fraction. One volume of 5X sample SDS loading buffer [250 mM Tris-Cl pH 6.8, 10% (v/v) sodium dodecyl sulphate, 50% (v/v) glycerol and 0.025% (w/v) bromophenol blue] was added to four volumes of the cytoplasmic fraction and the samples were heated for 5 min at 100^{o}C and subjected to SDS/PAGE. The remaining pellet containing the nuclear fraction was washed twice with ice cold 0.1% IGEPAL (v/v) in PBS and dissolved in 1X sample loading buffer [50 mM Tris-Cl pH 6.8, 2% (v/v) sodium dodecyl sulphate, 10% (v/v) glycerol and 0.005% (w/v) bromophenol blue] and heated for 5 min at 100^{o}C. The nuclear fractions were sonicated before subjecting them to SDS-PAGE.

2.7 Quantitative real-time PCR

The primers and probes for quantifying the levels of the mRNA species were from Applied Biosystems (hspa1a: Mm01159846_s1; HER2: HS01001580_m1 and RAF1: HS00234119_m1). Cells (2 x 10^5 per well) were seeded in 6-well plates. After 24 h, the cells were exposed to vehicle (0.1% acetonitrile) or PEITC for a further 8 (MEFs) or 16 h (MEFs and MDA-MB-231 cells). After cell lysis, total RNA was extracted using RNeasy Kit (Qiagen Ltd.), and 500 ng total RNA was reverse transcribed into cDNA with Omniscript Reverse Transcription Kit (Qiagen Ltd.). Real-time PCR was performed on Applied Biosystems 7900HT Fast Real-Time PCR System. The data were normalized using β-actin (mouse ACTB,

Applied Biosystems, Mm00607939_s1) as an internal control. Real-time PCR experiments shown in Section 3, Chapter 1 were performed in Professor Masayuki Yamamoto's Lab in Sendai, Japan.

2.8 Luciferase assay

HeLa-HSE-luc cells (10^5 per well) were seeded in each well of a 24-well plate, and 24 h later treated with PEITC or 0.1% (v/v) acetonitrile vehicle for 8-, 16-, 24-, or 48 h. Cells were washed twice with 0.1% PBS, and 100 µl of 1X reporter lysis buffer (Promega) was added to each well. The plate was placed at -20°C for a minimum for 2 h, and then transferred to thaw on a shaker at room temperature for 30 min. Cell lysates were collected into Eppendorf tubes and subjected to centrifugation at 15,000 x g for 2 min at 4°C. Luciferase activity was measured in 10 µl of cell lysate in opaque 96-well plates (Corning) using a microplate-reader based luminometer (Orion II, Berthold), and normalized for protein concentration determined by the Bradford's assay (BioRad).

2.9 ATP-binding assay

MDA-MB-231 cells (0.5 x 10^6 per dish) were seeded in 6-cm dishes. After 24 h, the cells were treated for a further 24 h with 0.1% acetonitrile as the vehicle control for sulfoxythiocarbamate alkyne (STCA, 75 µM) and PEITC (20 µM) treatments, or with 0.1% DMSO as the vehicle control for the geldanamycin (GA, 1 µM) and celastrol (CL, 0.8 µM) treatments. Cells were harvested by scraping into 300 µl of lysis buffer [10 mM Tris pH 7.5, 150 mM NaCl, 0.25% IGEPAL, with one protease inhibitor tablet (Roche) per 10.0 ml of buffer], frozen, thawed, and lysed for 30 min at 4°C. ATP-agarose beads (Jena Bioscience) were washed with

the incubation buffer (10 mM Tris pH 7.5, 150 mM NaCl, 20 mM $MgCl_2$, 0.05% IGEPAL, 1 mM DTT). Cell lysates (200 µg total protein) were added to a suspension of 30 µl of beads in 1.25 ml of buffer, and the samples were incubated rotating overnight at 4°C. The beads were collected by centrifugation and washed three times with the incubation buffer. 5 X SDS loading buffer (10 µl) and incubation buffer (40 µl) were added to the beads, and the samples were incubated for 5 min at 100°C. The beads were pelleted by centrifugation, and the supernatants were collected and subjected to western blot analysis.

2.10 Detection of HSF1 trimerization

MDA-MB-231 (2 x 10^6 per dish) cells were grown on 10-cm dishes for 24 h and treated with 0.1% acetonitrile or 20 µM PEITC for a further 3 h. Cells were then washed twice with PBS. 10 ml of 0.4% paraformaldehyde (w/v) in PBS (0.4% PFA-PBS) was added to the dishes over 10 min, where fresh 0.4% PFA-PBS was added every 5 min. Next, the PFA-PBS was removed and the reaction was quenched with the addition of 3 ml of ice-cold 1.25 M Glycine-PBS. After washing twice with PBS, nuclear and cytoplasmic fractions were obtained. Cells were lysed in buffer A [10 mM KCl, 5 mM $MgCl_2$, 50 mM Tris-Cl pH 7.5, 0.5% (v/v) IGEPAL, 1 mM DTT, one EDTA-free complete mini protease inhibitor cocktail tablet (Roche) and one phos-STOP tablet (Roche) per 10 ml of buffer]. The lysates were subjected to centrifugation at 1,000 x g for 5 min at 4^{o}C. The supernatant containing the cytoplasmic fraction was transferred to a fresh Eppendorf tube where one volume of 5X SDS sample loading buffer was added to four volumes of the cytoplasmic fraction. The pellet containing the nuclear fraction was washed three times with the buffer A before dissolving it in 1X

sample loading buffer [50 mM Tris-Cl pH 7.4, 2% (w/v) SDS, 10% (v/v) glycerol, and 0.005% (w/v) bromophenol blue]. The nuclear fractions were subjected to sonication. Both the cytoplasmic and the nuclear fractions were subjected to SDS-PAGE before immunoblotting.

2.11 Co-immunoprecipitation

MDA-MB-231 cells (4 x 10^6 per dish) were grown on 10-cm dishes for 24 h, and the treated with 0.1% DMSO or 20 μM PEITC for 45 min. The dishes with cells were placed on ice and washed twice with ice-cold PBS. Protein G Dynabeads (30 μl slurry, from Invitrogen) were washed twice for 5 min with PBS and incubated with 1 μg of mouse monoclonal HSF1 antibody (Santa Cruz) for 1 h at room temperature, after which the beads were washed three times every 10 min with PBS. Cells were lysed with 1.0 ml ice-cold CO-IP buffer (150 mM NaCl, 50 mM Tris-Cl, pH 7.4, 1 mM EDTA, 1% IGEPAL, 0.1% w/v sodium deoxycholate) supplemented with one EDTA-free protease cocktail inhibitor tablet (Roche) and one phosphatase inhibitor tablet (PhoSTOP Roche). Cell lysates were passed through a 23-gauge needle 10 times before they were clarified by centrifugation at 4°C for 30 min at 16,000 x g. Fifty μl of the clarified lysate (IP sample) was transferred to a fresh Eppendorf tube to serve as an input sample. To pre-clear the IP sample, 30 μl of Protein G Dynabeads slurry was washed twice for 5 min with PBS, and the beads were added to each of the IP sample (containing 0.8-1.0 mg protein), and incubated for 1 h at 4°C on a tube rotator. Subsequently, the Protein G Dynabead-antibody conjugate was added to the pre-cleared IP sample and incubated for 16 h at 4°C on a tube rotator. The immunoprecipitated complexes were washed three times with ice-cold CO-IP buffer every 10 min, and

were eluted from the beads by adding 70 µl of 1X LDS buffer (Invitrogen) and heating the sample at 70°C for 10 min. After cooling, 7 µl of sample reducing agent (SRA, Invitrogen) was added to the sample, and incubated for 15 min at room temperature. Immuproprecipitated proteins (35 µl) were resolved by electrophoresis. Antibodies against Hsp90 (monoclonal, BD Biosciences) and HSF1 (rabbit polyclonal, Enzo Life Sciences) were used for detection of the respective proteins.

2.12 Generation of p38δ and p38ɣ stable knockdown cell lines

p38δ and p38ɣ expression was reduced by RNA interference using Mission shRNA constructs (Sigma; plasmid clone IDs TRCN0000006145 and TRCN0000006147 for p38ɣ and TRCN0000000827 and TRCN0000009979 for p38δ. A lentivirus containing the control pLKO.1 or the shRNA plasmids was used to infect MDA-MB-231 cells. To produce the virus, HEK293T cells were transfected using Lipofectamine 2000 (Invitrogen) with empty pLKO.1-puro vector or the shRNA constructs against p38ɣ or p38δ together with the packaging vectors (psPAX2 and pMD2.G) in serum-reduced medium. On the following day, the medium was replaced with complete DMEM, and after 24 h, the lentivirus-containing supernatant was collected, filtered, and used to transduce MDA-MB-231 cells. Cells containing the shRNA plasmid were selected, expanded and maintained with supplementation of puromycin (2 mg/ml) for approximately three weeks, during which time cell lysates were collected every three to four days to ensure the respective p38 expression levels were reduced throughout the selection period.

2.13 Expression and purification of recombinant hexahistidine-tagged HSF1

Full-length HSF1 cDNA was amplified by PCR from a plasmid obtained from Addgene (Plasmid ID: #32537, in which the cDNA sequence was found to have a nucleotide substitution at position 1343 from a C to T, leading to a change from P to L at position 448 in the protein sequence) and subcloned into the bacterial expression vector pet15b using Nde1 and Xho1. Following transformation into E.coli (BL21(DE3)pLysS), the cells were grown to an optical density at 600 nm of 0.6, and induced for a further 3.5 h at 37°C with 400 mM isopropyl-β-D-thiogalactopyranoside (IPTG). The induced cells were harvested by centrifugation and resuspended in extraction buffer [20 mM Tris-Cl pH 7.9, 150 mM NaCl, 5 mM imidazole and 0.01% (v/v) IGEPAL CA-630]. After freezing and thawing, the cells were disrupted by sonication for 5 min on ice. Cell debris were then cleared by centrifugation at 10,000 x g for 15 min at 4^{o}C. The resultant supernatant was left on ice for 30 min before applying to nickel agarose resin (His-Trap^{TM}HP, GE Healthcare). The resin was washed with 20 mM Tris-Cl pH 7.9, 150 mM NaCl, 5 mM imidazole. The supernatant (20 ml) was then incubated for 1 h at 4°C with 1 ml resin. After three washes with buffer, the protein was eluted with 2 ml of 20 mM Tris-Cl pH 7.9, 150 mM NaCl, 250 mM imidazole. To remove the imidazole, the preparation was dialyzed in 50 mM Tris-Cl pH 7.4, 150 mM NaCl. Mutant S326A HSF1 was generated by site-directed mutagenesis of the plasmid vector pet15b containing the HSF1 cDNA by using the primers 5'-GTGGACACCCTCTTGGCCCCGACCGCCCTCATTG-3' and 5'CAATGAGGGCGGTCGGGGCCAAGAGGGTGTCCAC-3' and the QuikChange® II Mutagenesis kit (Stratagene). The hexahistidine-tagged mutant

S326A HSF1 recombinant protein was generated using the method described above.

2.14 High content microscopy and analysis

HSF1-knockout MEFs were seeded in black-walled 96-well plates (Corning Costar 3904) at 4 x 10^3 cells/well and transfected with 50ng/well GFP-tagged wild-type or S326A or S326E mutants of HSF1 using Lipofectamine LTX reagent (Invitrogen), using 8 replicate wells per condition. Twenty-four hours after transfection, cells were fixed using 4% paraformaldehyde in PBS for 10 min at room temperature, and permeabilised using methanol at -20°C for 5 min. Cells were blocked using 2.5% normal goat serum in PBS/0.1% sodium azide, and counterstained using rabbit anti-ERK1/2 mAb (clone 137F5, Cell Signaling Technology) and Alexa 546 labelled highly cross adsorbed goat anti-rabbit secondary antibody (Invitrogen). DNA was labelled with 300 nM DAPI (Sigma) in PBS and images were acquired using an IN Cell Analyzer 2000 robotic fluorescence microscope (GE Healthcare) using a 20x lens to capture 4 fields per well for each fluorophore (DAPI, GFP and Alexa 546) using 2x2 pixel binning to maximise signal/noise. Images were analyzed using a custom algorithm constructed within IN Cell Developer software (GE Healthcare), using DAPI and ERK1/2 images to identify nuclear and cytoplasmic regions, respectively, in order to assess fluorescence distribution within the GFP channel.

2.15 Kinase assays

The incubation mixtures contained purified recombinant kinase (at a specific activity of either 6 mU/µl or 0.06 mU/µl), recombinant HSF1 (1 µg) substrate, 10

mM $MgCl_2$, 0.1 mM [ɣ-^{32}P]-ATP (approximately 0.5 x 10^6 cpm/nmol), and kinase buffer [50 mM Tris-Cl, 0.03% (v/v) Brij-35, 0.1% (v/v) β-mercaptoethanol] in a total volume of 50 µl. The kinase assays were performed at 30°C. At the times indicated, a 15-µl aliquot of each incubation mixture was removed, the reaction was terminated by the addition of SDS gel loading buffer, the sample was loaded on SDS-PAGE, and the excess [ɣ-^{32}P]-ATP was removed by electrophoresis. The gels were dried and subjected to autoradiography. Protein-containing gel pieces (visualized by staining with Coomassie Brilliant Blue) were then excised, and phosphate incorporation into HSF1 was quantified by scintillation counting. Cold assays were performed in an analogous manner using purified recombinant kinase (at a specific activity of 0.06 mU/µl), recombinant HSF1 (1 µg) substrate, $MgCl_2$ (10 mM), and ATP (0.1 mM) instead of [ɣ-^{32}P]-ATP. For identification of the phosphorylated sites, the gel bands were excised, reduced with DTT (10 mM), alkylated with iodoacetamide (50 mM), and digested overnight (16 h) with trypsin (Modified Sequencing Grade, Roche) at 30°C. The resulting peptides were extracted from the gel, dried in a SpeedVac concentrator (Thermo Scientific), resuspended in 10 µl 5% formic acid, and diluted five times. Any residual particles were removed by centrifugation, the samples were then transferred to HPLC vials, and analyzed by LC/MS/MS on Ultimate3000 RSLCnano System (Thermo Scientific) coupled to a LTQ OrbiTrap VelosPro (Thermo Scientific) with EasySpray source. The data files were analyzed with Proteome Discoverer (Ver. 1.4.1) using Mascot (Ver. 2.4.1) as the search engine using Protein specific database (HisTag-HSF1) and IPI-Human (ipi.HUMAN.v3.87) database.

2.16 Generation of HSF1-knockout HeLa cell line

The CRISPR/Cas 9 technology was used in order to knockout endogenous HSF1 in the HeLa cells. The cells were transfected with the either the plasmid pLentiCRISPRv2, which contains sequences coding for Cas9, puromycin resistance or the pLentiCRISPRv2_HSF1, which contains sequences coding for Cas9, puromycin resistance, as well as the guideRNA (gRNA) sequence 5'-GTCCGGGTCGCTCACGA-3', which targets the region within the 1st exon at the 32nd amino acid region (at the translation level). The primers that were used to insert the HSF1 exon1 targeting gRNA into the pLentiCRISPRv2 plasmid were 5'-CCT ATT CCC TCC TTG CTC GAG ATG G-3' (forward) and 5'-CCG ATG TCC TCT GGG GCA TAG-3' (reverse).

HeLa cells (2 x 10^5) were plated in each well of a 6-well plate as transfected with 1.5 µg of plasmid and 4 µl of Lipofectamine 2000 complex. Twenty-four h after transfection, cells containing the pLentiCRISPRv2 or pLentiCRISPRv2_HSF1 were treated with 1 µg/ml of puromycin for a further 48 h. WT HeLa cells comprises of the pooled population of the surviving cells transfected with pLentiCRISPRv2 and treated with puromycin. The surviving cells containing the plasmid pLentiCRISPRv2_HSF1 that were puromycin resistant were replated into 96-well plates using the concentration of 1 cell/well that was achieved using serial dilution. The 96-well plates containing the single clones in each well were left to incubate in the 37^{o}C humidified incubator supplemented with 5% CO_2 for a further 2-3 weeks and were checked frequently.

The wells containing only one distinct colony were selected for expansion. Six colonies were selected to be expanded and were subsequently validated by western blotting to ensure that HSF1 was knocked out in these isogenic cell lines.

Five out of these six colonies were positive for HSF1 knockout. Subsequently, the genomic DNA from each isogenic cell line was extracted. Restriction digestion PCR was also conducted to test whether the clones were positive for HSF1 knockout using the forward primer 5'- CAC CGG GTG TCC GGG TCG CTC ACG A-3' and the reverse primer 5'- AAA CTC GTG AGC GAC CCG GAC ACC C-3'. A PCR was conducted in each of the lysates to expand the gRNA targeting region, gRNA was designed where it targeted a site within Exon1 of HSF1 that has a unique restriction digest site, Bst2BI, giving rise to two short (300 bp) fragments. In the event the restriction site was lost, the PCR product would not be able to be cut by this enzyme, further confirming that the pLentiCRISPRv2_HSF1 transfection led to the editing of the endogenous HSF1 DNA sequence to produce a HSF1 mRNA that is unable to be translated into the HSF1 protein. Unfortunately, human HSF1 exon1 region is highly GC-rich, hence, we were not able to amplify this region even though we used different methods and conditions to optimise the PCR.

2.17 Cell viability assay

Wild-type HeLa and HSF1-KO HeLa cells were seeded at a cell density of 5 x 10^3 cells per well of a clear and flat-bottomed 96-well plate (Corning). The cells were treated with 0.1% ACN (vehicle control) and varying concentrations of PEITC for 48 h. Four h before the 48 h treatments, the alamar blue dye (AbdSerotec) was added to the wells. The amount of alamar blue dye that was added is 10% of the total volume of mediawithin each well (100 µl). Therefore, in this experiment, 10 µl of alamar blue (AB) was added to each well. In the same plate, 100 µl of media was added to six empty wells (wells that do not contain any cells); these wells

served as the blank for the experiment. Ten µl of AB was added to each of the blank wells, and the plates are then returned to the humidified 37^{o}C incubator and kept for a further 4 hours after which. The plates were collected from the incubator and read using the plate reader (SpectraMax M2, Molecular Deivces) where the fluorescence in each well of the 96-well plate was measured with excitation wavelength of 560nm and emission of 590nm. The relative fluorescence units (RFU). The RFU values obtained for each of the treatments were averaged and subtracted for $RFU_{background}$ values and plotted. The values obtained were directly proportional to the number of viable cells and were represented as a percentage relative to the vehicle- treated cells, which served as the control.

2.18 Mitotic wash-off

U20S or HeLa cells were grown to a confluency of 70-80% in three 15 cm dishes where they were treated with 1.46 or 0.73 µM taxol, respectively. Following 14-16 h (for U2OS cells) or 12 h (for HeLa cells) of taxol treatment, the dishes were visualized under the microscope to ensure that the taxol treatment caused cells undergoing mitosis to be arrested. Mitotic cells appear rounded and are relatively less attached to the dishes compared to interphase cells exposed to taxol. The mitotic cells were “washed-off’ the dish by gentle pipetting with the media containing the taxol which they were growing in, and were transferred to a 50 ml tube. This step was repeated once more with PBS, and the remaining mitotic cells are washed off and transferred to the same 50 ml tube. The tubes containing the mitotic cells were subjected to centrifugation at 1000 rpm for 5 mins. The pellet obtained was resuspended in PBS and centrifuged once more. Subsequently,

the supernatant was removed and the cells were lysed with the SDS-lysis buffer. The remaining cells on the 15 cm dish represent interphase cells which had been exposed to taxol and were washed twice with PBS and subjected to lysis using SDS-lysis buffer. The protein concentrations are measured in the lysates, which were used for western blotting.

2.19 Immunofluorescence

$2.5x10^5$ U2OS cells ($2.5x10^5$) were seeded on 18mm by 18mm glass coverslips with a 1.5 thickness (VWR) placed in each well of a 6-well plate. Twenty to 24 h later the cells were washed thrice with 37^oC pre-warmed PBS and fixed with pre-warmed 3.7% paraformaldehyde in PBS at 37^oC for 15 min in order to preserve the cytoskeletal structure of the cells. The cells were permeabilised by washing them with 0.1% Triton X-100 in PBS (PBS-Tx) for a further 15 min. During all the fixation steps extra caution was taken so as so prevent the mitotic cells from being dislodged. Next, the cells were placed in blocking solution (3% normal donkey serum in PBS-Tx) for 30 min at room temperature (RT) after which they were incubated with mouse anti-total HSF1 (1:200) (E-4, Santa Cruz) or mouse anti-a-tubulin (1:10000) (DM1A, CST) and rabbit anti-HSF1 pS326 (1:200) (abcam, EP1713Y) antibodies diluted in the blocking solution for 1 – 1.5 h at RT. The cells were subjected to three washes every 5 min using PBS-Tx. Next, the cells were incubated with Alexa Flour 594 nM fluorophore-conjugated anti-rabbit (1:400) and Alexa Fluor 680 nM fluorophore-conjugated anti-mouse (1:400) secondary antibodies (Jackson Immunoresearch) diluted in the blocking solution for 1 h at kept protected from light. Next, the cells were washed three times every 5 min using PBS-Tx and were washed for a further 5 min with PBS. The cells were

incubated with DAPI dissolved in PBS at a final concentration of 2.5 µg/ml for 5 min at RT in the dark. The cells were quickly washed thrice with PBS and were subsequently mounted onto frosted glass slides (VWR) using 30 µl of ProLong gold anti-fade mounting medium (Invitrogen) and let to cure overnight at RT. The following day the samples were analysed and imaged using the confocal microscope (Zeiss LSM 710) (as a single optical section) or the widefield microscope (Deltavision Elite, GE Healthcare) (maximum intensity projection of 25 optical sections obtained with 0.2 µm thickness per section).

2.20 Generation of stable Keap1-knockout Keap1-rescued cell lines

Immortalized KEAP1-knockout (KKO) mouse embryonic fibroblasts (MEFs) were grown in with DMEM (Wako Chemical) with 9% fetal bovine serum (FBS). The PiggyBac transposon system was purchased from System Biosciences Inc. (California, USA) was utilized in KKO MEFs to generate stable cell lines expressing HA-tagged mouse Keap1 (HA-Keap1) by incorporating the cDNA encoding its protein sequence. KKO- MEFs were co-transfected with the PiggyBac expression vector and the plasmid encoding the transposase using electroporation pulsed with 100V for 30 ms. Fourty eight hours to 72 h post-transfection, the KKO-MEFs were selected with 2 mg/ml of puromycin for 1 week up to 10 days. The red fluorescent protein (RFP) expression was used as a marker for HA-KEAP cDNA incorporation and single colonies were isolated. The single colonies that were isolated were expanded and determined for the relative protein expression of endogenous NRF2 as well as HA-KEAP1 levels by western blotting. The generation of individual stable KKO-MEFs cell lines expressing HA-KEAP1 (wild-type, single mutant C151S, double mutant C273W/C288E or triple

mutant C151S/C273W/C288E) was performed by Dr. Ryota Saito in Professor Masayuki Yamamoto's lab at the University of Tohoku in Sendai, Japan.

2.21 Generation of Keap1 knock-in mice

The KEAP1$^{C151S/C151S}$ knock-in mice were generated in Professor Masayuki Yamamoto's lab at the University of Tohoku in Sendai, Japan following the detailed protocol described in the publication by Wang and colleagues (Wang et al., 2013b) and is also briefly explained in Saito et. al (Saito et al., 2015). In short, KEAP1$^{C151S/C151S}$ knock-in mice were generated using the CRISPR/Cas9 technology where B6D2F1 (C57B6 x DBA2) superovulating female mice were mated with B6D2F1 stud males and fertilized embryos were collected. A cocktail of Guide RNA (gRNA), Cas9 mRNA and the donor oligonucleotide were injected into the cytoplasm of fertilized embryos were injected into the pronuclei stage zygotes which were maintained with KSOM mouse embryo media placed in a 37^{o}C humidified incubator with 5% CO_2 in the air until they reached the blastocyst stage which occurred at 3 and a half days. Subsequently, 15 to 25 blastocysts were implanted into pseudopregnant B6D2F1 female mice. The mice containing the mutations on both alleles were crossed with wild-type C57B6 mice to produce heterozygote mice. Mice which were confirmed heterozygotes, were crossed to produce the homozygote KEAP1$^{C151S/C151S}$ mice. The KEAP $^{C151S/C151S}$ mice used at the time of the experiments were maintained for at most two generations by crossing with the wild-type C57B6 mice. Genotyping of mice were performed using real-time PCR (Taqman) to determine whether the mice carried the mutations. The oligos and gRNA sequences are provided upon request. The wild-type mice used in all the experiments were of C57B6 background.

2.22 Peritoneal macrophage isolation

Wild-type or KEAP $^{C151S/C151S}$ mice were injected with 3 ml of 4% thioglycolate solution into their intraperitoneal cavity. 4 days after injection, the peritoneal macrophages (PMφ) were extracted by carefully injecting to the peritoneal cavity and extracting the fluid containing the PMφ. The PMφ were immediately kept on ice and suspended in ice-cold PBS and RPMI without serum and centrifuged twice for 3 min at 1000 rpm. Next, the PMφ cells were resuspended in RPMI 1640 medium supplemented with 10 % FBS, counted, plated in 6-well plates with $1x10^6$ cells per well and placed in a 37^{o}C humidified incubator with 5% CO_2 in air. Within 4 h, the PMφ adheres to the plates and cells were washed twice with PBS before proceeding with further experiments. This procedure is also briefly explained in Saito et. al (Saito et. al, 2015).

2.23 In-cell western (ICW)

MCF7 cells (1×10^4) were seeded in each well of a 96-well plate, and 16 h after seeding, the cells were pre-treated with either the vehicle (0.1% DMSO) or the kinase inhibitors (Aloisine, BIRB796, CDK9I, SB202190 or ZM336372) dissolved in conditioned media for 1 h. Subsequently, the cells were treated with either the vehicle or 20 μM PEITC dissolved in conditioned media for a further 3 h, after which the cells were briefly washed thrice with PBS and fixed with ice-cold (-20^{o}C) methanol for 10 mins in -20^{o}C. Following methanol fixation, the fixed cells were washed three times every 5 mins in PBS, where the last wash was performed with PBS-T [0.1% (v/v) Tween 20 in PBS]. Next, the cells were blocked with 5% PBST-milk [0.1% (v/v) Tween 20, 5% (w/v) milk in PBS] for 1 h at RT. Next, the fixed cells were incubated with HSF1 pS326 primary antibody diluted

1:500 in PBST-milk for 2 h at RT. Following primary antibody incubation, the cells were washed thrice every 10 mins with PBST and were incubated with secondary goat anti-rabbit IRDye 680 nm (LiCOR) antibody diluted 1:800 in PBST-milk for 1 h at RT in the dark. The secondary antibody was removed by washing three times with 10 min intervals. Subsequently, the 96-well plate was scanned and quantified using the LI-COR® Odyssey® Infrared Imaging system. The background values were obtained from wells which contained cells that were not incubated with primary antibody, but were only incubated with the secondary antibody. Background values were subtracted for the quantification of the signal.

2.24 Statistical analysis

Values are means ± 1 SD. The differences between groups were determined by Student's t-test and one-way ANOVA and the analyses were performed using Excel (Microsoft Corp.) and GraphPad Prism 7.

Section 3: Results, Discussion and Conclusions

Chapter 1

Cyanoenone class of compounds are sensed by a specific cysteine residue in KEAP1

3.1.1 Introduction

As, described in Chapter A of Section 1, the KEAP1/NRF2/ARE pathway is at the forefront of cellular defense. Induction of this pathway is protective against various conditions of stress. Conversely, failure to upregulate the pathway leads to increased susceptibility and accelerated disease pathogenesis. Under basal conditions, transcription factor NRF2 is targeted for ubiquitination and proteasomal degradation by a repressor protein KEAP1, a substrate adaptor for Cullin 3-based E3 ubiquitin ligase (CUL3) (**Fig. A2**). Inducers of the pathway chemically modify specific cysteines within KEAP1, leading to loss of repressor function, NRF2 accumulation and enhanced transcription of genes encoding a large network of cytoprotective proteins.

Plant triterpenoids are secondary metabolites that are synthesized by the cyclization of 2,3-oxidosqualene and the mevalonate pathway. Oleanolic acid (3b-hydroxyolean-12-en-28-oic acid) (OA), a pentacyclic triterpenoid found in various plant species, is enriched in the Oleaceae family, especially the olive plant (*Olea europaea*) which it was named after (Castellano et al., 2013, Liu, 1995). Exciting ROS-scavenging (Wang et al., 2010), NRF2-activating (Feng et al., 2011, Reisman et al., 2009, Wang et al., 2010), anti-inflammatory

(Dharmappa et al., 2009, Singh et al., 1992, Cordova et al., 2014, Kim et al., 2014), anti-diabetic (Mukundwa et al., 2016, Wang et al., 2015), chemoprotective (George et al., 2012, Janakiram et al., 2008), hepatoprotective (Kim et al., 2004, Liu et al., 2013, Lu et al., 2014, Liu et al., 1995), neuroprotective (Sarkar et al., 2014, Mabandla et al., 2015, Caltana et al., 2014) as well as microbicidal (Jesus et al., 2015, Jimenez-Arellanes et al., 2013) properties of OA have emerged making it a promising compound for therapeutic use. On the other hand, poor water solubility and high metabolic clearance of OA limits its bioavailability in the body.

Although efforts have been made to improve the bioavailibity of OA, it was the chemical synthesis and biological analyses of its semi-synthetic derivatives that led to major leaps towards its potential use in clinical medicine. In particular, introduction of a cyanoenone group within the structure of the semi-synthetic pentacyclic OA derivative CDDO (2-cyano-3,12-dioxooleana-1, 9(11)-dien-28-oic acid) conferred potent NRF2-antioxidant response inducing and anti-inflammatory activities at low nanomolar concentrations, and the methyl ester analog of CDDO (CDDO-Me, also known as Bardoxolone methyl) significantly improved the estimated glomerular filtration rate of type II diabetic patients (T2DB) with severe chronic kidney disease (CKD) in Phase 2B placebo-controlled clinical trials (Clinicaltrials.gov). CDDO-Me progressed to Phase 3 clinical trials (BEACON study) to treat stage 4 CKD patients with T2DB, however, the trial was terminated one year later due to the escalation in the number of heart-related adverse events such as cardiovascular-related hospitalizations and deaths in the drug-treated group (Clinicaltrials.gov). To find an explanation for the

possible reasons for adverse cardiovascular events, further analyses on the primary outcome of this trial showed that CDDO-Me affected the endothelin pathway, increased sodium and fluid retention and elevated blood pressure (Chin et al., 2014). Apart from the adverse effects of CDDO-Me reported from these studies, one should appreciate the progress made towards the implementation of CDDO-Me in clinical medicine, which also highlights the need for synthesizing and testing new derivative compounds of oleanolic acid to improve the safety profile of the drug whilst retaining its powerful medicinal properties.

The cyanoenones, such as CDDO-Me, are the most potent NRF2 activators known. Cyanoenones bind to KEAP1 covalently and reversibly, and are suitable for chronic *in vivo* administration. However, the cysteine sensor for these compounds has not been established. Among the cysteine sensors of KEAP1, C151 in the BTB domain and C273 and C288 in the intervening region, are best characterized. In this study using KEAP1-knockout mouse embryonic fibroblasts (MEFs) rescued with wild-type (WT) or cysteine mutants of KEAP1, we tested a series of cyanoenones, and identified C151 as their main cysteine sensor.

3.1.2 RTA-408

The pentacyclic cyanoenone RTA-408 [N-(11-cyano-2,2,6a,6b,9,9,12a-heptmethyl-10,14-dioxo-1,3,4,5,6a,6b,7,8,8a,9,10,12a,14,14a,14b-hexadecahydro-2H-picen-4a-yl)-2-2-difluoro-propionamide, omaveloxolone] (**Fig. 1.1A**) is a semi-synthetic oleanane triterpenoid produced by Reata Pharmaceuticals (Irving, TX) (Reisman et al., 2014). The nonenolizable cyanonoenone in ring A of RTA-408 is a Michael acceptor which reacts readily with the sulfhydryl groups of cysteine moieties on proteins, particularly the substrate adaptor protein KEAP1, causing loss of its function and activation of transcription factor NRF2. RTA-408 is a potent NRF2 activator with a CD value (Concentration that Doubles the specific enzyme activity of the NRF2-target NQO1) of 2.5 nM in murine Hepa1c1c7 cells (Maureen Higgins, unpublished).

Topical application of RTA-408 has been found to protect mice from dermatitis caused by exposure to ionizing radiation by activating the NRF2-mediated antioxidant response and also by inhibiting the pro-inflammatory transcription factor nuclear factor-kappa b (NF-κB) mediated pathways (Reisman et al., 2014). In this study by Reisman and colleagues, RTA-408 lotion (at doses of 0.01%, 0.1% or 1%) was topically applied once daily on the skin of irradiated mice for 35 days, and at the end of the study, the researchers saw striking improvements in the appearance of the skin, which occurred in a dose-dependent manner. They also found that the group of mice treated with the highest concentration of RTA-408 did not present with dermal necrosis and had completely healed skin ulcers and hair regrowth (Reisman et al., 2014).

RTA-408 has also been shown to confer cytoprotection in the small intestine of mice exposed to lethal doses of radiation by promoting the survival of crypt cells (Alexeev et al., 2014). Additionally, in the same study, the authors found that RTA-408 selectively inhibited the growth of prostate cancer xenografts in mice whilst leaving the growth and survival of normal tissues unaffected (Alexeev et al., 2014) highlighting the potential for use in chemoradiation therapies.

Oxidative stress-induced injury in retinal pigment epithelial (RPE) cells has been implicated in the disease pathogenesis of age-related macular degeneration (AMD) (Lu et al., 2006). Liu *et al.* have shown that pre-treatment of RPE cells with RTA-408 protected them from hydrogen peroxide (H_2O_2)-induced oxidative stress through the activation of NRF2-antioxidant response pathway (Liu et al., 2015).

Parkinson's disease (PD) is the second most common neurodegenerative disease which affects 1-2% of the human population (Pickrell and Youle, 2015). There is no known cure for PD and the only available treatment options provide symptomatic relief with no amelioration of the disease progression. Mitochondrial dysfunction has been associated with PD pathogenesis and mitochondrial quality control is vital for disease progression. Mutations in the mitochondrial serine/threonine PTEN-induced putative kinase 1 (PINK1) have been implicated in hereditary juvenile PD. PINK1 accumulates on the outer membrane of dysfunctional mitochondria and activates Parkin, an E3 ubiquitin ligase, by phosphorylating it. PINK1-activated Parkin ubiquitinates the damaged

mitochondria and targets them for mitophagy (Geisler et al., 2010, Narendra et al., 2008). In PD, mutations in PINK1, prevents the recruitment of Parkin to the damaged mitochondria, hence, the cell is unable to degrade the dysfunctional mitochondria. In primary co-cultures of midbrain neurons and astrocytes of PINK1 knockout mice or NRF2 knockout mice which usually exhibit mitochondrial dysfunction, Dinkova-Kostova *et al.* showed that RTA-408 treatment reinstated the mitochondrial membrane potential (Dinkova-Kostova et al., 2015). They also showed that NRF2 activation by RTA-408 ameliorated dopamine-induced neurotoxicity in the primary co-cultures (Dinkova-Kostova et al., 2015). This study highlights the potential of RTA-408 as a drug that could be used to treat patients with PD to prevent disease progression.

More recently, in a Phase 1 clinical trial (https://clinicaltrials.gov/ct2/show/NCT02029716), in one group, RTA-408 lotion (0.5%, 1% and 3%) was applied twice daily on healthy human volunteers (male and female) aged 18-65 years old (Reisman et al., 2015) for two weeks on 4 cm^2 sites. In another group, 3% RTA-408 lotion was applied twice daily to 100 cm^2 sites or 500 cm^2 sites for two weeks and four weeks respectively (Reisman et al., 2015). At the end of the human study, it was established that application of RTA-408 lotion was well-tolerated at the highest concentration with the highest surface area and longest duration and that skin biopsies from these healthy volunteers showed upregulation of NQO1, a prototypical marker of NRF2 activation (Reisman et al., 2015).

Thus far, RTA-408 has been investigated in five Phase I clinical trials (Clinicaltrials.gov), including patients with advanced solid tumours, ocular

inflammation and pain, and risk of radiation-induced dermatitis. Currently, three new clinical trials involving treatment with RTA-408 capsules are recruiting patients with either advanced melanoma, mitochondrial myophathy or Friedrich's Ataxia (Clinicaltrials.gov).

3.1.2.1 KEAP1 cysteine 151 is a sensor for RTA-408 *in vitro* and *ex vivo*

As mentioned earlier, there is a growing pool of evidence that RTA-408 is a well-tolerated drug in animals and human that has beneficial effects in various disease models such as cancer, neurodegeneration and inflammation through its potent NRF2-activating capability and anti-inflammatory properties. The cysteine sensor(s) of KEAP1 which is modified by RTA-408 to activate NRF2, to our knowledge, is unknown. Since RTA-408 is being used in several clinical trials, it is vital to understand the underlying molecular mechanism by which it upregulates NRF2. Therefore, we sought to identify the cysteine residue(s) of KEAP1 that is the sensor of RTA-408 to allow for accumulation of NRF2 by using KEAP1 knockout (KKO) mouse embryonic fibroblast (MEF) cells rescued with N-terminally HA tagged mouse WT KEAP1 or cysteine mutants (C151S, C273E/C288W and C151S/C273W/C288W) of KEAP1. **Fig. 1.1B** clearly shows that upon a 3-h exposure to 25 or 50 nM RTA-408, NRF2 is stabilized in the WT and in the double mutant C273W/C288E KEAP1-rescued KKO MEFs (WT-KKO MEFs and C273W/C288E-KKO MEFs respectively). Contrastingly, in the single mutant C151S KEAP1-rescued KKO MEFs (C151S-KKO MEFs) and the triple mutant C151S/C273W/C288W KEAP1-rescued KKO MEFs

FIGURE 1.1

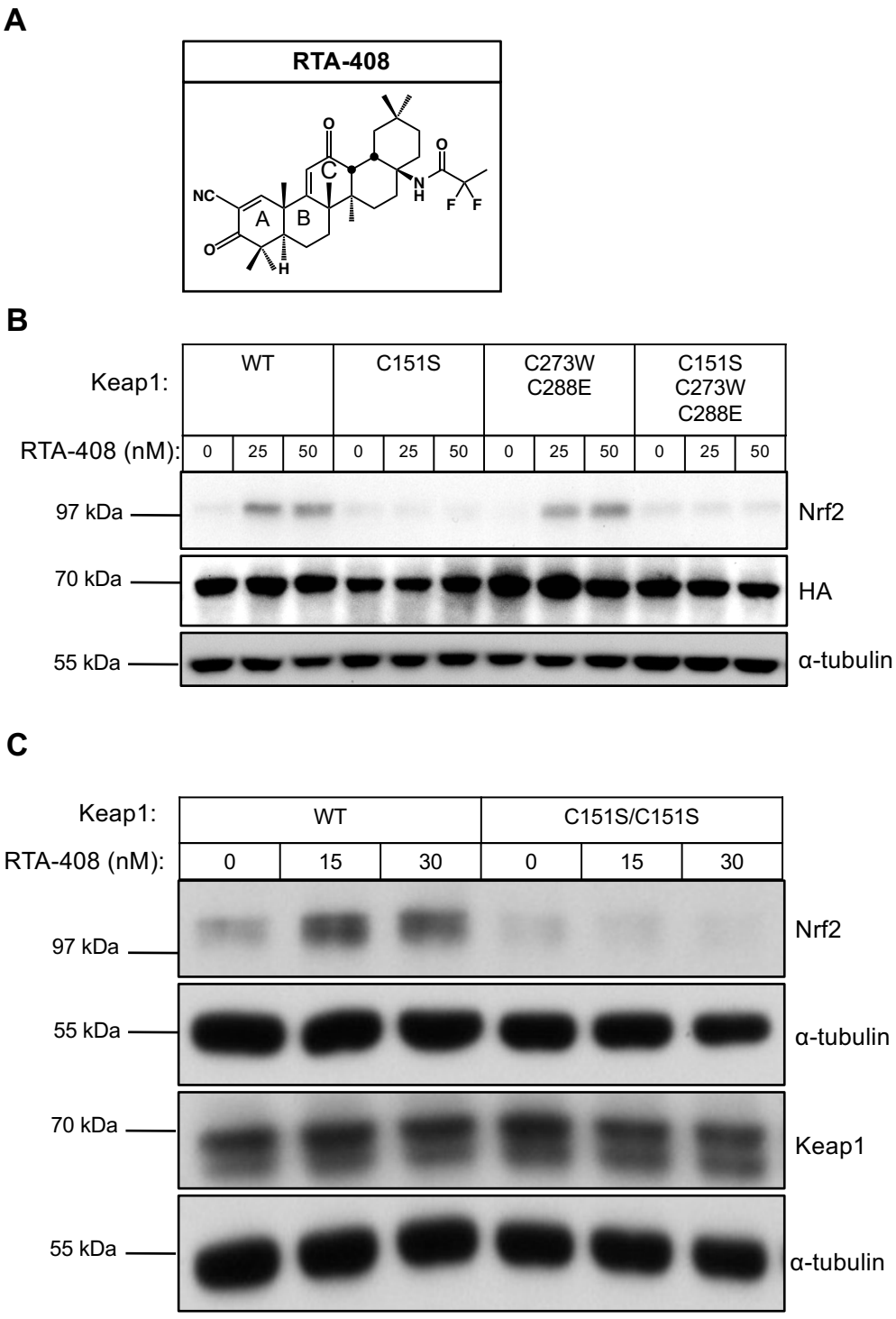

Figure 1.1. KEAP1 C151 is the primary sensor for RTA-408. A) The chemical structure of RTA-408. **B)** Western blot analyses of total cell lysates of KEAP1-knockout MEFs rescued with either wild-type (WT), single cysteine mutant C151S, double cysteine mutant C273W/C288E or triple cysteine mutant C151S/C273W/C288E of mouse N-terminally tagged HA-KEAP1. Cells were exposed to vehicle (0.1% DMSO) or varying concentrations of RTA-408 for 3 h after which the cells were lysed. Immunoblotting was performed on cell lysates using NRF2, HA and α-tubulin antibodies. **C)** Western blot analysis performed on total cell lysates of primary (WT) or $Keap^{C151S/C151S}$ mouse peritoneal macrophages that were treated with vehicle (0.1% DMSO) or varying concentrations of RTA-408 for 3 h. NRF2, KEAP1 and alpha-α-tubulin antibodies were used for detection. The data in this figure are representative of two independent experiments.

(C151S/C273W/C288W-KKO MEFs), these concentrations of RTA-408 are unable to cause the accumulation of NRF2 (**Fig. 1.1B**). Exposure to 15 or 30 nM RTA-408 of primary peritoneal macrophage (PMφ) cells isolated from wild-type C57B or from C57B/BDF1 KEAP1$^{C151S/C151S}$ knock-in mice generated using the CRISPR/Cas9 technology (**Fig. 1.1C**) also shows that NRF2 upregulation, at these concentrations, only occurs in the WT PMφ cells, but not in the KEAP1$^{C151S/C151S}$ PMφ cells. Taken together, these results establish that KEAP1 C151 is the primary sensor for RTA-408.

3.1.3 TBE-31

The acetylinic tricyclic bis(cyanoenone) (±)-(4b*S*,8a*R*,10a*S*)-10a-ethynyl-4b,8,8-trimethyl-3,7-dioxo-3.4b,7,8,8a,9,10,10a-octahydrophenanthrene-2,6-dicarbonitrile (TBE-31, **Fig. 1.2A**) is known to be one of the most potent inducers of the KEAP1/NRF2/ARE pathway (Kostov et al., 2015, Honda et al., 2011, Liby et al., 2008), with a CD value of 0.9 nM in the murine hepatoma Hepa1c1c7 cells (Zheng et al., 2012). TBE-31 is highly reactive with sulfhydryl groups as it contains two activated Michael acceptors found within the rings A and C (**Fig. 1.2A**) rendering it relatively more potent than most of the compounds in the cyanoenone group. Like RTA-408, TBE-31 has been shown to target KEAP1, hence allowing for activation of the NRF2-mediated antioxidant response. In vitro, TBE-31 binds reversibly to KEAP1 cysteines (Dinkova-Kostova et al. 2010) (Kostov et al., 2015). In various cellular systems and in mice, at low nanomolar concentrations, TBE-31 is able to activate the NRF2-mediated antioxidant response as well as inhibit pro-inflammatory pathways (Liby et al. 2008; Dinkova-Kostova et al. 2010; Kostov et al. 2015; Knatko et al. 2015). It has been reported that 1 nM of TBE-31 is sufficient to suppress nitric oxide (NO) production induced by exposure to interferon gamma (IFNɣ) in RAW 264.7 cells (Zheng et al., 2012).

In 2008, Liby and colleagues showed that exposure of TBE-31 in leukemia cells prevents cell proliferation and causes apoptotic cell death (Liby et al., 2008). They also found that oral administration of TBE-31 in rats protected them from aflatoxin-induced hepatocarcinogenesis by reducing the formation of DNA-aflatoxin adducts as well as the size and number of preneoplastic hepatocellular lesions (Liby et al., 2008) and suggested that this effect was mediated through

the activation of the transcription factor NRF2 and the inhibition of pro-inflammatory pathways. Importantly, it was this study that introduced the potential use of TBE-31 in cancer treatment as a chemotherapeutic and chemopreventive agent.

Solid organ transplant patients have a 65-250 times higher risk of developing cutaneous squamous cell carcinoma (cSCC) compared to the normal healthy population (Jensen et al., 2000, Hartevelt et al., 1990) mainly due to the treatment with immunosuppressive agents (Jiyad et al., 2016). Azathioprine, a purine antimetabolite, is a strong immunosuppressant and is often part of chronic life-long treatment of patients who have undergone solid organ transplant. Azathioprine increases skin photosensitivity to ultraviolet radiation and causes the incorporation of 6-thioguanine (6-TG) nucleotide in DNA of skin cells; upon exposure to ultraviolet radiation, 6-TG incorporated in DNA causes the production of reactive oxygen species (ROS), leading to oxidative stress and subsequent damage to DNA and DNA repair proteins, ultimately increasing the risk of developing cSCC (Zhang et al., 2007, Karran, 2006, Kalra et al., 2012). Since TBE-31 is a potent inducer of the KEAP1/NRF2/ARE pathway and a robust inhibitor of pro-inflammatory responses, in our lab, Kalra *et al.* investigated the effect of using TBE-31 to prevent the abovementioned effects of azathioprine treatment. It was found that at low nanomolar concentrations, TBE-31 protected cells containing 6-TG in their DNA against UVA-induced oxidative stress (Kalra et al., 2012). They also found that topical daily treatment of TBE-31 to the skin reduced the incorporation of 6-TG in mice treated with azathioprine. In a follow-up study, our lab found that compared to WT SKH-1 hairless mice, the incidence, multiplicity and tumour burden of cutaneous tumors formed after chronic

exposure to solar-simulated UV radiation was much lower in KEAP1-knockdown mice where the basal levels of NRF2 are higher and the latter is also constitutively activated (Knatko et al., 2015). Also, a study recently conducted and completed in our lab (Knatko et al. 2016) has shown that in NRF2 knockout / KEAP1 knockdown SKH-1 mice, the tumour incidence, multiplicity and burden after exposure to solar-simulated UV radiation were comparable to their WT counterparts, strongly signifying that NRF2 activation is the primary factor for maintaining a chemopreventive phenotype. Our lab has also found that genetic or TBE-31-mediated activation of NRF2 reduced the pro-inflammatory responses in the skin of mice irradiated with UV. In addition, TBE-31 treatment was well tolerated by the mice in both studies. Furthermore, recently, it was discovered that at concentrations in the sub-micromolar range, TBE-31 inhibits non-small cell lung cancer (NSCLC) cell migration and epithelial mesenchymal transition (EMT) by inhibiting TGF-β dependent actin stress fiber formation and also directly binding to actin, inhibiting its polymerization (Chan et al., 2016), highlighting the potential use of TBE-31 in metastatic cancers.

Taken together, these findings raise the potential for TBE-31 to be used for the treatment of patients suffering from cancer, chronic inflammatory and immunosuppresion-related diseases. Like RTA-408, although TBE-31 has been well-studied in the past eight years, the cysteine sensor in KEAP1 for TBE-31 has not been characterized. Discovering the mechanism by which TBE-31 activates NRF2 through chemical modification of KEAP1 would allow scientists to understand the molecular basis of its cytoprotective effects and potentially advance the use of TBE-31 in human studies.

3.A.3.1 KEAP1 cysteine 151 is the primary sensor for TBE-31 *in vitro* and *ex vivo*

KKO MEF cells stably expressing WT KEAP1 or several cysteine mutants were exposed to low nanomolar concentrations of TBE-31 for 3 h. In the WT-KKO and in the double cysteine mutant C273W/C288E-KKO MEFs, NRF2 accumulated upon treatment with 10 or 50 nM of TBE-31; however, under the same conditions, NRF2 did not accumulate in KKO MEFS harboring the single KEAP1 mutant C151S or the triple mutant C151S/C273W/C288E (**Fig 1.2B and 1.2C**). These results suggest that KEAP1 C151 is the primary sensor for TBE-31-mediated NRF2 upregulation. We also exposed primary WT PMφ and KEAP1$^{C151S/C151S}$ PMφ cells to 15, 30, 60 and 120 nM of TBE-31 for 3 h (**Fig. 1.2D**). In the primary WT PMφ cells, NRF2 accumulation was observed at all of the tested concentrations of TBE-31, whereas, in the primary KEAP1$^{C151S/C151S}$ PMφ cells NRF2 was unable to accumulate when exposed to lower concentrations (15, 30 or 60 nM) of TBE-31 (**Fig. 1.2D**). However, 120 nM TBE-31 (the highest concentration used) was able to cause upregulation of NRF2 in both the primary WT and KEAP1$^{C151S/C151S}$ PMφ cells. This could be due to the fact that the basal levels of KEAP1 proteins in the cells are kept very low, and increasing the concentration of a highly sulfhydryl reactive electrophile like TBE-31 would have saturated the modifications at KEAP1 C151 and the remaining freely available TBE-31 is allowed to target other reactive cysteines within KEAP1. Collectively, the results from Fig. 1.2B-D indicate that KEAP1 C151 is the primary sensor for TBE-31.

FIGURE 1.2

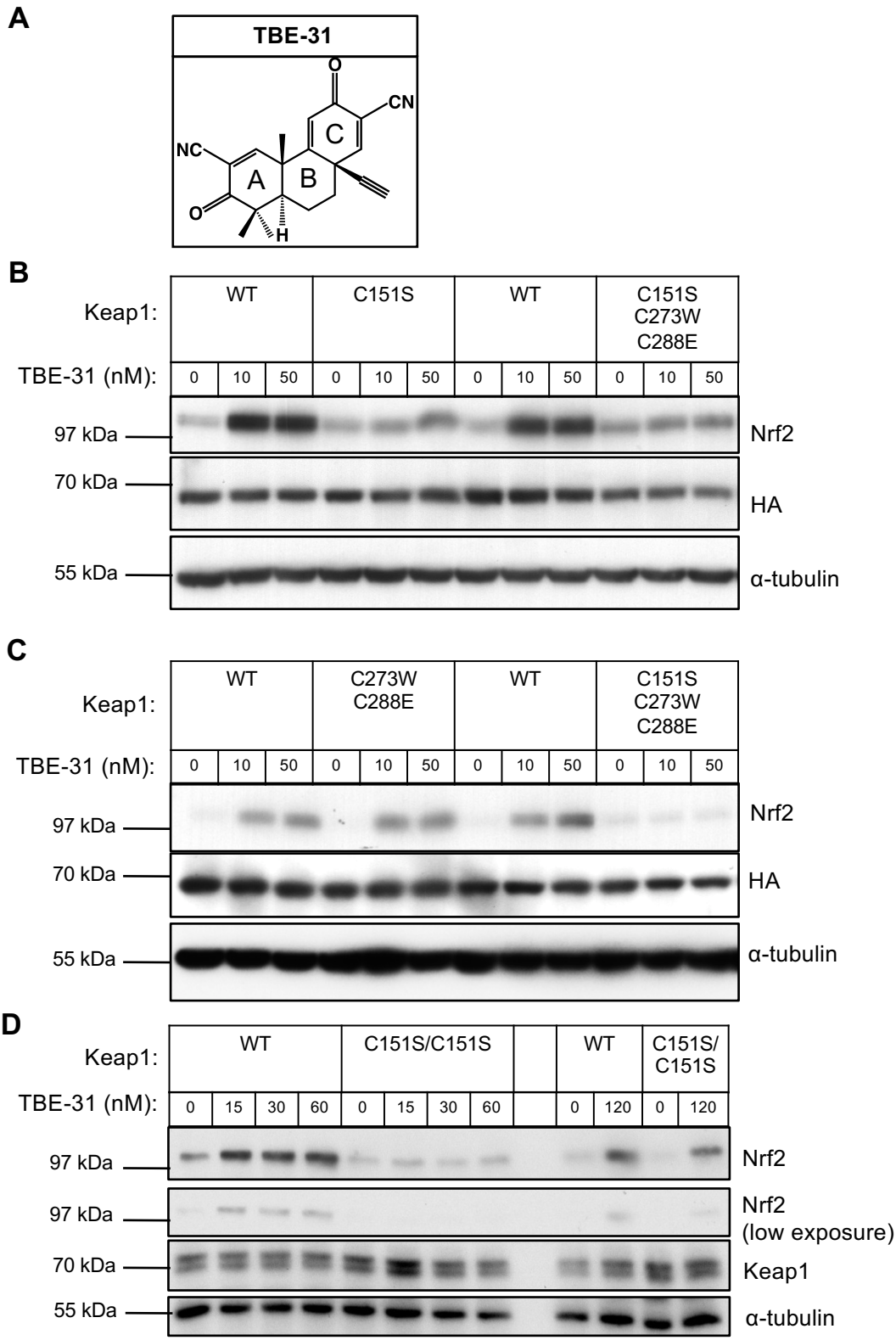

Figure 1.2. KEAP1 C151 is the primary sensor for TBE-31. A) The chemical structure of TBE-31 and its reaction with sulfhydryl groups. **B** and **C**) Western blot analyses of total cell lysates of KEAP1-knockout MEFs rescued with either wild-type (WT), single cysteine mutant C151S, double cysteine mutant C273W/C288E or triple cysteine mutant C151S/C273W/C288E of mouse N-terminally tagged HA-KEAP1. Cells were exposed to vehicle (0.1% DMSO) or varying concentrations of TBE-31 for 3 h after which the cells were lysed. Immunoblotting was performed on cell lysates using NRF2, HA and α-tubulin antibodies. **D**) Western blot analysis performed on total cell lysates of primary (WT) or Keap$^{C151S/C151S}$ mouse peritoneal macrophages that were treated with vehicle (0.1% DMSO) or varying concentrations of TBE-31 for 3 h. NRF2, KEAP1 and α-tubulin antibodies were used for detection. The data in this figure are representative of three independent experiments.

3.A.3.2 TBE-31 is a potent anti-inflammatory agent

Lipopolysaccharide (LPS) is a major component of the outer membrane of Gram-negative bacteria. Exposure of macrophages to LPS initiates toll-like receptor 4 (TLR4), CD14 and myeloid differentiation protein-2 (MD-2) to activate a battery of pro-inflammatory responses which results in the production of inflammatory cytokines such as tumour necrosis factor alpha (TNFα) (Fang et al., 2004, Fujihara et al., 2003). To investigate whether TBE-31, like other compounds in the cyanoenone class such as CDDO-Me and RTA-408, has the ability to repress inflammatory responses, we pretreated primary murine PMφ cells with 10 nM TBE-31 for 24 h, exposed the cells to LPS for a further 4 h, and used real-time PCR to evaluate the effect of TBE-31 on LPS-induced pro-inflammatory genes (**Fig. 1.3B-F**). First, we analyzed the transcript levels of the prototypic NRF2 target gene *NQO1* to assess the degree of activation of NRF2 by TBE-31. From **Fig. 1.3A**, it is evident that there was a significant induction of *NQO1* (14-17 fold) in the primary WT PMφ cells that were exposed to 10 nM TBE-31 for 24 h compared to the vehicle-treated cells. LPS treatment in the vehicle-treated primary PMφ cells resulted in the gene expression of the cytokines *interleukin1-β (IL-1β)*, *interleukin-6 (IL-6)*, *TNFα* as well as *cyclooxygenase 2 (COX2)* and *inducible nitric oxide synthase (iNOS)*. The LPS-induced inflammatory gene expression levels of *IL-1 β*, *IL-6*, *TNFα* and *iNOS* were significantly reduced by 30-60 % with pretreatment of TBE-31 for 24 hours indicating that TBE-31 acts as a powerful anti-inflammatory agent (**Fig. 1.3B-D and 1.3F**).

FIGURE 1.3

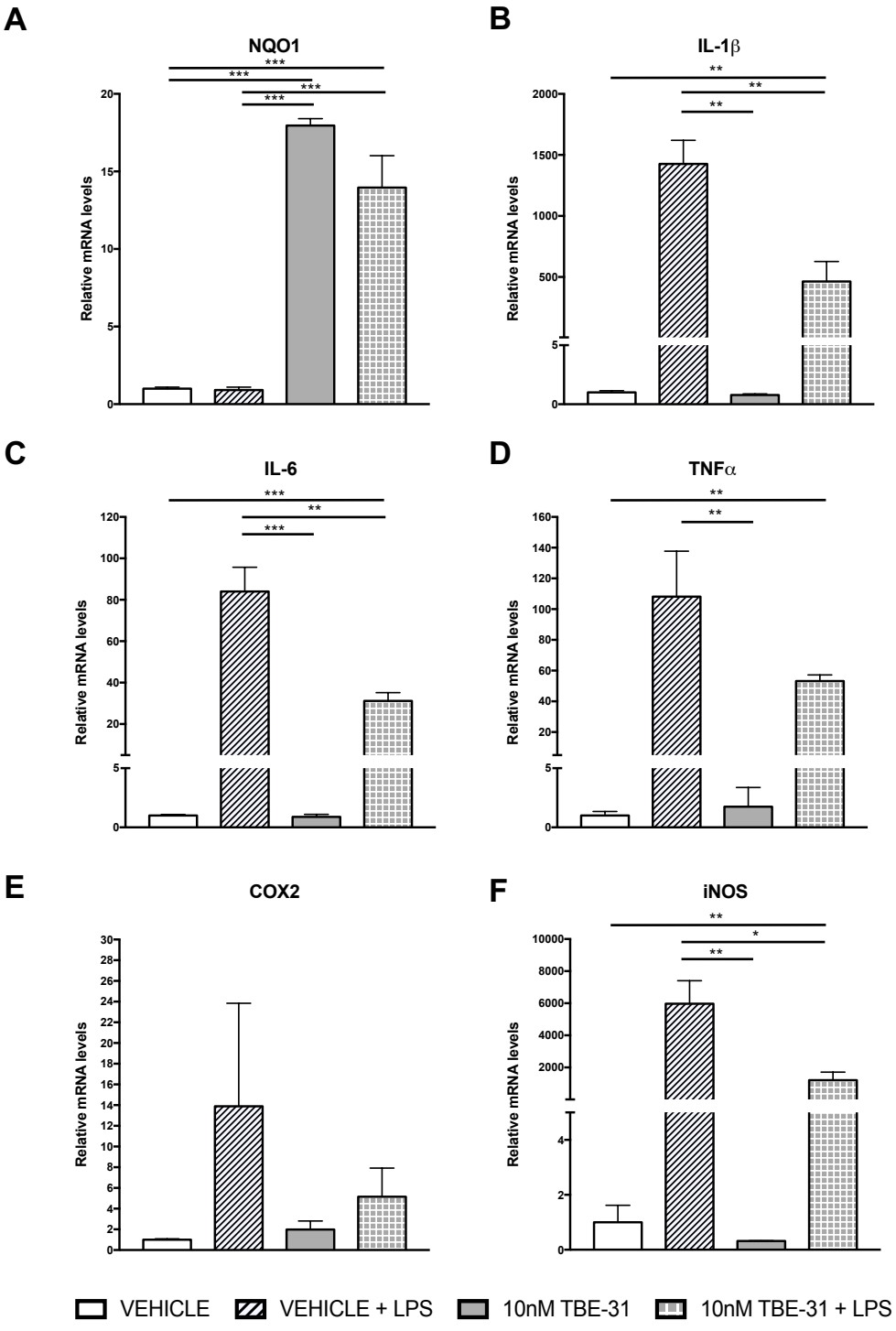

Figure 1.3. TBE-31 suppresses LPS-induced inflammation in WT mouse peritoneal macrophage cells. WT mouse peritoneal macrophages were treated with vehicle (0.1% DMSO) or 10 nM TBE-31 for 24 h and subsequently stimulated with 10 ng/ml of LPS for 4 h. **A-F**) Quantitative real-time PCR analyses showing relative mRNA levels of the NRF2 target gene NQO1 (**A**) and a panel of pro-inflammatory mediators and cytokines, namely, IL-1β (**B**), IL-6 (**C**), TNF-α (**D**), COX-2 (**E**) and iNOS (**F**). Statistical analyses were performed using one-way ANOVA with the Tukey-Kramer post-test; *, ** and *** represent p values lower than 0.05, 0.001 and 0.0001, respectively for triplicate wells. This experiment was conducted once..

3.A.3.3 TBE-31-mediated suppression of inflammation is potentially dependent on KEAP1 C151

To investigate whether TBE-31-mediated suppression of inflammation was dependent on KEAP1 C151, we obtained primary PMφ cells from WT and KEAP1$^{C151S/C151S}$ mice and treated them for 6 h with: (i) vehicle, (ii) vehicle + LPS, (iii) 50 nM TBE-31, and (iv) 50 nM TBE-31 + LPS. We used real-time PCR to measure the changes in gene expression of a panel of pro-inflammatory gene markers as well as the prototypic NRF2 target gene *NQO1*. In the primary WT PMφ cells *NQO1* is robustly upregulated (~10 fold) with the treatment of TBE-31, compared to a modest two-fold induction in the primary KEAP1$^{C151S/C151S}$ PMφ cells (Fig. 4A). In this preliminary experiment, since the cells were co-treated with TBE-31 and LPS for 6 h, a robust anti-inflammatory effect by TBE-31 was not observed when evaluating the expression at the pro-inflammatory genes (**Fig. 1.4C and 1.4D**). However, some of the genes such as *IL-1β* and *TNFα* displayed reduced expression, by 20-30% in the WT PMφ cells co-treated with LPS and TBE-31 compared to WT PMφ cells treated with only LPS. Interestingly, when comparing the same conditions in the KEAP1$^{C151S/C151S}$ PMφ cells, there was no reduction in expression levels of these genes (**Fig. 1.4B and 1.4E**). These preliminary data suggest that the TBE-31-mediated suppression of inflammation is dependent on KEAP1 C151. Due to time-constraints faced in Japan, I was not able to repeat this experiment. However, this experiment described in Fig. 1.4 will have to be conducted in the PMφ cells derived from both the WT and KEAP1$^{C151S/C151S}$ knock-in mice, where a pre-treatment of TBE-31 for 24 hours before exposure to LPS will be essential to allow the cells to show a clear effect

FIGURE 1.4

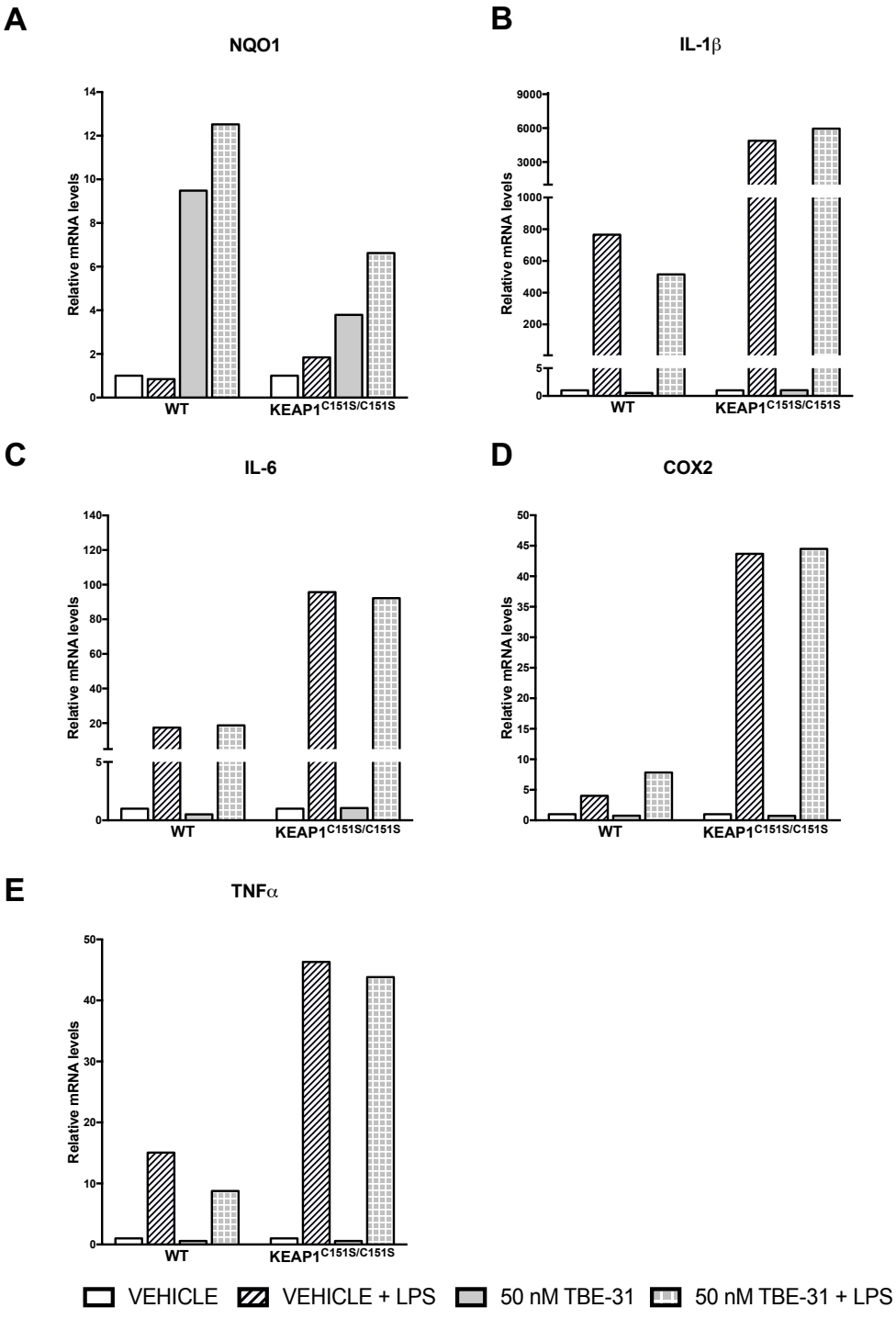

Figure 1.4. NRF2 activation of TBE-31 in mouse peritoneal macrophage cells is primarily through KEAP1 C151. WT or KEAP1$^{C151S/C151S}$ mouse peritoneal macrophages were treated with vehicle (0.1% DMSO) or 50 nM TBE-31 in combination with the presence or absence of 10 ng/ml of LPS for 6 h. **A-E**) Quantitative real-time PCR analyses showing relative mRNA levels of the NRF2 target gene NQO1 (**A**) and a panel of pro-inflammatory mediators and cytokines, namely, IL-1β (**B**), IL-6 (**C**), TNF-α (**D**), COX-2 (**E**). Statistical analyses were performed using one-way ANOVA with the Tukey-Kramer post-test; *, ** and *** represent p values lower than 0.05, 0.001 and 0.0001, respectively for triplicate wells. This experiment was conducted once.

of TBE-31 as an anti-inflammatory agent and be able to conclude whether this protective response observed can be attributed to the presence of C151 on KEAP1.

3.1.3.4 KEAP1$^{C151S/C151S}$ knock-in mice are more susceptible to LPS-induced inflammation than KEAP1 wild-type animals

In the presence of LPS, the gene expression levels of *IL-1β*, *IL-6*, *TNFα*, *COX2* and *iNOS* are greatly induced in both genotypes. Interestingly, WT and KEAP1$^{C151S/C151S}$ PMφ cells differ greatly in the magnitude of induction of LPS-induced inflammatory genes compared to their respective vehicle treatments, where the relative induction in the KEAP1$^{C151S/C151S}$ is 1.5- to 5-fold greater than that of the WT PMφ cells (**Fig. 1.5A-E**). Although the genetic background of the mice are slightly different, as explained in the Methods section, this finding raises the interesting possibility that the KEAP1$^{C151S/C151S}$ mice are more susceptible to inflammatory responses, and more importantly, that C151 of KEAP1 is mediating an anti-inflammatory response through activation of NRF2 thus acting as a central endogenous sensor during pro-inflammatory insults.

FIGURE 1.5

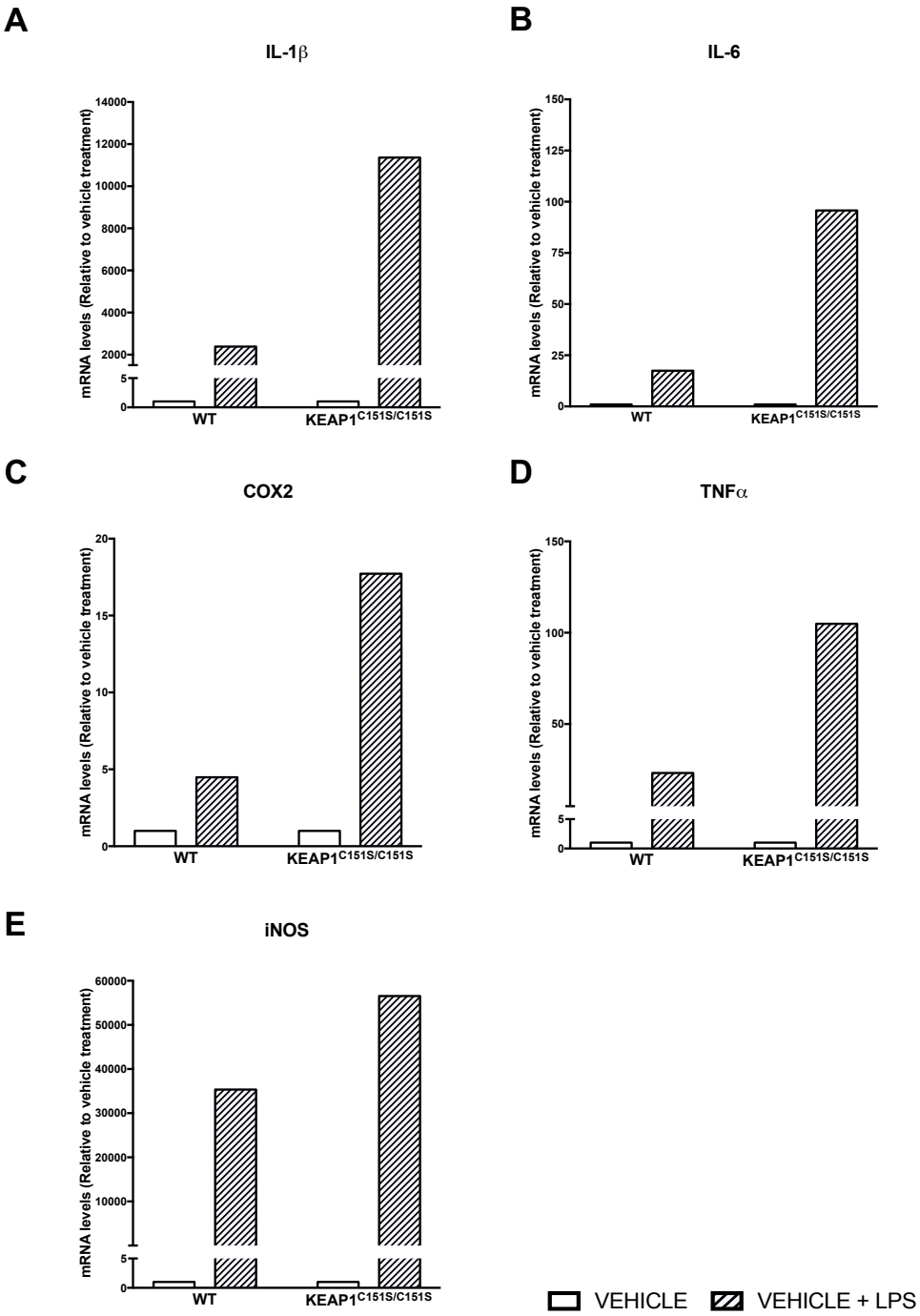

Figure 1.5. KEAP1$^{C151S/C151S}$ mouse peritoneal macrophages are much more sensitive to LPS-induced inflammation than their WT counterparts. WT or KEAP1$^{C151S/C151S}$ mouse peritoneal macrophages were treated with vehicle (0.1% DMSO) or 50 nM TBE-31 in the presence or absence of 10 ng/ml of LPS for 6 h. **A-E**) Quantitative real-time PCR analyses showing relative mRNA levels of a panel of pro-inflammatory mediators and cytokines, namely, IL-1β (**A**), IL-6 (**B**), COX-2 (**C**), TNF-α (**D**), iNOS **(E)**. This figure is representative of two independent experiments.

3.1.4 MCE-23

The cyanoenone MCE-23 [9a-ethynyl-3-oxo-9,9a-dihydro-3H-fluorene-2-carbonitrile] (Fig. 6A) is a tricyclic compound similar to TBE-31 (**Fig. 1.2A**); however, the carbonyl and cyanoenone groups are absent from ring A making MCE-23 comparatively much less reactive and less potent as an NRF2-inducer (CD = 41 nM in Hepa1c1c7 cells). Recently, by use of the crystalline-sponge method Duplan *et al.* have reported the structure of the Michael adduct of MCE-23 with a small molecule thiol (Duplan et al. 2016).

3.1.4.1 KEAP1 cysteine 151 is the primary sensor for MCE-23

To determine the cysteine sensor(s) of KEAP1 for MCE-23, KEAP1 KO MEFs rescued with either WT or cysteine mutants of KEAP1 were treated with 150 nM or 300 nM of MCE-23 for 3 hours (**Fig. 1.6B**). In the WT-KKO and double mutant C273/C288-KKO MEFs, NRF2 accumulated in a dose-dependent manner. On the other hand, treatment of the single mutant C151S-KKO or the triple mutant C151S/C273W/C288E-KKO MEFs, with 150 nM or 300 nM of MCE-23 failed to upregulate NRF2, indicating that C151 is the primary sensor in KEAP1 for this compound. Since, MCE-23 contains only one active reactive center, on ring C, and is sensed by C151 in KEAP1, this result suggests that ring C in TBE-31 is most important for its specificity and reactivity with KEAP1 C151.

FIGURE 1.6

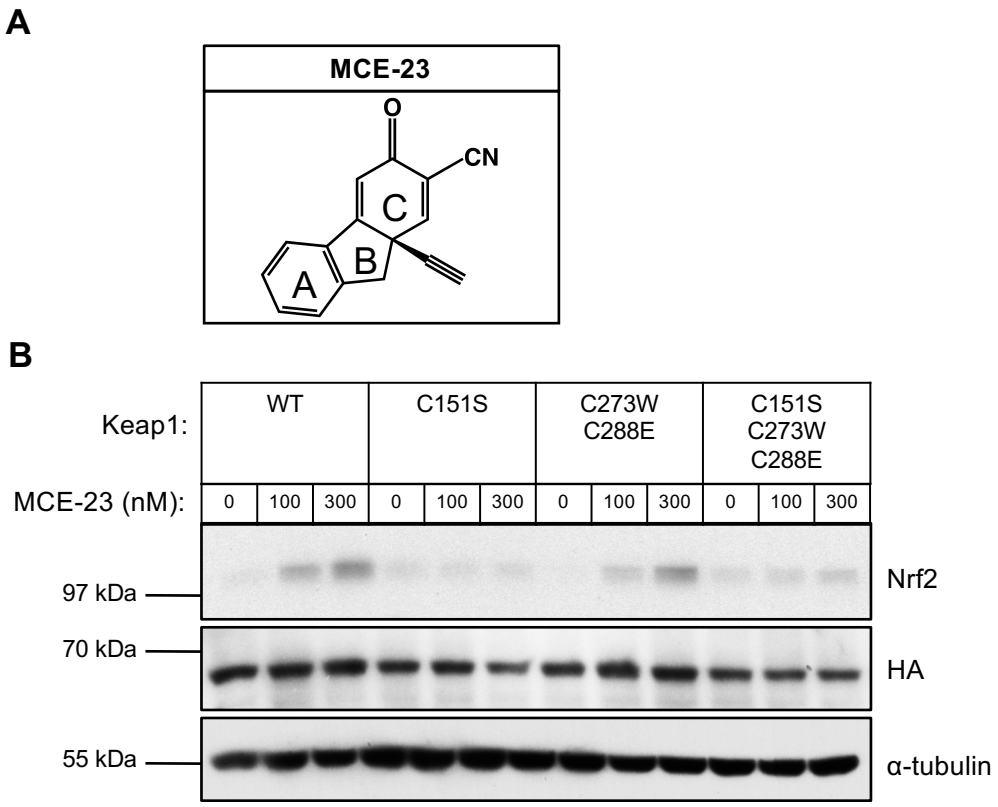

Figure 1.6. KEAP1 C151 is the primary sensor for MCE-23. A) The chemical structure of MCE-23. B) Western blot analyses of total cell lysates of KEAP1-knockout MEFs rescued with either wild-type (WT), single cysteine mutant C151S, double cysteine mutant C273W/C288E or triple cysteine mutant C151S/C273W/C288E of mouse N-terminally tagged HA-KEAP1. Cells were exposed to vehicle (0.1% DMSO) or varying concentrations of MCE-23 for 3 h after which the cells were lysed. Immunoblotting was performed on cell lysates using NRF2, HA and α-tubulin antibodies. The data in this figure are representative of two independent experiments.

3.1.5 MCE-1

The monocyclic cyanoenone MCE-1 (3-ethynyl-3-methyl-6-oxocyclohexa-1,4-dienecarbonitrile) (**Fig. 1.7A**) was derived from ring C of TBE-31 (**Fig. 1.2A and 1.2B**). It has been established that MCE-1 is a highly reactive Michael acceptor and that its addition to thiols is reversible (Dinkova-Kostova et al. 2010; Zheng et al., 2012). Like the other cyanoenones described, MCE-1 is a potent NRF2 inducer with a CD value of 22 nM in Hepa1c1c7 cells (Dinkova-Kostova et al. 2010), and has a strong anti-inflammatory effect in RAW 264.7 cells and primary murine PMφ cells (Zheng et al., 2012). Also, in their studies, Zheng *et al.* found that 5.8 nM of MCE-1 was sufficient to suppress NO production induced by exposure to IFNɣ in RAW 264.7 cells.

3.1.5.1 KEAP1 cysteine 151 is the primary sensor for MCE-1 *in vitro* and *ex vivo*

KKO-MEFs rescued with WT or cysteine mutants of KEAP1 were treated with 50 or 150 nM of MCE-1 for 3 h. The treatment of MCE-1 in the WT-KKO-MEFs as well as in the double mutant C273W/C288E-KKO MEFs caused upregulation of NRF2, whereas, this effect was not observed in the single mutant C151S-KKO MEFs or in the triple mutant C151S/C273W/C288E-KKO MEFs (**Fig. 1.7C**). Moreover, a 3-h exposure to 12.5 or 25 nM of MCE-1 in WT PMφ caused NRF2 accumulation, whilst this effect was not observed in the PMφ KEAP1$^{C151S/C151S}$ cells (**Fig. 1.7C**). These findings confirm that the mechanism of NRF2 activation by MCE-1 is mediated through the sensing by KEAP1 C151S.

FIGURE 1.7

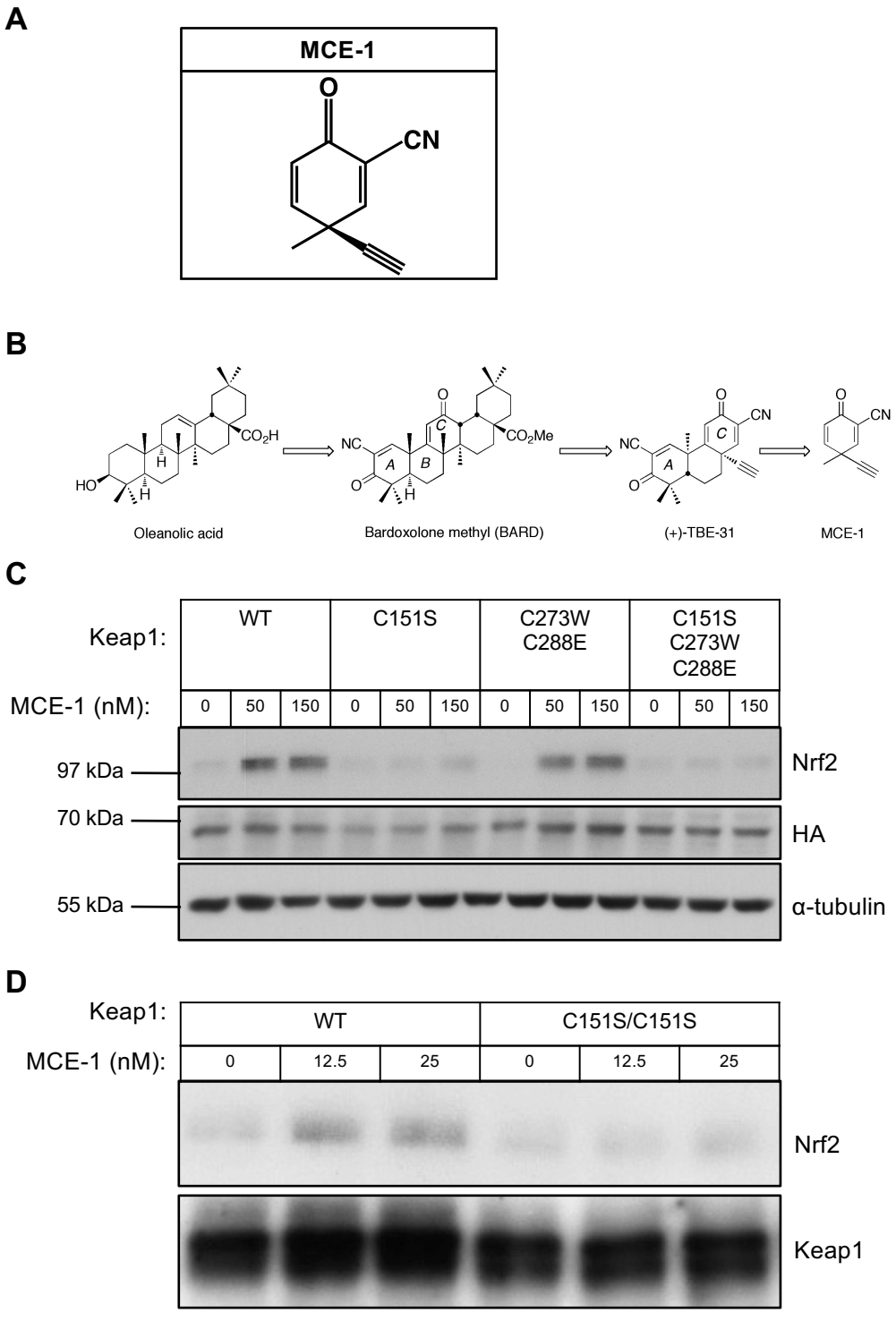

Figure 1.7. KEAP1 C151 is the primary sensor for MCE-1. A) The chemical structure of MCE-1. B) Synthesis of CDDO (Image taken from http://www.stonybrook.edu/commcms/chemistry/faculty/honda.tadashi.html.)
C) Western blot analyses of total cell lysates of KEAP1-knockout MEFs rescued with either wild-type (WT), single cysteine mutant C151S, double cysteine mutant C273W/C288E or triple cysteine mutant C151S/C273W/C288E of mouse N-terminally tagged HA-KEAP1. Cells were exposed to vehicle (0.1% DMSO) or varying concentrations of MCE-1 for 3 h after which the cells were lysed. Immunoblotting was performed on cell lysates using NRF2, HA and α-tubulin antibodies. **D)** Western blot analysis performed on total cell lysates of primary (WT) or $Keap^{C151S/C151S}$ mouse peritoneal macrophages that were treated with vehicle (0.1% DMSO) or varying concentrations of MCE-1 for 3 h. NRF2, KEAP1 and α-tubulin antibodies were used for detection. The data in this figure are representative of two independent experiments.

3.1.6 Conclusions

Activation of the NRF2/KEAP1/ARE pathway is critical for cytoprotection. Although this pathway has been studied extensively, there is still much to discover. In our study, we have shown that all of the cyanonenone compounds tested are able to upregulate NRF2 at low nanomolar concentrations, and are specifically sensed by KEAP1 C151. We have also found that TBE-31 has potent NRF2-inducing and strong anti-inflammatory properties and these properties should be explored further. Another exciting revelation of this study is that KEAP1$^{C151/C151S}$ mice peritoneal macrophages are more sensitive to LPS-induced inflammation, suggesting that C151 is an important endogenous stress sensor, and that the absence of this cysteine may be detrimental to the organism in the face of infections.

It is extraordinary that a 5-ringed molecule like RTA-408 can be reduced in size to a 3-ringed molecule like TBE-31 or MCE-23, which can be further reduced to a single-ringed molecule like MCE-1, and still maintain specificity for the same cysteine sensor in KEAP1, C151. This finding implies that preserving the reactive cyanoenone center is sufficient to confer specificity, and that chemical reactivity (rather than shape or size) is the most important feature of the cyanoenone inducers. Recently, Saito and colleagues reported that the pentacyclic semisynthetic triterpenoid CDDO-Im (1-[2-cyano-3,12-dioxooleana-1,9(11)-dien-28-oyl]imidazole) (**Fig. 1.8A**), an imidazolide derivative of CDDO, is sensed by KEAP1 C151 (Saito et al., 2015). Strikingly, to further support the findings from this and our study, the recently crystallized structure of the human KEAP1 BTB domain in complex with CDDO has shown that the reactive

FIGURE 1.8

A

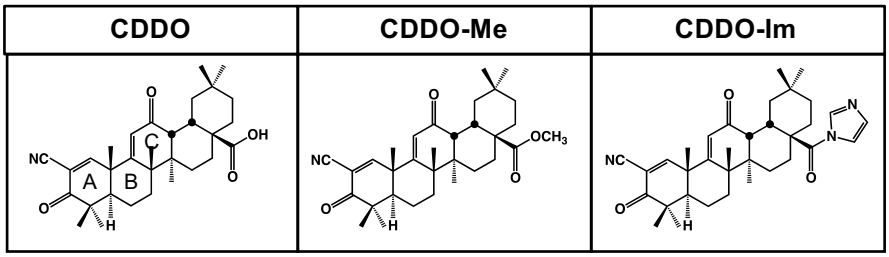

B

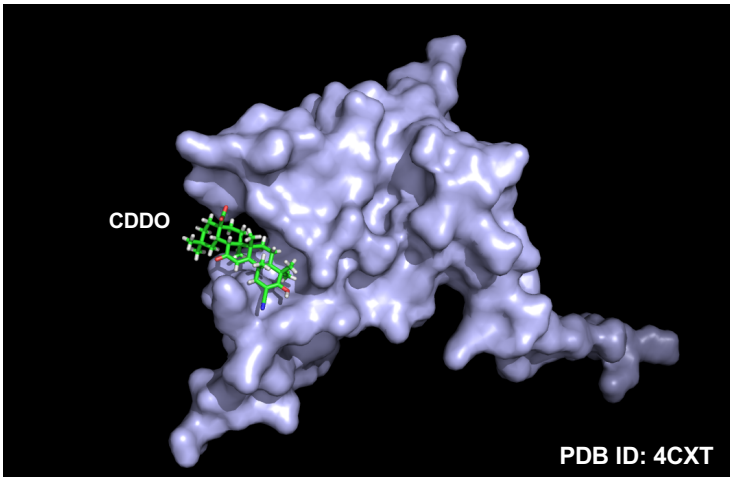

C

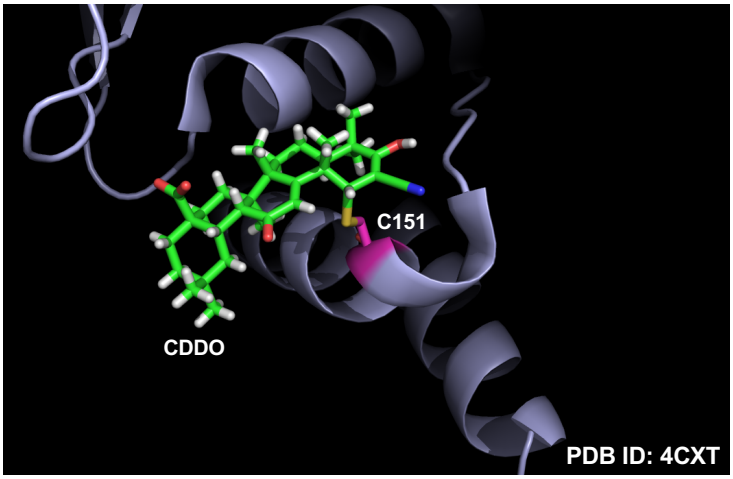

Figure 1.8. Structure of CDDO and its complex with KEAP1 BTB domain. A) The chemical structure of CDDO and its derivatives, CDDO-Me and CDDO-Im **B)** The crystal structure of human KEAP1 BTB domain bound to CDDO **C)** Crystal structure showing C151 of human KEAP1 BTB domain covalently binding to the CDDO compound. Structure drawn using PyMol using PBD entry 4XCT.

cyanoenone center of CDDO (in Ring A) is the only part of the molecule that binds covalently to KEAP1, and that this binding occurs with the C151 residue (Caltana et al., 2014).

Section 3: Results, Discussion and Conclusions

Chapter 2

Heat Shock Factor 1 is a substrate for p38 MAPKs

3.2.1 Phenethyl isothiocyanate (PEITC)

The naturally occurring isothiocyanates are a class of dietary compounds which are secondary metabolites found enriched in plants mostly belonging to the Cruciferae (also called Brassicaceae) family (e.g. Brussels sprouts, broccoli, watercress). In humans, diets rich in cruciferous vegetables are known to be protective against neurodegenerative, cardiovascular and cancer-related diseases. Numerous reports have indicated that these cruciferous vegetables belonging to the *Brassica* genus have many chemopreventive attributes. *Nasturtium officinale* or watercress, a vegetable that belongs to the Cruciferae family, contains a glucosinolate precursor, gluconasturtiin. Phenethyl isothiocyanate (PEITC) is an isothiocyanate (ITC) that is derived from the modification of gluconasturtiin through the participation of myrosinase (a beta-thioglucosidase) during plant tissue injury (Fahey et al., 2001). PEITC has been shown to have promising anticancer properties where it has been shown to prevent human glioblastoma GBM 8401 cell migration and inhibition (Chou et al., 2015). PEITC inhibited tumourigenesis in $Apc^{min/+}$ mice (Khor et al., 2008) and also lowered the tumour incidence in azoxymethane-initiated colon cancer in mice (Cheung et al., 2010). Interestingly, in a very recent case study, a 53-year-old man with end-stage B-cell prolymphocytic leukemia (B-LL), a rare and aggressive disease which is chemoresistant and has a median survival of three

years, was treated concurrently with PEITC for 8 weeks with 6 cycles of R-CHOP (Rituximab, Cyclophosphamide, Hydroxydaunorubicin [doxorubicin hydrochloride], Oncovin [vincristine sulfate], Prednisolone) chemotherapy presented with normal white blood cell count and disease stabilization, allowing the patient to qualify for allogenic peripheral blood stem cell transplant. During the time of publication, 43 months after initial diagnosis and treatment, the patient was reported to be doing well with no occurrence of CD20+ small B-cell. The authors suggested that PEITC sensitized B-LL cells to chemotherapeutic drugs and proposed that PEITC should be used in synergy with other drugs for future treatments (Nachat et al., 2016).

One of the potential mechanisms by which PEITC exerts its anti-tumour effect is possibly through its well-established ability to upregulate the transcription factor Nrf2 by activating the KEAP1/NRF2/ARE pathway. The gluthathione-S-transferases (GSTs), which are well-established transcriptional targets of Nrf2, play vital role in benzene metabolism. A recent publication by Yuan et. al. shows that in PEITC administration in smokers null for *GSTM1* and *GSTT1* exhibited a strong protective effect by enhancing benzene detoxification (Yuan et al., 2016). Another potential mechanism by which PEITC could mediate cytoprotective effects could be due to the upregulation of heat shock proteins. Although there have been many publications demonstrating that PEITC, like many isothiocyanates, is able to activate the KEAP1/NRF2/ARE pathway, the exact mechanism by which it does so is not clear. It has been suggested that PEITC and other isothiocyanates cause Nrf2 stabilisation by modifying cysteine residues in Keap1 to inactivate its function. PEITC is highly cysteine reactive due to the

presence of the electron withdrawing isothiocyanate (N=C=S) group (**Fig. 2.1A**). Therefore, we wanted to identify the cysteine residue(s) in Keap1 that sense(s) PEITC.

3.2.2 PEITC causes stabilisation of NRF2 through reacting with cysteine 151 of KEAP1

We used KEAP1-knockout mouse embryonic fibroblasts (KKO MEFs) rescued with either the wild-type (WT) or the KEAP1 mutants C151S, C273W/C288E and C151S/ C273W/C288E. Exposure to 2.5 and 7.5 μM PEITC caused the stabilisation of Nrf2 in all genotypes regardless of the mutation status of KEAP1 (**Fig 2.1B**). This result suggests that the intracellular concentration of PEITC is much higher than the amount of KEAP1, hence it is able to react with multiple cysteines in Keap1 in order to stabilise NRF2. The same experiment was repeated using lower concentrations of PEITC, and this time it was clear that 2 μM PEITC was sufficient to cause upregulation of NRF2 in the KKO MEFS rescued with either the WT or the double mutant C273W/C288E KEAP1. In contrast, this dose of PEITC was not able to upregulate NRF2 in the KKO MEFs rescued with the single mutant C151S or triple mutant C151S/C273W/C288E KEAP1, indicating that C151 is the main sensor for PEITC (**Fig. 2.1C**). Interestingly, the results from **Fig. 1B and C** suggest that there is a very narrow window of stabilisation of NRF2 by PEITC through KEAP1 C151 between the range of 0.5 μM to 2 μM.

In another experiment, primary peritoneally derived macrophage (PMO) cells from either the WT or KEAP1$^{C151S/C151S}$ mice exposed to concentrations ranging from 0.94 to 7.5 μM of PEITC caused the stabilisation of NRF2 in both genotypes (**Fig. 2.1D**). Primary cells could be more sensitive to PEITC than the immortalised KKO MEFs, hence, lower concentrations should be used in the future to elucidate whether Keap1 C151 is the main sensor for PEITC in the primary PMO cells. Collectively, the results from **Fig 2.1B, C and D** raise the possibility of other Keap1 cysteine(s) potentially sensing PEITC. It is interesting to note that the highest concentration of PEITC (7.5 μM) used causes a significant reduction in the protein levels of tubulin (**Fig. 2.1D**). It has been reported that the isothiocyanates BITC, PEITC and SF covalently modify α-tubulin in cells by reacting with its cysteine residues and as a consequence preventing its polymerisation (Xiao et al., 2012). PEITC has also been reported to cause the degradation of both α and β-tubulin in prostate cancer cells PC3 and that the degradation could be rescued by co-incubation of the antioxidant N-acetyl-L-cysteine (NAC) (Yin et al., 2009). Together, these results confirm that cysteine reactivity underlies the multiple biological activities of PEITC.

We have previously reported that structurally diverse NRF2 activators, all of which react with sulfhydryl groups, induce the heat shock response, and demonstrated the essential requirement for HSF1 (Zhang et al., 2011b). The isothiocyanates represent a prominent class of NRF2 activators, which have shown chemoprotective effects in numerous animal models of chronic disease; some have been and/or currently are in clinical trials (Dinkova-Kostova and Kostov, 2012, Dinkova-Kostova, 2013, Kensler et al., 2012). We therefore

FIGURE 2.1

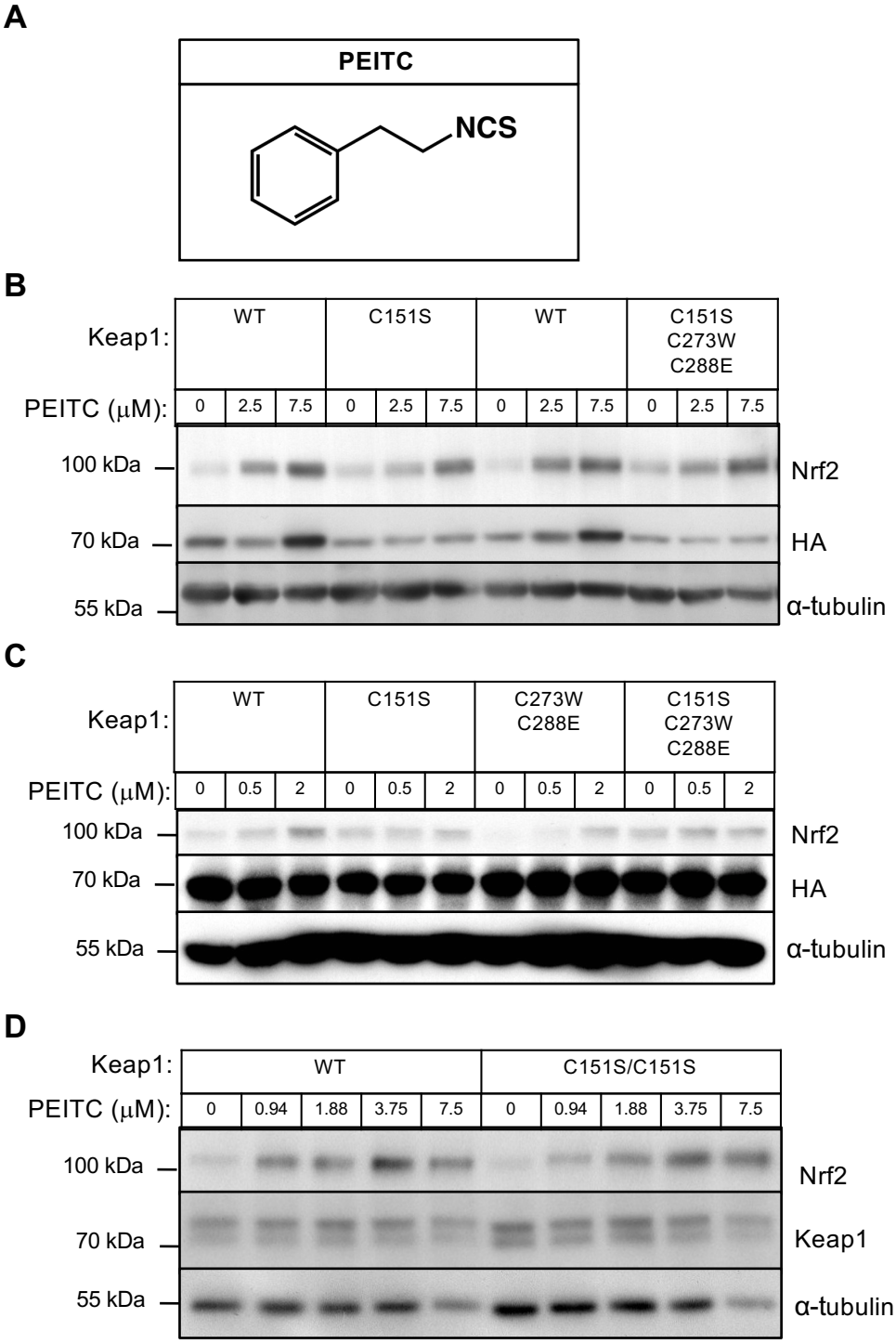

Figure 2.1. KEAP1 C151 is the primary sensor for PEITC. A) The chemical structure of PEITC. **B and C)** Western blot analyses of KEAP1-knockout MEFs rescued with either wild-type (WT), single mutant C151S, double mutant C273W/C288E or triple mutant C151S/C273W/C288E of mouse N-terminally tagged HA-KEAP1 which were exposed to vehicle (0.1% DMSO) or varying concentrations of PEITC for 3 h. Immunoblotting was performed on cell lysates using NRF2, HA and α-tubulin antibodies for detection. **D)** Western blot analysis performed on primary (WT) or $Keap^{C151S/C151S}$ mouse peritoneal macrophages that were treated with vehicle (0.1% DMSO) or varying concentrations of PEITC for 3 h. NRF2, KEAP1 and alpha-tubulin antibodies were used for detection. The data are representative of two independent experiments.

examined the potential heat shock response-inducer activity of three representative isothiocyanates: allyl- (AITC), benzyl- (BITC), and phenethyl isothiocyanate (PEITC) (**Fig. 2.2A**) in the human breast cancer cell line MDA-MB-231, using Hsp70 as a prototypic heat shock protein.

3.2.3 Cysteine-reactive PEITC induces the heat shock response

When cells were exposed for 24 h to the aromatic isothiocyanates BITC or PEITC at a concentration of 10 μM, the levels of Hsp70 increased by ~12- and ~10-fold, respectively, whereas the levels of Hsp70 remained unchanged upon exposure to 10 μM of the aliphatic isothiocyanate AITC (**Fig. 2.2B**). PEITC is in clinical trials for prevention of lung cancer and for depletion of oral cells expressing mutant p53 (ClinicalTrials.gov). We therefore focused our subsequent studies on this isothiocyanate.

We wanted to find out whether the upregulation of Hsp70 by PEITC was mediated by HSF1, therefore we exposed cells which were HSF1-deficient and their wild-type counterparts to PEITC and observed the levels of Hsp70 in these cells.

FIGURE 2.2

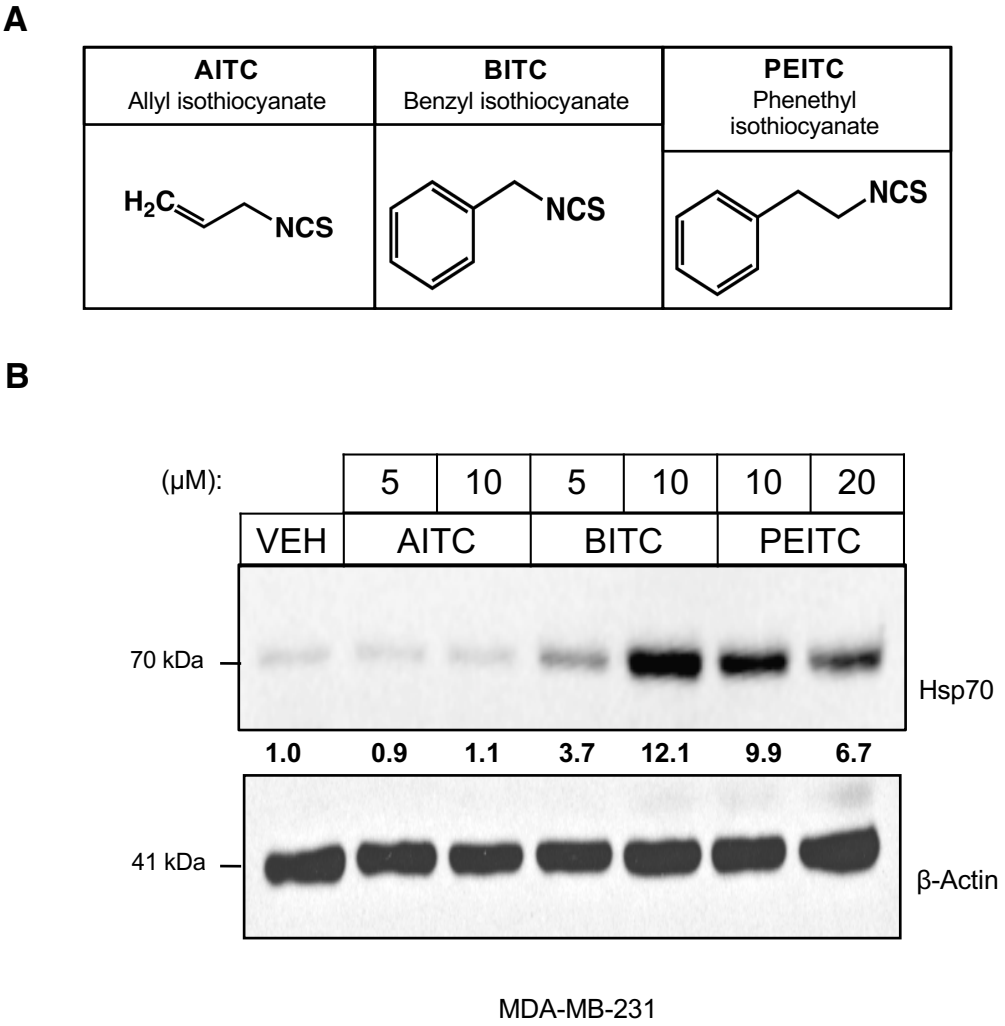

Figure 2.2. PEITC is a robust inducer of the heat shock response. (**A**) Chemical structures of allyl isothiocyanate (AITC), benzyl isothiocyanate (BITC), and phenethyl isothiocyanate (PEITC). (**B**) MDA-MB-231 cells (2.5 x 10^5 per well) growing in 6-well plates were exposed to vehicle (0.1% acetonitrile), AITC, BITC, or PEITC for 16 h. Cells were lysed in RIPA buffer, proteins were resolved by SDS/PAGE, transferred to immobilon-P membranes, and probed with an antibody against Hsp70. The levels of β-actin served as loading control.

3.2.4 PEITC requires HSF1 for the induction of Hsp70

Western blot analysis of human cervical cancer HeLa cells with either WT HSF1 (HSF1 WT HeLa) or HSF1 knocked-out (HSF1-KO HeLa) generated using the CRISPR/Cas9 technology confirmed the requirement of HSF1 for the induction of Hsp70 by PEITC. In the HSF1 WT HeLa cells, exposure to 7.5 μM or 15 μM PEITC caused an induction of Hsp70 by ~1.1 and ~1.5-fold respectively (**Fig 2.3A**), whereas in the HSF1-KO HeLa cells exposed to the same concentrations showed no induction of Hsp70. Importantly, the basal levels of Hsp70 were reduced by 60% in the HSF1-KO HeLa cells compared to their wild-type counterparts, suggesting the partial requirement of the presence of HSF1 under homeostatic conditions. Further validation of the requirement of HSF1 for Hsp70 induction was observed in experiments conducted in mouse embryonic fibroblasts (MEFs). In wild-type MEFs, exposure to 7.5- or 10 μM PEITC for 24 h caused an upregulation of Hsp70 by ~2- and ~3.2-fold, respectively, whereas the levels of this heat shock protein remained unchanged in their HSF1-deficient counterparts (**Fig. 2.3B**).

We wanted to find out whether the loss of HSF1 would affect the efficacy of PEITC, therefore we conducted a cytotoxicity assay using the cell permeable reagent known as reazurin (blue), which is weakly fluorescent and an oxidation-reduction indicator, that undergoes colourimetric and flourometric changes in response to cellular metabolic changes. When reazurin is reduced, it forms resofurin (bright pink) which is highly fluorescent and the intensity of the

FIGURE 2.3

A

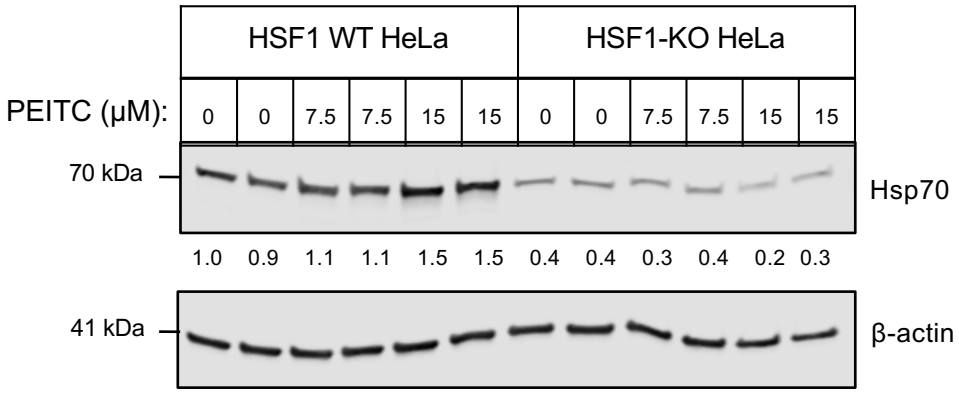

B

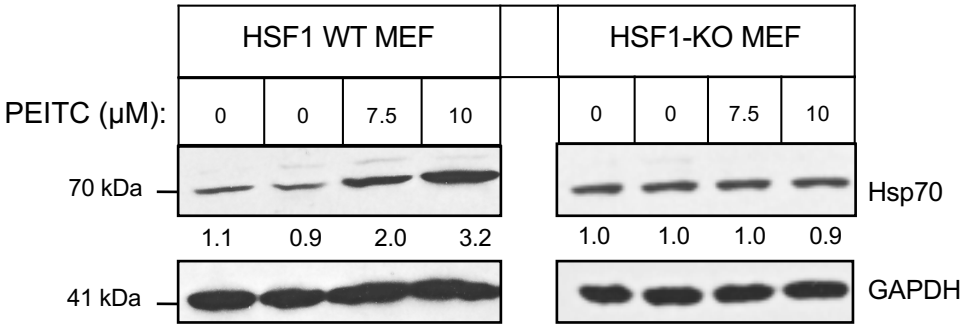

Figure 2.3. PEITC requires HSF1 for the induction of Hsp70. (**A**) HSF1 WT or HSF1-KO HeLa cells (3.5 x 10^5 per well) (**B**) or mouse embryonic fibroblasts (MEF, 2 x 10^5 per well) growing in 6-well plates were exposed to vehicle (0.1% acetonitrile) or PEITC for 24 h. Experimental data from panel B was obtained by Dr. Ying Zhang. Cells were lysed in SDS lysis buffer, proteins were resolved by SDS/PAGE, transferred to immobilon-P membranes, and probed with an antibody against Hsp70. The levels of β-actin or glyceraldehyde-3-phosphate dehydrogenase (GAPDH) served as loading control.

fluorescence has been found to be directly proportional to the number of respiring cells.

3.2.5 Loss of HSF1 enhances the cytotoxicity of PEITC

The dose of PEITC required to cause 50 % cell death (IC_{50} value) in HSF1 WT HeLa cells is 16 μM, whereas it is 12 μM in the HSF1-KO HeLa cells (**Fig. 2.4**). This result suggests that loss of HSF1 renders the cells more sensitive to PEITC, probably due to inability to mount the pro-survival heat shock response where upregulation of heat shock proteins have been shown to promote cell survival. However, the difference between the two cell lines is relatively modest, indicating that other transcription factors (such as NRF2) may compensate for the absence of HSF1.

Under unstressed conditions, HSF1 is mostly cytoplasmic and is found to be in complex with its negative regulators Hsp70 and Hsp90. Upon exposure to stress, HSF1 is released from this complex, and translocates into the nucleus. It is clear from the literature that during exposure to heat stress, HSF1 forms a homotrimer within 15 min and the HSF1 trimer binds to heat shock elements (HSE) (Guettouche et al., 2005, Ahn et al., 2005). To our knowledge, it is not known whether the trimerization of HSF1 precedes its nuclear translocation during stress conditions. We decided to answer this question by performing a nuclear and cytoplasmic separation after cells were exposed to either the solvent control [0.1% (v/v) acetonitrile] or PEITC. Before performing the subcellular fractionation, we fixed the cells with 0.4% paraformaldehyde to ensure that the

FIGURE 2.4

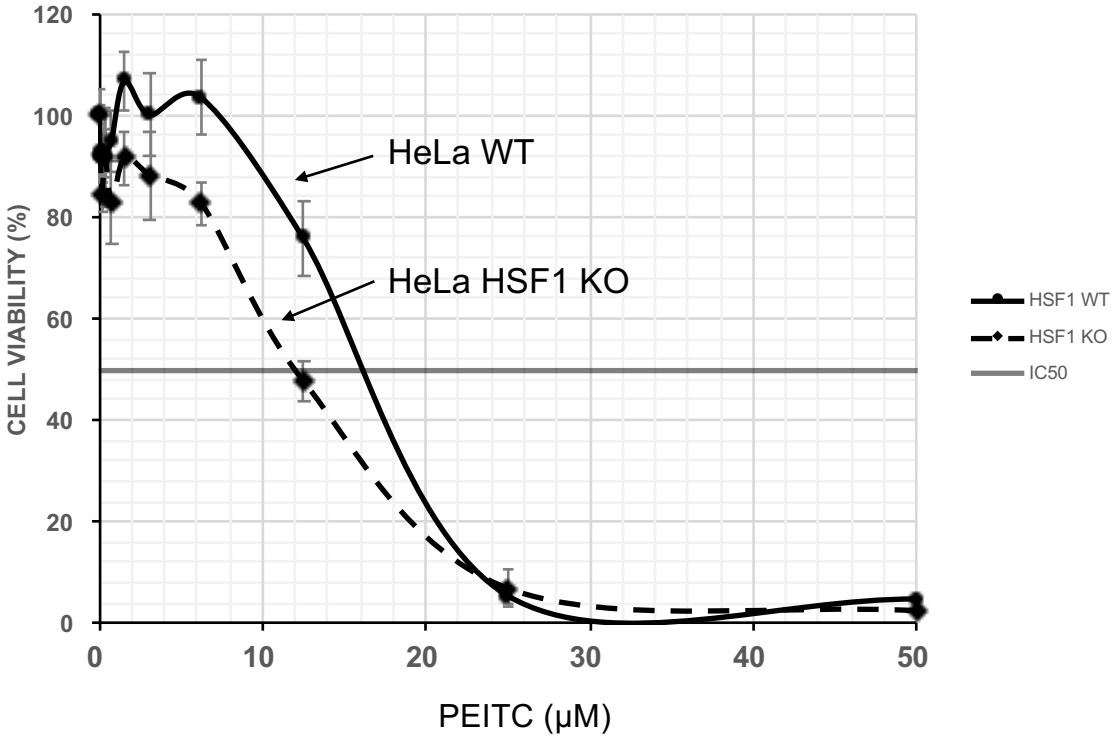

Figure 2.4. Loss of HSF1 enhances cytotoxicity of PEITC. HSF1 WT or HSF1-KO HeLa cells (5 x 10^3 per well) in 96-well plates were exposed to vehicle (0.1% acetonitrile) or various concentrations of PEITC for 48 h. AlamarBlue reagent was added to all the wells 4 h before the 48 h time point. The fluorescence was measured (ex. 560 nm/em. 590 nm) 4 h after AlamarBlue addition and the fluorescence values obtained were corrected for blank and normalised as a percentage against the wells treated with the vehicle.

monomeric, dimeric and trimeric forms of HSF1 would be preserved and ultimately be able to be detected by western blotting.

3.2.6 PEITC causes nuclear accumulation of HSF1 and its trimerization

Nuclear-cytoplasmic separation experiments conducted in MDA-MB-231 cells showed that PEITC caused nuclear translocation of HSF1 (**Fig. 2.5**). Thus, in vehicle-treated cells, HSF1 was present in both the cytoplasmic and nuclear fractions. In sharp contrast, in the cytoplasmic fraction of cells treated with PEITC for 3 h, there was no detectable HSF1, and essentially all HSF1 was in the nuclear fraction. Furthermore, the presence of monomeric, dimeric and trimeric HSF1 species was readily detectable in the nuclear fraction of PEITC-treated cells. Notably, the gel electrophoretic mobility of monomeric HSF1 in the nuclear fraction of PEITC-treated cells was slower than in their vehicle-treated counterparts (**Fig. 2.5**), indicative of occurrence of post-translational modifications. This experiment shows that upon PEITC treatment, HSF1 undergoes nuclear translocation and trimerization.

Trimerization is required for the transcriptional activity of HSF1 (Sorger and Nelson, 1989, Perisic et al., 1989, Peteranderl and Nelson, 1992, Rabindran et al., 1993). To test whether the HSF1 trimers that form upon treatment with PEITC are able to enhance transcription through heat shock elements (HSEs), we used the cervical cancer HeLa HSE-luciferase reporter cell line (HeLa-HSE-

FIGURE 2.5

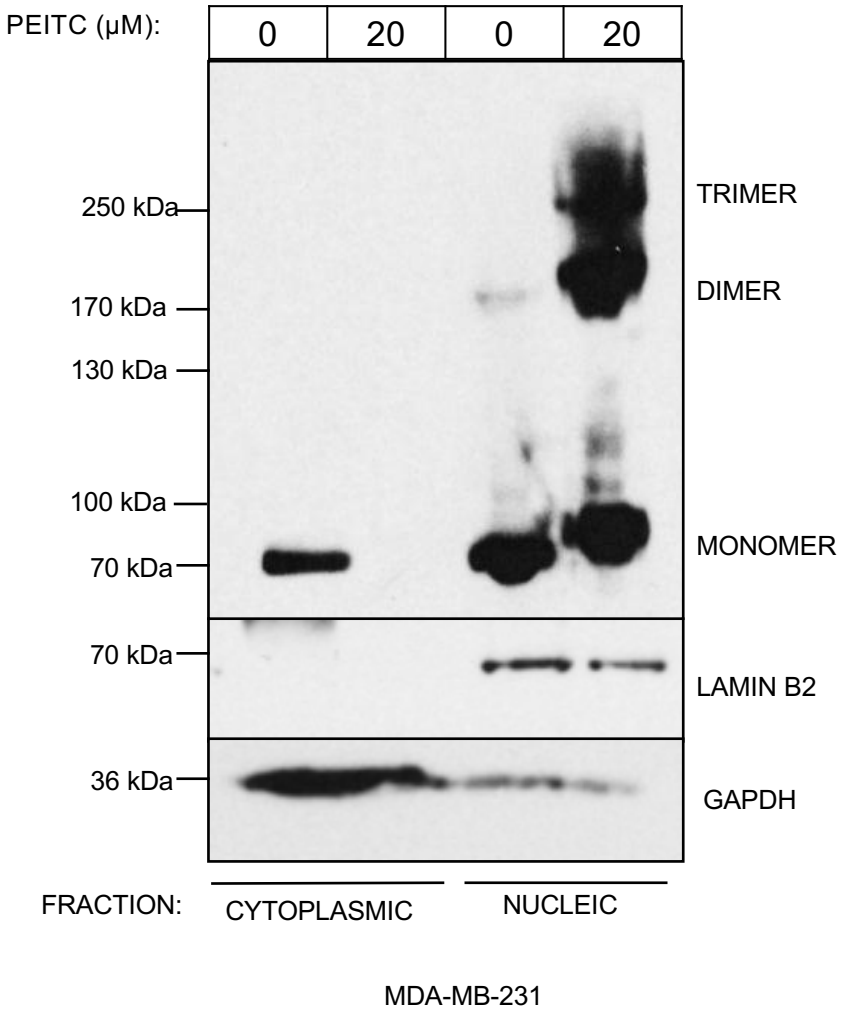

Figure 2.5. PEITC causes nuclear accumulation of HSF1 and its trimerization. MDA-MB-231 cells (2.5 x 10^5 per well) growing in 6-well plates were exposed to vehicle (0.1% acetonitrile) or 20 μM PEITC for 3 h. Cells were then fixed with 0.8% (w/v) paraformaldehyde. Cell lysates were subjected to nuclear (N) and cytoplasmic (C) separation, proteins were resolved by SDS/PAGE (10% gel), transferred to immobilon-P membranes, and probed with an antibody against HSF1. The levels of lamin B2 and GAPDH served as fraction purity indicators and as loading controls.

luc) stably transfected with the *HSP70.1* promoter fused to the luciferase gene (Calamini et al., 2012).

3.2.7 PEITC causes an increase in Hsp70.1 promoter activity as well as Hsp70 mRNA levels

Remarkably, PEITC led to a dramatic dose- and time-dependent induction of the reporter, with a maximal increase of more than 1000-fold (**Fig. 2.6A**). Consistent with the increase in the protein levels of Hsp70 (**Fig. 2.3B**), the mRNA levels for *hspa1a* were upregulated by 4.1- and 3.5-fold after exposure of wild-type MEF cells to 10 μM PEITC for 8- or 16 h, respectively (**Fig. 2.6B**). Together, these results demonstrate that PEITC is a potent and robust inducer of the heat shock response.

Activation of HSF1 requires release from its negative regulators; indeed, inhibition of Hsp90, the main negative regulator of HSF1, often leads to induction of the heat shock response (Jhaveri et al., 2012). To test whether PEITC inhibits the function of Hsp90, we evaluated the stability of two well-established Hsp90 client oncoproteins, the tyrosine kinase HER2 and the serine/threonine kinase RAF1, both of which bind strongly to Hsp90 (Taipale et al., 2012).

3.2.8 PEITC inhibits Hsp90

Following treatment with PEITC, the levels of HER2 and RAF1 were decreased by ~60- and ~35%, respectively, consistent with Hsp90 inhibition (**Fig.**

FIGURE 2.6

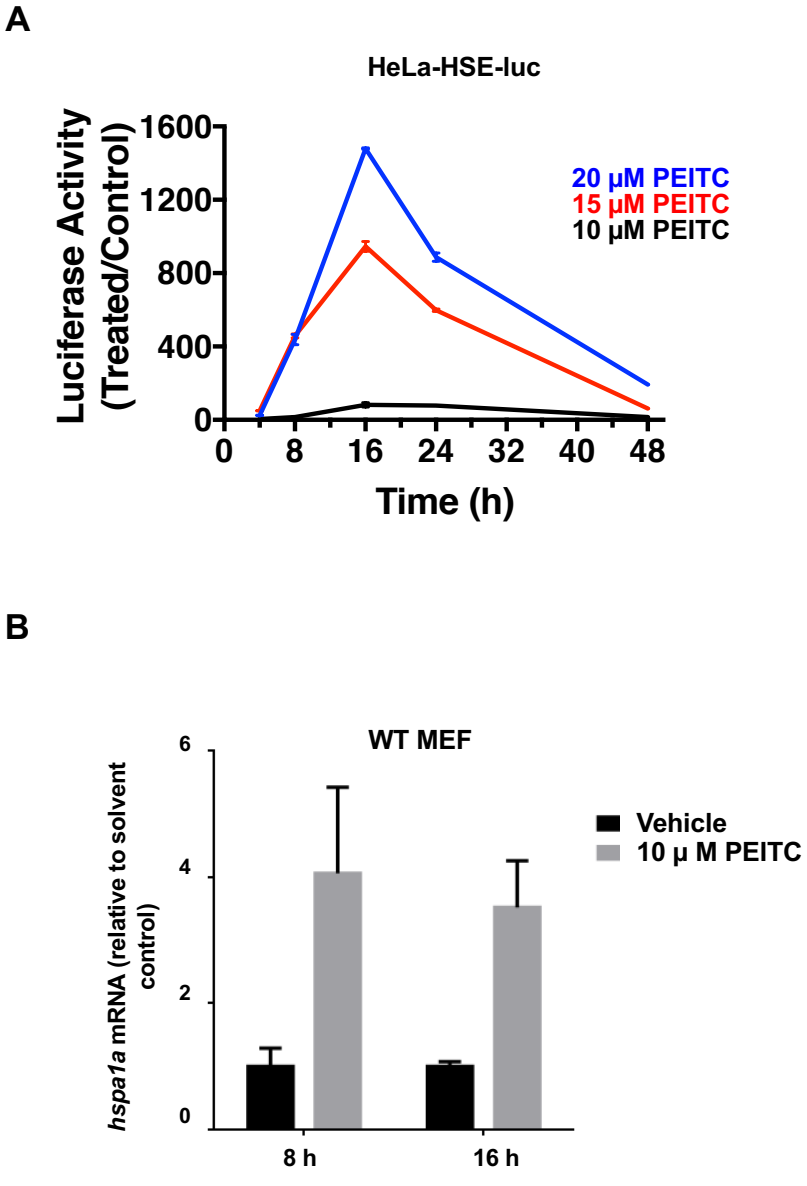

Figure 2.6 PEITC causes an increase in Hsp70.1 promoter activity as well as Hsp70 mRNA levels. (**A**) HeLa-HSE-luc cells (1.3 x 10^5 per well) stably transfected with the luciferase gene under the control of the *HSP70.1* promoter, were grown in 12-well plates and exposed to vehicle (0.1% acetonitrile) or PEITC. Luciferase activity was determined in cell lysates. The relative luminescence units (RLU) were quantified and normalized with respect to the vehicle control treatment. (**B**) Wild-type MEF cells (2 x 10^5 per well) in 6-well plates were exposed to vehicle (0.1% acetonitrile) or PEITC for 8 or 16 h. Cells were lysed, total RNA was extracted, and reverse transcribed into cDNA. The mRNA levels for *hspa1a* were quantified using real-time PCR. The data were normalized using β-actin as an internal control. Data represent means ± SD and are expressed as ratio of the relative transcripts in treated over control samples. These experiments were performed by Dr. Ying Zhang.

2.7A). Treatment with 10 μM PEITC did not lead to any changes in the transcription of either of these genes, as quantified by real-time PCR. Interestingly however, the 20- μM PEITC treatment led to a significant (p = 0.002, n = 3) 45% decrease in the mRNA levels for HER2, although the mRNA levels for RAF1 were not affected (not shown). The reason for this decrease in HER2 expression, and its potential contribution to the decreased HER2 protein levels at the high concentration of PEITC is presently unknown. In contrast to geldanamycin (GA), an Hsp90 inhibitor that competes with ATP, but similarly to celastrol (CL) and sulfoxythiocarbamate alkyne (STCA), which inhibit Hsp90 by modifying its cysteine residues without interfering with ATP binding (Zhang et al., 2014), PEITC did not prevent the ability of the chaperone to bind ATP (**Fig. 2.7B**). These results support the notion that PEITC, by virtue of its cysteine reactivity inhibits Hsp90, and further suggest that, by inhibiting Hsp90, the isothiocyanate may trigger the release of HSF1. Indeed, immunoprecipitation experiments showed that the amount of HSF1 bound to Hsp90 is greatly reduced upon exposure to PEITC (**Fig. 2.7C**).

3.2.9 PEITC causes phosphorylation of HSF1 at S326

In addition to release from Hsp90, full transcriptional activation of HSF1 requires its phosphorylation at S326 (Guettouche et al., 2005, Chou et al., 2012). The shift in gel electrophoretic mobility of the monomeric form of HSF1 in nuclear fractions of PEITC-treated cells (**Fig. 2.5, 2.8A**) indicated the occurrence of post-translational modifications. Given the dramatic activation of the HSE-luciferase reporter by PEITC (**Fig. 2.6A**), we tested the possibility that exposure to PEITC

FIGURE 2.7

A

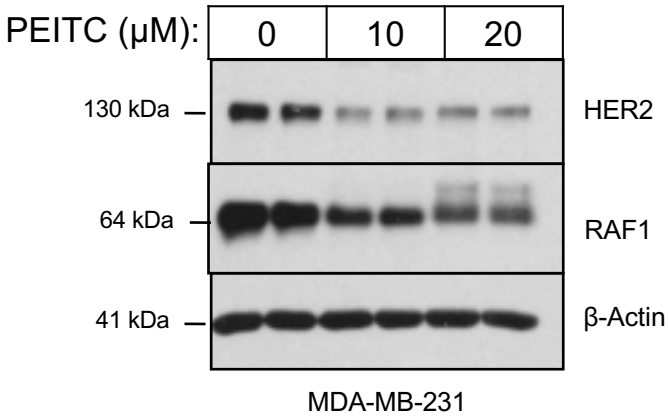

B

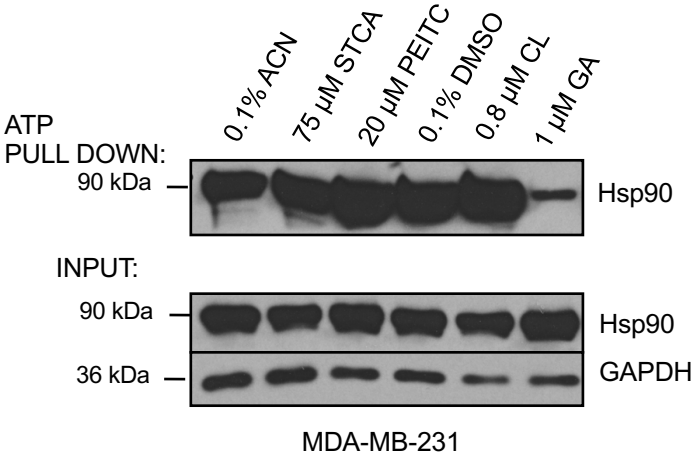

C

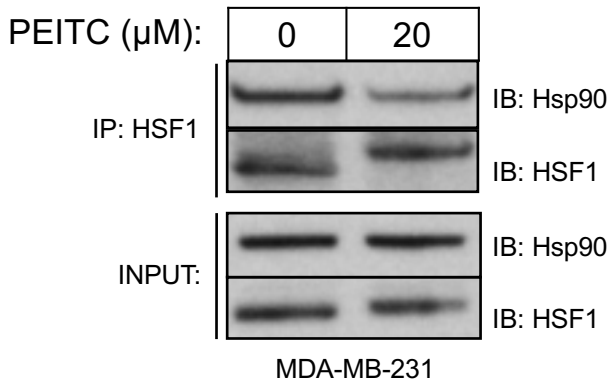

Figure 2.7. PEITC inhibits Hsp90. (**A**) MDA-MB-231 cells (2.5 x 10^5 per well) in 6-well plates were treated with vehicle (0.1% acetonitrile) or PEITC for 24 h. The levels of HER2 and RAF1 were detected by western blot analysis. The levels of β-actin served as loading control. (**B**) MDA-MB-231 cells (0.5 x 10^6 per dish) were grown in 6-cm dishes. After 24 h, the cells were treated for a further 24 h with 0.1% acetonitrile (ACN) as the vehicle control for sulfoxythiocarbamate alkyne (STCA) and PEITC treatments, or with 0.1% DMSO as the vehicle control for the geldanamycin (GA) and celastrol (CL) treatments. Cells were lysed and subjected to ATP pulldown using ATP-agarose beads. For the ATP pull-down and input samples, Hsp90 or GAPDH were detected by western blot analyses. This experiment was performed with Dr. Ying Zhang. (**C**) MDA-MB-231 cells (1 x 10^6 per well) were grown in 6-cm dishes and treated with vehicle (0.1% acetonitrile) or PEITC for 45 min. cells were lysed and subjected to immunoprecipitation with an anti-HSF1 antibody, and then immunoblotted with an anti-Hsp90 antibody. An aliquot of total lysate was subjected to immunoblot analysis with anti-Hsp90 and anti-HSF1 antibodies.

was causing HSF1 phosphorylation at S326. The use of a pS326-phosphospecific antibody revealed a time- and dose-dependent increase in pS326 HSF1 and an upregulation of Hsp70 upon exposure to PEITC (**Fig. 2.8A**). Notably and in full agreement with the shift in electrophoretic mobility of HSF1 in nuclear fractions of PEITC-treated cells (**Fig. 2.5**) as well as in the immunoprecipitation experiment (**Fig. 2.7C**), in this experiment the migration of HSF1 was slower in lysates from cells treated with 20 μM PEITC than from vehicle- or 10 μM PEITC-treated cells (**Fig. 2.8A**). Surprisingly however, although HSF1 S326 phosphorylation was more extensive upon treatment with the higher concentration (20 μM) of PEITC, induction of Hsp70 appeared to be greater at the lower concentration (10 μM) of the isothiocyanate. Nuclear-cytoplasmic separation further confirmed the accumulation of pS326 HSF1 in both cytoplasmic and nuclear fractions (**Fig. 2.8B**). The results from this shorter time-course experiment also indicated that HSF1 phosphorylation occurred in the cytoplasm and preceded the nuclear translocation of the transcription factor. Also, the phosphorylated HSF1 at S326 in the 20 μM PEITC treatment enters the nucleus within 15 min, indicating a rapid activation of the transcriptional response by the isothiocyanate.

Only a stringent subset of kinases, known as CMGC kinases are able to phosphorylate proline-directed sites (Ubersax and Ferrell, 2007). There are 14 proline-directed phosphorylation sites on HSF1 (**Fig. 2.9**) many of which have been reported to play a role in either activating or repressing the transcriptional capability of HSF1. S326 of HSF1 represents a proline-directed phosphorylation site. Phosphorylation of S326 of HSF1 has been implicated in increasing the

FIGURE 2.8

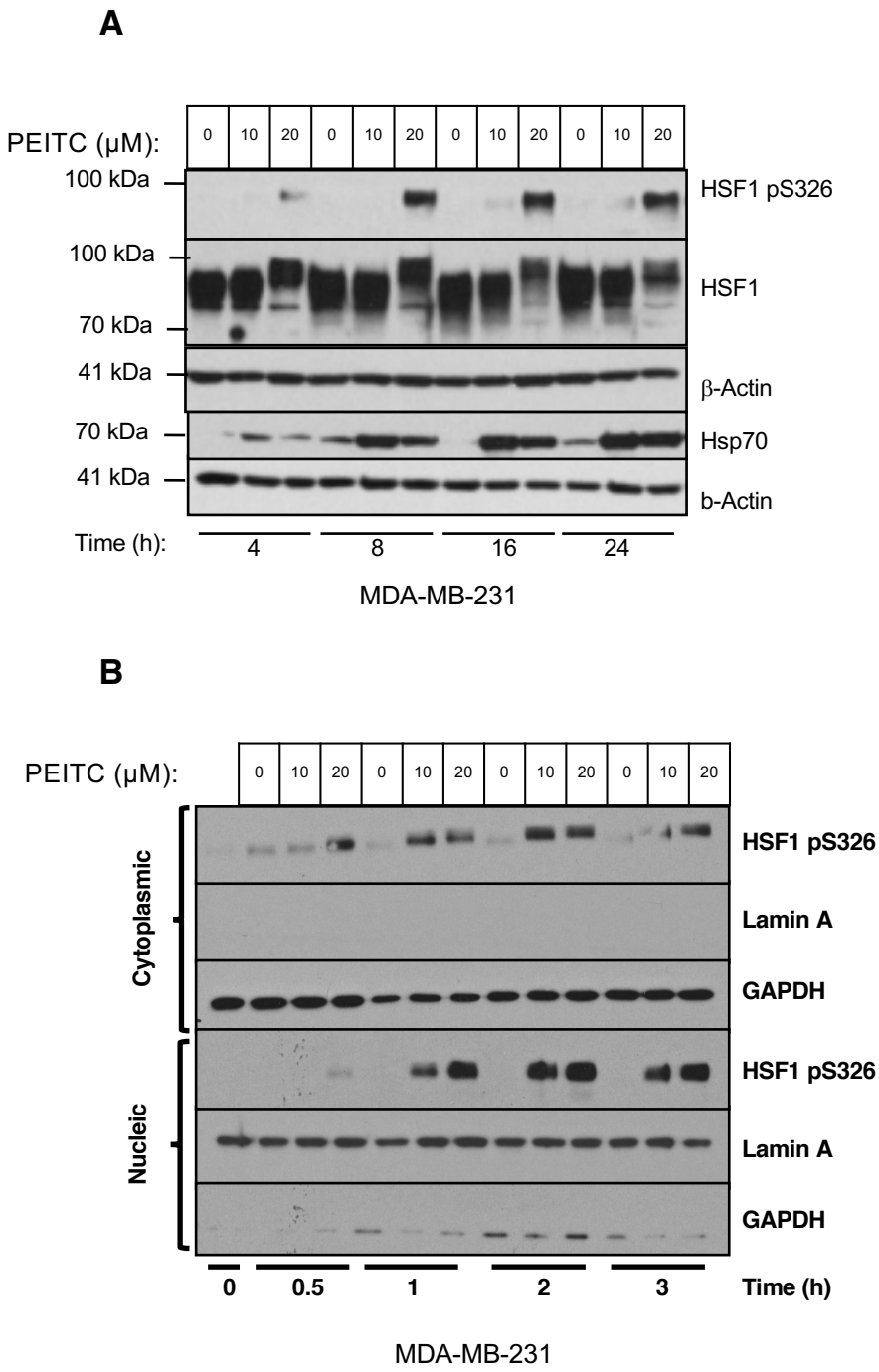

Figure 2.8. PEITC causes phosphorylation of HSF1 at S326. MDA-MB-231 cells (2.5 x 10^5 per well) in 6-well plates were treated with vehicle (0.1% acetonitrile) or PEITC for either 24 h **(A)** or for the indicated periods of time **(B)**. In **(A)**, the levels of pS326 HSF1, total HSF1, and Hsp70 were detected by western blot analysis in cell lysates, and the levels of β-actin served as loading control. In **(B)**, the levels of pS326 HSF1 were detected by western blot analysis in cytoplasm and nucleus following nuclear-cytoplasmic separation. The levels of lamin A and GAPDH served as fraction purity indicators and as loading controls.

FIGURE 2.9

Proline-directed sites on HSF1

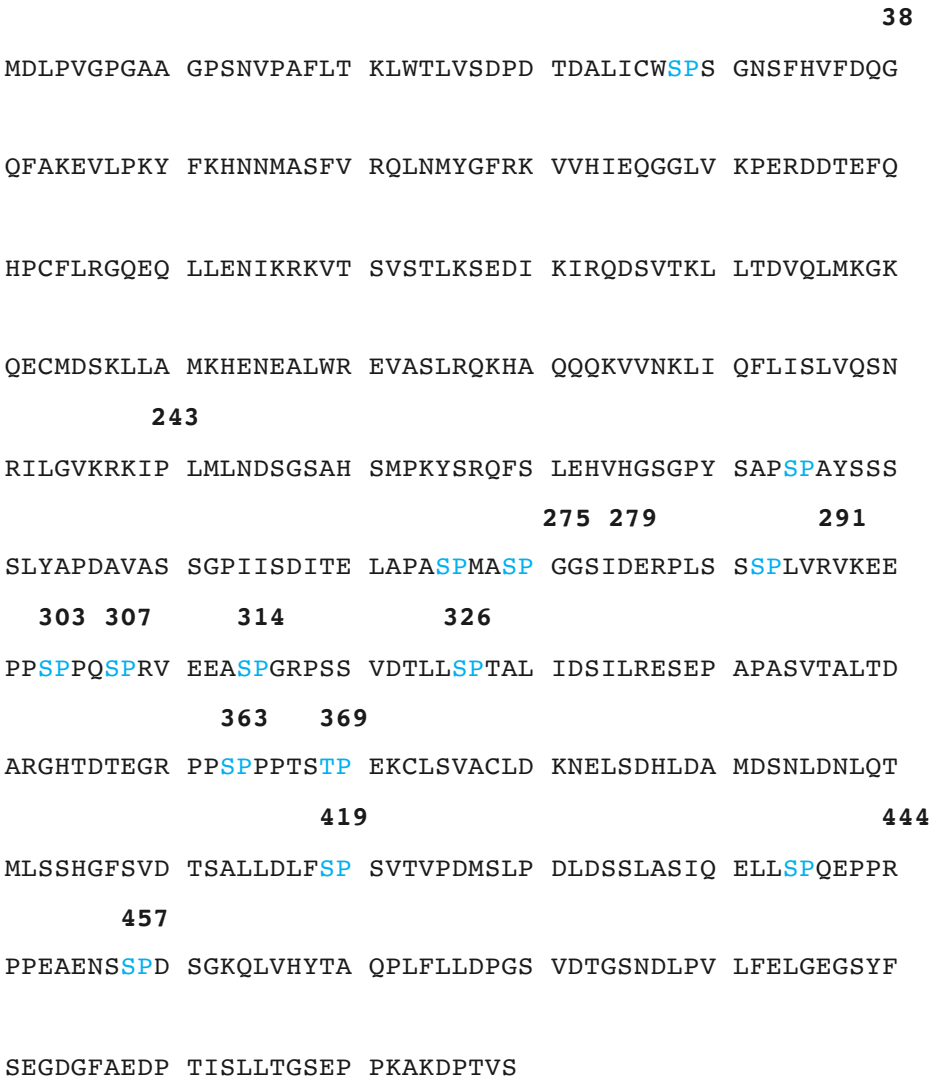

Figure 2.9. Predicted proline-directed phosphorylation sites on HSF1. The human HSF1 protein sequence was obtained from the protein database www.uniprot.org using the unique entry ID Q00613. There are 14 proline-directed sites, either SP or TP, on HSF1.

transcriptional capability of the transcription factor. Several studies have reported that mutation of the S326 to an alanine decreases the transcriptional capability of HSF1 (Chou et al., 2012, Guettouche et al., 2005, Tang et al., 2015). There have been reports that the kinases that phosphorylates this site could be either mTORC1 (Chou et al., 2012) or MEK (Tang et al., 2015). However, none of them are proline-directed kinases, which makes them unlikely to be the kinases that phosphorylate this proline-directed S326 site. In addition, these experiments have used near stoichiometric amounts of each kinase and HSF1 *in vitro*, which, in our opinion 'forces' the interaction between the two. Furthermore, in these experiments the researchers used kinase inhibitors for 24 h in order to see a decrease in phosphorylation of S326 of HSF1. Usually 30-60 min incubation with a kinase inhibitor is sufficient to inhibit a kinase, hence, a 24 h incubation with an inhibitor could ultimately produce off-target effects.

Given these caveats, we conducted a small screen using several CMGC kinase inhibitors. We first developed a high-throughput cell-based assay for the detection of HSF1 S326 phosphorylation by taking advantage of a technique known as the 'In-Cell Western" (ICW). In short, ICW is a procedure that is usually conducted in a 96-well or 384-well format, where cells are plated in the wells are fixed and subjected to immunostaining, where the secondary antibody used is conjugated to infrared-excitable flourophores for quantitative detection by the Oddessey Scanner (Licor). We seeded MCF7 cells in 96-well plates and treated them with varying concentrations of kinase inhibitors for 1 h. After treatment with the inhibitors, either vehicle (0.1% DMSO) or 20 μM PEITC was added for 4 h, after which the cells were subjected to the ICW procedure for quantification of the

HSF1 pS326 levels in each of the wells. From this screen we found that inhibition of p38 mitogen-activated protein kinases (MAPK) led to a decrease in basal phosphorylation of HSF1 at S326 by the p38 MAPK inhibitor ZM33673 (**Appendix Fig. 5.1C**). Also, as PEITC has been reported to activate p38 MAPK (Cheung et al., 2008), we next examined their status in MDA-MB-231 cells.

3.2.10 PEITC activates p38 MAPK

A dose-dependent phosphorylation of p38 MAPK was readily detectable, and increased by ~30- and ~90-fold, after treatment with 10- and 20 μM of PEITC, respectively (**Fig. 2.10A**). Importantly, the levels of p38 MAPK were unchanged, showing that PEITC did not cause any alterations in protein expression or stability of the kinases. In contrast to the activation of p38 MAPK, exposure to PEITC decreased the phosphorylation of the ribosomal subunit S6 at S235/236 (**Fig. 2.10B**), indicating inhibition of the mechanistic target of rapamycin (mTOR), a kinase that had been previously implicated in the phosphorylation of HSF1 at S326 (Chou et al., 2012). Moreover, the dose-dependent PEITC-mediated phosphorylation of p38 MAPK correlates well with the extent of phosphorylation of HSF1 at S326, which increased by 30- and 55-fold, after treatment with 10- and 20 μM PEITC, respectively (**Fig. 2.10A**).

Recently, it was reported that HSF1 physically interacts and is phosphorylated at S326 by MAPKK (also known as MEK) (Tang et al., 2015). We therefore next examined the effect of inhibiting MEK on HSF1 S326 phosphorylation using the highly selective MEK1/2 inhibitor 1,4-diamino-2,3-

FIGURE 2.10

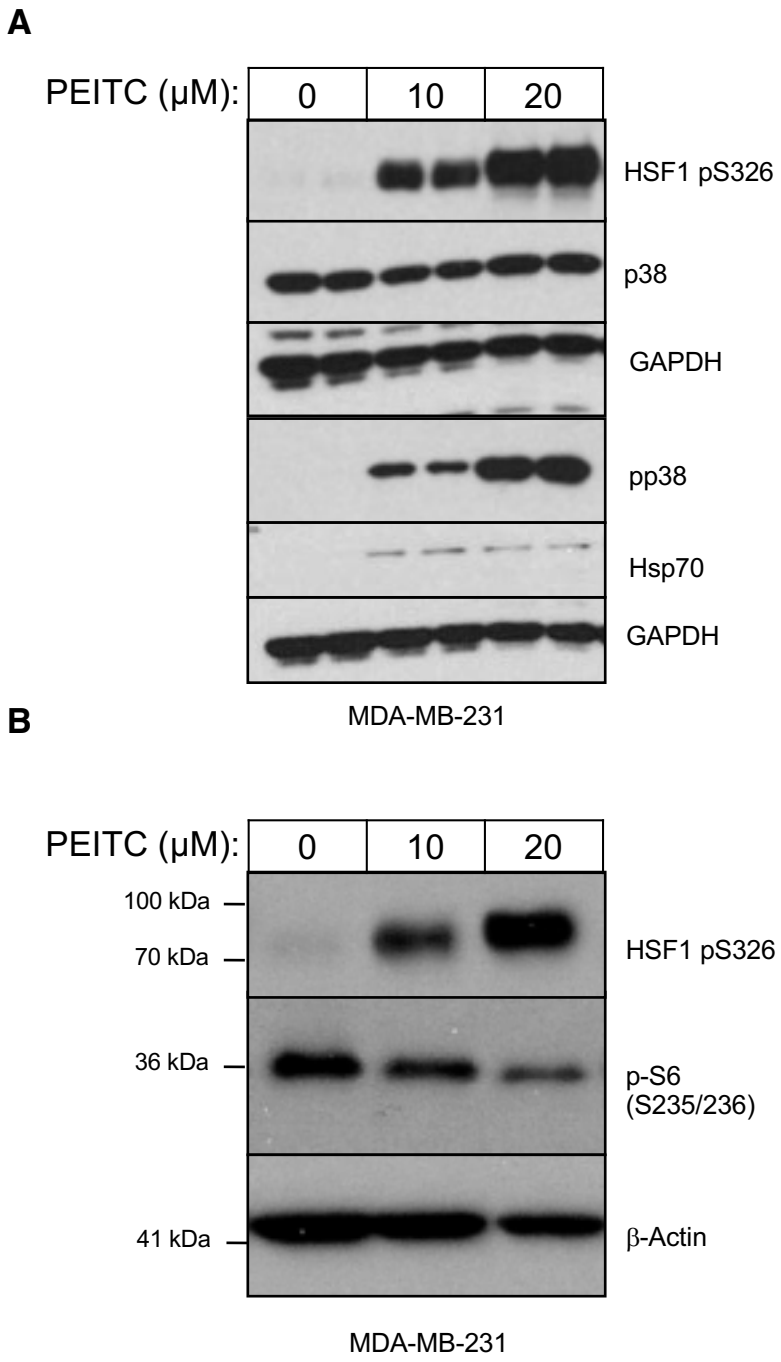

Figure 2.10. PEITC activates p38 MAPK. PEITC activates p38 and inhibits mTOR. MDA-MB-231 cells (2.5 x 10^5 per well) growing in 6-well plates were treated with vehicle (0.1% acetonitrile) or PEITC for either 24 h (**A**), 3 h (**B**) or for the indicated periods of time (**D**). The levels of HSF1, pS326 HSF1, pS235/6 S6, Hsp70, phosphorylated p38 (pp38), p3, were detected by western blot analysis.

dicyano-1, 4-bis[2-aminophenylthio]butadiene (U0126) (Favata et al., 1998). In agreement with the published report (Tang et al., 2015), we were able to detect reduced levels of phosphorylation of HSF1 at S326 in lysates of heat-shocked cells that had been pre-treated for 24 h with U0126 (**Fig. 2.11A**). However, the MEK inhibitor had no effect on the phosphorylation of HSF1 at S326 in heat-shocked cells that had been pre-treated with U0126 for 1 h (**Fig. 2.11B**). Overall, these findings raise the possibility that p38 MAPK could represent one group of the long-sought catalysts for the phosphorylation of this key residue.

3.2.11 p38 MAPK phosphorylate HSF1 at S326 *in vitro*

Next, we used recombinant HSF1 to test the ability of purified recombinant p38 MAPK isoforms to phosphorylate HSF1 *in vitro*. HSF1 was expressed as a His-tagged fusion protein in *Escherichia coli*. Purified His-HSF1 migrated as a major band during NuPAGE® at the expected molecular weight, and showed a tendency to form spontaneously dimeric and trimeric species (**Fig. 2.12A**). The four p38 MAPK isoforms (α, β, γ and δ) were expressed individually in *Escherichia coli* from human cDNAs as inactive GST-fusion proteins, and purified by affinity chromatography on glutathione-Sepharose. Recombinant MKK6 was then used to activate the p38 proteins, and subsequently removed by passage through amylose resin. The enzyme activity of each p38 isoform was quantified by the phosphorylation of a standard substrate, myelin basic protein. Each kinase was used at an equivalent specific enzyme activity in reactions with HSF1 as a substrate.

FIGURE 2.11

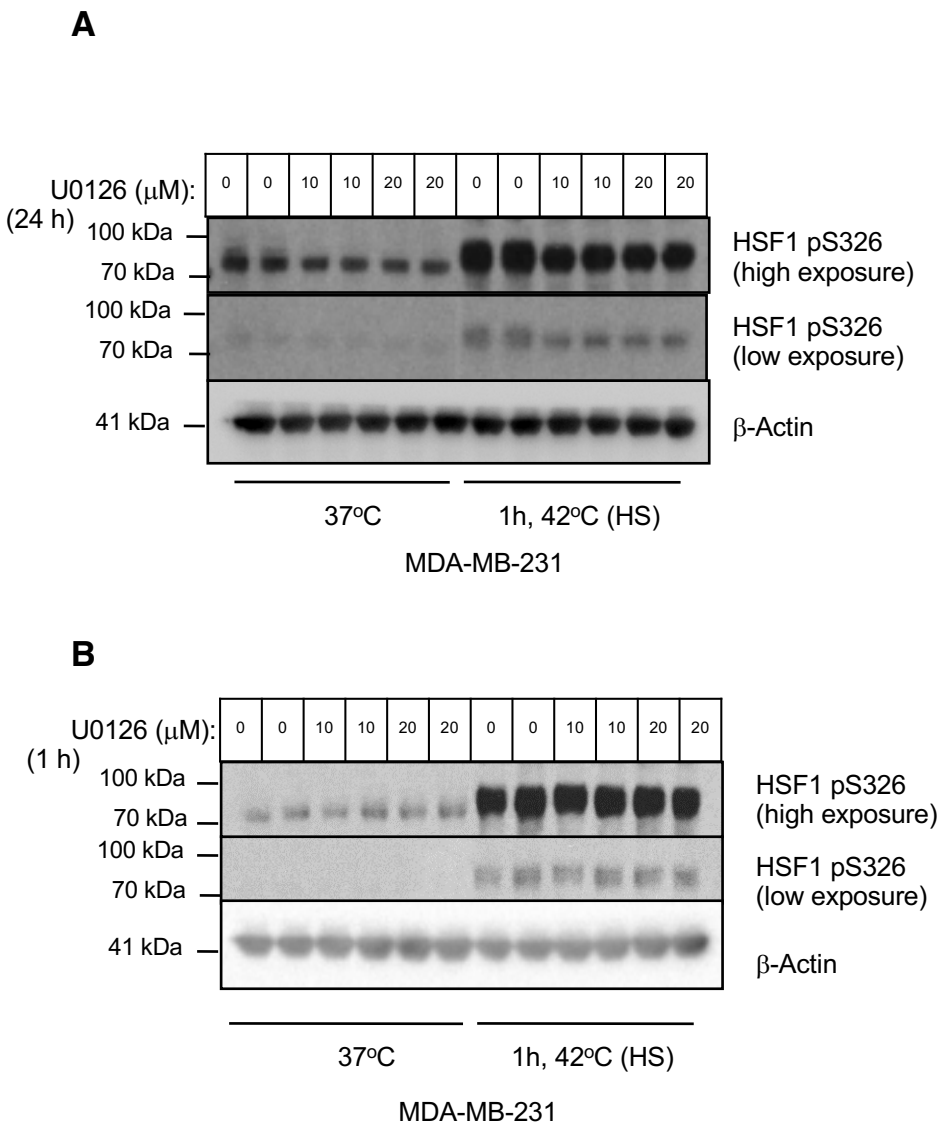

Figure 2.11. The MEK inhibitor U0126 reduces the levels of heat-shock induced phosphorylation of HSF1 at S326 after a 24 h pre-treatment, but 1 h pre-treatment has no effect. MDA-MB-231 cells (2.5 x 10^5 per well) in 6-well plates were pre-treated with U0126 for either 24 h (**A**) or 1 h (**B**), and subsequently subjected to heat shock (HS). The levels of HSF1 and pS326 HSF1 were detected by western blot analysis. The levels of β-actin served as loading control.

FIGURE 2.12

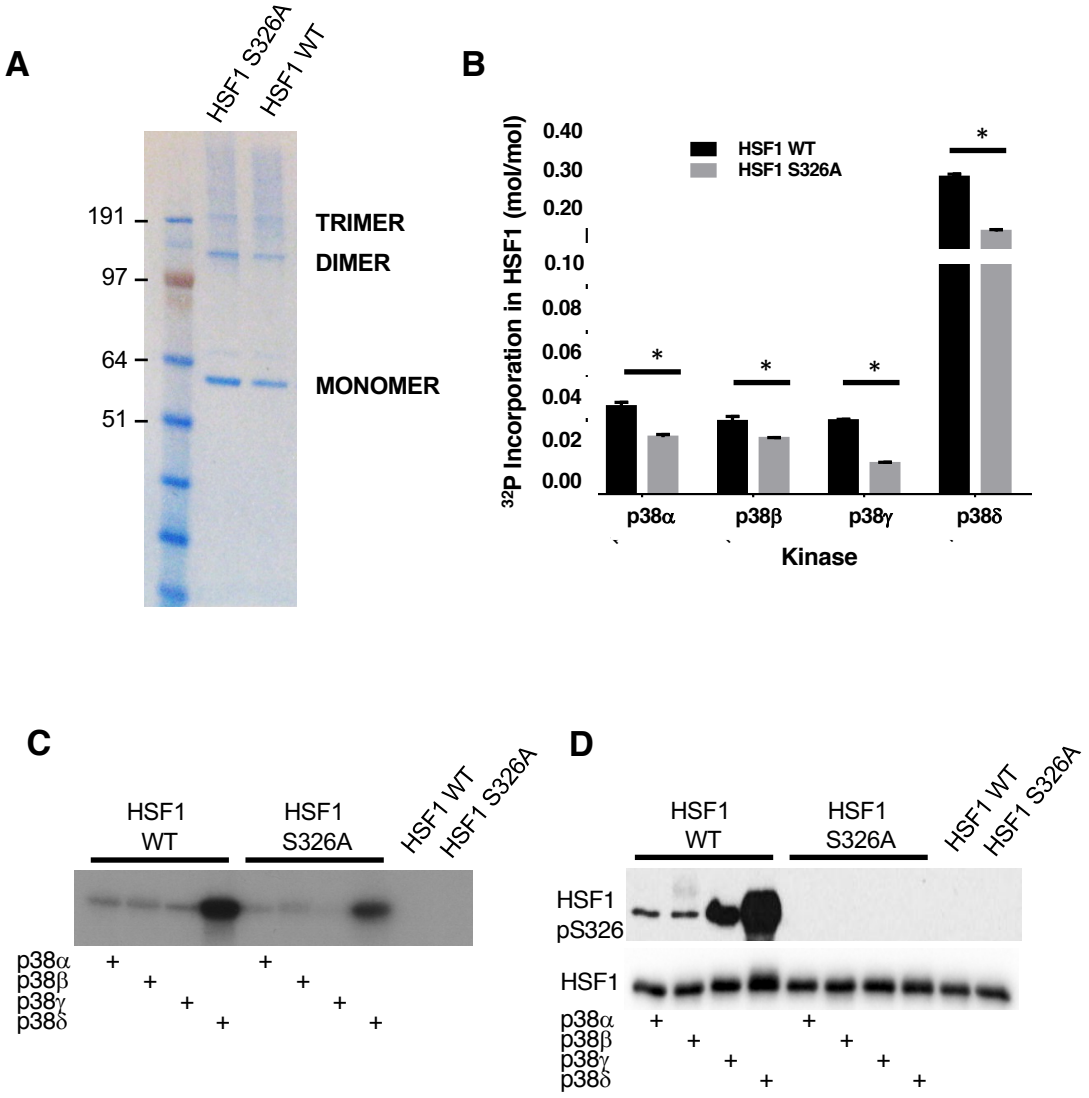

Figure 2.12. p38 MAPK phosphorylate HSF1 *in vitro*. (**A**) Electrophoretic mobility (NuPAGE NoVex Bis-Tris 4-12% gradient gel) of recombinant hexahistidine-tagged HSF1 wild-type (WT) and S326A mutant. (**B-D**) Purified activated recombinant p38 MAPK isoforms (0.06 mU/µl) were incubated with recombinant wild-type (WT), S326A mutant HSF1, or (all 0.1 µg/µl at 30°C for 15 min in the presence of 10 mM $MgCl_2$ and 0.1 mM [ɣ-^{32}P]-ATP. Identical reactions were carried out in the presence of increasing concentrations of the p38α/β inhibitor SB202190 or BIRB0796, which inhibits all p38 isoforms. The reactions were terminated by addition of SDS gel loading buffer, the samples were loaded on SDS/PAGE, and the excess [ɣ-^{32}P]-ATP was removed by electrophoresis. The gels were dried and subjected to autoradiography (**C**). After staining with Coomassie Brilliant Blue, the protein bands were excised and the incorporated radioactivity (**B**) was determined by scintillation counting. *, $p < 0.05$. (**D**) Purified activated recombinant p38α (0.06 mU/µl) was incubated with recombinant wild-type (WT) or S326A mutant HSF1 (0.1 µg/µl) at 30°C for 15 min in the presence of 10 mM $MgCl_2$ and 0.1 mM ATP. The reactions were terminated by addition of SDS gel loading buffer, the samples were loaded on SDS/PAGE, and the phosphorylation of HSF1 at S326 and the levels of total HSF1 were detected by western blotting. These experiments were performed in collaboration with Dr. Calum D. Sutherland.

All p38 isoforms were able to rapidly phosphorylate HSF1 (**Fig. 2.12B,** black bars). Quantitative analysis of incubation reactions of HSF1 with either p38α, p38β, p38ɣ or p38δ and Mg-[γ^{32}P]-ATP revealed that p38δ phosphorylated HSF1 at a higher rate and stoichiometry than did p38α, p38β or p38ɣ, indicating that HSF1 is a better substrate for p38δ than for any of the other p38 isoforms (**Fig. 2.12B,** black bars and **Fig. 2.12C**). Parallel reactions in the absence of HSF1 showed that, under these experimental conditions, there was no detectable autophosphorylation of any of the kinases (not shown), and the radioactivity in these samples (as quantified by scintillation counting) was identical to that of the buffer blank. Western blot analysis using the S326-phosphospecific antibody confirmed this conclusion and clearly demonstrated that S326 was one of the phosphorylation sites (**Fig. 2.12D**).

The extent of phosphorylation of HSF1 was dependent on the kinase concentration as well as the incubation time. Thus, with 6 mU/µl of enzyme and 60 min incubation (when phosphate incorporation had reached or was approaching a plateau), the stoichiometry of the reaction was 2, 1.3, 0.8, and 2.2 mol/mol for the α, β, ɣ and δ isoforms, respectively, suggesting that, under these experimental conditions, p38α, p38β and p38δ were able to phosphorylate at least two sites on HSF1. With 0.06 mU/µl of enzyme and 15 min incubation, the stoichiometry of the reaction for HSF1 was 0.04, 0.03, 0.03, and 0.28 mol/mol for p38α, p38β, p38ɣ and p38δ, respectively (**Fig. 2.12B,** black bars), indicating that p38δ was the most efficient catalyst among the isoforms. The p38δ-mediated phosphorylation of HSF1 was inhibited by BIRB0796 (**Fig. 2.13A**), which inhibits all p38 MAPK isoforms (Kuma et al., 2005). In contrast to wild-type (WT) HSF1,

FIGURE 2.13

A

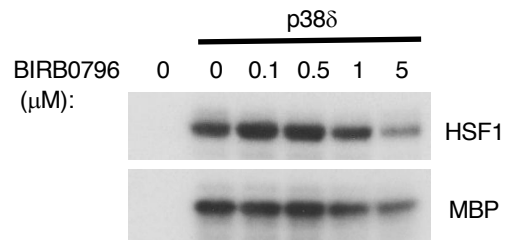

B

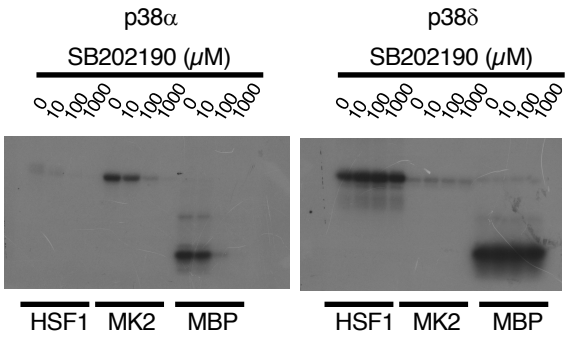

C

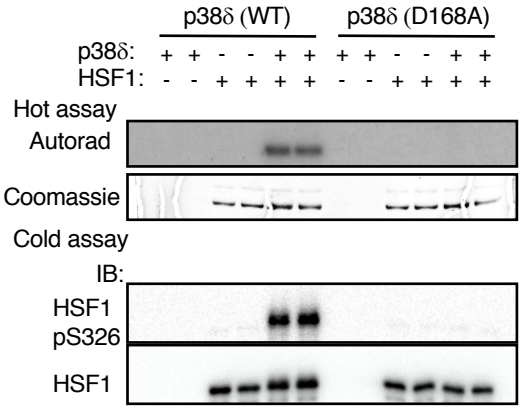

Figure 2.13. p38 MAPK phosphorylate HSF1 *in vitro*. (**A-C**) Purified activated recombinant p38 MAPK isoforms (0.06 mU/μl) were incubated with recombinant wild-type (WT), S326A mutant HSF1, MK2, or myelin basic protein (MBP) (all at 0.1 μg/μl) at 30° C for 15 min in the presence of 10 mM $MgCl_2$ and 0.1 mM [γ-^{32}P]-ATP. Identical reactions were carried out in the presence of increasing concentrations of the p38α/β inhibitor SB202190 or BIRB0796, which inhibits all p38 isoforms. The reactions were terminated by addition of SDS gel loading buffer, the samples were loaded on SDS/PAGE, and the excess [γ-^{32}P]-ATP was removed by electrophoresis. The gels were dried and subjected to autoradiography. (**B-C**) Purified activated recombinant p38α (0.06 mU/μl) was incubated with recombinant wild-type (WT) or S326A mutant HSF1 (0.1 μg/μl) at 30° C for 15 min in the presence of 10 mM $MgCl_2$ and 0.1 mM ATP. The reactions were terminated by addition of SDS gel loading buffer, the samples were loaded on SDS/PAGE, and the phosphorylation of HSF1 at S326 and the levels of total HSF1 were detected by western blotting. These experiments were performed in collaboration with Dr. Calum D. Sutherland.

under the same experimental conditions, the stoichiometry of the reaction for mutant HSF1, in which S326 was replaced with alanine (S326A) was 0.02, 0.02, 0.01 and 0.14 mol/mol for the p38α, β, ɣ and δ isoforms, respectively (**Fig. 2.12B,** grey bars and **Fig. 2.12C**), implicating S326 as one of the phosphorylation sites, and confirming the existence of additional site(s) within HSF1 which are also phosphorylated by p38 MAPK. Interestingly, this experiment also showed that, although not as robust as p38δ, p38ɣ was the most selective isoform in phosphorylating S326.

To confirm the unusually high substrate preference of p38δ for HSF1 relative to the more widely studied p38α and β isoforms, we carried out analogous reactions with MK2 as a substrate. In comparison with p38δ, the initial rates of activation of this physiological substrate are ~20 times faster for the α or β isoforms (Goedert et al., 1997). Indeed, p38δ was far less effective in phosphorylating MK2 than was p38α (**Fig. 2.13B**). In sharp contrast, p38δ was more than 20-fold more efficient than p38α in catalyzing the phosphorylation of HSF1. As expected, the p38α-, but not p38δ-mediated phosphorylation of all three substrates was dose-dependently inhibited by the p38α/β inhibitor SB202190.

As mentioned above, we employed MBP-MKK6 to obtain active bacterially produced human p38 MAPK. To make absolutely certain that the phosphorylation of HSF1 was not due to any residual MKK6, a new preparation of p38δ was made in parallel with a preparation of a kinase-dead mutant (D168A) version of the enzyme under identical conditions. After incubation and removal of the activating

kinase, each protein was used at an equivalent concentration in a reaction with HSF1 as a substrate. Phosphorylation of HSF1 only occurred with the active, but not kinase-dead p38δ, as revealed by autoradiography and western blot analysis (**Fig. 2.13C**), establishing the p38δ enzyme as the only HSF1 kinase activity in the preparation.

Together, these data demonstrate that HSF1 can be phosphorylated *in vitro* by all p38 MAPK isoforms at S326, and that p38δ is the most efficient catalyst among the isoforms, whereas p38Ɣ is the most specific. However, it is important to note that S326 is not the only site of phosphorylation by these kinases as the S326A mutant HSF1 was also phosphorylated, albeit with the expected reduction in stoichiometry. To identify the phosphorylation sites precisely, we employed a protease-mass spectrometric approach. Recombinant HSF1 was incubated with recombinant p38α or p38δ and, after electrophoretic separation and in-gel proteolytic digestion, the resulting tryptic peptides were analyzed by mass spectrometry. Under these conditions, the sequence coverage was ~50%. We found that the two p38 isoforms phosphorylated identical sites (**Table 2.1**), suggesting that the increased phosphate incorporation with p38δ was due to a faster rate of phosphorylation of the same sites that were phosphorylated by p38α and not due to phosphorylation of additional site(s). Three phosphorylated peptides were identified in each sample. The corresponding mass (m/z 2902.4659 for p38α and m/z 2902.4683 for p38δ) of the longest peptide was in precise agreement with the calculated molecular weight of a peptide containing phosphorylated S326 (m/z 2902.4689, R.VEEASPGRPSSVDTLL**S**^{326}PTALIDSILR.E). The mass of the shorter peptides

Table 2.1

p38 MAPKα + HSF1 Peptide sequence	Phospho-S	M (calc.)	M (expt.)
K.EEPPS[303]PPQS[307]PR.V	S303/307	1299.5496	1299.5487
R.VKEEPPS[303]PPQS[307]PR.V	S303/307	1526.7130	1526.7121
R.VEEASPGRPSSVDTLLS[326]PTALIDSILR.E	S326	2902.4689	2902.4659
p38 MAPKδ + HSF1 Peptide sequence	Phospho-S	M (calc.)	M (expt.)
K.EEPPS[303]PPQS[307]PR.V	S303/307	1299.5496	1299.5493
R.VKEEPPS[303]PPQS[307]PR.V	S303/307	1526.7130	1526.7121
R.VEEASPGRPSSVDTLLS[326]PTALIDSILR.E	S326	2902.4689	2902.4683

Table 2.1. Phosphopeptides identified by liquid chromatography tandem mass spectrometry after 60-min incubation of recombinant human HSF1 (1.0 µg) with p38 MAPKα or p38 MAPKδ (0.06 mU/µl), followed by SDS/PAGE separation, and in-gel tryptic digestion.

(m/z 1299.5487 and 1526.7121 for p38α and m/z 1299.5493 and 1526.7121 for p38δ) corresponded exactly to the molecular weight of peptides K.EEPPSPPQ**S**^{307}PR.V (m/z 1299.5496) and R.VKEEPP**S**^{303}PPQ**S**^{307}PR.V (m/z 1526.7130), in which both S303 and S307 were phosphorylated. Notably, S303 was found in both phosphorylated as well as unphosphorylated forms. The phosphorylation of HSF1 at S303/307 by the same kinase which phosphorylates the transcription factor at S326 was at first glance surprising, because in contrast to the activating S326 phosphorylation, phosphorylation at S303/307 is inhibitory (Kline and Morimoto, 1997, Chu et al., 1998, Xavier et al., 2000). However, this finding provides a possible explanation for the observation that although PEITC treatment causes a concentration-dependent increase in HSF1 phosphorylation (**Fig. 2.8A** and **2.10A**), induction of Hsp70 is lower at the higher PEITC concentration (**Fig. 2.2B**, **2.8A** and **2.10A**). Immunoblotting performed by our collaborators at the Centro Nacional de Biotechnologia/CSIC in Madrid (Dr. Ana Cuenda and colleagues) with isoform-specific antibodies showed that p38α, p38γ and p38δ are well expressed in MDA-MB-231 cells, and confirmed that the levels of these kinases did not change upon exposure to PEITC (**Appendix 5.2C**).

We established that PEITC causes the phosphorylation of the p38 MAPKs the MDA-MB-231 cells and showed that all isoforms for the p38 MAPKs are able to phosphorylate HSF1 *in vitro*. We also determined *in vitro* that amongst the p38 MAPK isoforms, p38γ was the isoform that showed the highest specificity to HSF1 in terms of mediating its phosphorylation at S326. On the other hand, from our *in vitro* studies p38δ was the isoform that had a 10-fold greater efficiency in phosphorylating HSF1.

3.2.12 Deletion or inhibition of p38γ decreases the phosphorylation of HSF1 at S326 in cells

To address whether p38γ and p38δ play a role in the phosphorylation of HSF1 at S326 in cells, we first used the human epidermoid cancer cell line A431, in which both p38γ and p38δ are expressed, along with its derivatives in which p38γ or p38δ had been stably knocked down by more than 90%, using selective short hairpin RNA (shRNA) (**Fig. 2.14A**) (Zur et al., 2015). In comparison to the parental cells or cells deficient in p38δ, the heat shock-mediated phosphorylation of HSF1 at S326 was reduced by 60% in cells lacking p38γ (**Fig. 2.14B**), in close agreement with the high selectivity of this isoform for the S326 phosphorylation *in vitro* (**Fig. 2.12B-D**). Treatment with the p38α/β-specific inhibitor SB202190 had no further effect, indicating that p38α and p38β do not contribute significantly to the phosphorylation of S326 in these cells (**Fig. 2.14B**).

Similar results were obtained in MDA-MB-231 cells: shRNA-mediated knockdown (by more than 90%) of p38γ led to a substantial reduction (by ~50%) in the phosphorylation of HSF1 at S326 at basal cell culture conditions, whereas the knockdown of p38δ did not have this effect (**Fig. 2.15**). The knockdown of p38γ led a corresponding decrease in the levels of Hsp70 (**Fig. 2.15**). Interestingly, the levels of Hsp70 were also reduced upon p38δ knockdown, even though the phosphorylation of HSF1 at S326 was not affected. These data suggest that p38δ might be involved in catalyzing the phosphorylation of other (than S326) sites, which activate HSF1, consistent with the highest stoichiometry

FIGURE 2.14

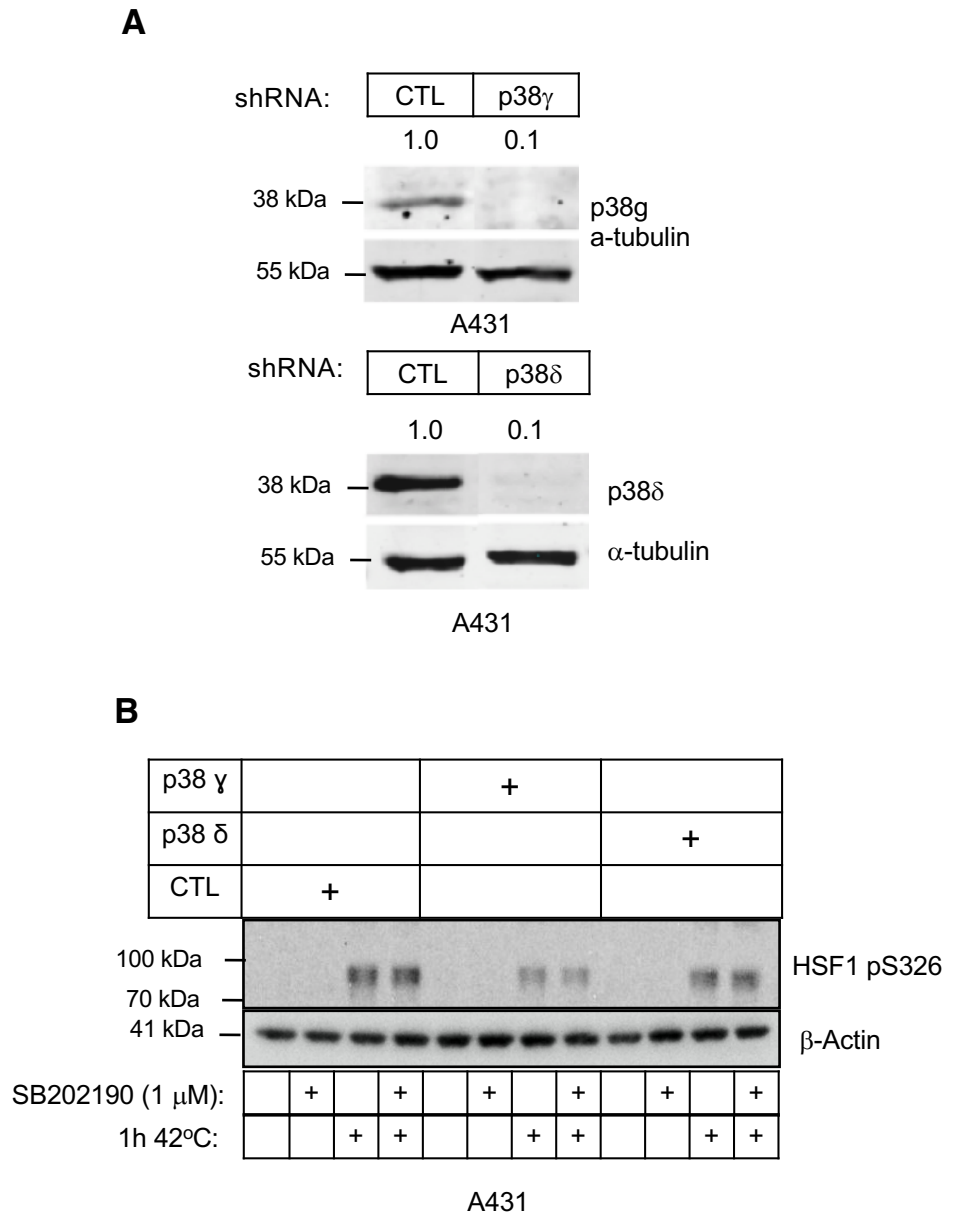

Figure 2.14. Deletion or inhibition of p38ɣ MAPK reduces the levels of pS326 HSF1 in cells. (**A**) Immunoblotting for p38 ɣ and δ in A431 cells, which either express both p38ɣ and p38δ (WT), or in which p38ɣ or p38δ had been stably knocked down using selective shRNA. (**B**) A431 cells (5 x 10^5 per well, WT or p38ɣ- or p38δ-deficient) were pre-incubated for 1 h with vehicle (0.1% acetonitrile) or SB202190, and exposed to heat shock (42 °C) for a further 1 h. The levels of HSF1 phosphorylated at S326 was detected by western blot analysis. The levels of α-tubulin (**A**) or β-actin (**B**) served as loading controls.

FIGURE 2.15

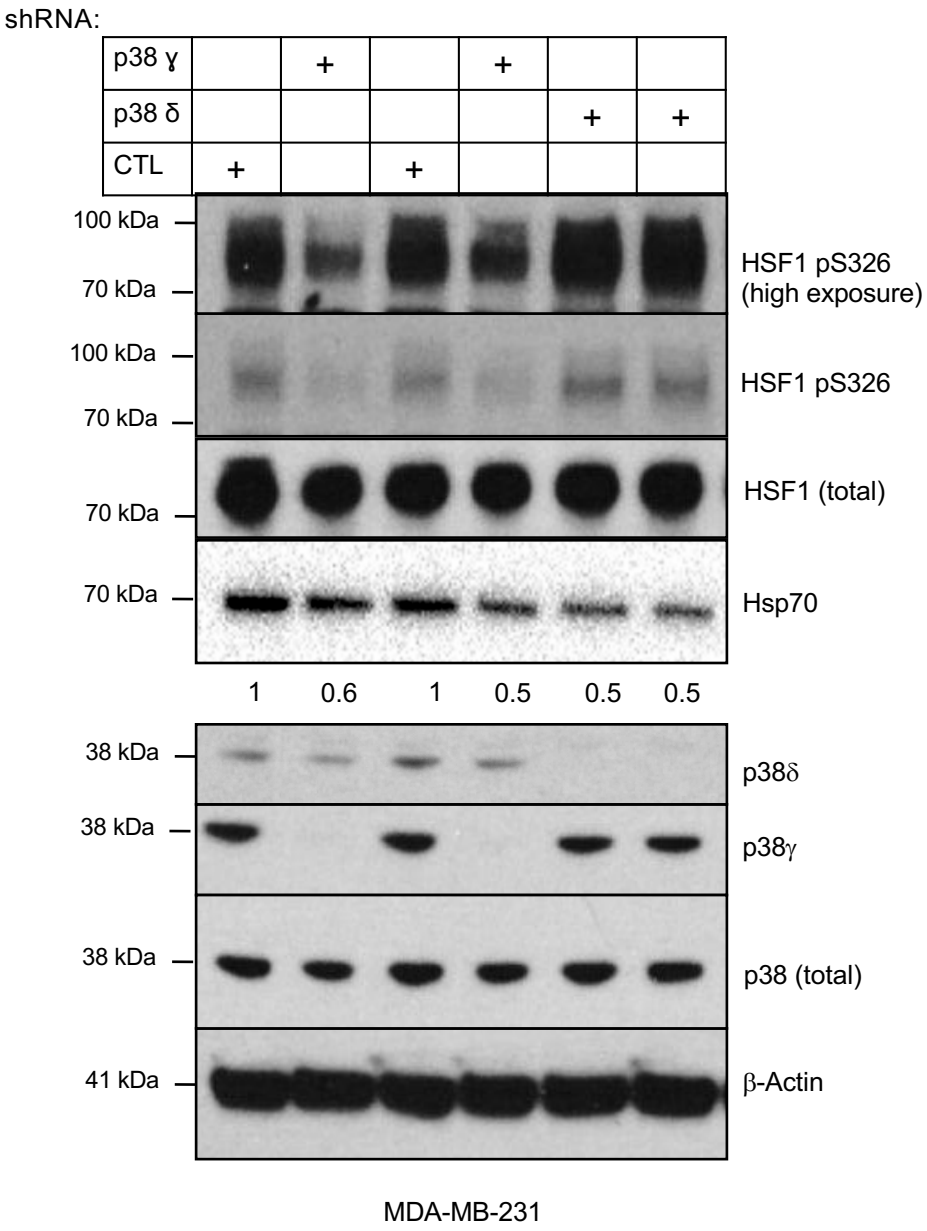

Figure 2.15. Deletion or inhibition of p38ɣ MAPK reduces the levels of pS326 HSF1 in cells. p38ɣ or p38δ was stably knocked down in MDA-MB-231 cells using selective shRNA. The levels of total HSF1, HSF1 phosphorylated at S326, total p38, p38ɣ, and p38δ, and Hsp70 were detected by western blot analysis.

of the reaction of this p38 isoform *in vitro* with both WT and S326A mutant HSF1 (**Fig. 2.12B and C**); the identity of these potential sites is presently unknown.

The conclusion that p38α and p38β do not contribute significantly to the phosphorylation of S326 in A431 cells was further supported by studies in PEITC-treated MDA-MB-231 cells, where SB202190 either had no effect (at the high concentration of PEITC) or even enhanced by 2.5-fold (at the low concentration of PEITC) the levels of pS326 HSF1 after exposure to the isothiocyanate (**Fig. 2.16A**). The activation of p38α/β by PEITC and the efficacy of SB202190 were confirmed by monitoring the levels of phosphorylated (at T334) MK2 (**Fig. 2.16A**). Finally, we used BIRB0796, which inhibits all four p38 MAPK isoforms (Kuma et al., 2005). Pre-treatment with BIRB0796 for 1 h reduced the phosphorylation of S326 in PEITC-treated MDA-MB-231 cells (**Fig. 2.16B**). Together, these findings strongly suggest that p38γ is the principal p38 MAPK isoform responsible for the phosphorylation of HSF1 at S326 in cells.

Phosphorylation at S326, but not at any of the other serine residues identified by Guettouche *et al.*, has been shown to affect the heat shock-induced transcriptional activity of HSF1 without affecting the trimerization of nuclear translocation of the transcription factor. In agreement, we found that both purified recombinant wild-type and S326A mutant HSF1 have the propensity to form dimers and trimers spontaneously (**Fig. 2.12A**). In collaboration with Jim Caunt (University of Bath), we used quantitative high content imaging to examine the nuclear and cytoplasmic distribution of wild-type, S326A or S326E mutant GFP-HSF1 fusion proteins after their ectopic expression in HSF1 knockout (HSF1-KO)

FIGURE 2.16

A

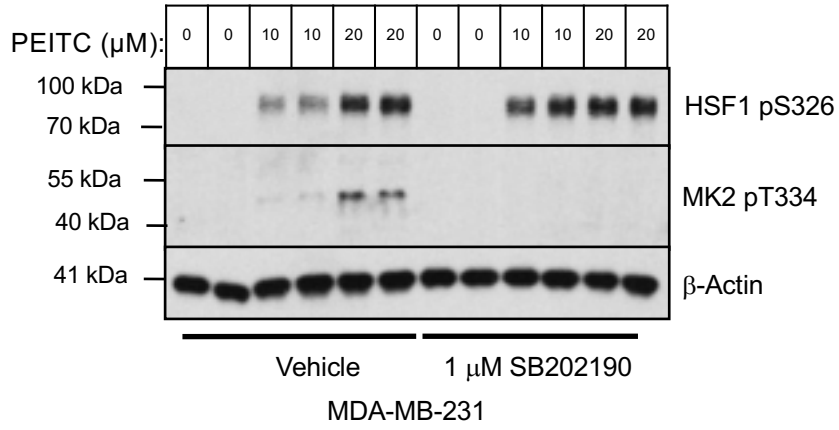

B

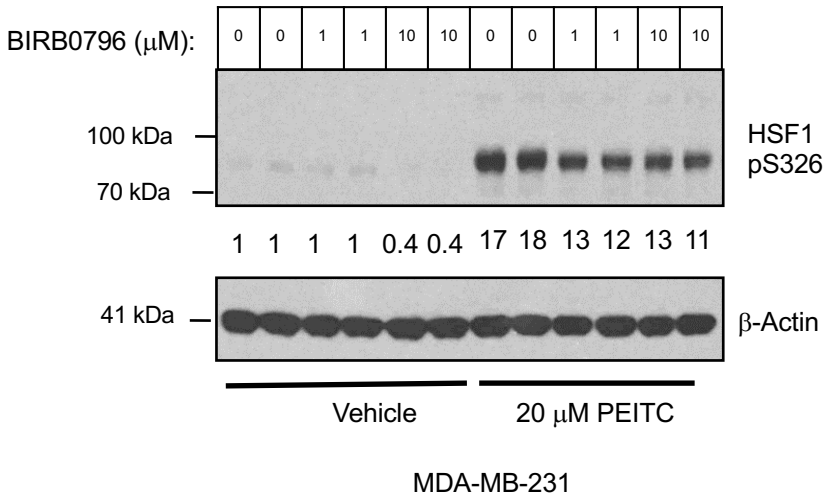

Figure 2.16. Deletion or inhibition of p38ɣ MAPK reduces the levels of pS326 HSF1 in cells. MDA-MB-231 cells (5 x 10^5 per well) grown in 6-well plates were pre-treated with vehicle (0.1% acetonitrile), SB202190 (**A**) or BIRB0796 (**B**) for 1 h, and subsequently either treated with vehicle (0.1% acetonitrile) or PEITC for a further 1.5 h. (**A,B**) HSF1 phosphorylated at S326 and MK2 phosphorylated at T334 were detected by western blot analysis. β-actin served as a loading control.

MEFs, and did not observe any significant differences among the genotypes (**Fig. 2.17**). Notably however, these results should be interpreted with caution: it is well documented that in *C. elegans,* ectopic expression of HSF1 produces a gain-of-function phenotype (Morley and Morimoto, 2004, Chiang et al., 2012), indicating that any level of overexpression of HSF1 may not accurately reflect the physiological properties of the endogenous protein.

As mentioned earlier, several reports have emerged showing that when the S326 is mutated to an alanine (A), the transcriptional activity of HSF1 is compromised (Tang et al., 2015, Chou et al., 2012, Guettouche et al., 2005). We wanted to find out whether performing similar experiments in our system would also allow us to reproduce the effect that these authors have observed.

3.2.13 HSF1 S326A, S326D and S326E mutants do not affect the binding at the Hsp70.1 promoter under basal conditions

To investigate whether the phosphorylation of S326 could affect the transcriptional activity of HSF1, we generated the phospho-deficient alanine mutant S326A and the phospho-mimetic aspartic acid and glutamic acid mutants S326D and S326E. We overexpressed either the WT, S326A, S326D or S326E FLAG-HSF1 constructs in the HeLa-HSE-luc cells stably expressing the Hsp70.1 promoter fused upstream of the luciferase gene and measured the luciferase activity in these cells (**Fig. 2.18A**). We normalized the luciferase activity to the protein expression levels of the individual constructs that were transfected. There were no differences between the WT and mutant HSF1, indicating that the

FIGURE 2.17

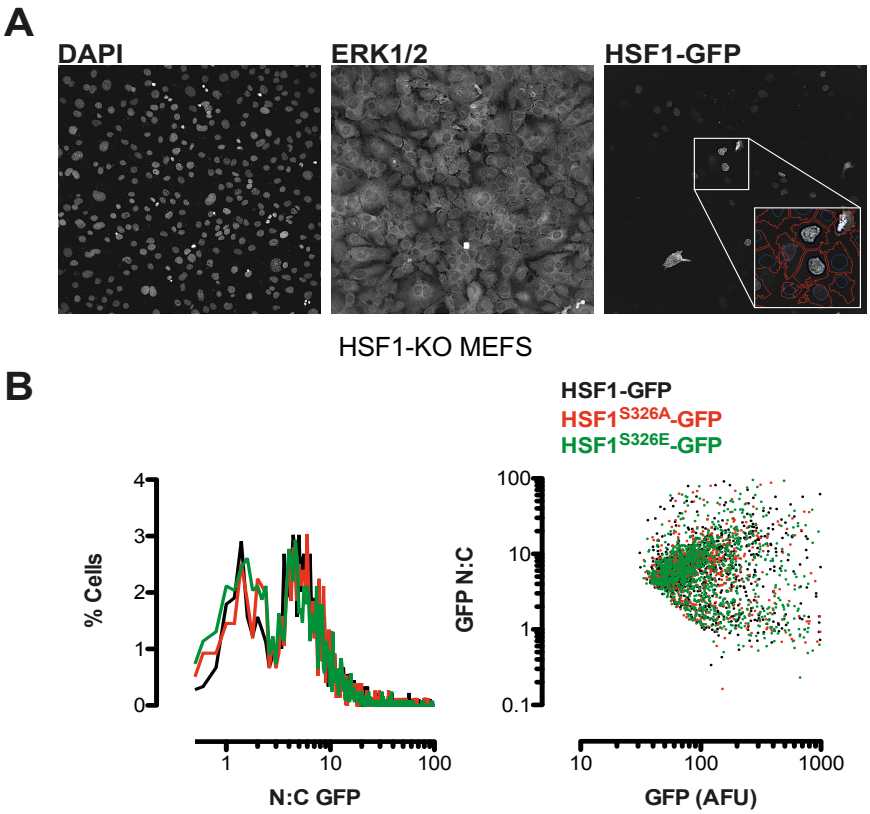

Figure 2.17. S326A/E mutation does not influence the nucleo-cytoplasmic distribution of ectopically expressed HSF1-GFP. HSF1-knockout MEFs were transfected with GFP-tagged wild-type or S326A/E mutants of HSF1 prior to counter staining with anti-ERK1/2 antibodies and DAPI. Four fields of view per well of eight replicate wells per condition were imaged using a robotic high content microscope. Automated and systematic analysis of images was performed using a custom algorithm. (**A**) A single representative field of view is shown from one well. DAPI and ERK1/2 images were used to define nuclear and cytoplasmic regions, respectively, and GFP fluorescence was recorded from each region (as indicated in the inset screengrab showing automated cell definition), accepting >70 AFU per cell as positively transfected. (**B**) Plots of single cell data show a frequency histogram of nuclear : cytoplasmic GFP fluorescence (left panel) indicating a bimodal distribution of HSF1, which is unaffected by S326A/E mutation. The right hand panel shows a comparison of whole cell GFP fluorescence in the same cell populations versus nucleo-cytoplasmic distribution, indicating that the bimodal distribution is apparent across a 10-fold difference in HSF1-GFP levels, and is again unaffected by S326A/E substitution. This experiment was conducted by Dr. Jim Caunt at the University of Bath.

phosphorylation at this site was not crucial for activating the transcriptional capability of HSF1 (**Fig. 2.18A**). Furthermore, we conducted a similar experiment in HSF1-KO MEFs, where we co-transfected the Hsp70.1 promoter luciferase, renilla luciferase and HSF1 WT or mutants, and measured the luciferase activity in these cells, however, we were unable to obtain conclusive data as the RLU levels were too low to be detectable. One of the shortcomings of the experiments of this nature is that the protein expression levels of the mutants vary greatly which could be due to differences in their turnover.

Since we have established that the p38 MAPKs, specifically, p38γ is the main kinase that phosphorylates HSF1 at S326 in A431 and MDA-MB-231 cells, we wanted to uncover the mechanism by which PEITC activates the p38 MAPK. It has been well-documented that the p38 MAPKs are activated by the upstream kinase, apoptosis signal-regulating kinase 1 (ASK1) (Dorion et al., 2002, Hsieh et al., 2010, Ichijo et al., 1997, Tobiume et al., 2001). Also, during basal conditions, the reduced form of thioredoxin (TXN1) has been shown to inhibit the function of ASK1 by directly binding to the N-terminal domain of the latter (Saitoh et al., 1998). When intracellular ROS levels increase, TXN1 is oxidized, and is unable to bind to and inhibit ASK1. When ASK1 fully dissociates from TXN1, it undergoes autophosphorylation at T845(murine)/T838(human) which is located within its kinase domain, which is followed by its subsequent oligomerization through its N-terminal coiled-coiled domain (NCC) which leads to its activation (Soga et al., 2012, Zhang and Zhang, 2002, Bunkoczi et al., 2007). Interestingly, exposure to PEITC increases intracellular ROS levels (Xiao et al., 2010, Hong et al., 2015, Jutooru et al., 2014) and the levels of oxidised TXN1, and

FIGURE 2.18

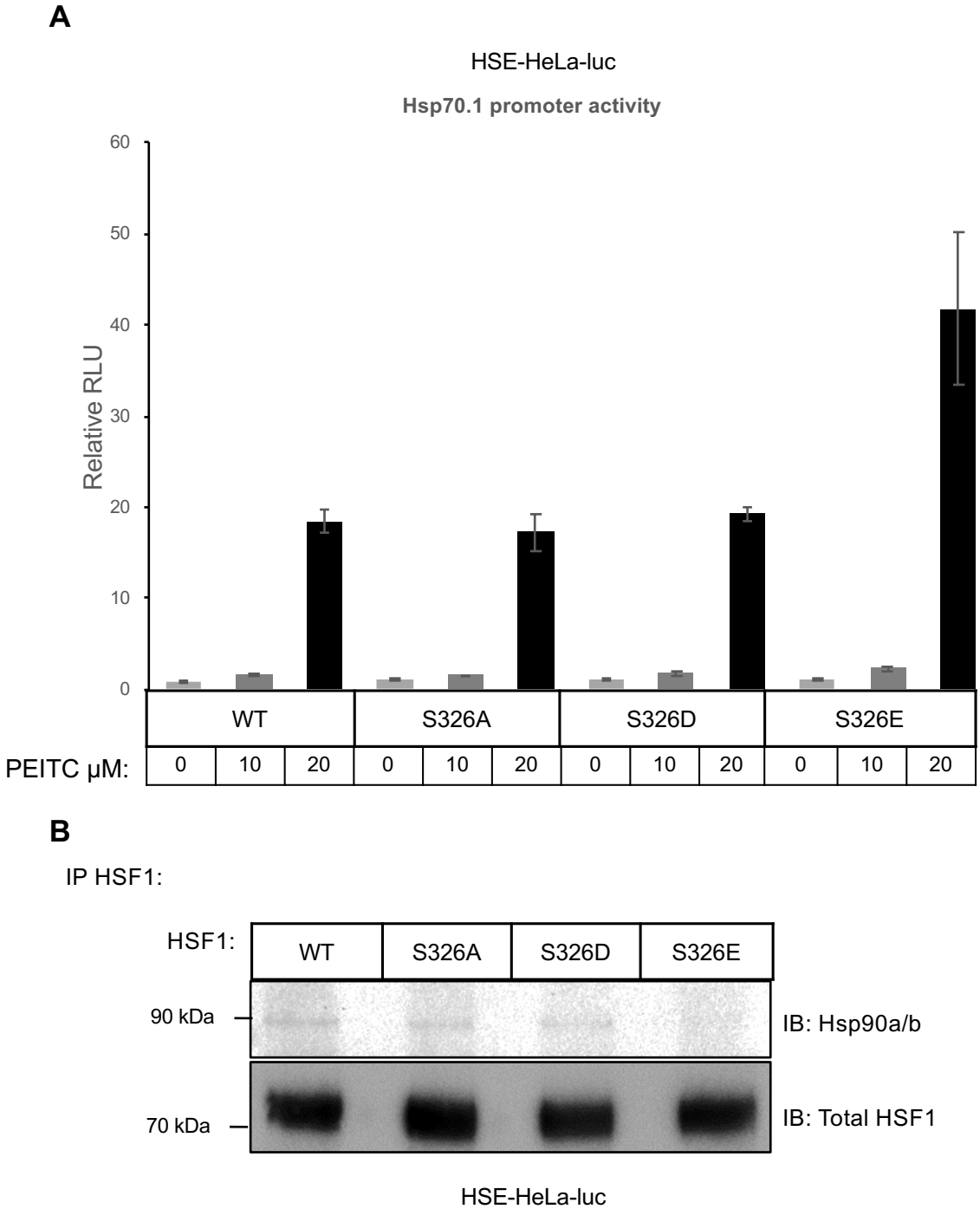

Figure 2.18. HSF1 S326A, S326D and S326E mutants do not affect the Hsp70.1 promoter activity under basal conditions. (**A**) HeLa-HSE-luc cells (1.3 x 10^5 per well) of a 12-well plate, stably expressing the luciferase gene under the control of the *HSP70.1* promoter, were transfected with either FLAG-WT HSF1 or the mutants FLAG-S326A, FLAG-S326D and FLAG-S326E constructs for 24 h after which they were exposed to vehicle (0.1% acetonitrile) or PEITC. Luciferase activity was determined in cell lysates. The relative luminescence units (RLU) were quantified and normalized with respect to the vehicle control treatment. (**B**) MDA-MB-231 cells (1 x 10^6 per well) were grown in 6-cm dishes and transfected with either FLAG-WT HSF1 or the mutants FLAG-S326A, FLAG-S326D and FLAG-S326E constructs for 24 h. Cells were lysed and subjected to immunoprecipitation with an anti-HSF1 antibody, and then immunoblotted with an anti-Hsp90 antibody. An aliquot of total lysate was subjected to immunoblot analysis with anti-Hsp90 and anti-HSF1 antibodies.

correspondingly decreases the levels of reduced TXN1 (Zhang et al., 2012). Therefore, we conducted a preliminary study to perform the knockdown of ASK1 using siRNA. We initially performed the knockdown experiments in the HeLa-HSE-luc cells as they were highly transfectable cells and would give us information on the efficiency of the knockdown.

3.2.14 siRNA-mediated knockdown of ASK1 in HeLa-HSE-luc cells greatly reduces the basal and PEITC-mediated phosphorylation of HSF1 at S326

The mRNA levels of *ASK1* at 24 and 48 h after siRNA transfection were greatly reduced by 10, 20 and 40 nM of the siRNA compared to the non-targeting negative control siRNA (siCONTROL). Relative to siCONTROL knockdown treatment, when comparing the *ASK1* transcript levels, knockdown of ASK1 at 48 h post-transfection was three times more efficient when compared to 24 h post-transfection. Hence, for all future experiments associated with siRNA-mediated ASK1 KD, we analysed and conducted experiments on cells 48 h post-transfection. Next, we treated HeLa-HSE-luc cells which we knocked down with the siCONTROL or siASK1 for 48 h and exposed the cells to vehicle, 10 μM or 20 μM PEITC for 5 h. The siASK1 knockdown cells showed greatly reduced levels of HSF1 pS326 in all treatments compared to the mock transfected cells. Excitingly, PEITC was unable to cause the phosphorylation of HSF1 at S326 in the ASK1 knockdown cells (**Fig. 2.19**) indicating that PEITC-mediated phosphorylation of HSF1 at S326 was mediated through the ASK1-p38 MAPK signaling cascade. We spent our efforts finding for an antibody that recognized

FIGURE 2.19

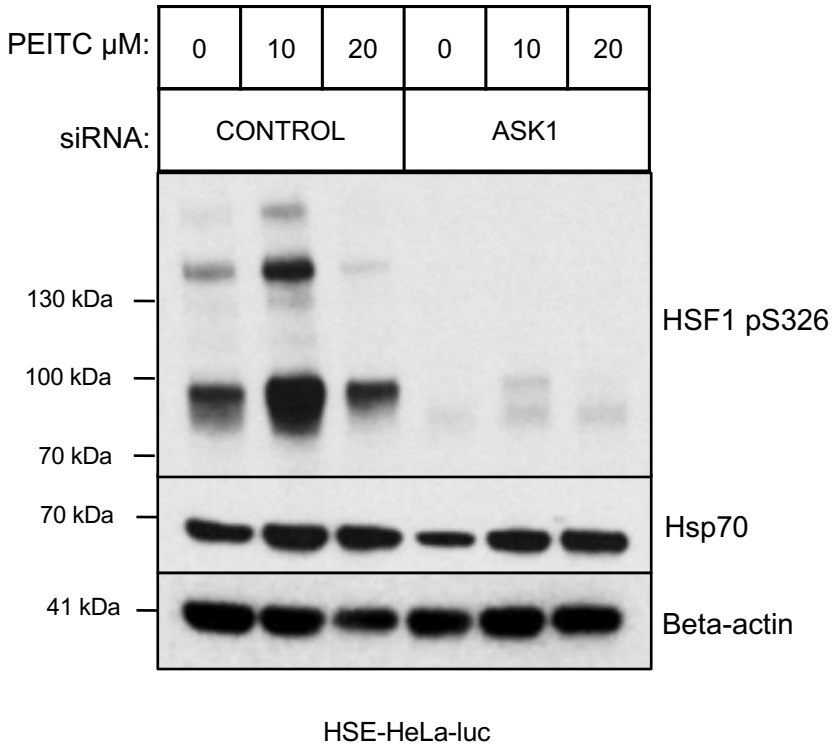

Figure 2.19. Knockdown of ASK1 in HSE-HeLa-luc cells greatly reduces the phosphorylation of HSF1 at S326. HSE-HeLa-luc cells (2.5 x 10^5 per well) growing in 6-well plates were transfected with either the negative control siRNA (siCONTROL) or ASK1 siRNA (siASK) for 48 h after which the cells were treated with vehicle (0.1% acetonitrile) or PEITC for a further 5 h. The levels of pS326 HSF1 and Hsp70 and β-actin were detected by western blot analysis, where β-actin served as a loading control.

the endogenous form of ASK1, therefore, we purchased 7 different commercially available ASK1 antibodies, however, we were unable to blot for ASK1. Interestingly, we observed a slight reduction in Hsp70 levels in the ASK1 knockdown cells compared to the mock transfected cells. Hsp70 is a prototypic marker of transcriptional activation of HSF1, it is likely that reduction of HSF1 pS326 levels could indicate that HSF1 is not as transcriptionally active compared to when it is phosphorylated at this particular site in these cells.

Since we observed that ASK1 knockdown profoundly decreases the HSF1 pS326 levels and slightly decrease Hsp70 protein levels in the HeLa-HSE-luc cells, we wanted to find out whether this effect would decrease the *Hsp70.1* promoter activity basally or when stimulated with PEITC in these cells.

3.2.15 siRNA-mediated knockdown of ASK1 in HeLa-HSE-luc cells increases the *Hsp70.1* promoter activity during PEITC-mediated heat shock response activation

We found that knockdown of ASK1, did not affect the basal *Hsp70.1* promoter-driven luciferase activity. However, surprisingly, compared to the mock transfected cells under the same conditions of PEITC treatment, knockdown of ASK1 caused an increase in *Hsp70.1* promoter activity by ~2 and 2.5-fold with 10 μM and 20 μM PEITC, respectively (**Fig. 2.20**). Together, these results suggest that, contrary to published work, phosphorylation of HSF1 at S326 is not always necessary for increasing the transcriptional activity of HSF1.

FIGURE 2.20

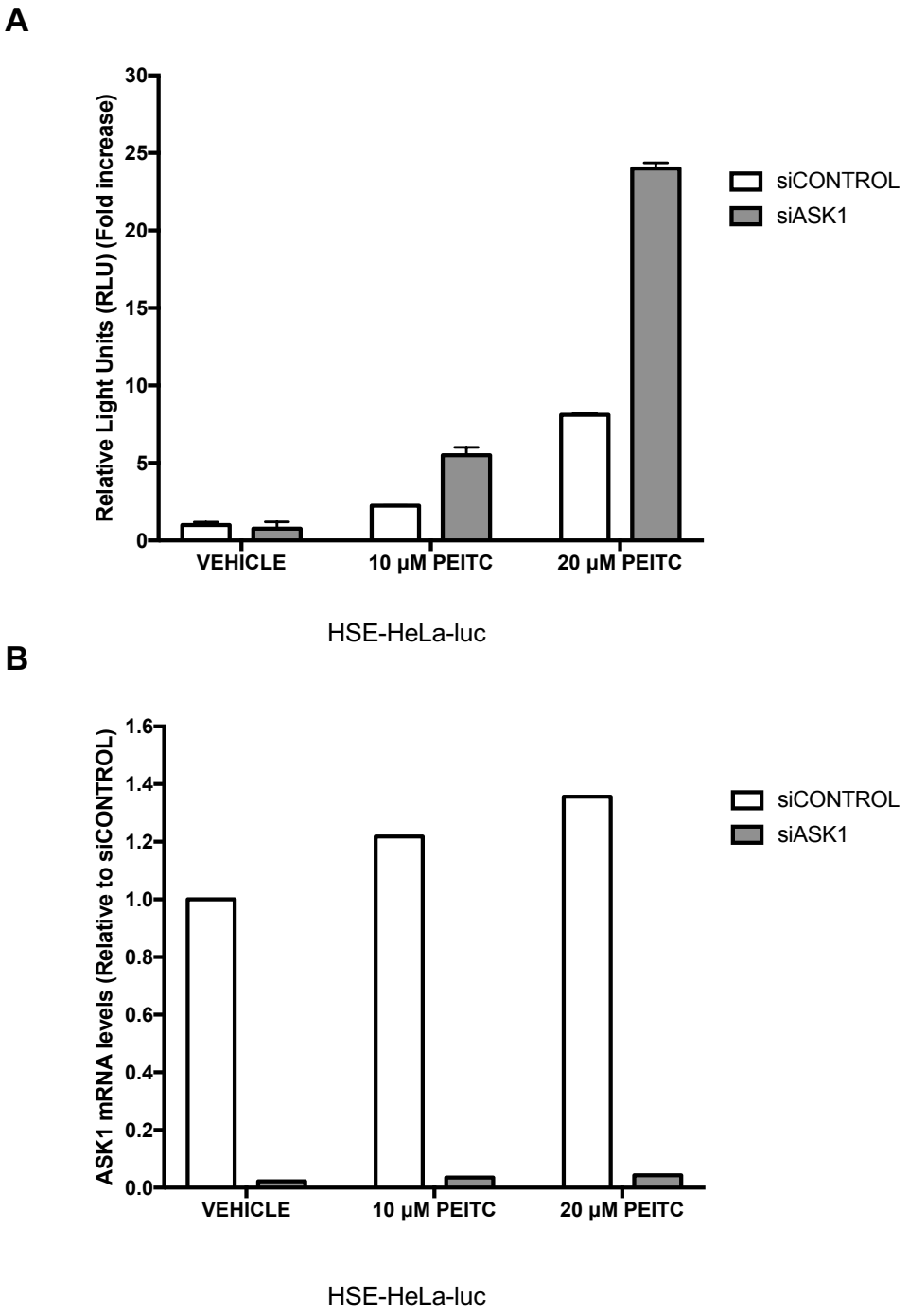

Figure 2.20. siRNA-mediated knockdown of ASK1 in HSE-HeLa-luc cells increases the Hsp70.1 promoter activity during PEITC-mediated heat shock response activation. HSE-HeLa-luc cells (1.3 x 10^5 per well) of a 12-well plate stably expressing the luciferase gene under the control of the *HSP70.1* promoter were transfected with either the negative control siRNA (siCONTROL) or ASK1 siRNA (siASK) for 48 h after which the cells were treated with vehicle (0.1% acetonitrile) or PEITC for a further 16 h. Luciferase activity was determined in cell lysates. The relative luminescence units (RLU) were quantified and normalized with respect to the vehicle siCONTROL treatment.

3.2.16 siRNA-mediated knockdown of ASK1 and exposure to the ASK1 inhibitor (NDQI-1) in MDA-MB-231 cells does not affect phosphorylation of HSF1 at S326.

Since we observed a reduction of HSF1 pS326 in ASK1 knockdown HeLa-HSE-luc cells, we wanted to investigate whether we would be able to observe a similar effect in the MDA-MB-231 cells. Therefore, we conducted a similar experiment where we treated MDA-MB-231 cells with either the siCONTROL or siASK1 for 48 h and exposed them to vehicle, 10 μM or 20 μM PEITC for 5 h post-transfection. Unlike the HeLa-HSE-luc cells, in the MDA-MB-231 cells, the levels of HSF1 pS326 remained unchanged despite the reduction of ASK1 levels (**Fig. 2.21A**). The efficiency of the siRNA knockdown was validated by analyzing the transcript levels of *ASK1* using real-time PCR (**Fig. 2.22**). In another experiment, we pretreated MDA-MB-231 cells with the commercially available ASK1 inhibitor 2,7-Dihydro-2,7-dioxo-3*H*-naphtho[1,2,3-*de*]quinoline-1-carboxylic acid ethyl ester (NDQI-1) for 1 h, exposed these cells to PEITC for a further 2 h, analyzed the levels of phosphorylated HSF1 S326 by western blotting (**Fig 2.21B**), and found no reproducible reduction in pS326 HSF1. The combination of NDQI-1 and PEITC led to increased cytotoxicity, hence, the HSF1 S326 phosphorylated levels were difficult to interpret.

Taken together, these results indicate that the phosphorylation of HSF1 at S326 might not be critical for its transcriptional activation, contrary to what has been published in the literature thus far (**Fig. 2.21, 2.22**). However, it is important to note that phosphorylation of HSF1 at S326 is a prominent marker for activation

FIGURE 2.21

A

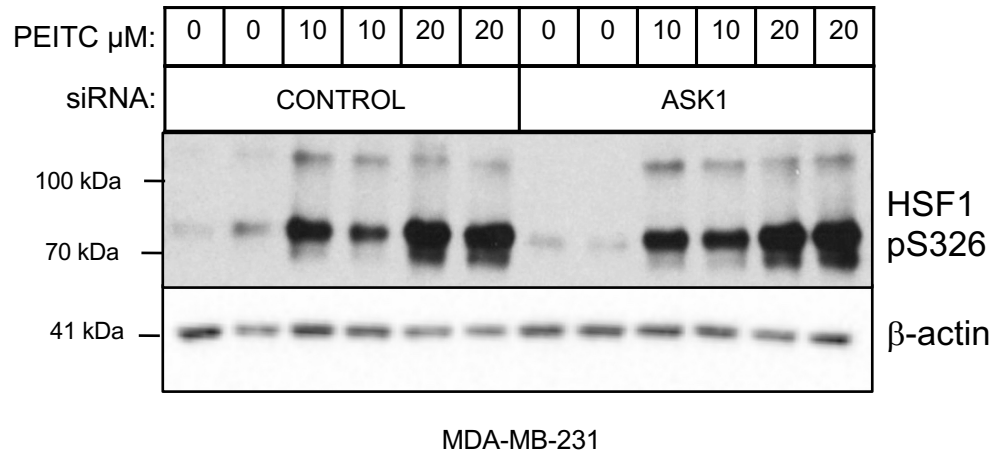

B

Figure 2.21 Knockdown of ASK1 and exposure to the ASK1 inhibitor (NDQI-1) in MDA-MB-231 cells does not affect phosphorylation of HSF1 at S326. (**A**) MDA-MB-231 cells (3 x 10^5 per well) transfected with either the negative control siRNA (siCONTROL) or ASK1 siRNA (siASK) for 48 h after which the cells were treated with vehicle (0.1% acetonitrile) or PEITC for a further 3 h. (**B**)MDA-MB-231 cells (5 x 10^5 per well) grown in 6-well plates were pre-treated with vehicle (0.1% acetonitrile) or NDQI-1 for 1 h, and subsequently either treated with vehicle (0.1% acetonitrile) or PEITC for a further 3 h. (**A,B**) HSF1 phosphorylated at S326 was detected by western blot analysis. β-actin served as a loading control.

FIGURE 2.22

A

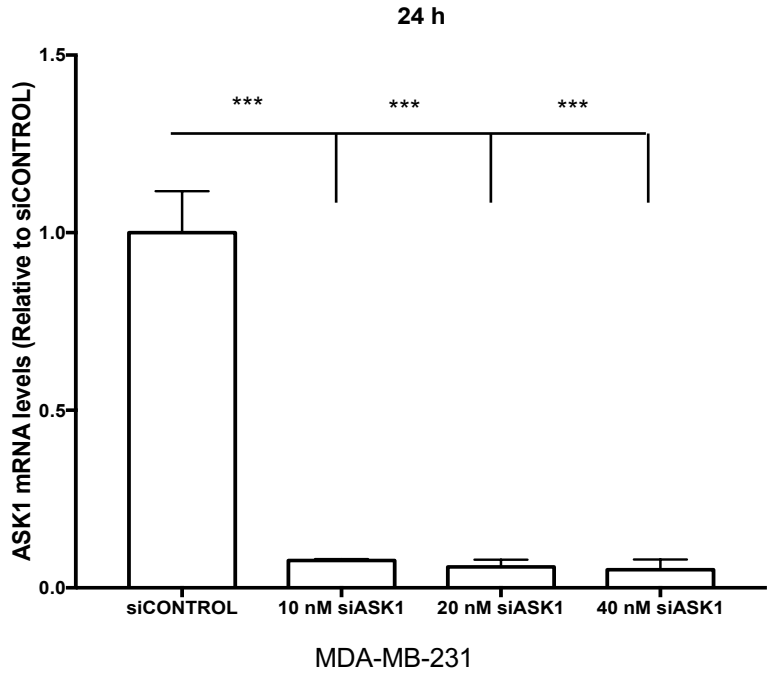

B

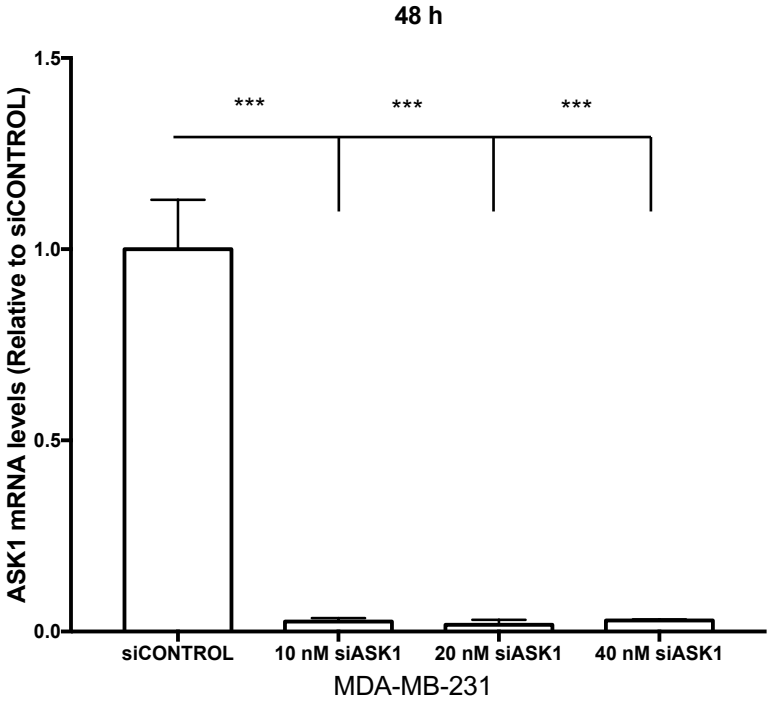

Figure 2.22 siRNA for ASK1 efficiently reduces *ASK1* mRNA levels. (**A**) MDA-MB-231 cells (3 x 10^5 per well) transfected with either the negative control siRNA (siCONTROL) or ASK1 siRNA (siASK) for 24 (**A**) or 48 h (**B**). Cells were lysed, total RNA was extracted, and reverse transcribed into cDNA. The mRNA levels for *ASK1* were quantified using real-time PCR. The data were normalized using 18S as an internal control. Data represent means ± SD and are expressed as ratio of the relative transcripts in treated over control samples. *** is when $p < 0.01$.

of the heat shock response as it occurs rapidly upon exposure to heat stress or electrophiles such as PEITC. These results beg the question as to why this site, S326, is rapidly phosphorylated during the activation of the heat shock response. As described earlier, during homeostatic conditions, monomeric HSF1 is bound to the Hsp90 multichaperone complex in the cytoplasm. Upon exposure to stress, HSF1 is released from the Hsp90 multichaperone complex and undergoes posttranslational modifications, mainly phosphorylation events, and is then able to translocate to the nucleus where it assumes its transcriptionally active trimeric form. Perhaps the phosphorylation of HSF1 at S326 during stress, prevents its binding to its negative regulator Hsp90, and hence allows it to function as a transcription factor. We tested this possibility in the next set of experiments.

3.2.17 HSF1 S326E phospho-mimetic mutant is unable to bind to Hsp90

We transfected constructs encoding the FLAG-tagged WT HSF1 and its mutants S326A, S326D and S326E into HeLa-HSE-luc cells and performed a co-immunoprecipitation experiment 24 h later. We pulled down HSF1 using a total HSF1 antibody and immunoblotted for endogenous Hsp90. We found that the phosphomimetic mutant HSF1 S326E was unable to bind to endogenous Hsp90 (**Fig. 2.18B**). This result suggests that phosphorylation of HSF1 S326 may dissociate the transcription factor from its negative regulator Hsp90, perhaps facilitating its translocation into the nucleus to trimerize and bind to heat shock elements.

3.2.18 Discussion

By use of mass spectrometry and protein sequencing, Guettouche *et al.* (Guettouche et al., 2005) found that in cells subjected to heat shock, human HSF1 is phosphorylated at 12 serine residues: S121, S230, S292, S303, S307, S314, S319, S326, S344, S363, S419, and S444. More recently, using mass spectrometry-based proteomics, Xu *et al.* (Xu et al., 2012) reported the phosphorylation at five additional serine residues (S127, S195, S216, S320, and S368), and at four threonine residues (T142, T323, T367, and T369). The functional significance of most threonine phosphorylations is unknown, except for T142, the phosphorylation of which by casein kinase 2 (CK2) has been reported to increase the transcriptional activity of HSF1 (Soncin et al., 2003). It is well established that phosphorylations at S303/307, S121 and S363 inhibit the function of the transcription factor and are involved in the attenuation phase of the heat shock response (Kline and Morimoto, 1997, Chu et al., 1998, Xavier et al., 2000, Wang et al., 2006), whereas phosphorylation at S216 by Polo-like kinase 1 (PLK1) promotes the ubiquitination and degradation of HSF1 during mitosis (Lee et al., 2008a). Curiously, PLK1 also phosphorylates HSF1 at S419, but in contrast to the inhibitory S216 phosphorylation, phosphorylation at S419 is activating and promotes the nuclear translocation of the transcription factor (Kim et al., 2005). Phosphorylation at S320 by protein kinase A (PKA) also activates HSF1 (Murshid et al., 2010). Another activating phosphorylation occurs at S230; it is catalyzed by calcium/calmodulin-dependent protein kinase II (CaMKII) and enhances the magnitude of the response upon heat stress (Holmberg et al.,

2001). Although the DNA-binding ability of the S230A mutant of HSF is retained, its transcriptional activity is reduced by ~50% in comparison with wild-type HSF1.

Phosphorylation at S326 is a hallmark for HSF1 activation, and several studies have attempted to identify the kinase(s) phosphorylating this site. It was reported that the mechanistic target of rapamycin (mTOR) is able to catalyze the phosphorylation of HSF1 at S326 (20). However, PEITC inhibits mTOR (Cavell et al., 2012). In full agreement, we also found that the mTOR pathway was inhibited by PEITC, as evidenced by the decreased phosphorylation of the ribosomal subunit S6 at S235/236 (**Fig. 2.10B**). Overall, our data presented in this contribution imply that mTOR is not the primary kinase responsible for the phosphorylation of S326 on HSF1 in response to treatment with PEITC, and further implicate the family of proline-directed p38 MAPK as highly efficient catalysts, which phosphorylate HSF1 rapidly and stoichiometrically. Notably however, neither pharmacological inhibition of p38 MAPK by small molecule inhibitors or genetic downregulation of p38γ or p38δ eliminated completely the phosphorylation of HSF1 at S326 (**Fig. 2.16B**). These results imply that although p38γ is the principal isoform within the p38 MAPK family that phosphorylates this site, inactivation of p38γ allows for compensation by other kinases. One such candidate is JNK1/2, which is also activated by PEITC, albeit at a later time point in comparison with p38 MAPK. It has been reported that p38 MAPK engage in feedback control loops that suppress the activities of upstream MAP kinase kinase kinases (MAP3Ks), which participate in the activation JNK, and by disrupting these feedback control loops, inhibition of p38 leads to hyperactivation

of JNK (Cohen, 2009). The possibility that JNK1/2 could phosphorylate HSF1 at S326 requires a further study.

Interestingly and unexpectedly, we found that in addition to S326, p38 MAPK can also catalyze the phosphorylation of HSF1 at S303/307 (**Table 2.1**). In contrast to the activating function of the S326 phosphorylation, phosphorylation at S303/307 inhibits the function of HSF1 (14-16). Although surprising, the fact that the same kinase can catalyze phosphorylation of two distinct sites on HSF1 with opposing functional consequences is not unprecedented. As mentioned above, phosphorylation at S216 by PLK1 inhibits HSF1, whereas phosphorylation at S419 by the same kinase activates the transcription factor (Kim et al., 2005, Lee et al., 2008a). Our results imply that either p38 MAPK phosphorylate S326 at a faster rate than at S303/307, thus giving a “window” of HSF1 activation due to S326 phosphorylation before the repressive effect of S303/307 phosphorylation takes place, or alternatively, that there is a threshold of MAPK p38 activation below which S326 is the principal target, and above which the S303/307 phosphorylation becomes dominant. The second possibility is supported by the fact that induction of Hsp70 is lower upon treatment with the higher (20 μM) compared to the lower (10 μM) concentration of PEITC, whereas the extent of HSF1 phosphorylation is dependent on the dose of PEITC. In addition, the identity of the phosphatases involved may also influence the relative turnover rates of phosphorylation at each site. Dissecting these possibilities requires better tools for quantitation of relative stoichiometry of phosphorylation at S303/307 vs. S326 in different cell compartments.

Previous investigations have suggested the possible involvement of MAPK signaling in the activation of HSF1. Thus, loss of the tumor suppressor neurofibromatosis type 1 (NF1) leads to activation of MAPK signaling and HSF1 (Dai et al., 2012). Chronic exposure of rodent fibroblast cells to heat stress causes phosphorylation of p38 MAPK and induction of Hsp70 (Banerjee Mustafi et al., 2009). In addition, the anti-inflammatory agent sodium salicylate, has been reported to activate p38 MAPK, promote HSF1 DNA binding and transcriptional activity, and induce Hsp70 expression (Seo et al., 2005). Most recently, it was reported that HSF1 physically interacts and is phosphorylated by MEK (Tang et al., 2015). However, to our knowledge, there are no prior publications linking HSF1 phosphorylation at S326 directly with p38 MAPK activation. In our study, the identification of p38 MAPK as one family of kinases, which phosphorylate HSF1 at S326 was greatly facilitated by the observation that PEITC is an exceptionally robust activator of HSE-dependent transcription (**Fig. 2.6A**). PEITC shares the ability to induce the heat shock response with celastrol (Dayalan Naidu et al., 2015, Trott et al., 2008, Westerheide et al., 2004a), another natural product which like PEITC, has a characteristic chemical signature, reactivity with sulfhydryl groups (Trott et al., 2008). Notably, in a screen comprising ~900 000 small molecules, Calamini *et al.* (Calamini et al., 2012) discovered new classes of HSF1 activators, all of which, although structurally diverse, bear the same chemical signature. We propose that this chemical property underlies the ability of PEITC to both inhibit Hsp90 as well as activate p38 MAPK. The role of phosphorylation in the activation of NRF2 is not well-established, and it a subject of investigation by multiple groups. Although PEITC causes NRF2 stabilisation through cysteine modifications of KEAP1, we also considered the possibility that

by activating p38 MAPK, PEITC might further contribute to NRF2 activation. In a preliminary experiment, we conducted an in vitro kinase assay by incubating the recombinant human NRF2 Neh6 fragment with the p38 β, ɣ and δ isoforms and found that they were all able to phosphorylate NRF2. Interestingly, p38 β and ɣ selectively phosphorylate NRF2 at the S324 site, whereas the δ isoform's preferred phosphorylation site was S347 (**Fig. 2.23**). As discussed in the Introduction of Section 1, Chapter B, NRF2 and HSF1-regulated cytoprotective pathways and target genes at times overlap depending on the stressors, and this data presents the idea that these two transcription factors could be regulated by the same, if not, similar subset of proteins such as the p38 MAPKs.

3.2.18 Conclusions

Pharmacological targeting of p38γ and p38δ has been recently proposed for the treatment of autoimmune and inflammatory diseases, as well as cancer (Escos et al., 2016). As HSF1 activation supports malignant transformation (Santagata et al., 2011, Mendillo et al., 2012), this approach holds promise for targeting HSF1 for cancer treatment. Also, we have discovered that the upstream kinase ASK1, is responsible for mediating phosphorylation of HSF1 at S326 (**Fig. 2.19**), possibly through activation of p38 MAPKs, however, this effect is only observed in the HeLa-HSE-luc cells and not in the MDA-MB-231 cells (**Fig. 2.21**). It is possible that there are different upstream kinases activated by PEITC, which in turn activate the p38 MAPK signaling cascade in different cell lines, hence, uncovering these pathways will be vital for our understanding of activation of the heat shock response. Interestingly, dual-specificity phosphatase 26 (DUSP26)

FIGURE 2.23

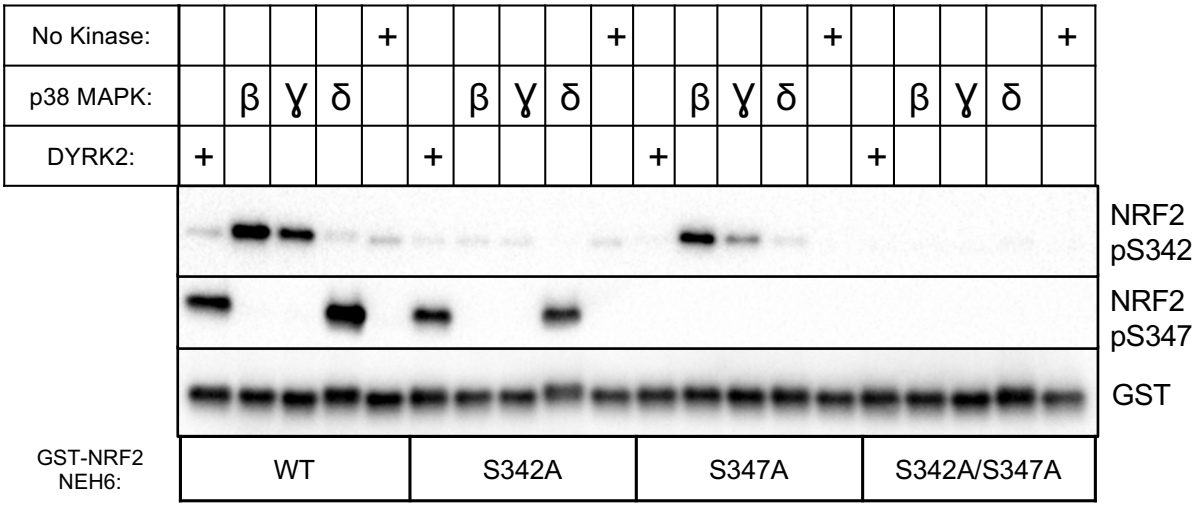

Figure 2.23. p38 MAPKs are able to phosphorylate the Neh6 domain of NRF2. Purified activated recombinant DYRK2, p38 β, ɣ and δ (0.06 mU/µl) was incubated with recombinant wild-type GST-tagged NEH6 domain of NRF2 (0.1 µg/µl) at 30° C for 15 min in the presence of 10 mM $MgCl_2$ and 0.1 mM ATP. The reactions were terminated by addition of SDS gel loading buffer, the samples were loaded on SDS/PAGE, and the phosphorylation of NRF2 at S342 and S347 and the levels of total GST were detected by western blotting.

directly dephosphorylates p38 MAPK and represses its downstream kinase activity; mutation of cysteine 151 in its active site to a serine, inactivates the phosphatase (Vasudevan et al., 2005). It is possible that PEITC is able to inactivate DUSP26 by targeting C151, hence allowing for continued p38 phosphorylation resulting in the sustained phosphorylation of HSF1 at S326. Further studies need to be conducted to test this hypothesis.

Chapter 3

Physiological significance of HSF1 phosphorylation at S326

3.3.1 Introduction

As described in Chapter 2 of Section 3, we have found that all four p38 MAPK isoforms are able to catalyse the phosphorylation of HSF1 at S326 in vitro (Dayalan Naidu et al., 2016). We further identified p38ɣ as the main isoform that phosphorylates HSF1 at S326 in cells (Dayalan Naidu et al., 2016). We have also shown evidence that phosphorylation of HSF1 at S326 does not affect its transcriptional activity of HSF1, in contrast to previous reports (Guettouche et al., 2005, Chou et al., 2012). Nevertheless, it is clear from the work from our lab and other groups that phosphorylation of HSF1 at S326 is a marker of activation of the HSR (Dai et al., 2012). Upon exposure to the Hsp90 inhibitor and the HSR activator PEITC, phosphorylation of HSF1 at S326 occurs within 15 min in the cytoplasm, and subsequently the phosphorylated HSF1 S326 accumulates in the nucleus (Dayalan Naidu et al., 2016). Under basal conditions, HSF1 pS326 levels are significantly lower than when the HSR is activated. Apart from the two observations that phosphorylated HSF1 at S326 levels dramatically increase upon HSR activation and that increase of these levels correlates with poor cancer prognosis (Yih et al., 2012, Li et al., 2014, Chou et al., 2012), the question of the physiological significance of this phosphorylation still remains.

We first wanted to compare the sub-cellular localisation of HSF1 pS326 to that of the total HSF1. To address this question, we performed immunofluorescence experiments using the osteosarcoma cell line U2OS as these cells have a well-functioning HSR and express HSF1 pS326 basally. Unsynchronised U2OS cells were fixed using 37^{o}C pre-warmed 3.7% paraformaldehyde to preserve most of the cellular structures including cytoskeletal filaments and DNA orientation, and co-stained with antibodies against total HSF1 and HSF1 pS326. We also used DAPI (4',6-diamidino-2-phenylindole), a fluorescent nucleic acid stain, to allow for identification of the localisation of the chromosomes.

3.3.2 HSF1 pS326 and HSF1 differ in their sub-cellular localisation

In U2OS interphase cells, HSF1 is mainly localised in the cytoplasm and is mostly concentrated at the periphery of the nucleus (**Fig. 3.1 and 3.2**); its staining pattern is reminiscent of that of proteins found in the Golgi apparatus such as GOLGB1 (Asante et al., 2013) and GOLM1 (Byrne et al., 2015). Although not as intense, it is evident that the total HSF1 antibody recognises HSF1 pS326 as it stains the regions where HSF1 pS326 is present. In contrast to the total HSF1, the HSF1 pS326 staining shows that the phosphorylated protein is localised predominantly in the cytoplasm. In the cytoplasm, HSF1 pS326 seems to be localised to a particular cytoskeletal structure within the cell (**Fig. 3.1 and 3.2**). Overall, it is striking that the localisation of HSF1 phosphorylated at S326 in interphase cells is almost mutually exclusive to the total HSF1 localisation (**Fig. 3.1 and 3.2**).

FIGURE 3.1

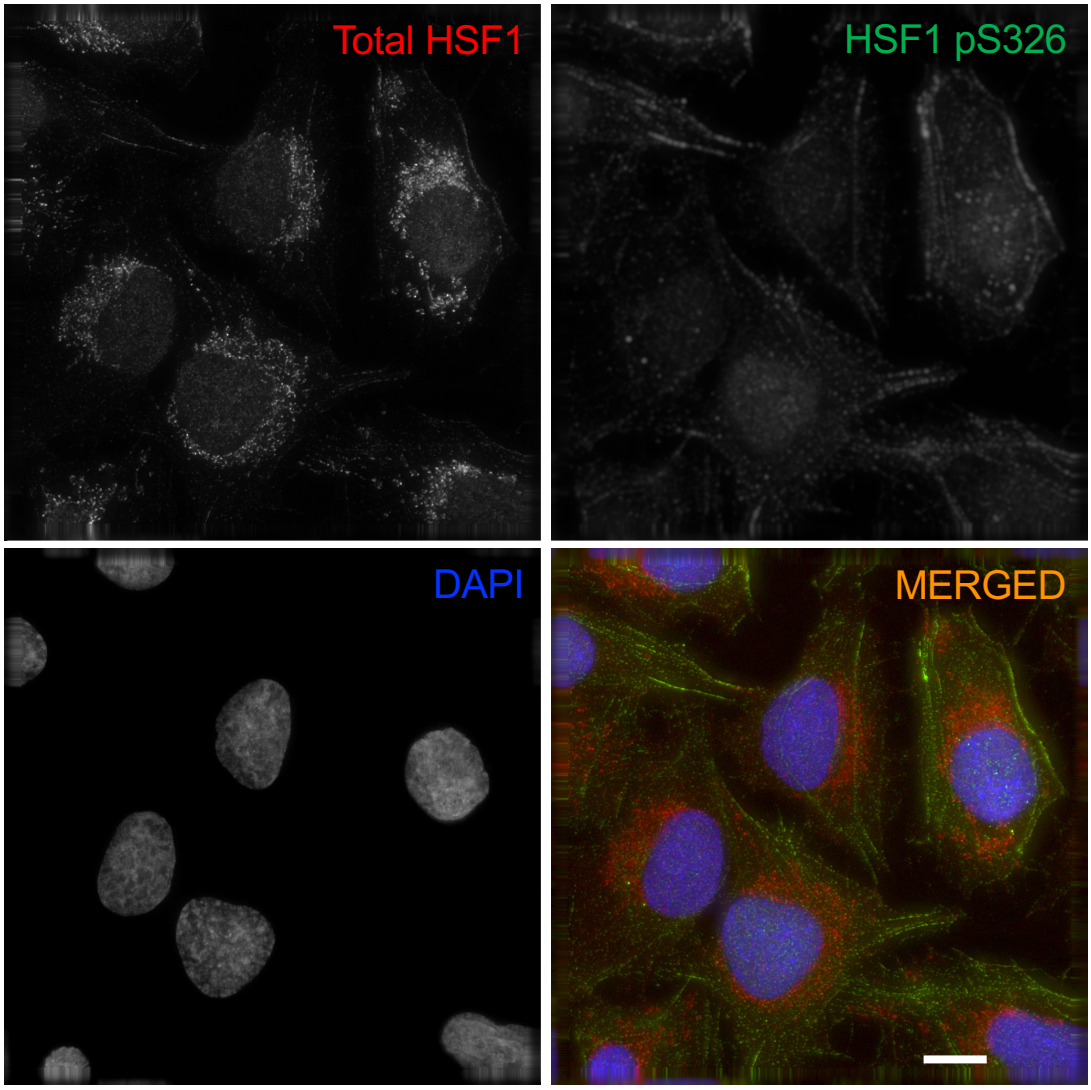

Figure 3.1. Localisation of HSF1 phosphorylated at S326 in interphase or resting cells is almost mutually exclusive to total HSF1 localisation. Representative image of unsynchronised U2OS cells stained with antibodies against total HSF1 (left top panel, red on overlay), HSF1 pS326 (right top panel, green on overlay) and with DAPI (left bottom panel, blue on overlay). The bottom right image is a merged image of all three channels. The image was obtained and deconvolved using the Deltavision™ Elite (GE Healthcare) microscope and imaging system. Maximum intensity of 25 optical sections is shown. The scale bar represents 25 μm.

FIGURE 3.2

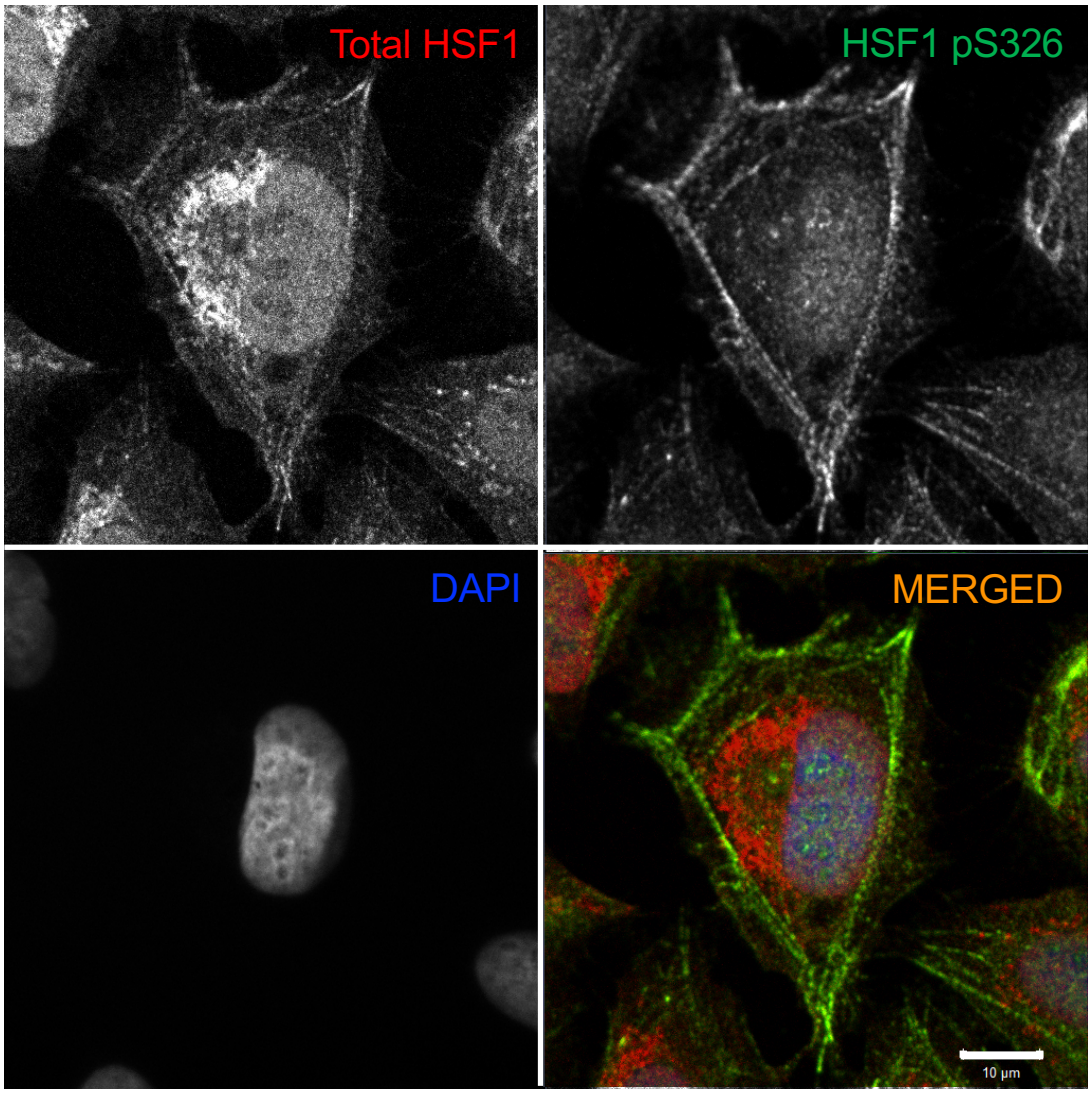

Figure 3.2. Localisation of HSF1 phosphorylated at S326 in interphase or resting cells is almost mutually exclusive to total HSF1 localisation. Representative image of unsynchronised U2OS cells stained with antibodies against total HSF1 (left top panel, red on overlay), HSF1 pS326 (right top panel, green on overlay) and with DAPI (left bottom panel, blue on overlay). The bottom right image is a merged image of all three channels. The individual channels are displayed without colour. The bottom right image is a merged image of all three channels. The image was obtained using the Zeiss LSM 710 (Zeiss) microscope and imaging system. A single optical section is shown. The white scale bar represents 10 µm.

3.3.3 The levels of HSF1 pS326 are significantly higher in mitotic cells compared to interphase cells

Interestingly, we noticed that a small number of fixed cells stained with HSF1 pS326 had exceptionally high staining intensity compared to the other cells (**Fig. 3.1**). Upon examination of DAPI staining, we discovered that these cells were at various stages of mitosis. **Fig. 3.3 and 3.4** show representative images of such cells from over three independent experiments. In **Fig. 3.3**, the cell indicated by an arrow, is likely to be at the late prometaphase, as apparent from the image of compacted chromosomes in the DAPI channel (bottom left panel). The cell indicated by arrowhead is in metaphase, with the chromosomes (DAPI channel, bottom left image) aligned at the metaphase plate. Both cells display strongly elevated levels of HSF1 (top left panel) and HSF1 pS326 (top right panel), compared to the surrounding cells in this field of view. In **Fig. 3.4**, the two cells with the highest intensity of total HSF1 (top left) and HSF1 pS326 (top right) are both undergoing different stages of mitosis: telophase (arrow) and metaphase (arrowhead). Thus, it appears that mitotic cells have higher levels of HSF1 and/or HSF1 pS326, compared to the neighbouring interphase cells. At this point, it is precarious to assume that total HSF1 levels are increased during mitosis, as the total HSF1 antibody is also able to recognise the HSF1 pS326, and since HSF1 pS326 levels are increased in mitotic cells, the total antibody will be able to bind it as well. A western blot analysis comparing total and pS326 HSF1 levels in interphase versus mitotic cells would solve the question of whether total HSF1 levels are increased during mitosis. We have addressed this later in this section.

FIGURE 3.3

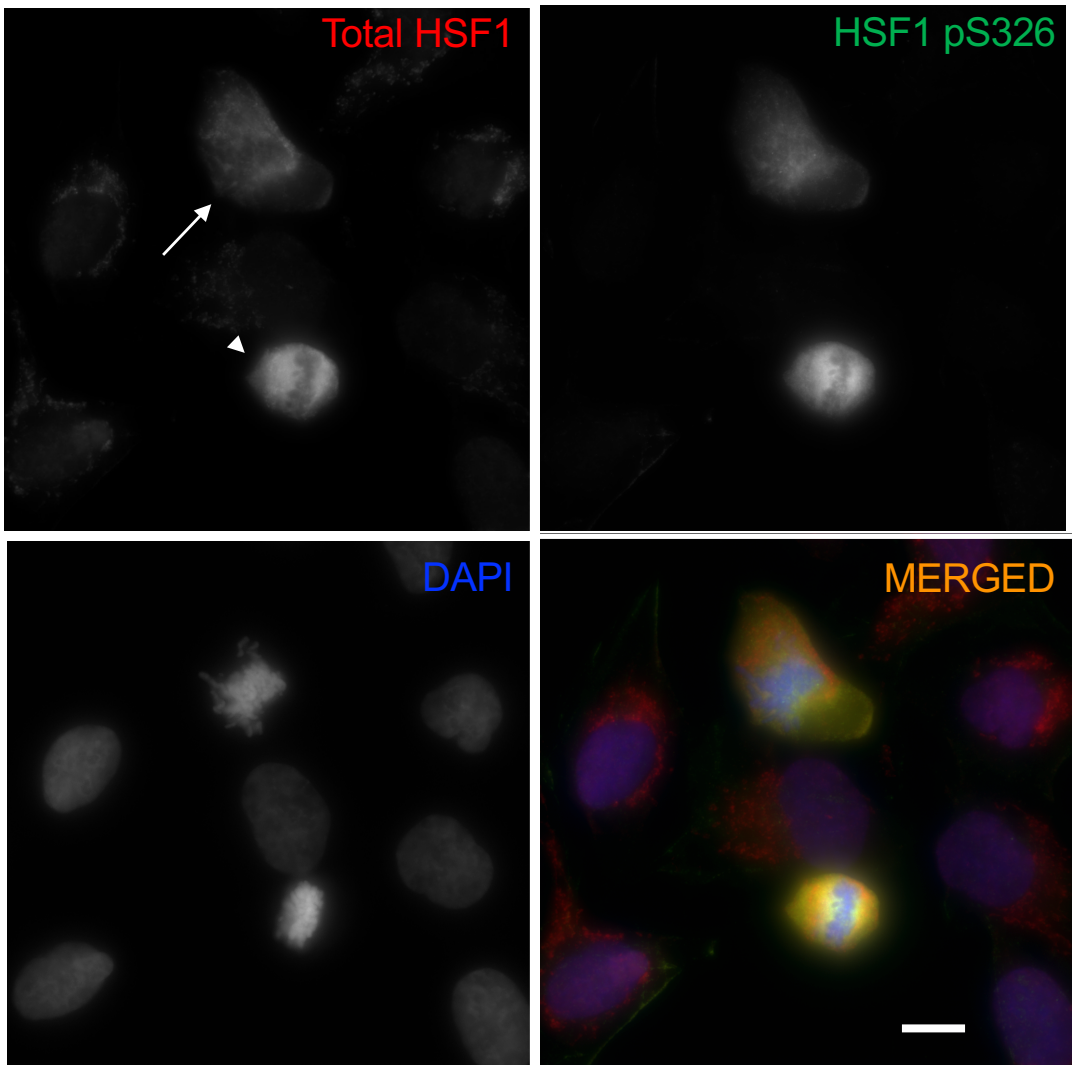

Figure 3.3. Phosphorylation of HSF1 at S326 is significantly higher in mitotic cells compared to interphase cells. Representative confocal immunofluorescence image of unsynchronised U2OS cells stained with antibodies against total HSF1 (red), HSF1 pS326 (green) and the DNA stain, 4′,6-Diamidino-2-phenylindole dihydrochloride (DAPI) (blue). The individual channels are displayed without colour. The bottom right image is a merged image of all three channels. There are two mitotic cells in this figure, where they are at the following stages of mitosis: 1) prometaphase (top, arrow) and 2) metaphase (bottom, arrowhead). The image was obtained using the Zeiss LSM 710 (Zeiss) microscope and imaging system. A single optical section is shown. The white scale bar represents 10 μm.

FIGURE 3.4

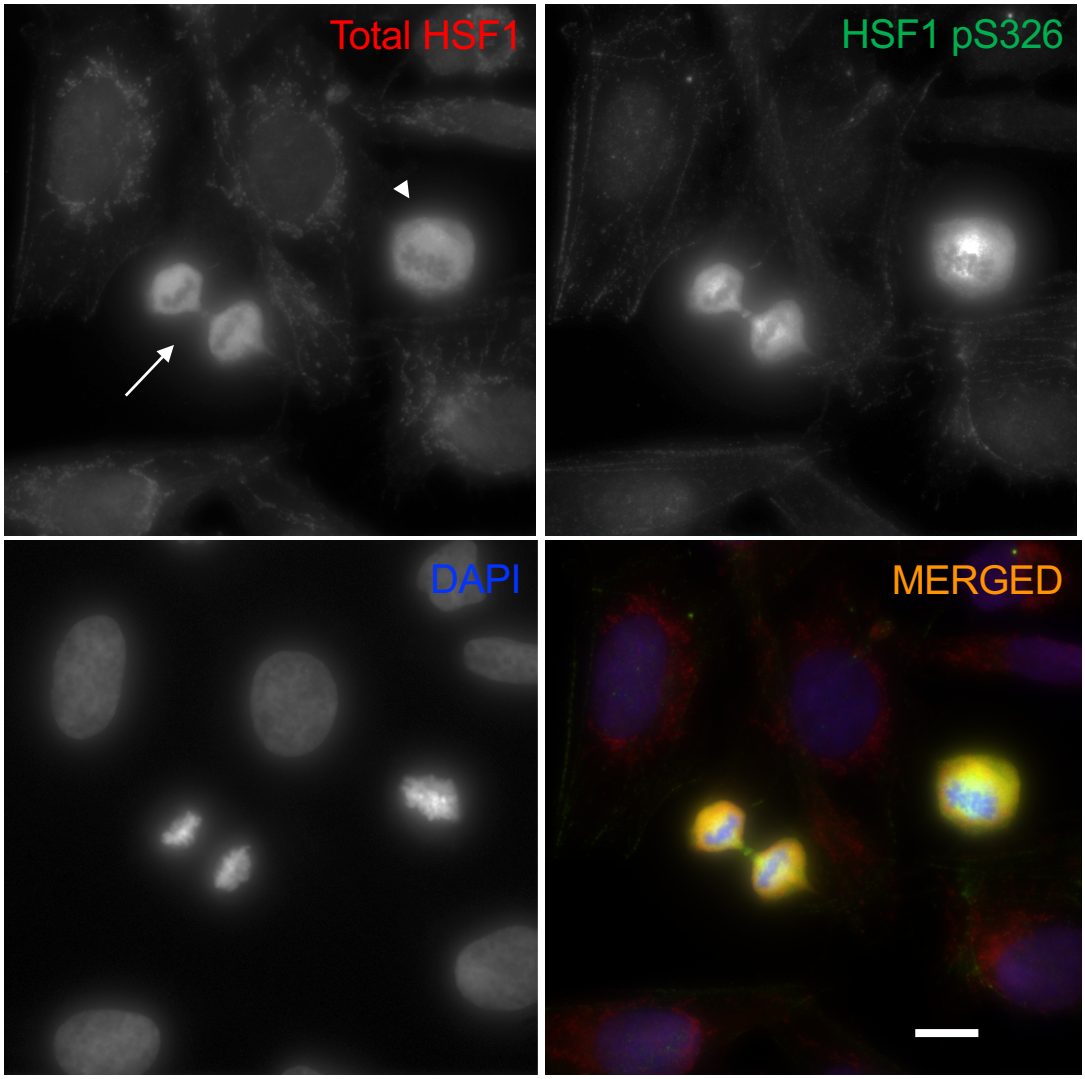

Figure 3.4. Phosphorylation of HSF1 at S326 is significantly higher in mitotic cells compared to interphase cells and colocalises with total HSF1. Representative confocal immunofluorescence image of unsynchronised U2OS cells stained with antibodies against total HSF1 (red), HSF1 pS326 (green) and the DNA stain, 4′,6-Diamidino-2-phenylindole dihydrochloride (DAPI) (blue). The individual channels are displayed without colour. The bottom right image is a merged image of all three channels. There are two mitotic cells in this figure, where they are at the following stages of mitosis: 1) telophase (left, arrow) and 2) metaphase (right, arrowhead). The image was obtained using the Zeiss LSM 710 (Zeiss) microscope and imaging system. A single optical section is shown. The white scale bar represents 10 μm.

FIGURE 3.5

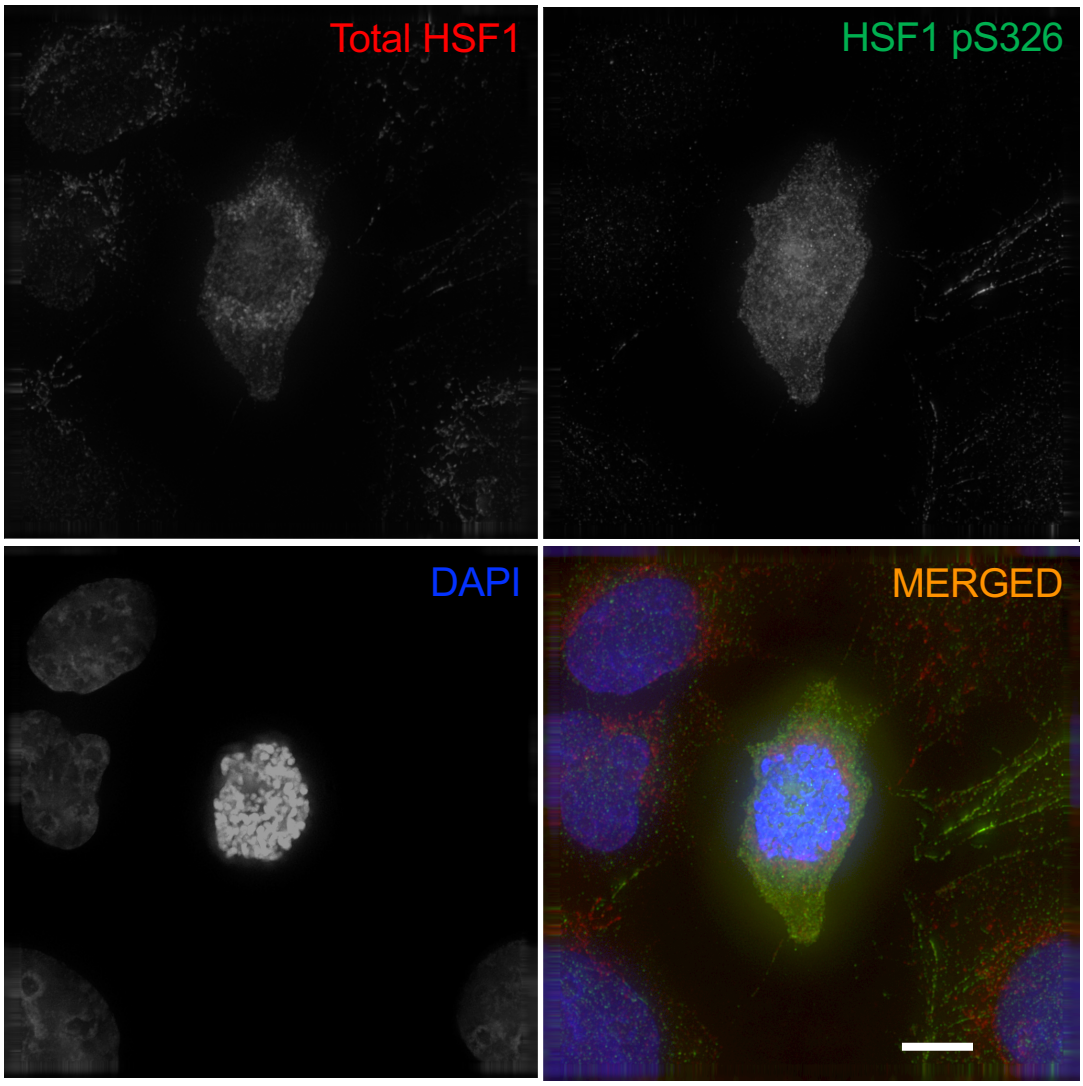

Figure 3.5. Total HSF1 and HSF1 pS326 co-localise in an U2OS cell undergoing prophase. Representative confocal immunofluorescence image of unsynchronised U2OS cells stained with antibodies against total HSF1 (left top panel, red on overlay), HSF1 pS326 (right top panel, green on overlay) and with DAPI (left bottom panel, blue on overlay). The bottom right image is a merged image of all three channels. The individual channels are displayed without colour. The bottom right image is a merged image of all three channels. The image was obtained using the Zeiss LSM 710 (Zeiss) microscope and imaging system. A single optical section is shown. The white scale bar represents 10 µm.

FIGURE 3.6

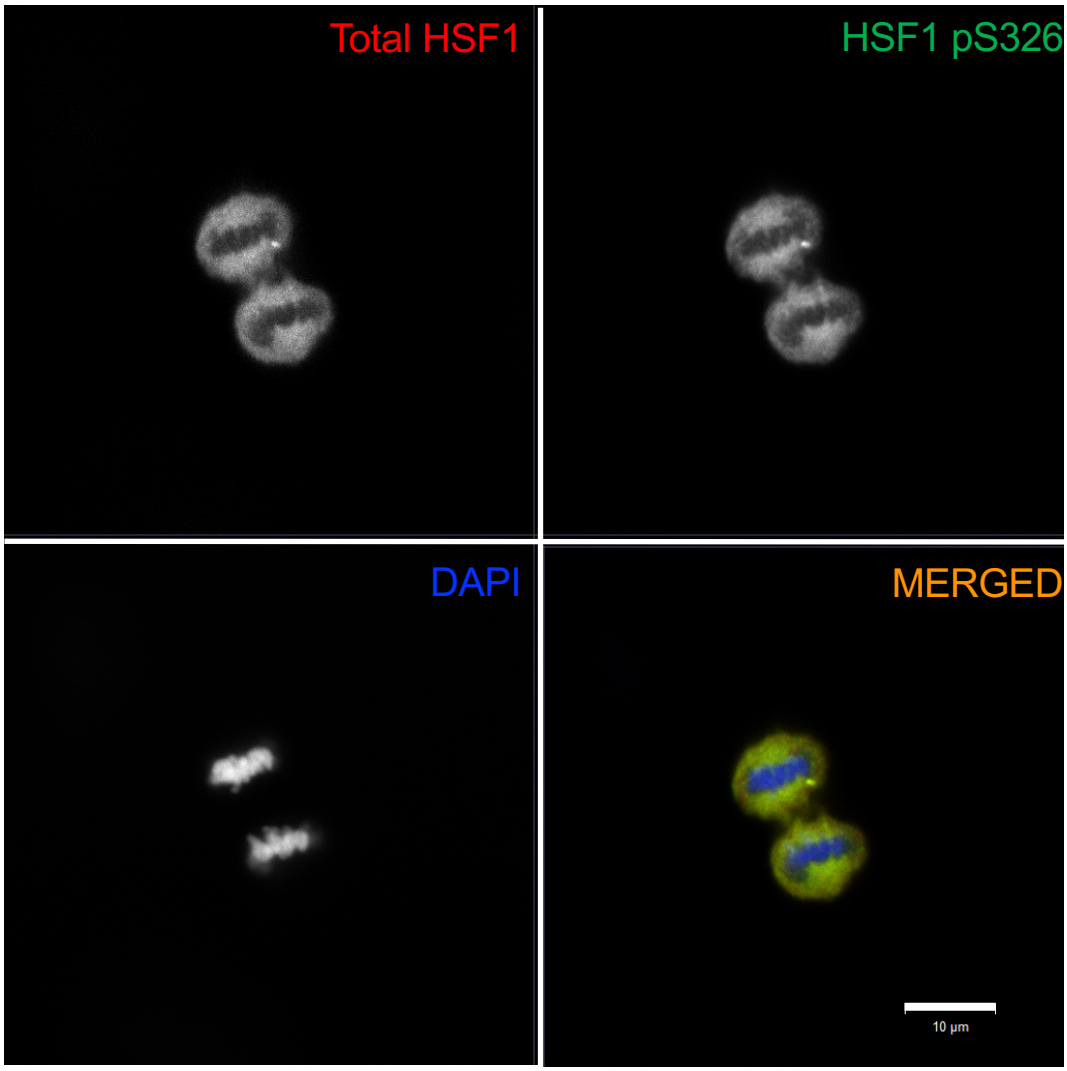

Figure 3.6. Total HSF1 and HSF1 pS326 co-localise in an U2OS cell undergoing telophase. Representative confocal immunofluorescence image of unsynchronised U2OS cells stained with antibodies against total HSF1 (left top panel, red on overlay), HSF1 pS326 (right top panel, green on overlay) and with DAPI (left bottom panel, blue on overlay). The bottom right image is a merged image of all three channels. The individual channels are displayed without colour. The bottom right image is a merged image of all three channels. The image was obtained using the Zeiss LSM 710 (Zeiss) microscope and imaging system. A single optical section is shown. The white scale bar represents 10 µm.

FIGURE 3.7

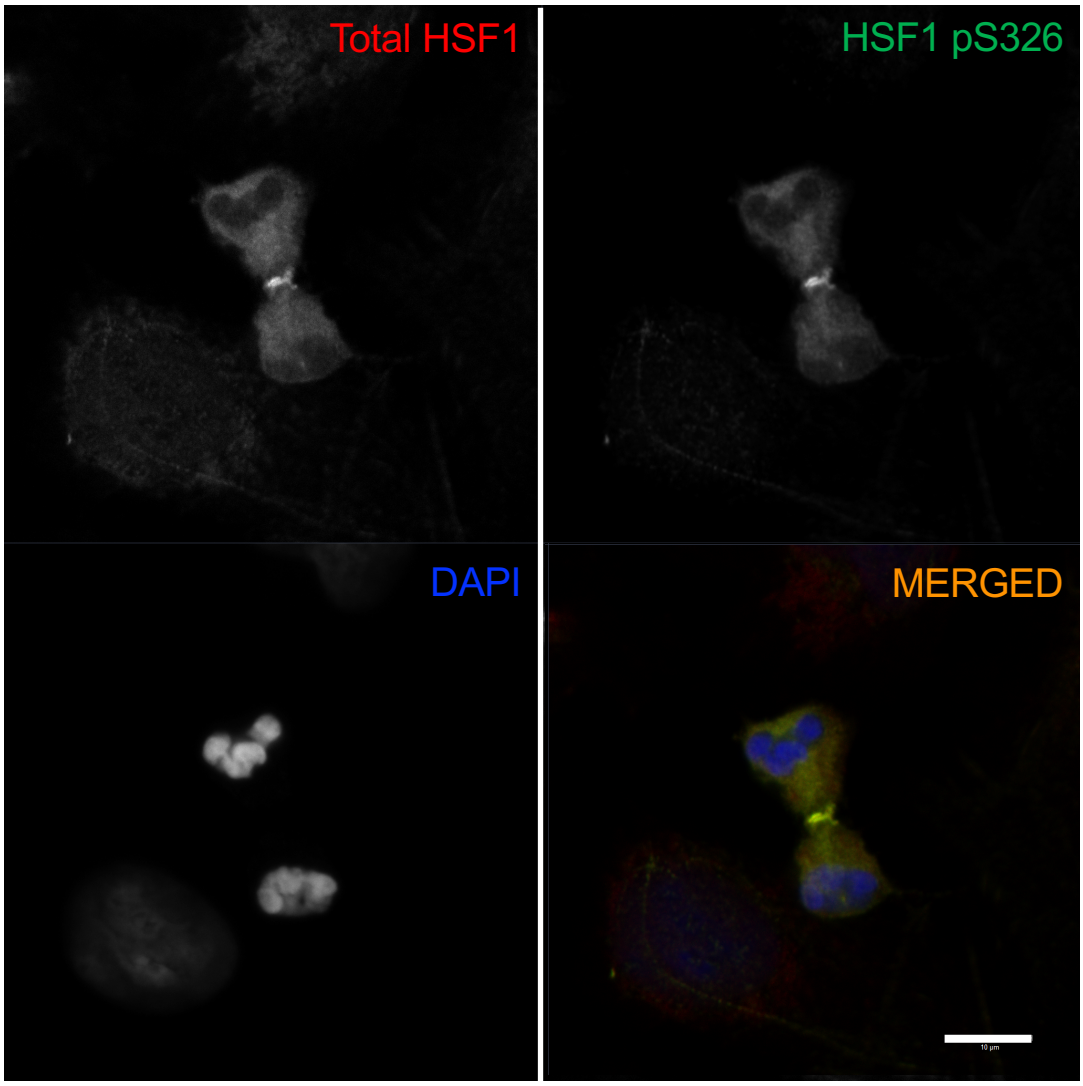

Figure 3.7. Total HSF1 and HSF1 pS326 co-localise in an U2OS cell undergoing telophase and are present at the midbody. Representative confocal immunofluorescence image of unsynchronised U2OS cells stained with antibodies against total HSF1 (left top panel, red on overlay), HSF1 pS326 (right top panel, green on overlay) and with DAPI (left bottom panel, blue on overlay). The bottom right image is a merged image of all three channels. The individual channels are displayed without colour. The bottom right image is a merged image of all three channels. The image was obtained using the Zeiss LSM 710 (Zeiss) microscope and imaging system. A single optical section is shown. The white scale bar represents 10 μm.

3.3.4 The localisation of HSF1 pS326 and α-tubulin are mutually exclusive in interphase cells

Since we observed the staining of HSF1 pS326 to be localised to cytoskeletal structures, we wondered whether HSF1 could be bound to α-tubulin, a major cytoskeletal structure found in most cells. An α-tubulin/β-tubulin heterodimer is the basic subunit of microtubules (Nogales et al., 1998). Microtubules are essential for intracellular structure and transport, and are the primary component of the spindle fibres required for mitosis to occur (Tuszynski et al., 2006).

However, co-staining of HSF1 pS326-stained U2OS cells with α-tubulin-specific antibody ruled out the microtubular localisation of phosphorylated HSF1. Representative images of interphase cells in **Fig. 3.8 and 3.9** show that the localisation of HSF1 pS326 and α-tubulin are mutually exclusive. The α-tubulin staining (top left) shows that the microtubules have a more curved and stringy fibrous appearance in contrast to HSF1 pS326 staining (top right) that is fibrous in appearance but localises in relatively straight and angular lines. Interestingly, HSF1 pS326 staining shows a rhomboidal-like pattern (**Fig. 3.9**). The data from this experiment suggests that HSF1 pS326 bind to other cytoskeletal elements other than microtubules (**Fig. 3.8 and 3.9**). For example, it is possible that HSF1 pS326 binds to β-actin or other intermediate filaments.

FIGURE 3.8

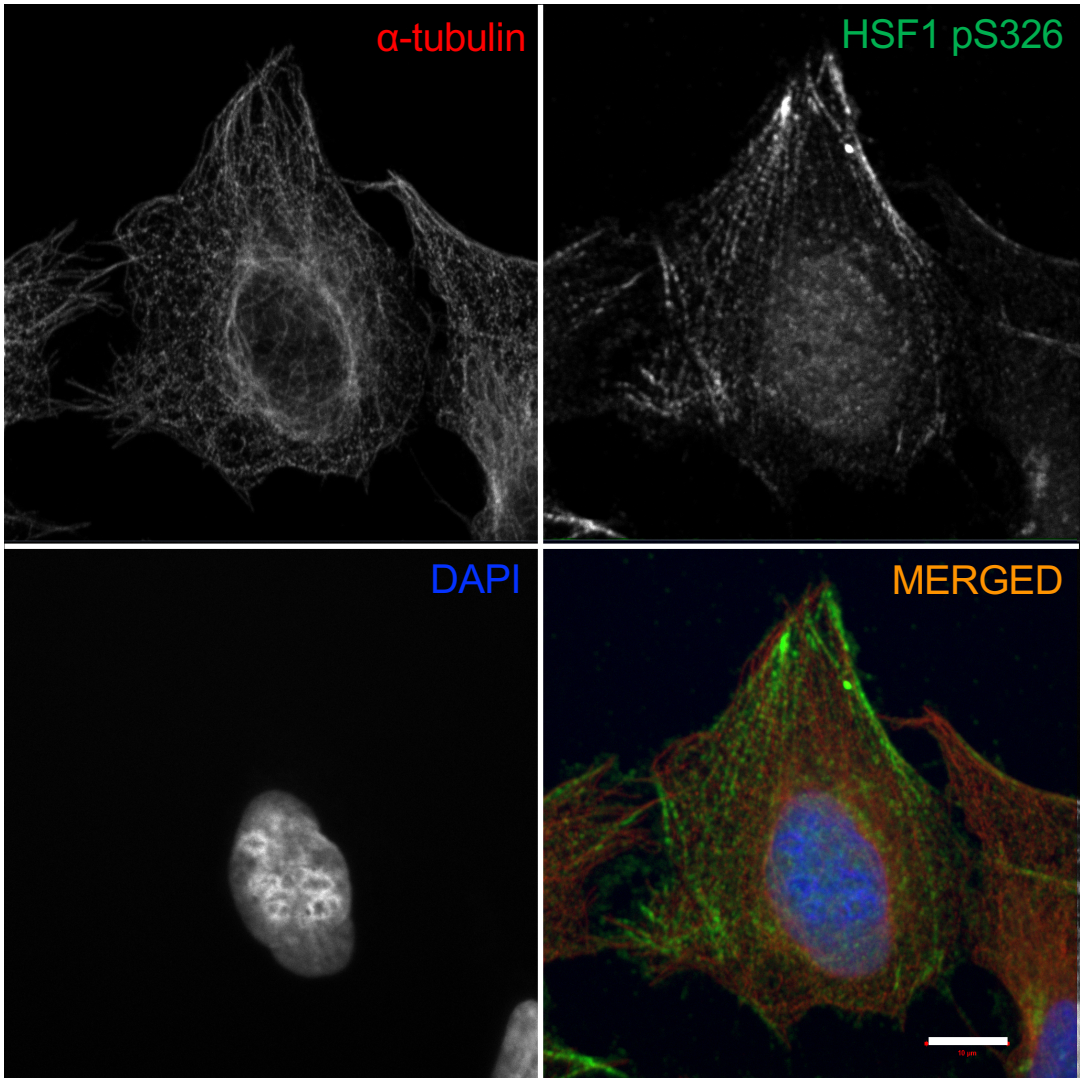

Figure 3.8. HSF1 pS326 shows a filamentous localisation that does not co-localise with in an U2OS cell in interphase. Representative confocal immunofluorescence image of unsynchronised U2OS cells stained with antibodies against α-tubulin (left top panel, red on overlay), HSF1 pS326 (right top panel, green on overlay) and with DAPI (left bottom panel, blue on overlay). The bottom right image is a merged image of all three channels. The individual channels are displayed without colour. The bottom right image is a merged image of all three channels. The image was obtained using the Zeiss LSM 710 (Zeiss) microscope and imaging system. A single optical section is shown. The white scale bar represents 10 μm.

FIGURE 3.9

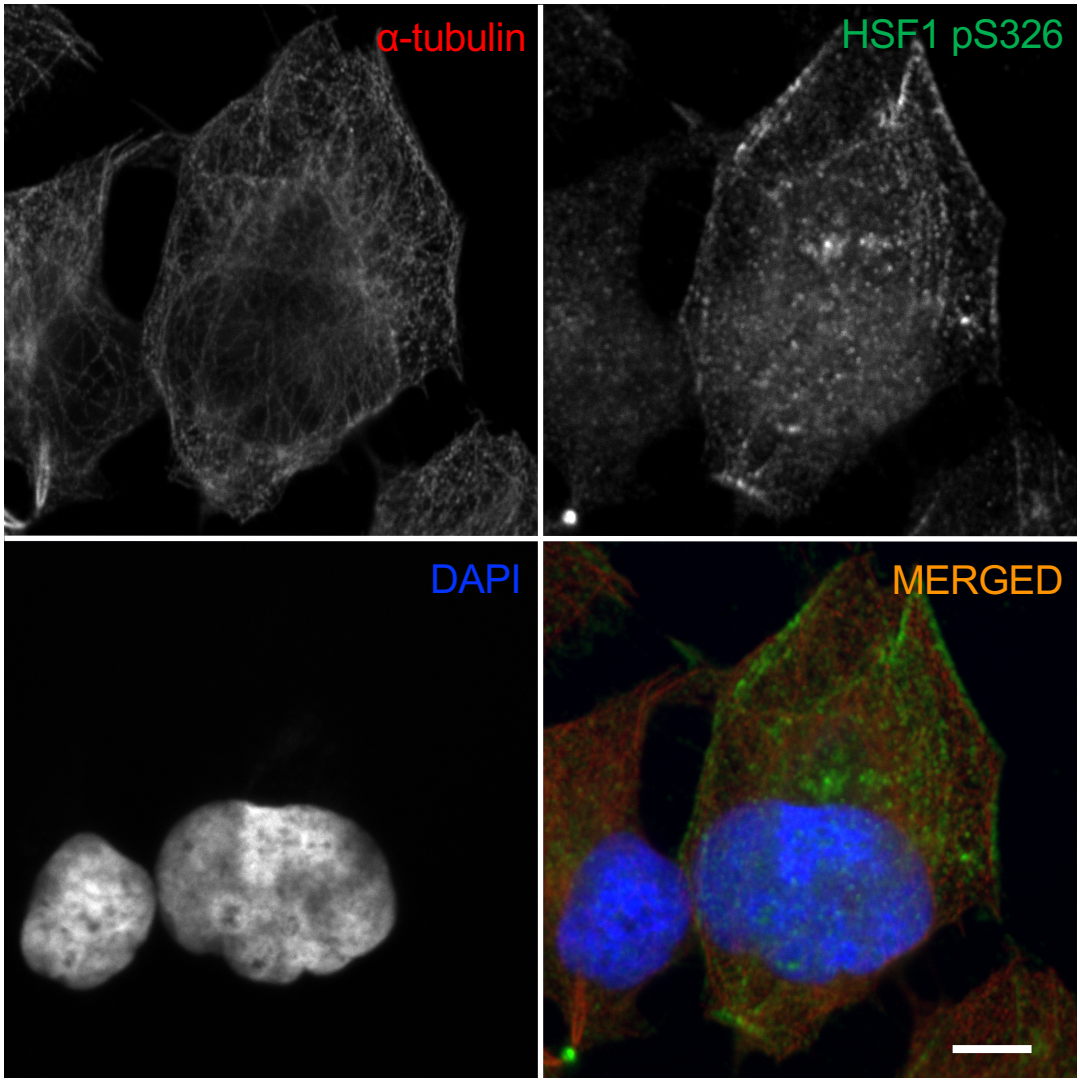

Figure 3.9. HSF1 pS326 shows a filamentous localisation that does not co-localise with in an U2OS cell in interphase. Representative confocal immunofluorescence image of unsynchronised U2OS cells stained with antibodies against α-tubulin (left top panel, red on overlay), HSF1 pS326 (right top panel, green on overlay) and with DAPI (left bottom panel, blue on overlay). The bottom right image is a merged image of all three channels. The individual channels are displayed without colour. The bottom right image is a merged image of all three channels. The image was obtained using the Zeiss LSM 710 (Zeiss) microscope and imaging system. A single optical section is shown. The white scale bar represents 10 μm.

3.3.5 HSF1 pS326 localisation is diffused throughout the mitotic cell and is not present at the chromosomes

The staining pattern of HSF1 pS326 in interphase U2OS cells contrasts greatly with that in mitotic cells (**Fig. 3.1-3.9**). In interphase cells, it has a structured filamentous appearance (**Fig. 3.1, 3.2, 3.8 and 3.9**), whereas in most mitotic cells, the staining pattern of HSF1 pS326 is unstructured and diffused throughout the cell (**Fig. 3.5-3.7 and 3.10-3.13**). This could be due to the disassembly or absence of the cytoskeletal structure that HSF1 pS326 binds to during interphase.

3.3.6 HSF1 pS326 concentrates at the midbody during telophase

To date, not much is known about the function of the midbody. Cytoskeletal elements have been found to be concentrated within the midbody. The midbody comprises of three main molecular machineries: 1) the chromosomal passenger complex containing Aurora B kinase, 2) Protein regulator of cytokinesis 1 (PRC1), a microtubule cross-linking protein and 3) the centralspindlin complex containing mitotic kinesin-like protein (MKLP1) (Green et al., 2013, Hu et al., 2012). Polo-like kinase 1 (PLK1) has been found to be a major regulator for midbody assembly (Hu et al., 2012).

Interestingly and strikingly, U2OS cells undergoing telophase, exhibit HSF1 pS326 concentrated at their midbodies (**Fig 3.4, 3.7, 3.14-16**). HSF1 pS326 is also diffused throughout the cells, however the staining intensity at the

FIGURE 3.10

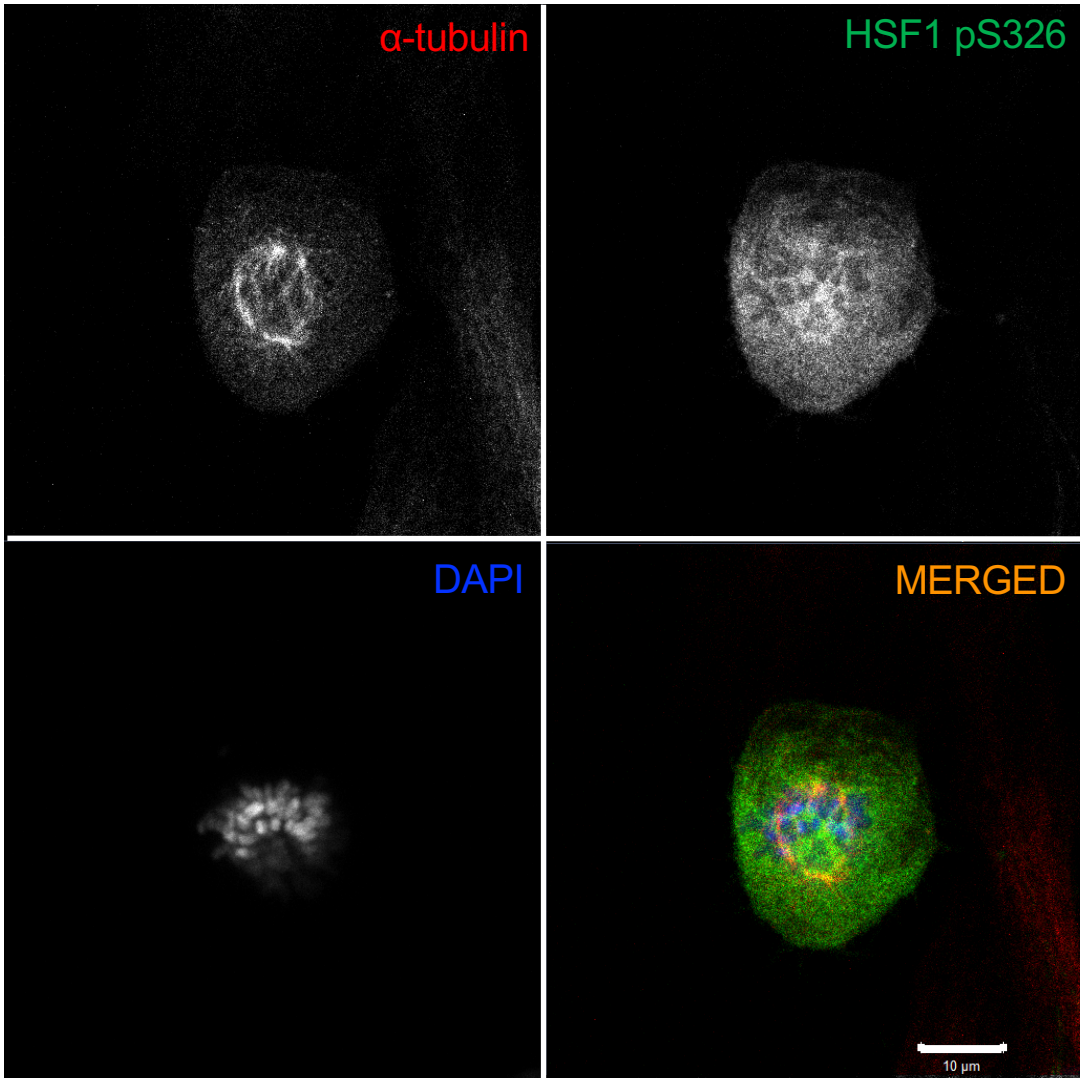

Figure 3.10. HSF1 pS326 is ubiquitously expressed in an U2OS cell undergoing mitosis with lower expression at the chromosomes. Representative confocal immunofluorescence image of U2OS cells stained with antibodies against α-tubulin (left top panel, red on overlay), HSF1 pS326 (right top panel, green on overlay) and with DAPI (left bottom panel, blue on overlay). The bottom right image is a merged image of all three channels. The individual channels are displayed without colour. The bottom right image is a merged image of all three channels. The image was obtained using the Zeiss LSM 710 (Zeiss) microscope and imaging system. A single optical section is shown. The white scale bar represents 10 µm.

FIGURE 3.11

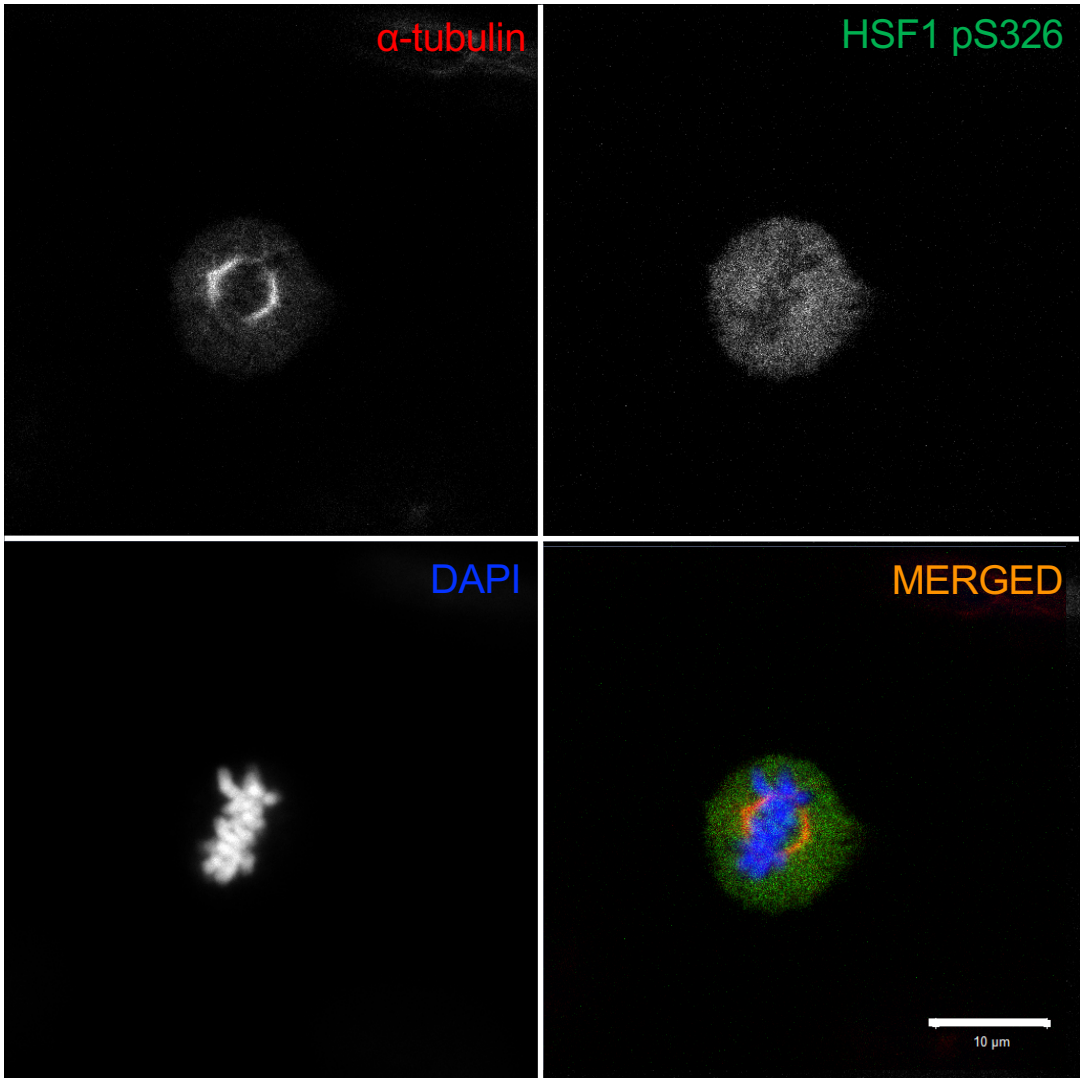

Figure 3.11. HSF1 pS326 is ubiquitously expressed in an U2OS cell undergoing at metaphase with lower expression at the chromosomes. Representative confocal immunofluorescence image of unsynchronised U2OS cells stained with antibodies against α-tubulin (left top panel, red on overlay), HSF1 pS326 (right top panel, green on overlay) and with DAPI (left bottom panel, blue on overlay). The bottom right image is a merged image of all three channels. The individual channels are displayed without colour. The bottom right image is a merged image of all three channels. The image was obtained using the Zeiss LSM 710 (Zeiss) microscope and imaging system. A single optical section is shown. The white scale bar represents 10 µm.

FIGURE 3.12

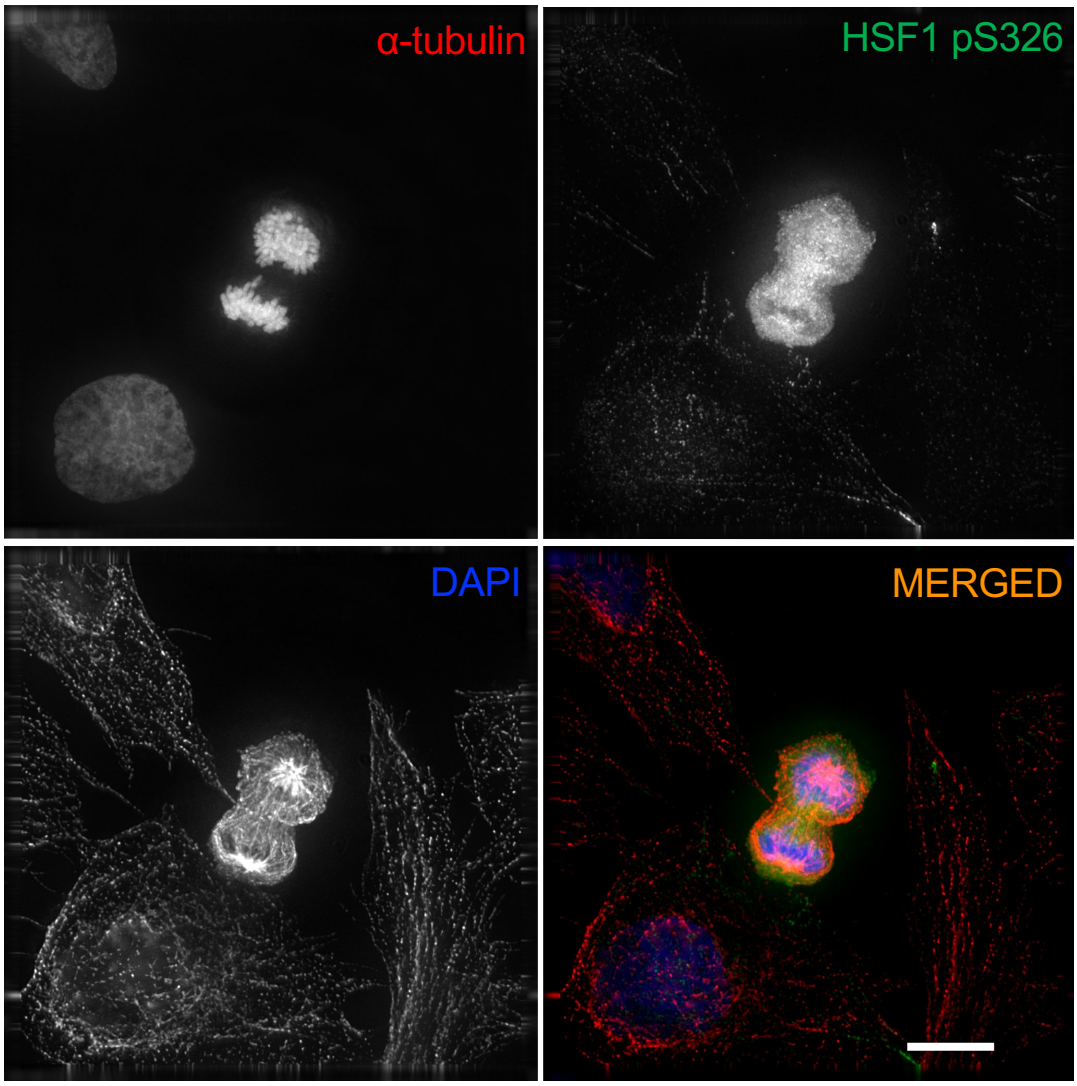

Figure 3.12. HSF1 pS326 is ubiquitously expressed in an U2OS cell in late anaphase with lower expression at the chromosomes. U2OS cells stained with antibodies against α-tubulin (left top panel, red on overlay), HSF1 pS326 (right top panel, green on overlay) and with DAPI (left bottom panel, blue on overlay). The bottom right image is a merged image of all three channels. The individual channels are displayed without colour. The bottom right image is a merged image of all three channels. The image was obtained using the Deltavision™ Elite (GE Healthcare) microscope and imaging system. Maximum intensity of 25 optical sections is shown. The white scale bar represents 10 μm.

FIGURE 3.13

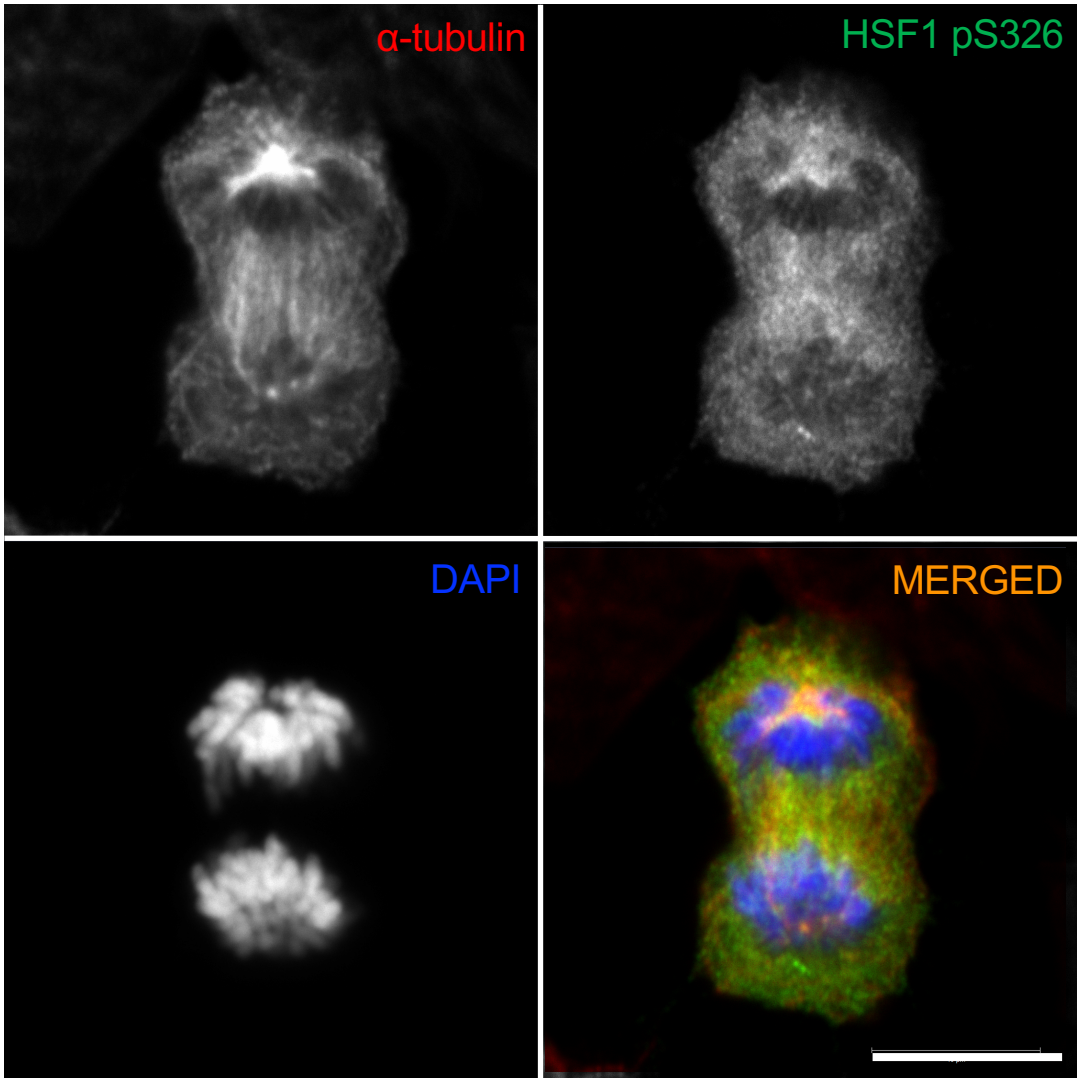

Figure 3.13. HSF1 pS326 is ubiquitously expressed in an U2OS cell in late anaphase with lower expression at the chromosomes. U2OS cells stained with antibodies against α-tubulin (left top panel, red on overlay), HSF1 pS326 (right top panel, green on overlay) and with DAPI (left bottom panel, blue on overlay). The bottom right image is a merged image of all three channels. The individual channels are displayed without colour. The bottom right image is a merged image of all three channels. The image was obtained using the Zeiss LSM 710 (Zeiss) microscope and imaging system. A single optical section is shown. The white scale bar represents 10 µm.

FIGURE 3.14

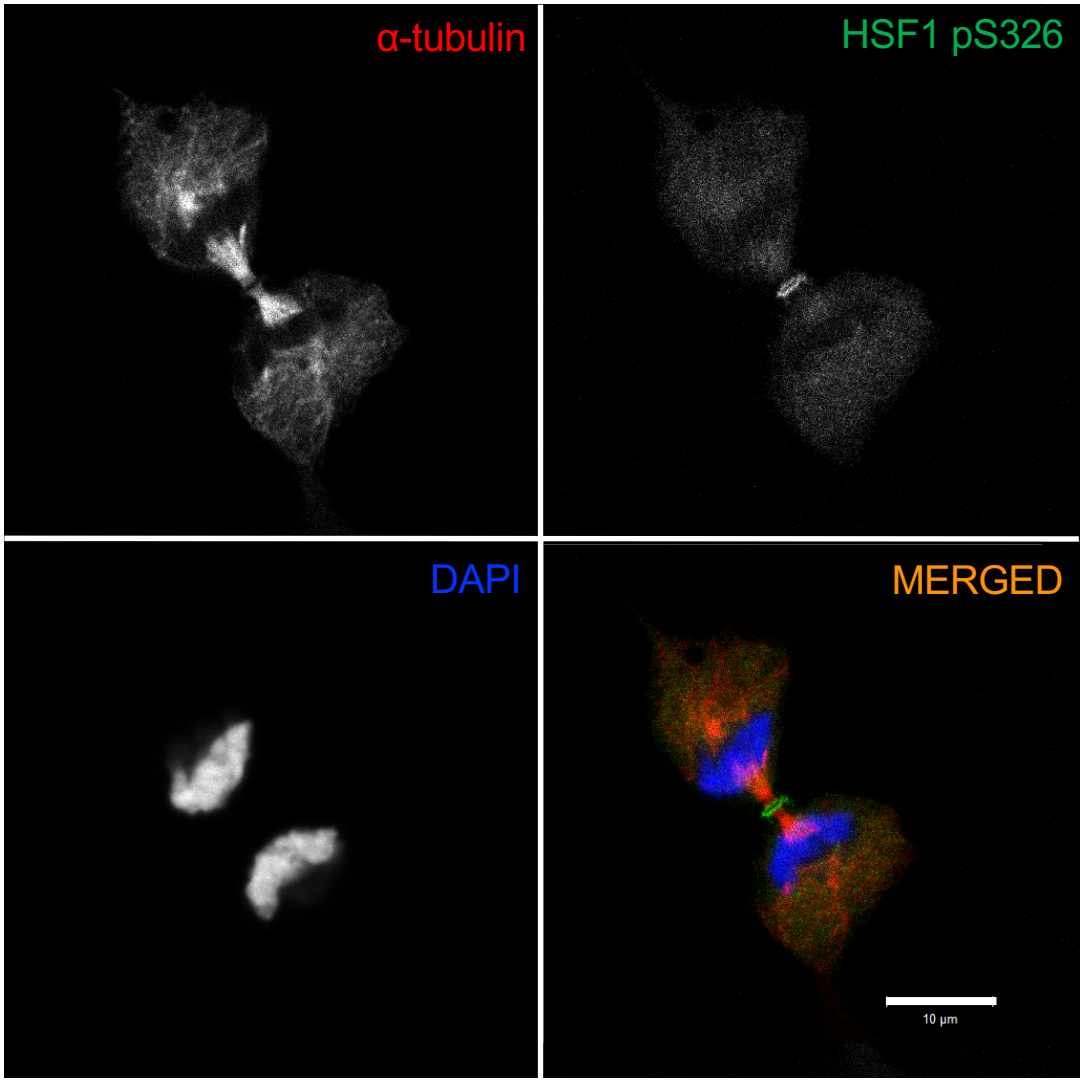

Figure 3.14. HSF1 pS326 is highly expressed at the midbody of an U2OS cell undergoing telophase. U2OS cells stained with antibodies against α-tubulin (left top panel, red on overlay), HSF1 pS326 (right top panel, green on overlay) and with DAPI (left bottom panel, blue on overlay). The bottom right image is a merged image of all three channels. The bottom right image is a merged image of all three channels. The image was obtained using the Zeiss LSM 710 (Zeiss) microscope and imaging system. A single optical section is shown. The white scale bar represents 10 µm.

FIGURE 3.15

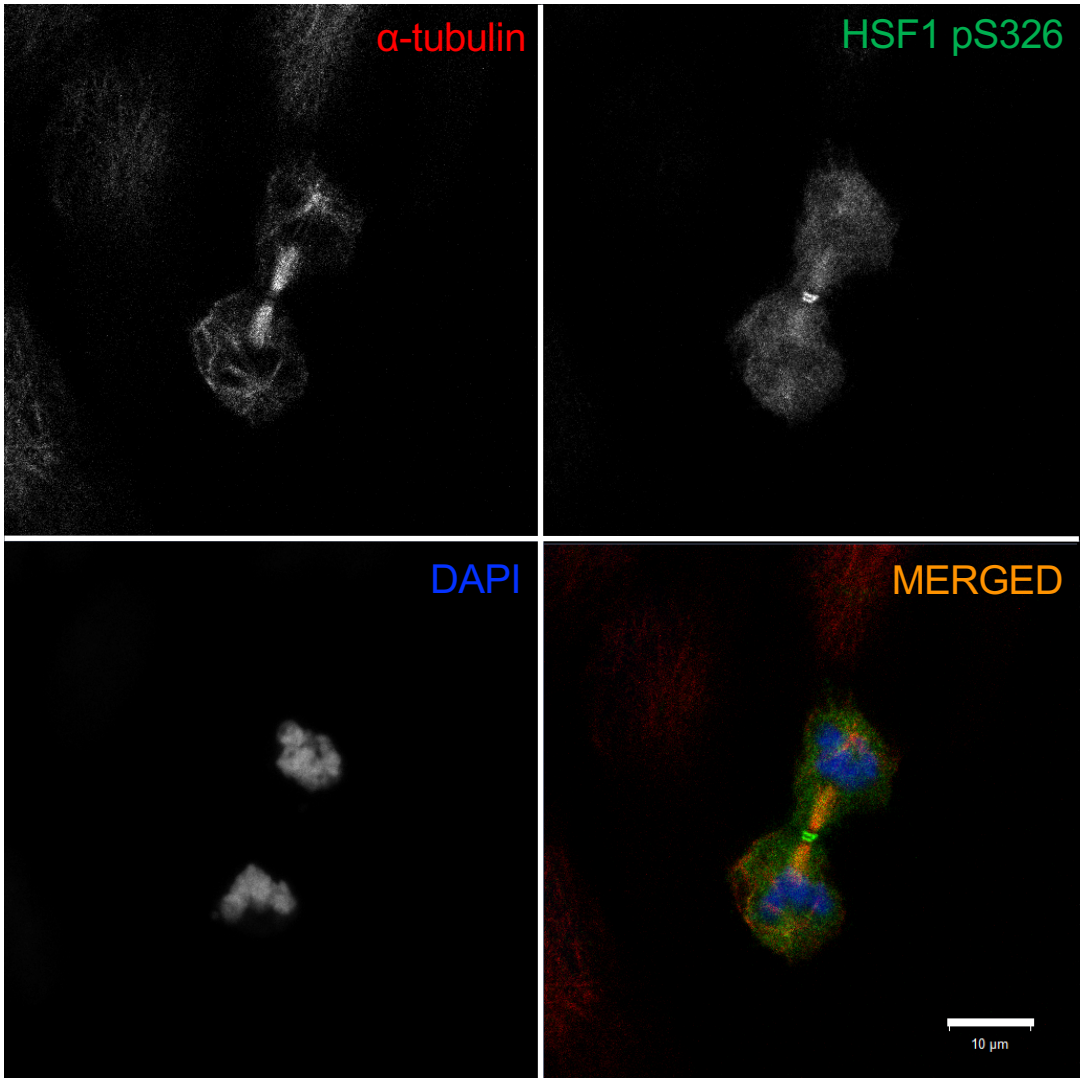

Figure 3.15. HSF1 pS326 is highly expressed at the midbody of an U2OS cell undergoing telophase. U2OS cells stained with antibodies against α-tubulin (left top panel, red on overlay), HSF1 pS326 (right top panel, green on overlay) and with DAPI (left bottom panel, blue on overlay). The bottom right image is a merged image of all three channels. The bottom right image is a merged image of all three channels. The image was obtained using the Zeiss LSM 710 (Zeiss) microscope and imaging system. A single optical section is shown. The white scale bar represents 10 µm.

FIGURE 3.16

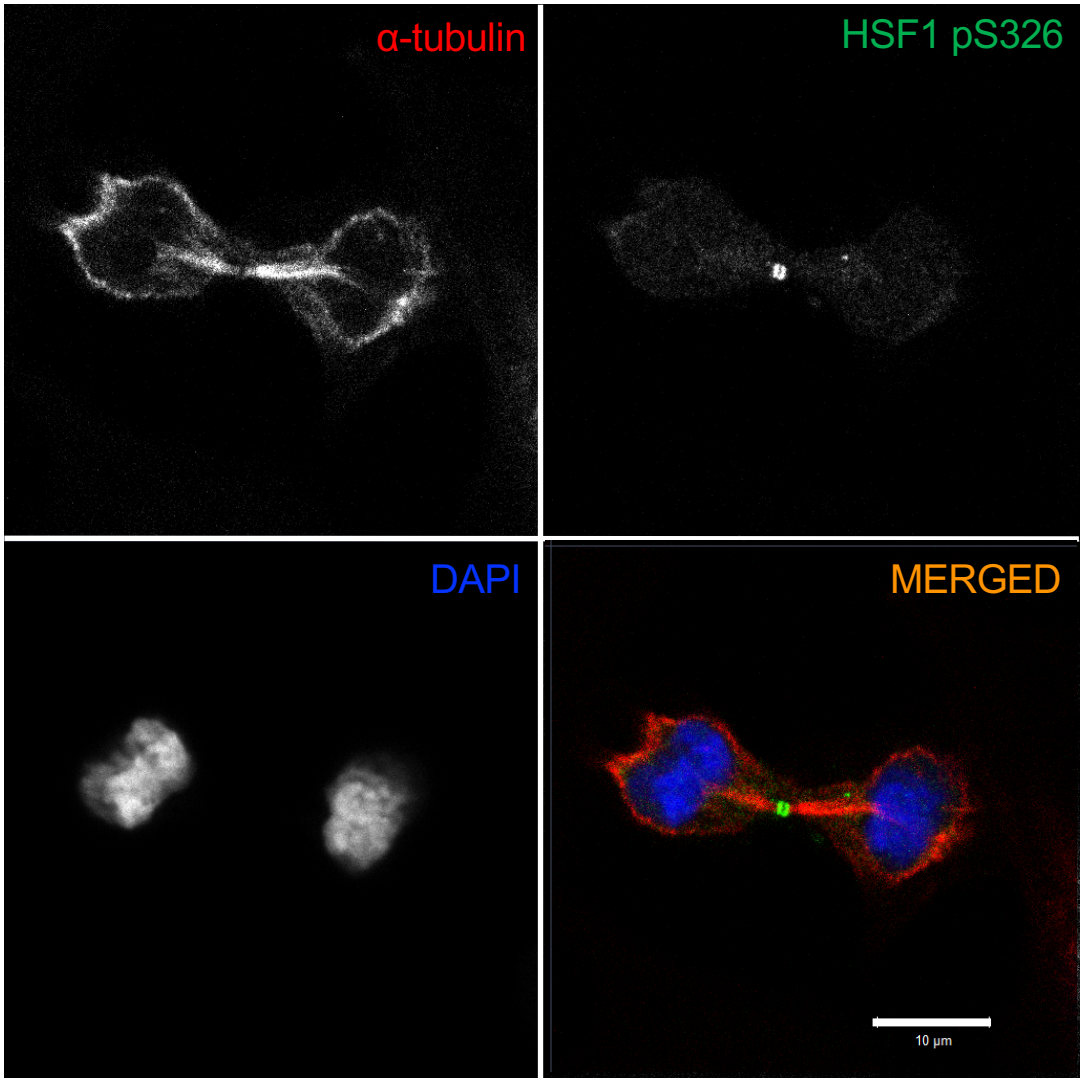

Figure 3.16. HSF1 pS326 is highly expressed at the midbody of an U2OS cell undergoing telophase. Representative confocal immunofluorescence image of unsynchronised U2OS cells stained with antibodies against α-tubulin (left top panel, red on overlay), HSF1 pS326 (right top panel, green on overlay) and with DAPI (left bottom panel, blue on overlay). The bottom right image is a merged image of all three channels. The individual channels are displayed without colour. The bottom right image is a merged image of all three channels. The image was obtained using the Zeiss LSM 710 (Zeiss) microscope and imaging system. A single optical section is shown. The white scale bar represents 10 µm.

midbody is significantly higher than the staining intensity in other compartments of the cell. It is plausible that HSF1 could play other roles in the cell apart from being a transcription factor.

In order to further validate the data obtained using immunofluorescence, where we discovered that mitotic U2OS cells highly express HSF1 pS326 compared to interphase cells (**Fig. 3.3 and 3.4**), we performed a western blot analysis comparing the levels of HSF1 pS326 and total HSF1 levels in taxol-arrested mitotic U2OS cells and interphase U2OS cells. To control for possible effects of drug treatment, we used interphase cells that were exposed to the same concentration of the taxol as the mitotically-arrested cells as a control population. We used the microtubule toxin, taxol, which stabilises microtubules and arrests cells in mitosis (Gascoigne and Taylor, 2009), possibly via preventing spindle checkpoint satisfaction or by delaying stable kinetochore attachments. We collected the taxol-arrested mitotic cells by selectively detouching them from the dish using the “mitotic shake-off” method (explained in detail in the Methods Section 2.18). The cells remaining on the dish after mitotic cells were collected were further vigorously washed and collected for taxol-treated interphase-cell control. The total population of asynchronous U2OS were used as an additional control.

3.3.7 The HSF1 pS326 levels are significantly higher in taxol-arrested mitotic cells compared to interphase cells

Various amounts of U2OS cell lysate from each experimental group were loaded as follows: 1) Unsynchronised cells, 2) taxol-treated interphase cells and, 3) taxol-arrested mitotic cells (**Fig. 3.17**). Western blot analysis of these samples shows that in U2OS cells, there are minimal differences in the levels of HSF1 pS326 between untreated unsynchronised cells and taxol-treated interphase cells **(Fig. 3.18)**. However, in comparison with interphase cells treated with taxol, HSF1 pS326 is more highly expressed in taxol-arrested mitotic cells (**Fig. 3.18**). The same phenomenon is observed in a similar experiment conducted in HeLa cells (**Fig. 3.19**). These results further support our previous observations using immunofluorescence **(Fig. 3.3 and 3.4)**.

Interestingly, in both U2OS and HeLa cells, two distinct bands are observed in the HSF1 pS326 immunoblot: ~70 kDa and ~130 kDa. However, in the U2OS cells, the 130 kDa band is expressed more highly than the 70 kDa band (**Fig. 3.18**), whereas in the HeLa cells, it is the opposite: the 70 kDa band is expressed more highly than the 130 kDa (**Fig. 3.19**). Since the actual molecular weight of HSF1 is ~65 kDa, the upper band could represent a homodimeric species. Alternatively, the upper band could be a conjugation of HSF1 with multiple SUMO proteins as HSF1 has been previously reported to be SUMO-modified (Hong et al., 2001, Hilgarth et al., 2003, Hietakangas et al., 2003, Goodson et al., 2001). Also interestingly, in both HeLa and U2OS cells, only in the taxol-arrested mitotic cells, HSF1 pS326 appears as a smear, suggesting

FIGURE 3.17

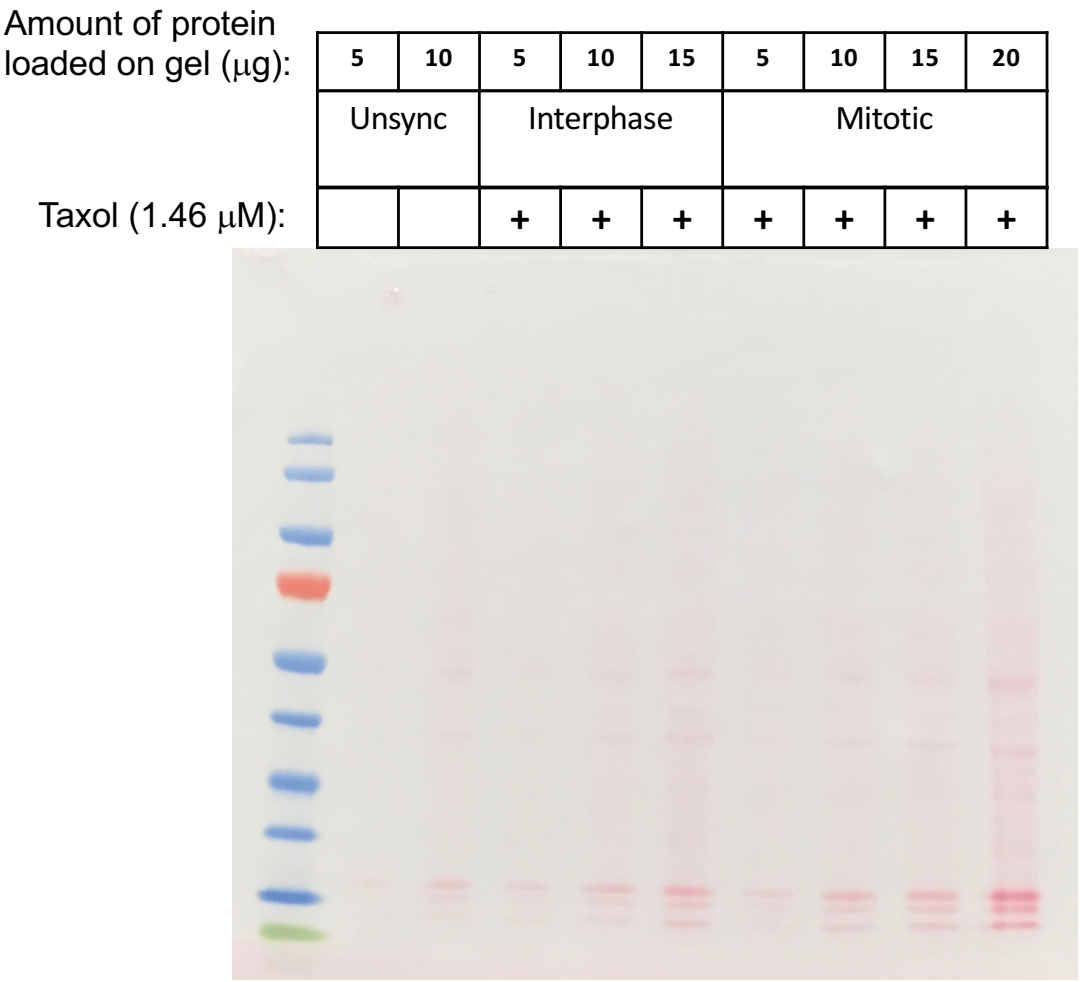

Figure 3.17. Ponceau S staining of a western blot membrane. U2OS cells were exposed to 1.46 μM taxol for 14 h in order to arrest cells in mitosis. Mitotic cells were collected by mitotic wash-off and lysed immediately with SDS-lysis buffer. The remaining cells consisted of non-mitotic (interphase) cells exposed to taxol were lysed directly using the same buffer. Increasing amounts of protein (μg) from each group were loaded and resolved using the NuPAGE system. The proteins from the gels were immobilised onto 0.2 μm nitrocellulose (NC) membranes. The NC membranes were stained using a water-soluble and reversible protein stain Ponceau S to ensure an even protein transfer and loading.

FIGURE 3.18

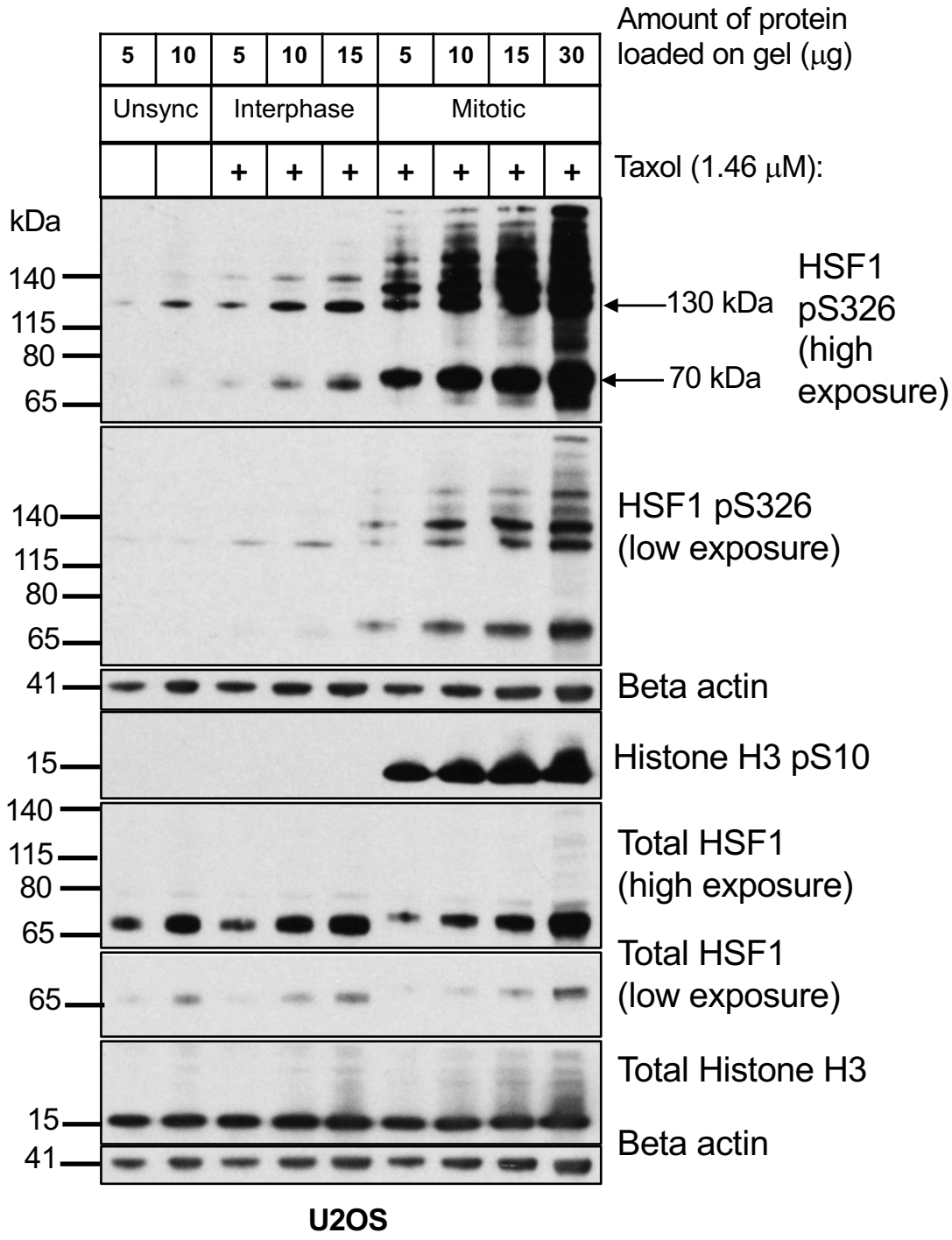

Figure 3.18. HSF1 pS326 levels are significantly higher in taxol-arrested mitotic cells compared to interphase cells. U2OS cells were exposed to 1.46 μM taxol for 14 h in order to arrest cells in mitosi or left without treatment (unsynchronised). Mitotic cells were collected from the taxol-treated dish and lysed immediately with SDS-lysis buffer. The remaining attached (interphase) cells that were exposed to the same Taxol treatment were lysed directly using the same buffer. Unsynchronised cells were trypsinised and lysed in SDS-lysis buffer without separation. Increasing amounts of protein (mg) from each group were loaded and resolved using the NuPAGE system. The proteins from the gels were immobilised onto 0.2 μm nitrocellulose (NC) membranes. The western blot membranes were probed with antibodies against total HSF1, HSF1 pS326, Histone H3, Histone H3 pS10 and β-actin. Histone H3 pS10 was used as a mitotic marker and to ensure the purity of the separation. β-actin and Histone H3 served as loading controls. This experiment was performed with Dr. Dina Dikovskaya.

FIGURE 3.19

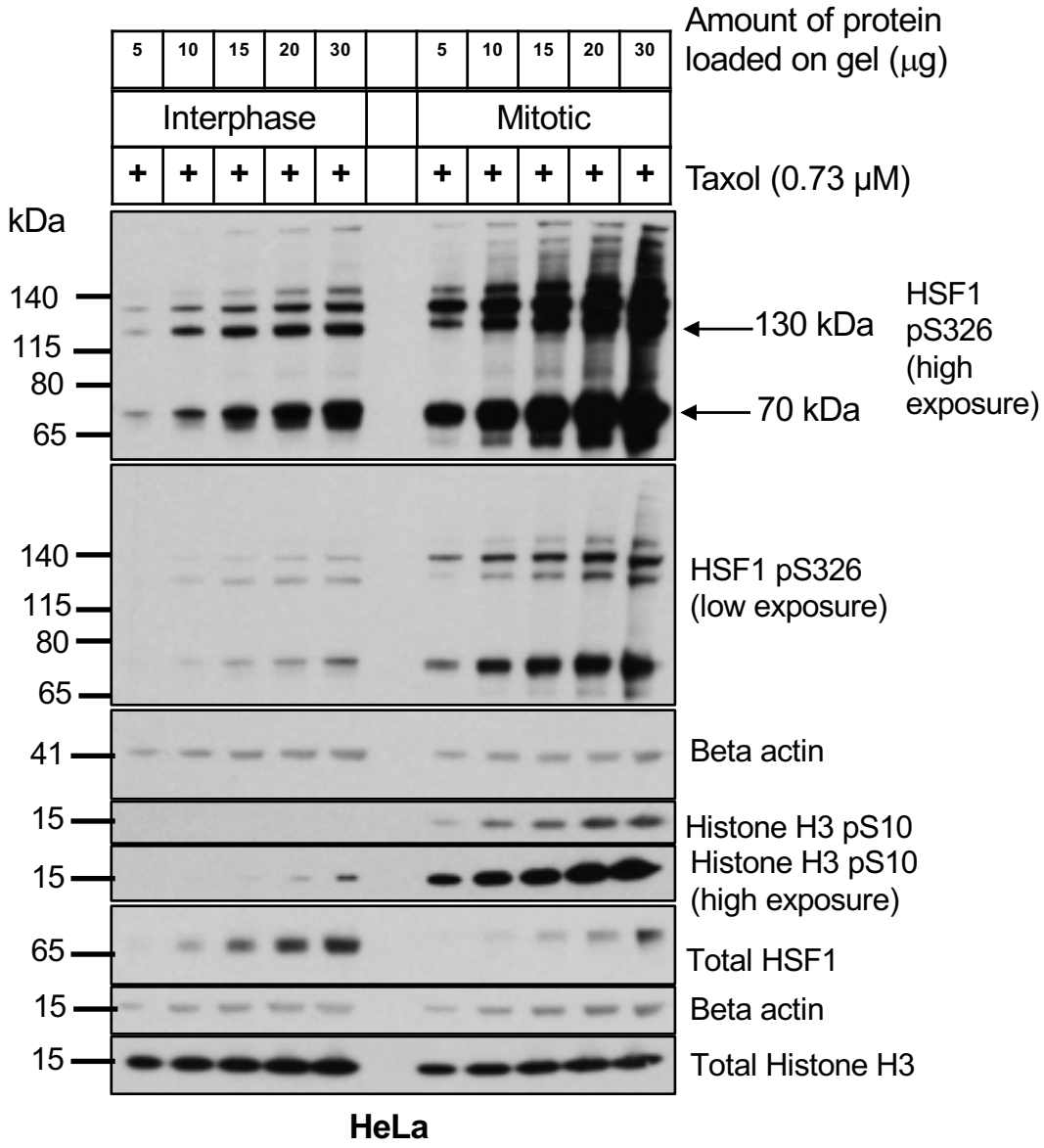

Figure 3.19. Total HSF1 is degraded, whereas, HSF1 pS326 levels are significantly higher in taxol-arrested mitotic cells than in interphase cells. HeLa cells were exposed to 0.73 μM taxol for 12 h in order to arrest cells in mitosi or left without treatment (unsynchronised). Mitotic cells were collected from the taxol-treated dish and lysed immediately with SDS-lysis buffer. The remaining attached (interphase) cells that were exposed to the same Taxol treatment were lysed directly using the same buffer. Unsynchronised cells were trypsinised and lysed in SDS-lysis buffer without separation. Increasing amounts of protein (mg) from each group were loaded and resolved using the NuPAGE system. The proteins from the gels were immobilised onto 0.2 μm nitrocellulose (NC) membranes. The western blot membranes were probed with antibodies against total HSF1, HSF1 pS326, Histone H3, Histone H3 pS10 and β-actin. Histone H3 pS10 was used as a mitotic marker and to ensure the purity of the separation. β-actin and Histone H3 served as loading controls. This experiment was performed with Dr. Dina Dikovskaya.

potential ubiquitination of the protein (**Fig. 3.18 and Fig. 3.19**). Furthermore, in these cells, the HSF1 pS326 migrates more slowly than in the taxol-exposed interphase cells, suggesting that there could be other post-translation modification(s) occurring on the phosphorylated HSF1 S326 species. The additional post-translation modification(s) could include PLK1-catalysed phosphorylation of HSF1 at S216 that has been reported to occur during mitosis (Lee et al., 2008a).

3.3.8 The total HSF1 levels decrease in taxol-arrested mitotic cells and interphase cells

In U2OS cells, the total HSF1 levels are slightly lower in taxol-arrested mitotic cells compared to taxol-exposed interphase cells (**Fig. 3.18**). A more dramatic decrease in total HSF1 levels is observed in mitotic HeLa cells arrested with taxol compared to the interphase cells treated with taxol (**Fig. 3.19**). These results clarify the immunofluorescence data (**Fig. 3.3 and 3.4**) where total HSF1 levels seemed to be higher in mitotic cells compared to interphase cells. It is now obvious that in the immunofluorescence data using the total HSF1 antibody, the apparent increased intensity observed in mitosis is not a reflection of the total HSF1 levels, but more likely of the HSF1 pS326 that is increased during mitosis.

We wanted to find out if there were any other phosphorylation events occurring on HSF1 during mitosis as we observed that HSF1 undergoes a further posttranslational event(s) during this cell cycle phase (**Fig. 3.18 and 3.19**). Using

the available antibodies, we probed for HSF1 pS303 and HSF1 pS121, both of which have been reported to repress the transcriptional activity of HSF1.

3.3.9 HSF1 pS303 and pS121 levels are decreased in U2OS cells arrested in mitosis with taxol compared to interphase cells

In **Fig. 3.20**, HSF1 pS303 and pS121 levels are decreased in U2OS cells arrested in mitosis with taxol compared to interphase cells exposed to taxol. It is interesting that phosphorylation of these sites, which inhibits HSF1 transcriptional activity (Wang et al., 2006, Hietakangas et al., 2003), is downregulated in mitosis, suggesting that perhaps HSF1 has to be active and able to bind to the HSEs during mitosis as reported by Vihervaara et. al. (Vihervaara et al., 2013). However, the decrease in the levels of HSF1 pS303 and pS121 that we observed could also be due to the total HSF1 protein decrease during mitosis **(Fig. 3.18 and Fig. 3.19)**. Notably, we found that these “phosphospecific” antibodies are able to recognise unphosphorylated recombinant HSF1 (data not shown), hence the specificities of these antibodies are highly questionable and the detected species could represent a mixed population of total HSF1 as well as the phosphorylated residues on HSF1 it is supposed to recognise. Interestingly, in contrast to the levels of HSF1 p326, the levels of transcription factor NRF2 are decreased in taxol-arrested mitotic U2OS cells (**Fig. 3.20**).

Because we discovered that all members of the p38 MAPK family are able to efficiently catalyse the phosphorylation of HSF1 at S326 (Dayalan Naidu et al., 2016), we next wanted to find out if these kinases were mediating the increase in

FIGURE 3.20

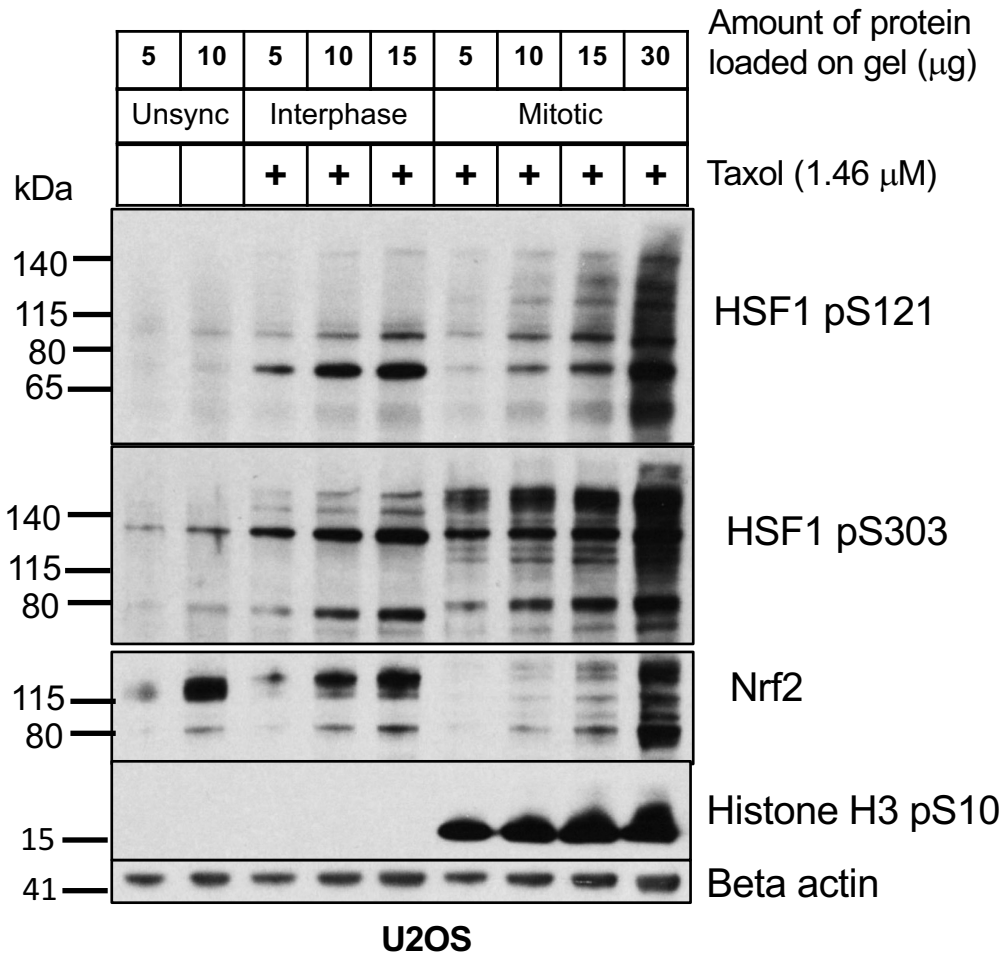

Figure 3.20. HSF1 pS303 and HSF1 pS121 levels are lower in taxol-arrested mitotic cells compared to interphase cells. U2OS cells were exposed to 1.46 μM taxol for 14 h in order to arrest cells in mitosi or left without treatment (unsynchronised). Mitotic cells were collected from the taxol-treated dish and lysed immediately with SDS-lysis buffer. The remaining attached (interphase) cells that were exposed to the same Taxol treatment were lysed directly using the same buffer. Unsynchronised cells were trypsinised and lysed in SDS-lysis buffer without separation. Increasing amounts of protein (mg) from each group were loaded and resolved using the NuPAGE system. The proteins from the gels were immobilised onto 0.2 μm nitrocellulose (NC) membranes. The western blot membranes were probed with antibodies against HSF1 pS121, HSF1 pS303, Nrf2, Histone H3 pS10 and β-actin. Histone H3 pS10 was used as a mitotic marker and to ensure the purity of the separation. β-actin served as a loading control. These lysates belong to the experiment described in **Figure 3.17**. This experiment was performed with Dr. Dina Dikovskaya.

HSF1 pS326 levels in taxol-arrested mitotic cells. We therefore determined the levels of all p38 isoforms as well as the phosphorylated (i.e. active) total p38 in the U2OS cell lysates described in **Fig. 3.18**.

3.3.10 p38α and p38β are active in interphase cells whereas, p38β is predominantly active in taxol -arrested mitotic cells

The levels of all of the individual p38 isoforms are very similar when comparing taxol-arrested mitotic U2OS cells and taxol-exposed interphase cells (**Fig. 3.21**). The phosphospecific p38 antibody recognises all four isoforms of p38, and it can be seen in **Fig. 3.21** that p38α and p38β are phosphorylated in taxol-exposed interphase cells, whereas p38β is predominantly phosphorylated in taxol-arrested mitotic cells. It is thus possible that in mitotic cells, p38β mediates the phosphorylation of HSF1 at S326 observed in **Fig. 3.18**.

3.3.10 Discussion

Here we have shown that the basal sub-cellular localisation of HSF1 pS326 is very different compared to the overall HSF1. In resting cells, HSF1 pS326, although also present in the nucleus, is mainly localised to cytoskeletal filaments and appears as straight and angular lines **(Fig. 3.1 and 3.2).** Basally, most of the HSF1 has a more globular appearance and is mainly localised at structures resembling the Golgi bodies.

FIGURE 3.21

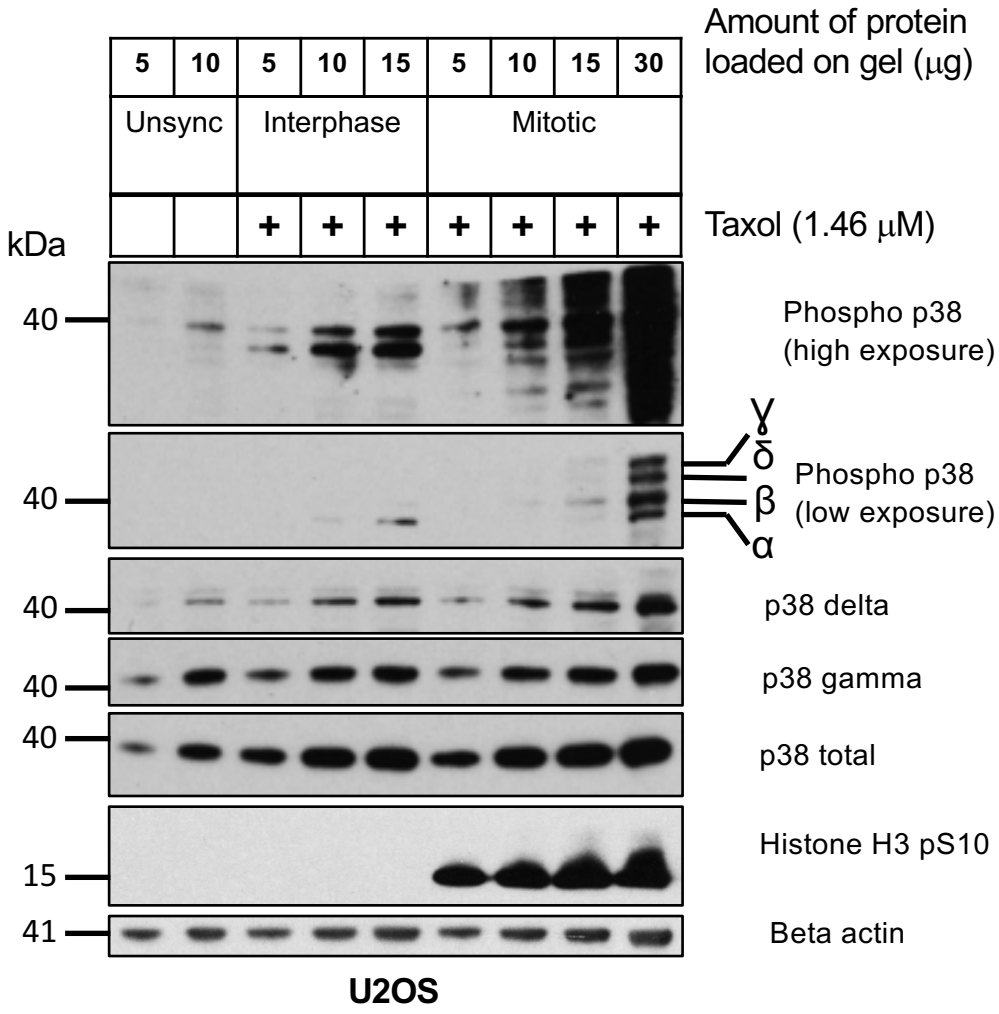

Figure 3.21. Different p38 isoforms are phosphorylated during taxol-arrested mitosis compared to interphase cells. U2OS cells were exposed to 1.46 μM taxol for 14 h in order to arrest cells in mitosi or left without treatment (unsynchronised). Mitotic cells were collected from the taxol-treated dish and lysed immediately with SDS-lysis buffer. The remaining attached (interphase) cells that were exposed to the same Taxol treatment were lysed directly using the same buffer. Unsynchronised cells were trypsinised and lysed in SDS-lysis buffer without separation. Increasing amounts of protein (mg) from each group were loaded and resolved using the NuPAGE system. The proteins from the gels were immobilised onto 0.2 μm nitrocellulose (NC) membranes. The western blot membranes were probed with antibodies against total p38, p38α, p38β, p38γ, p38δ, phospho p38, Histone H3 pS10 and β-actin. Histone H3 pS10 was used as a mitotic marker and to ensure the purity of the separation. β-actin served as a loading control. These lysates belong to the experiment described in **Figure 3.17**. This experiment was performed with Dr. Dina Dikovskaya.

We have shown by immunofluorescence and western blotting that HSF1 pS326 levels are significantly higher in taxol-arrested mitotic cells compared to interphase cells (**Fig. 3.3, 3.4, 3.18 and 3.21**). HSF1 pS326 is highly expressed at all stages of mitosis. We also found that HSF1 pS326 localises and concentrates at the midbody of cells undergoing telophase and cytokinesis (**Fig. 3.4, 3.7 and 3.14-3.16**). It is interesting that HSF1 pS326 adopts this localisation pattern during cell division. Since the midbody is a hub for cytoskeletal filaments, such as actin and myosin filaments (Green et al., 2013), it is possible that HSF1 phosporylated at S326 has a high affinity to a particular protein, possibly a cytoskeletal protein, that is concentrated at the midbody. This finding exposes the intriguing possibility that HSF1 could have a role beyond its function as a transcription factor. The kinase that phosphorylates and maintains the phosphorylation of HSF1 at S326 could potentially be p38β (**Fig 3.21**). On the other hand, as observed in Chapter 2, **Fig. 2.16A**, treatment of cells with the p38a and p38b inhibitor SB202190 did not reduce HSF1 pS326 levels, however these data were obtained in unsynchronised cells and do not represent the mitotic cell population.

Preliminary western blot analysis of cells pre-treated with the CDK9 inhibitor (CDK9I) showed a decrease in HSF1 pS326 levels (**Fig. 3.22**) CDK9 could potentially be the kinase involved in the phosphorylation of HSF1 at S326 during mitosis. Another obvious candidate is CDK1, a kinase that is activated in late G2 and throughout mitosis. Notably, in yeast, a heat-sensitive mutant HSF1 has been linked with a defect in spindle pole body (the equivalent to the centrosome in mammalian cells) duplication (Zarzov et al., 1997). The spindle

FIGURE 3.22

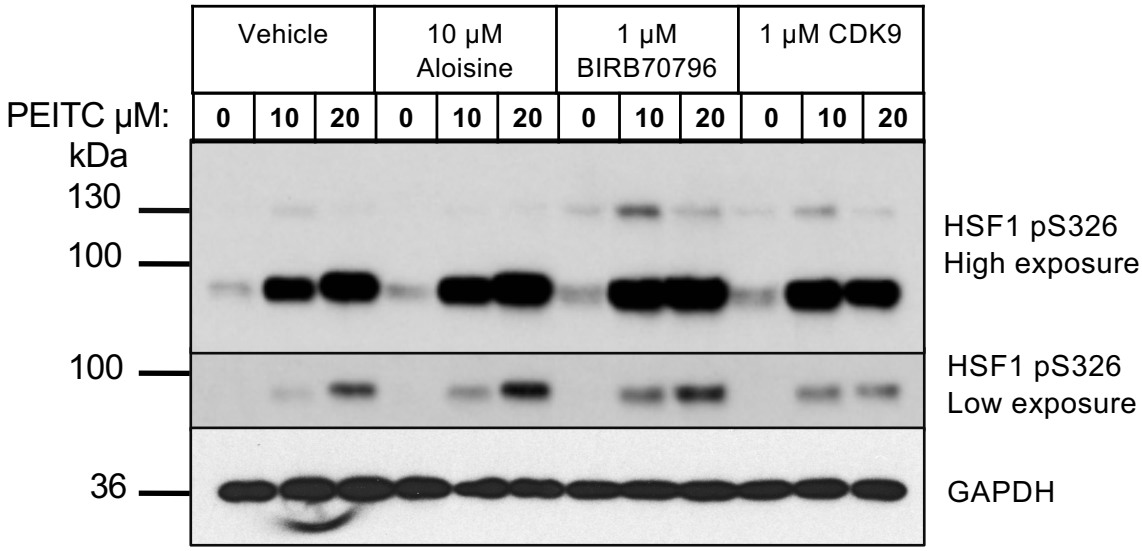

Figure 3.22. CDK9 Inhibitor reduces HSF1 pS326 in MCF7 cells. 5 x 10^5 MCF7 cells per well of a 6 well plated were seeded. 20 h after seeding the MCF7 cells were pretreated with either 10 µM Aloisine, 1 µM BIRB0796 or 1 µM CDK9 Inhibitor for 1 h. Subsequently the cells were exposed to vehicle (0.1% DMSO) or 10 or 20 µM PEITC for a further 3 h afterwhich cells were lysed immediately with SDS-lysis buffer. Cell lysates (10 µg) were loaded and resolved using the SDS-PAGE system. The proteins from the gels were immobilised onto 0.45 µm nitrocellulose (NC) membranes. The western blot membranes were probed with antibodies against HSF1 pS326 and GAPDH were used, where the latter served as a loading control.

pole body organises the microtubule cytoskeleton. Importantly, this particular mutant was isolated as a co-lethal allele with cdc28-109 (the yeast equivalent of the mammalian CDK1). This observation agrees with the staining pattern of HSF1 pS326 in the cells, and indicates that CDK1 could be a potential kinase that mediates the phosphorylation of this site. Like p38 MAPK, the CDKs belong to the CMGC family of proline-directed kinases known for their promiscuity and functional redundancies. It is entirely plausible that HSF1 is phosphorylated by one or more of these kinases during mitosis. Also, since the overall HSF1 total protein levels drop during mitosis (**Fig. 3.18 and 3.19**), it could be that phosphorylation of HSF1 at S326 promotes the acetylation of HSF1 at key lysine residues such as K208, which has been reported to promote its protein stability by preventing it from ubiqutination and degradation by the proteasome (Raychaudhuri et al., 2014).

3.3.11 Future Perspectives

This study presented in Chapter 3 has raised many important and interesting questions regarding the physiological significance of HSF1 phosphorylation at S326 during mitosis: 1) Is this phosphorylation a prerequisite for entering into mitosis? 2) Is this phosphorylation a consequence of high CDK activity during mitosis? 3) How is the dephosphorylation of this site mediated when exiting mitosis and does this occur through the midbody expulsion, or are phosphatases involved? 4) Why is HSF1 pS326 sequestered to cytoskeletal elements in interphase cells? Further experiments need to be conducted to address all of these questions.

Concluding Remarks

HSF1 and NRF2 orchestrate comprehensive transcriptional programs that include genes encoding antioxidant and drug-metabolizing enzymes, chaperones which prevent protein misfolding and aggregation, as well as proteins which take part in the repair and clearance of damaged macromolecules, thus maintaining the cellular redox and intermediary metabolism. These programs provide powerful means for adaptation and survival under conditions of electrophilic, oxidative, inflammatory, and thermal stress due to the extraordinary functional diversity of their downstream target genes. However, although the functions of both HSF1 and NRF2 are undoubtedly broadly cytoprotective, the consequences of their activation are both context- and duration-dependent and may have not only beneficial, but also negative effects for the organism, such as promoting cardiomyopathy, facilitating tumor growth, and may even reduce longevity. This dichotomy should be very carefully considered when these transcription factors are targeted for disease prevention or treatment.

Although HSF1 and NRF2 are currently considered as drug targets, and both inducers and inhibitors are being developed for use as pharmacological agents, many questions still need to be answered before such agents can enter clinical practice. The initial signal that triggers release of HSF1 from its main negative regulators is still unclear. The primary cellular sensor for electrophilic small-molecule activators of HSF1 in the mammalian cell has not been established, although based on the ability of these compounds to react with sulfhydryl groups, it could be speculated that this sensor is a protein(s) equipped with reactive cysteine(s). It is also not clear whether small-molecule dual activators of HSF1 and NRF2 activate both pathways sequentially

or simultaneously. The requirement for higher inducer concentrations for HSF1 than for NRF2 activation suggests that the Keap1/NRF2 pathway is activated first, and the heat shock response follows. It would be important to establish, whether, in addition to HSF1, heat shock can also activate (or repress) NRF2 function, and if so, whether this requires HSF1, and whether there might be a physical interaction between the two transcription factors. Although both NRF2 and HSF1 affect mitochondrial function, how this occurs is not known at present. It is possible that genes encoding critical mitochondrial proteins are direct transcriptional targets of HSF1 and/or NRF2. Alternatively, by compromising the cellular proteostasis and redox balance, the absence of HSF1 and/or NRF2 may affect the catalytic function of thermodynamically unstable and/or redox-sensitive mitochondrial proteins indirectly. Finally, it would be very interesting to generate HSF1/NRF2-double knockout mice and, if they are viable, to examine their responses to stress of different types and performance in various models of human disease.

Section 4: References

ABRAVAYA, K., MYERS, M. P., MURPHY, S. P. & MORIMOTO, R. I. 1992. The human heat shock protein hsp70 interacts with HSF, the transcription factor that regulates heat shock gene expression. *Genes Dev,* 6**,** 1153-64.

AHN, S. G., KIM, S. A., YOON, J. H. & VACRATSIS, P. 2005. Heat-shock cognate 70 is required for the activation of heat-shock factor 1 in mammalian cells. *Biochem J,* 392**,** 145-52.

AHN, S. G. & THIELE, D. J. 2003. Redox regulation of mammalian heat shock factor 1 is essential for Hsp gene activation and protection from stress. *Genes Dev,* 17**,** 516-28.

AHN, Y. H., HWANG, Y., LIU, H., WANG, X. J., ZHANG, Y., STEPHENSON, K. K., BORONINA, T. N., COLE, R. N., DINKOVA-KOSTOVA, A. T., TALALAY, P. & COLE, P. A. 2010. Electrophilic tuning of the chemoprotective natural product sulforaphane. *Proc Natl Acad Sci U S A,* 107**,** 9590-5.

AKERFELT, M., MORIMOTO, R. I. & SISTONEN, L. 2010. Heat shock factors: integrators of cell stress, development and lifespan. *Nat Rev Mol Cell Biol,* 11**,** 545-55.

AL-AYOUBI, A. M., ZHENG, H., LIU, Y., BAI, T. & EBLEN, S. T. 2012. Mitogen-activated protein kinase phosphorylation of splicing factor 45 (SPF45) regulates SPF45 alternative splicing site utilization, proliferation, and cell adhesion. *Mol Cell Biol,* 32**,** 2880-93.

ALASTALO, T. P., HELLESUO, M., SANDQVIST, A., HIETAKANGAS, V., KALLIO, M. & SISTONEN, L. 2003. Formation of nuclear stress granules involves HSF2 and coincides with the nucleolar localization of Hsp70. *J Cell Sci,* 116**,** 3557-70.

ALBENA T. DINKOVA-KOSTOVA , Y. Z., SHARADHA DAYALAN NAIDU, RUMEN V. KOSTOV, ASHLEY PHEELY, VITTORIO CALABRESE 2013. Sulfhydryl-Reactive Phytochemicals as Dual Activators of Transcription Factors NRF2 and HSF1. *In:* GANG, D. (ed.) *50 Years of Phytochemistry Research.* 1 ed.: Springer International Publishing.

ALEXEEV, V., LASH, E., AGUILLARD, A., CORSINI, L., BITTERMAN, A., WARD, K., DICKER, A. P., LINNENBACH, A. & RODECK, U. 2014. Radiation protection of the gastrointestinal tract and growth inhibition of prostate cancer xenografts by a single compound. *Mol Cancer Ther,* 13**,** 2968-77.

ALI, A., BHARADWAJ, S., O'CARROLL, R. & OVSENEK, N. 1998. HSP90 interacts with and regulates the activity of heat shock factor 1 in Xenopus oocytes. *Mol Cell Biol,* 18**,** 4949-60.

ALLISON, A. C., CACABELOS, R., LOMBARDI, V. R., ALVAREZ, X. A. & VIGO, C. 2001. Celastrol, a potent antioxidant and anti-inflammatory drug, as a possible treatment for Alzheimer's disease. *Prog Neuropsychopharmacol Biol Psychiatry,* 25**,** 1341-57.

ALMEIDA, D. V., NORNBERG, B. F., GERACITANO, L. A., BARROS, D. M., MONSERRAT, J. M. & MARINS, L. F. 2010. Induction of phase II enzymes and hsp70 genes by copper sulfate through the electrophile-responsive element (EpRE): insights obtained from a transgenic zebrafish model carrying an orthologous EpRE sequence of mammalian origin. *Fish physiology and biochemistry,* 36**,** 347-53.

ANCKAR, J. & SISTONEN, L. 2011. Regulation of HSF1 function in the heat stress response: implications in aging and disease. *Annu Rev Biochem,* 80**,** 1089-115.

ANDERICA-ROMERO, A. C., GONZALEZ-HERRERA, I. G., SANTAMARIA, A. & PEDRAZA-CHAVERRI, J. 2013. Cullin 3 as a novel target in diverse pathologies. *Redox Biol,* 1**,** 366-72.

ARIDON, P., GERACI, F., TURTURICI, G., D'AMELIO, M., SAVETTIERI, G. & SCONZO, G. 2011. Protective role of heat shock proteins in Parkinson's disease. *Neurodegener Dis,* 8**,** 155-68.

ARRIGO, A. P., VIROT, S., CHAUFOUR, S., FIRDAUS, W., KRETZ-REMY, C. & DIAZ-LATOUD, C. 2005. Hsp27 consolidates intracellular redox homeostasis by upholding glutathione in its reduced form and by decreasing iron intracellular levels. *Antioxid Redox Signal,* 7**,** 414-22.

ASANTE, D., MACCARTHY-MORROGH, L., TOWNLEY, A. K., WEISS, M. A., KATAYAMA, K., PALMER, K. J., SUZUKI, H., WESTLAKE, C. J. & STEPHENS, D. J. 2013. A role for the Golgi matrix protein giantin in ciliogenesis through control of the localization of dynein-2. *J Cell Sci,* 126**,** 5189-97.

AU, Q., KANCHANASTIT, P., BARBER, J. R., NG, S. C. & ZHANG, B. 2008. High-content image-based screening for small-molecule chaperone amplifiers in heat shock. *J Biomol Screen,* 13**,** 953-9.

BADRINARAYAN, P. & SASTRY, G. N. 2011. Sequence, structure, and active site analyses of p38 MAP kinase: exploiting DFG-out conformation as a strategy to design new type II leads. *J Chem Inf Model,* 51**,** 115-29.

BAIRD, L. & DINKOVA-KOSTOVA, A. T. 2013. Diffusion dynamics of the Keap1-Cullin3 interaction in single live cells. *Biochem Biophys Res Commun,* 433**,** 58-65.

BAIRD, L., LLERES, D., SWIFT, S. & DINKOVA-KOSTOVA, A. T. 2013. Regulatory flexibility in the Nrf2-mediated stress response is conferred by conformational cycling of the Keap1-Nrf2 protein complex. *Proc Natl Acad Sci U S A,* 110**,** 15259-64.

BALER, R., DAHL, G. & VOELLMY, R. 1993. Activation of human heat shock genes is accompanied by oligomerization, modification, and rapid translocation of heat shock transcription factor HSF1. *Mol Cell Biol,* 13**,** 2486-96.

BALI, P., PRANPAT, M., BRADNER, J., BALASIS, M., FISKUS, W., GUO, F., ROCHA, K., KUMARASWAMY, S., BOYAPALLE, S., ATADJA, P., SETO, E. & BHALLA, K. 2005. Inhibition of histone deacetylase 6 acetylates and disrupts the chaperone function of heat shock protein 90: a novel basis for antileukemia activity of histone deacetylase inhibitors. *J Biol Chem,* 280**,** 26729-34.

BANERJEE MUSTAFI, S., CHAKRABORTY, P. K., DEY, R. S. & RAHA, S. 2009. Heat stress upregulates chaperone heat shock protein 70 and antioxidant manganese superoxide dismutase through reactive oxygen species (ROS), p38MAPK, and Akt. *Cell Stress Chaperones,* 14**,** 579-89.

BAST, A., WESELER, A. R., HAENEN, G. R. & DEN HARTOG, G. J. 2010. Oxidative stress and antioxidants in interstitial lung disease. *Curr Opin Pulm Med,* 16**,** 516-20.

BENJAMIN, I. J., GUO, Y., SRINIVASAN, S., BOUDINA, S., TAYLOR, R. P., RAJASEKARAN, N. S., GOTTLIEB, R., WAWROUSEK, E. F., ABEL, E. D. & BOLLI, R. 2007. CRYAB and HSPB2 deficiency alters cardiac metabolism and paradoxically confers protection against myocardial ischemia in aging mice. *Am J Physiol Heart Circ Physiol,* 293**,** H3201-9.

BENJAMIN, I. J., KROGER, B. & WILLIAMS, R. S. 1990. Activation of the heat shock transcription factor by hypoxia in mammalian cells. *Proc Natl Acad Sci U S A,* 87**,** 6263-7.

BERMAN, K., MCKAY, J., AVERY, L. & COBB, M. 2001. Isolation and characterization of pmk-(1-3): three p38 homologs in Caenorhabditis elegans. *Mol Cell Biol Res Commun,* 4**,** 337-44.

BERSUKER, K., HIPP, M. S., CALAMINI, B., MORIMOTO, R. I. & KOPITO, R. R. 2013. Heat shock response activation exacerbates inclusion body formation in a cellular model of Huntington disease. *J Biol Chem,* 288**,** 23633-8.

BIAMONTI, G. 2004. Nuclear stress bodies: a heterochromatin affair? *Nat Rev Mol Cell Biol,* 5**,** 493-8.

BIAMONTI, G. & VOURC'H, C. 2010. Nuclear stress bodies. *Cold Spring Harb Perspect Biol,* 2**,** a000695.

BLAKE, M. J., FARGNOLI, J., GERSHON, D. & HOLBROOK, N. J. 1991. Concomitant decline in heat-induced hyperthermia and HSP70 mRNA expression in aged rats. *Am J Physiol,* 260**,** R663-7.

BOELLMANN, F., GUETTOUCHE, T., GUO, Y., FENNA, M., MNAYER, L. & VOELLMY, R. 2004. DAXX interacts with heat shock factor 1 during stress activation and enhances its transcriptional activity. *Proc Natl Acad Sci U S A,* 101**,** 4100-5.

BONELLI, M. A., ALFIERI, R. R., POLI, M., PETRONINI, P. G. & BORGHETTI, A. F. 2001. Heat-induced proteasomic degradation of HSF1 in serum-starved human fibroblasts aging in vitro. *Exp Cell Res,* 267**,** 165-72.

BOVA, M. P., YARON, O., HUANG, Q., DING, L., HALEY, D. A., STEWART, P. L. & HORWITZ, J. 1999. Mutation R120G in alphaB-crystallin, which is linked to a desmin-related myopathy, results in an irregular structure and defective chaperone-like function. *Proc Natl Acad Sci U S A,* 96**,** 6137-42.

BRANCHO, D., TANAKA, N., JAESCHKE, A., VENTURA, J. J., KELKAR, N., TANAKA, Y., KYUUMA, M., TAKESHITA, T., FLAVELL, R. A. & DAVIS, R. J. 2003. Mechanism of p38 MAP kinase activation in vivo. *Genes Dev,* 17**,** 1969-78.

BRANDT, G. E., SCHMIDT, M. D., PRISINZANO, T. E. & BLAGG, B. S. 2008. Gedunin, a novel hsp90 inhibitor: semisynthesis of derivatives and preliminary structure-activity relationships. *J Med Chem,* 51**,** 6495-502.

BRAVI, M. C., ARMIENTO, A., LAURENTI, O., CASSONE-FALDETTA, M., DE LUCA, O., MORETTI, A. & DE MATTIA, G. 2006. Insulin decreases intracellular oxidative stress in patients with type 2 diabetes mellitus. *Metabolism,* 55**,** 691-5.

BREWER, A. C., MUSTAFI, S. B., MURRAY, T. V., RAJASEKARAN, N. S. & BENJAMIN, I. J. 2013. Reductive stress linked to small HSPs, G6PD, and Nrf2 pathways in heart disease. *Antioxid Redox Signal,* 18**,** 1114-27.

BRUNET SIMIONI, M., DE THONEL, A., HAMMANN, A., JOLY, A. L., BOSSIS, G., FOURMAUX, E., BOUCHOT, A., LANDRY, J., PIECHACZYK, M. & GARRIDO, C. 2009. Heat shock protein 27 is involved in SUMO-2/3 modification of heat shock factor 1 and thereby modulates the transcription factor activity. *Oncogene,* 28**,** 3332-44.

BRYAN, H. K., OLAYANJU, A., GOLDRING, C. E. & PARK, B. K. 2013. The Nrf2 cell defence pathway: Keap1-dependent and -independent mechanisms of regulation. *Biochem Pharmacol,* 85**,** 705-17.

BU, L., JIN, Y., SHI, Y., CHU, R., BAN, A., EIBERG, H., ANDRES, L., JIANG, H., ZHENG, G., QIAN, M., CUI, B., XIA, Y., LIU, J., HU, L., ZHAO, G., HAYDEN, M. R. & KONG, X. 2002. Mutant DNA-binding domain of HSF4 is associated with autosomal dominant lamellar and Marner cataract. *Nat Genet,* 31**,** 276-8.

BUDZYNSKI, M. A., PUUSTINEN, M. C., JOUTSEN, J. & SISTONEN, L. 2015. Uncoupling Stress-Inducible Phosphorylation of Heat Shock Factor 1 from Its Activation. *Mol Cell Biol,* 35**,** 2530-40.

BUNKOCZI, G., SALAH, E., FILIPPAKOPOULOS, P., FEDOROV, O., MULLER, S., SOBOTT, F., PARKER, S. A., ZHANG, H., MIN, W., TURK, B. E. & KNAPP, S. 2007. Structural and functional characterization of the human protein kinase ASK1. *Structure,* 15**,** 1215-26.

BURTON, E. R., GAFFAR, A., LEE, S. J., ADESHUKO, F., WHITNEY, K. D., CHUNG, J. Y., HEWITT, S. M., HUANG, G. S., GOLDBERG, G. L., LIBUTTI, S. K. & KWON, M. 2011. Downregulation of Filamin A interacting protein 1-like is associated with promoter methylation and induces an invasive phenotype in ovarian cancer. *Mol Cancer Res,* 9**,** 1126-38.

BYRNE, A. M., BEKIARIS, S., DUGGAN, G., PRICHARD, D., KIRCA, M., FINN, S., REYNOLDS, J. V., KELLEHER, D. & LONG, A. 2015. Golgi phosphoprotein 2 (GOLPH2) is a novel bile acid-responsive modulator of oesophageal cell migration and invasion. *Br J Cancer,* 113**,** 1332-42.

CALAMINI, B., SILVA, M. C., MADOUX, F., HUTT, D. M., KHANNA, S., CHALFANT, M. A., ALLAIS, C., OUIZEM, S., SALDANHA, S. A., FERGUSON, J., MERCER, B. A., MICHAEL, C., TAIT, B. D., GARZA, D., BALCH, W. E., ROUSH, W. R., MORIMOTO, R. I. & HODDER, P. 2010. ML346: A Novel Modulator of Proteostasis for Protein Conformational Diseases. *Probe Reports from the NIH Molecular Libraries Program.* Bethesda (MD).

CALAMINI, B., SILVA, M. C., MADOUX, F., HUTT, D. M., KHANNA, S., CHALFANT, M. A., SALDANHA, S. A., HODDER, P., TAIT, B. D., GARZA, D., BALCH, W. E. & MORIMOTO, R. I. 2012. Small-molecule proteostasis regulators for protein conformational diseases. *Nat Chem Biol,* 8**,** 185-96.

CALTANA, L., RUTOLO, D., NIETO, M. L. & BRUSCO, A. 2014. Further evidence for the neuroprotective role of oleanolic acid in a model of focal brain hypoxia in rats. *Neurochem Int,* 79**,** 79-87.

CANNING, P., COOPER, C. D., KROJER, T., MURRAY, J. W., PIKE, A. C., CHAIKUAD, A., KEATES, T., THANGARATNARAJAH, C., HOJZAN, V., AYINAMPUDI, V., MARSDEN, B. D., GILEADI, O., KNAPP, S., VON DELFT, F. & BULLOCK, A. N. 2013. Structural basis for Cul3 protein assembly with the BTB-Kelch family of E3 ubiquitin ligases. *J Biol Chem,* 288**,** 7803-14.

CANNING, P., SORRELL, F. J. & BULLOCK, A. N. 2015. Structural basis of Keap1 interactions with Nrf2. *Free Radic Biol Med,* 88**,** 101-7.

CAO, H., XUE, L., XU, X., WU, Y., ZHU, J., CHEN, L., CHEN, D. & CHEN, Y. 2011. Heat shock proteins in stabilization of spontaneously restored sinus rhythm in permanent atrial fibrillation patients after mitral valve surgery. *Cell Stress Chaperones,* 16**,** 517-28.

CARBONE, D. L., DOORN, J. A., KIEBLER, Z., ICKES, B. R. & PETERSEN, D. R. 2005. Modification of heat shock protein 90 by 4-hydroxynonenal in a rat model of chronic alcoholic liver disease. *J Pharmacol Exp Ther,* 315**,** 8-15.

CARNEMOLLA, A., LABBADIA, J. P., LAZELL, H., NEUEDER, A., MOUSSAOUI, S. & BATES, G. P. 2014. Contesting the dogma of an age-related heat shock response impairment: implications for cardiac-specific age-related disorders. *Hum Mol Genet*.

CASANOVAS, O., JAUMOT, M., PAULES, A. B., AGELL, N. & BACHS, O. 2004. P38SAPK2 phosphorylates cyclin D3 at Thr-283 and targets it for proteasomal degradation. *Oncogene,* 23**,** 7537-44.

CASTELLANI, R., SMITH, M. A., RICHEY, P. L. & PERRY, G. 1996. Glycoxidation and oxidative stress in Parkinson disease and diffuse Lewy body disease. *Brain Res,* 737**,** 195-200.

CASTELLANO, J. M., GUINDA, A., DELGADO, T., RADA, M. & CAYUELA, J. A. 2013. Biochemical basis of the antidiabetic activity of oleanolic acid and related pentacyclic triterpenes. *Diabetes,* 62**,** 1791-9.

CASTILLO, E. F., RAY, A. L. & BESWICK, E. J. 2016. MK2: an unrecognized regulator of tumor promoting macrophages in colorectal cancer? *Macrophage (Houst),* 3.

CAVELL, B. E., SYED ALWI, S. S., DONLEVY, A. M., PROUD, C. G. & PACKHAM, G. 2012. Natural product-derived antitumor compound phenethyl isothiocyanate inhibits mTORC1 activity via TSC2. *J Nat Prod,* 75**,** 1051-7.

CERIELLO, A. 2006. Oxidative stress and diabetes-associated complications. *Endocr Pract,* 12 Suppl 1**,** 60-2.

CHADLI, A., FELTS, S. J., WANG, Q., SULLIVAN, W. P., BOTUYAN, M. V., FAUQ, A., RAMIREZ-ALVARADO, M. & MER, G. 2010. Celastrol inhibits Hsp90 chaperoning of steroid receptors by inducing fibrillization of the Co-chaperone p23. *J Biol Chem,* 285**,** 4224-31.

CHAN, E., SAITO, A., HONDA, T. & DI GUGLIELMO, G. M. 2016. The acetylenic tricyclic bis(cyano enone), TBE-31, targets microtubule dynamics and cell polarity in migrating cells. *Biochim Biophys Acta,* 1863**,** 638-49.

CHAN, H. Y., WARRICK, J. M., GRAY-BOARD, G. L., PAULSON, H. L. & BONINI, N. M. 2000. Mechanisms of chaperone suppression of polyglutamine disease: selectivity, synergy and modulation of protein solubility in Drosophila. *Hum Mol Genet,* 9**,** 2811-20.

CHANDRA, V., GANGULI, M., RATCLIFF, G., PANDAV, R., SHARMA, S., BELLE, S., RYAN, C., BAKER, C., DEKOSKY, S. & NATH, L. 1998. Practical issues in cognitive screening of elderly illiterate populations in developing countries. The Indo-US Cross-National Dementia Epidemiology Study. *Aging (Milano),* 10**,** 349-57.

CHEN, H. W., YU, S. L., CHEN, J. J., LI, H. N., LIN, Y. C., YAO, P. L., CHOU, H. Y., CHIEN, C. T., CHEN, W. J., LEE, Y. T. & YANG, P. C. 2004. Anti-invasive gene expression profile of curcumin in lung adenocarcinoma based on a high throughput microarray analysis. *Mol Pharmacol,* 65**,** 99-110.

CHEN, Y., WANG, B., LIU, D., LI, J. J., XUE, Y., SAKATA, K., ZHU, L. Q., HELDT, S. A., XU, H. & LIAO, F. F. 2014. Hsp90 chaperone inhibitor 17-AAG attenuates Abeta-induced synaptic toxicity and memory impairment. *J Neurosci,* 34**,** 2464-70.

CHENG, F., JIA, P., WANG, Q. & ZHAO, Z. 2014. Quantitative network mapping of the human kinome interactome reveals new clues for rational kinase inhibitor discovery and individualized cancer therapy. *Oncotarget,* 5**,** 3697-710.

CHEUNG, K. L., KHOR, T. O., HUANG, M. T. & KONG, A. N. 2010. Differential in vivo mechanism of chemoprevention of tumor formation in azoxymethane/dextran sodium sulfate mice by PEITC and DBM. *Carcinogenesis,* 31**,** 880-5.

CHEUNG, K. L., KHOR, T. O., YU, S. & KONG, A. N. 2008. PEITC induces G1 cell cycle arrest on HT-29 cells through the activation of p38 MAPK signaling pathway. *AAPS J,* 10**,** 277-81.

CHIANG, W. C., CHING, T. T., LEE, H. C., MOUSIGIAN, C. & HSU, A. L. 2012. HSF-1 regulators DDL-1/2 link insulin-like signaling to heat-shock responses and modulation of longevity. *Cell,* 148**,** 322-34.

CHIN, D., HUEBBE, P., PALLAUF, K. & RIMBACH, G. 2013. Neuroprotective properties of curcumin in Alzheimer's disease--merits and limitations. *Curr Med Chem,* 20**,** 3955-85.

CHIN, M. P., REISMAN, S. A., BAKRIS, G. L., O'GRADY, M., LINDE, P. G., MCCULLOUGH, P. A., PACKHAM, D., VAZIRI, N. D., WARD, K. W., WARNOCK, D. G. & MEYER, C. J. 2014. Mechanisms contributing to adverse cardiovascular events in patients with type 2 diabetes mellitus and stage 4 chronic kidney disease treated with bardoxolone methyl. *Am J Nephrol,* 39**,** 499-508.

CHOI, H. S., LIN, Z., LI, B. S. & LIU, A. Y. 1990. Age-dependent decrease in the heat-inducible DNA sequence-specific binding activity in human diploid fibroblasts. *J Biol Chem,* 265**,** 18005-11.

CHOI, Y., ASADA, S. & UESUGI, M. 2000. Divergent hTAFII31-binding motifs hidden in activation domains. *J Biol Chem,* 275**,** 15912-6.

CHOO, Y. Y. & HAGEN, T. 2012. Mechanism of cullin3 E3 ubiquitin ligase dimerization. *PLoS One,* 7**,** e41350.

CHOU, S. D., PRINCE, T., GONG, J. & CALDERWOOD, S. K. 2012. mTOR is essential for the proteotoxic stress response, HSF1 activation and heat shock protein synthesis. *PLoS One,* 7**,** e39679.

CHOU, Y. C., CHANG, M. Y., WANG, M. J., YU, F. S., LIU, H. C., HARNOD, T., HUNG, C. H., LEE, H. T. & CHUNG, J. G. 2015. PEITC inhibits human brain glioblastoma GBM 8401 cell migration and invasion through the inhibition of uPA, Rho A, and Ras with inhibition of MMP-2, -7 and -9 gene expression. *Oncol Rep,* 34**,** 2489-96.

CHOWDHRY, S., ZHANG, Y., MCMAHON, M., SUTHERLAND, C., CUADRADO, A. & HAYES, J. D. 2013. Nrf2 is controlled by two distinct beta-TrCP recognition motifs in its Neh6 domain, one of which can be modulated by GSK-3 activity. *Oncogene,* 32**,** 3765-81.

CHRISTIANS, E., DAVIS, A. A., THOMAS, S. D. & BENJAMIN, I. J. 2000. Maternal effect of Hsf1 on reproductive success. *Nature,* 407**,** 693-4.

CHU, B., ZHONG, R., SONCIN, F., STEVENSON, M. A. & CALDERWOOD, S. K. 1998. Transcriptional activity of heat shock factor 1 at 37 degrees C is repressed through phosphorylation on two distinct serine residues by glycogen synthase kinase 3 and protein kinases Calpha and Czeta. *J Biol Chem,* 273**,** 18640-6.

CICERO, M. P., HUBL, S. T., HARRISON, C. J., LITTLEFIELD, O., HARDY, J. A. & NELSON, H. C. 2001. The wing in yeast heat shock transcription factor (HSF) DNA-binding domain is required for full activity. *Nucleic Acids Res,* 29**,** 1715-23.

CLEASBY, A., YON, J., DAY, P. J., RICHARDSON, C., TICKLE, I. J., WILLIAMS, P. A., CALLAHAN, J. F., CARR, R., CONCHA, N., KERNS, J. K., QI, H., SWEITZER, T., WARD, P. & DAVIES, T. G. 2014. Structure of the BTB domain of Keap1 and its interaction with the triterpenoid antagonist CDDO. *PLoS One,* 9**,** e98896.

CLEREN, C., CALINGASAN, N. Y., CHEN, J. & BEAL, M. F. 2005. Celastrol protects against MPTP- and 3-nitropropionic acid-induced neurotoxicity. *J Neurochem,* 94**,** 995-1004.

CLINICALTRIALS.GOV. Available: https://clinicaltrials.gov/ct2/results?term=rta+408&Search=Search [Accessed 18 May 2016 2016].

COHEN, P. 2009. Targeting protein kinases for the development of anti-inflammatory drugs. *Curr Opin Cell Biol,* 21**,** 317-24.

CONNOR, R. E., MARNETT, L. J. & LIEBLER, D. C. 2011. Protein-selective capture to analyze electrophile adduction of hsp90 by 4-hydroxynonenal. *Chem. Res. Toxicol.,* 24**,** 1275-82.

CONWAY, E. M., LIU, L., NOWAKOWSKI, B., STEINER-MOSONYI, M. & JACKMAN, R. W. 1994. Heat shock of vascular endothelial cells induces an up-regulatory transcriptional response of the thrombomodulin gene that is delayed in onset and does not attenuate. *J Biol Chem,* 269**,** 22804-10.

COPPLE, I. M., LISTER, A., OBENG, A. D., KITTERINGHAM, N. R., JENKINS, R. E., LAYFIELD, R., FOSTER, B. J., GOLDRING, C. E. & PARK, B. K. 2010. Physical and functional interaction of sequestosome 1 with Keap1 regulates the Keap1-Nrf2 cell defense pathway. *J Biol Chem,* 285**,** 16782-8.

CORDOVA, C., GUTIERREZ, B., MARTINEZ-GARCIA, C., MARTIN, R., GALLEGO-MUNOZ, P., HERNANDEZ, M. & NIETO, M. L. 2014. Oleanolic acid controls allergic and inflammatory responses in experimental allergic conjunctivitis. *PLoS One,* 9**,** e91282.

COSTA, S., REINA-COUTO, M., ALBINO-TEIXEIRA, A. & SOUSA, T. 2016. Statins and oxidative stress in chronic heart failure. *Rev Port Cardiol,* 35**,** 41-57.

COTTO, J. J., KLINE, M. & MORIMOTO, R. I. 1996. Activation of heat shock factor 1 DNA binding precedes stress-induced serine phosphorylation. Evidence for a multistep pathway of regulation. *J Biol Chem,* 271**,** 3355-8.

CRAIG, E. A., STEVENS, M. V., VAILLANCOURT, R. R. & CAMENISCH, T. D. 2008. MAP3Ks as central regulators of cell fate during development. *Dev Dyn,* 237**,** 3102-14.

CUADRADO, A. & NEBREDA, A. R. 2010. Mechanisms and functions of p38 MAPK signalling. *Biochem J,* 429**,** 403-17.

CUENDA, A. & ROUSSEAU, S. 2007. p38 MAP-kinases pathway regulation, function and role in human diseases. *Biochim Biophys Acta,* 1773**,** 1358-75.

CURRIE, R. W. & KARMAZYN, M. 1990. Improved post-ischemic ventricular recovery in the absence of changes in energy metabolism in working rat hearts following heat-shock. *J Mol Cell Cardiol,* 22**,** 631-6.

CURRIE, R. W., KARMAZYN, M., KLOC, M. & MAILER, K. 1988. Heat-shock response is associated with enhanced postischemic ventricular recovery. *Circ Res,* 63**,** 543-9.

CURRIE, R. W., TANGUAY, R. M. & KINGMA, J. G., JR. 1993. Heat-shock response and limitation of tissue necrosis during occlusion/reperfusion in rabbit hearts. *Circulation,* 87**,** 963-71.

DAI, C., SANTAGATA, S., TANG, Z., SHI, J., CAO, J., KWON, H., BRONSON, R. T., WHITESELL, L. & LINDQUIST, S. 2012b. Loss of tumor suppressor NF1 activates HSF1 to promote carcinogenesis. *The J Clin Invest*, 122, 3742-54,

DAI, C., WHITESELL, L., ROGERS, A. B. & LINDQUIST, S. 2007. Heat shock factor 1 is a powerful multifaceted modifier of carcinogenesis. *Cell,* 130**,** 1005-18.

DARVESH, A. S., CARROLL, R. T., BISHAYEE, A., NOVOTNY, N. A., GELDENHUYS, W. J. & VAN DER SCHYF, C. J. 2012. Curcumin and neurodegenerative diseases: a perspective. *Expert Opin Investig Drugs,* 21**,** 1123-40.

DAVIES, T. G., WIXTED, W. E., COYLE, J. E., GRIFFITHS-JONES, C., HEARN, K., MCMENAMIN, R., NORTON, D., RICH, S. J., RICHARDSON, C., SAXTY, G., WILLEMS, H. M., WOOLFORD, A. J., COTTOM, J. E., KOU, J. P., YONCHUK, J. G., FELDSER, H. G., SANCHEZ, Y., FOLEY, J. P., BOLOGNESE, B. J., LOGAN, G., PODOLIN, P. L., YAN, H., CALLAHAN, J. F., HEIGHTMAN, T. D. & KERNS, J. K. 2016. Monoacidic Inhibitors of the Kelch-like ECH-Associated Protein 1: Nuclear Factor Erythroid 2-Related Factor 2 (KEAP1:NRF2) Protein-Protein Interaction with High Cell Potency Identified by Fragment-Based Discovery. *J Med Chem,* 59**,** 3991-4006.

DAYALAN NAIDU, S., KOSTOV, R. V. & DINKOVA-KOSTOVA, A. T. 2015. Transcription factors Hsf1 and Nrf2 engage in crosstalk for cytoprotection. *Trends Pharmacol Sci,* 36**,** 6-14.

DAYALAN NAIDU, S., SUTHERLAND, C., ZHANG, Y., RISCO, A., DE LA VEGA, L., CAUNT, C. J., HASTIE, C. J., LAMONT, D. J., TORRENTE, L., CHOWDHRY, S., BENJAMIN, I. J., KEYSE, S. M., CUENDA, A. & DINKOVA-KOSTOVA, A. T. 2016. Heat Shock Factor 1 is a Substrate for p38 Mitogen-Activated Protein Kinases. *Mol Cell Biol*. (in press)

DE WIT, R., VAN DER ZEE, J., VAN DER BURG, M. E., KRUIT, W. H., LOGMANS, A., VAN RHOON, G. C. & VERWEIJ, J. 1999. A phase I/II study of combined weekly systemic cisplatin and locoregional hyperthermia in patients with previously irradiated recurrent carcinoma of the uterine cervix. *Br J Cancer,* 80**,** 1387-91.

DEACON, K. & BLANK, J. L. 1997. Characterization of the mitogen-activated protein kinase kinase 4 (MKK4)/c-Jun NH2-terminal kinase 1 and MKK3/p38 pathways regulated by MEK kinases 2 and 3. MEK kinase 3 activates MKK3 but does not cause activation of p38 kinase in vivo. *J Biol Chem,* 272**,** 14489-96.

DEL BARCO BARRANTES, I., COYA, J. M., MAINA, F., ARTHUR, J. S. & NEBREDA, A. R. 2011. Genetic analysis of specific and redundant roles for p38alpha and p38beta MAPKs during mouse development. *Proc Natl Acad Sci U S A,* 108**,** 12764-9.

DEL REINO, P., ALSINA-BEAUCHAMP, D., ESCOS, A., CEREZO-GUISADO, M. I., RISCO, A., APARICIO, N., ZUR, R., FERNANDEZ-ESTEVEZ, M., COLLANTES, E., MONTANS, J. & CUENDA, A. 2014. Pro-oncogenic role of alternative p38 mitogen-activated protein kinases p38gamma and p38delta, linking inflammation and cancer in colitis-associated colon cancer. *Cancer Res,* 74**,** 6150-60.

DESAI, S., LIU, Z., YAO, J., PATEL, N., CHEN, J., WU, Y., AHN, E. E., FODSTAD, O. & TAN, M. 2013. Heat shock factor 1 (HSF1) controls chemoresistance and autophagy through transcriptional regulation of autophagy-related protein 7 (ATG7). *J Biol Chem,* 288**,** 9165-76.

DHARMAPPA, K. K., KUMAR, R. V., NATARAJU, A., MOHAMED, R., SHIVAPRASAD, H. V. & VISHWANATH, B. S. 2009. Anti-inflammatory activity of oleanolic acid by inhibition of secretory phospholipase A2. *Planta Med,* 75**,** 211-5.

DINKOVA-KOSTOVA, A. T. 2013. Chemoprotection against cancer by isothiocyanates: a focus on the animal models and the protective mechanisms. *Top Curr Chem,* 329**,** 179-201.

DINKOVA-KOSTOVA, A. T., BAIRD, L., HOLMSTROM, K. M., MEYER, C. J. & ABRAMOV, A. Y. 2015. The spatiotemporal regulation of the Keap1-Nrf2 pathway and its importance in cellular bioenergetics. *Biochem Soc Trans,* 43**,** 602-10.

DINKOVA-KOSTOVA, A. T., HOLTZCLAW, W. D., COLE, R. N., ITOH, K., WAKABAYASHI, N., KATOH, Y., YAMAMOTO, M. & TALALAY, P. 2002. Direct evidence that sulfhydryl groups of Keap1 are the sensors regulating induction of phase 2 enzymes that protect against carcinogens and oxidants. *Proc Natl Acad Sci U S A,* 99**,** 11908-13.

DINKOVA-KOSTOVA, A. T. & KOSTOV, R. V. 2012. Glucosinolates and isothiocyanates in health and disease. *Trends Mol Med,* 18**,** 337-47.

DINKOVA-KOSTOVA, A. T., MASSIAH, M. A., BOZAK, R. E., HICKS, R. J. & TALALAY, P. 2001. Potency of Michael reaction acceptors as inducers of enzymes that protect against carcinogenesis depends on their reactivity with sulfhydryl groups. *Proc Natl Acad Sci U S A,* 98**,** 3404-9.

DONNELLY, T. J., SIEVERS, R. E., VISSERN, F. L., WELCH, W. J. & WOLFE, C. L. 1992. Heat shock protein induction in rat hearts. A role for improved myocardial salvage after ischemia and reperfusion? *Circulation,* 85**,** 769-78.

DORION, S., LAMBERT, H. & LANDRY, J. 2002. Activation of the p38 signaling pathway by heat shock involves the dissociation of glutathione S-transferase Mu from Ask1. *J Biol Chem,* 277**,** 30792-7.

DUDA, D. M., BORG, L. A., SCOTT, D. C., HUNT, H. W., HAMMEL, M. & SCHULMAN, B. A. 2008. Structural insights into NEDD8 activation of cullin-RING ligases: conformational control of conjugation. *Cell,* 134**,** 995-1006.

DUNGU, J. N., ANDERSON, L. J., WHELAN, C. J. & HAWKINS, P. N. 2014. Cardiac transthyretin amyloidosis. *Heart,* 98**,** 1546-54.

ELIA, G., POLLA, B., ROSSI, A. & SANTORO, M. G. 1999. Induction of ferritin and heat shock proteins by prostaglandin A1 in human monocytes. Evidence for transcriptional and post-transcriptional regulation. *Eur J Biochem,* 264**,** 736-45.

ENGEL, F. B., SCHEBESTA, M., DUONG, M. T., LU, G., REN, S., MADWED, J. B., JIANG, H., WANG, Y. & KEATING, M. T. 2005. p38 MAP kinase inhibition enables proliferation of adult mammalian cardiomyocytes. *Genes Dev,* 19**,** 1175-87.

ESCOS, A., RISCO, A., ALSINA-BEAUCHAMP, D. & CUENDA, A. 2016. p38gamma and p38delta Mitogen Activated Protein Kinases (MAPKs), New Stars in the MAPK Galaxy. *Front Cell Dev Biol,* 4**,** 31.

FAHEY, J. W., ZALCMANN, A. T. & TALALAY, P. 2001. The chemical diversity and distribution of glucosinolates and isothiocyanates among plants. *Phytochemistry,* 56**,** 5-51.

FANG, H., PENGAL, R. A., CAO, X., GANESAN, L. P., WEWERS, M. D., MARSH, C. B. & TRIDANDAPANI, S. 2004. Lipopolysaccharide-induced macrophage inflammatory response is regulated by SHIP. *J Immunol,* 173**,** 360-6.

FARGNOLI, J., KUNISADA, T., FORNACE, A. J., JR., SCHNEIDER, E. L. & HOLBROOK, N. J. 1990. Decreased expression of heat shock protein 70 mRNA and protein after heat treatment in cells of aged rats. *Proc Natl Acad Sci U S A,* 87**,** 846-50.

FARKAS, T., KUTSKOVA, Y. A. & ZIMARINO, V. 1998. Intramolecular repression of mouse heat shock factor 1. *Mol Cell Biol,* 18**,** 906-18.

FAVATA, M. F., HORIUCHI, K. Y., MANOS, E. J., DAULERIO, A. J., STRADLEY, D. A., FEESER, W. S., VAN DYK, D. E., PITTS, W. J., EARL, R. A., HOBBS, F., COPELAND, R. A., MAGOLDA, R. L., SCHERLE, P. A. & TRZASKOS, J. M. 1998. Identification of a novel inhibitor of mitogen-activated protein kinase kinase. *J Biol Chem,* 273**,** 18623-32.

FELLNER, L. & STEFANOVA, N. 2013. The role of glia in alpha-synucleinopathies. *Mol Neurobiol,* 47**,** 575-86.

FENG, J., ZHANG, P., CHEN, X. & HE, G. 2011. PI3K and ERK/Nrf2 pathways are involved in oleanolic acid-induced heme oxygenase-1 expression in rat vascular smooth muscle cells. *J Cell Biochem,* 112**,** 1524-31.

FENG, Y., HUANG, W., MENG, W., JEGGA, A. G., WANG, Y., CAI, W., KIM, H. W., PASHA, Z., WEN, Z., RAO, F., MODI, R. M., YU, X. & ASHRAF, M. 2014. Heat shock improves Sca-1+ stem cell survival and directs ischemic cardiomyocytes toward a prosurvival phenotype via exosomal transfer: a critical role for HSF1/miR-34a/HSP70 pathway. *Stem Cells,* 32**,** 462-72.

FORSHEW, T., JOHNSON, C. A., KHALIQ, S., PASHA, S., WILLIS, C., ABBASI, R., TEE, L., SMITH, U., TREMBATH, R. C., MEHDI, S. Q., MOORE, A. T. & MAHER, E. R. 2005. Locus heterogeneity in autosomal recessive congenital cataracts: linkage to 9q and germline HSF4 mutations. *Hum Genet,* 117**,** 452-9.

FOURQUET, S., GUEROIS, R., BIARD, D. & TOLEDANO, M. B. 2010. Activation of NRF2 by nitrosative agents and H2O2 involves KEAP1 disulfide formation. *J Biol Chem,* 285**,** 8463-71.

FU, Q., WANG, J., BOERMA, M., BERBEE, M., QIU, X., FINK, L. M. & HAUER-JENSEN, M. 2008. Involvement of heat shock factor 1 in statin-induced transcriptional upregulation of endothelial thrombomodulin. *Circ Res,* 103**,** 369-77.

FUJIHARA, M., MUROI, M., TANAMOTO, K., SUZUKI, T., AZUMA, H. & IKEDA, H. 2003. Molecular mechanisms of macrophage activation and deactivation by lipopolysaccharide: roles of the receptor complex. *Pharmacol Ther,* 100**,** 171-94.

FUJIMOTO, M., HAYASHIDA, N., KATOH, T., OSHIMA, K., SHINKAWA, T., PRAKASAM, R., TAN, K., INOUYE, S., TAKII, R. & NAKAI, A. 2010. A novel mouse HSF3 has the potential to activate nonclassical heat-shock genes during heat shock. *Mol Biol Cell,* 21**,** 106-16.

FUJIMOTO, M., IZU, H., SEKI, K., FUKUDA, K., NISHIDA, T., YAMADA, S., KATO, K., YONEMURA, S., INOUYE, S. & NAKAI, A. 2004. HSF4 is required for normal cell growth and differentiation during mouse lens development. *EMBO J,* 23**,** 4297-306.

FUJIMOTO, M., OSHIMA, K., SHINKAWA, T., WANG, B. B., INOUYE, S., HAYASHIDA, N., TAKII, R. & NAKAI, A. 2008. Analysis of HSF4 binding regions reveals its necessity for gene regulation during development and heat shock response in mouse lenses. *J Biol Chem,* 283**,** 29961-70.

FUKAGAWA, N. K. 1999. Aging: is oxidative stress a marker or is it causal? *Proc Soc Exp Biol Med,* 222**,** 293-8.

FUKUTOMI, T., TAKAGI, K., MIZUSHIMA, T., OHUCHI, N. & YAMAMOTO, M. 2014. Kinetic, thermodynamic, and structural characterizations of the association between Nrf2-DLGex degron and Keap1. *Mol Cell Biol,* 34**,** 832-46.

GAN, N., WU, Y. C., BRUNET, M., GARRIDO, C., CHUNG, F. L., DAI, C. & MI, L. 2010. Sulforaphane activates heat shock response and enhances proteasome activity through up-regulation of Hsp27. *J Biol Chem,* 285**,** 35528-36.

GARRIDO, C., SCHMITT, E., CANDE, C., VAHSEN, N., PARCELLIER, A. & KROEMER, G. 2003. HSP27 and HSP70: potentially oncogenic apoptosis inhibitors. *Cell Cycle,* 2**,** 579-84.

GASCOIGNE, K. E. & TAYLOR, S. S. 2009. How do anti-mitotic drugs kill cancer cells? *J Cell Sci,* 122**,** 2579-85.

GEISLER, S., HOLMSTROM, K. M., TREIS, A., SKUJAT, D., WEBER, S. S., FIESEL, F. C., KAHLE, P. J. & SPRINGER, W. 2010. The PINK1/Parkin-mediated mitophagy is compromised by PD-associated mutations. *Autophagy,* 6**,** 871-8.

GEORGE, V. C., KUMAR, D. R., SURESH, P. K. & KUMAR, R. A. 2012. Apoptosis-induced cell death due to oleanolic acid in HaCaT keratinocyte cells--a proof-of-principle approach for chemopreventive drug development. *Asian Pac J Cancer Prev,* 13**,** 2015-20.

GIBBS, A., SCHWARTZMAN, J., DENG, V. & ALUMKAL, J. 2009. Sulforaphane destabilizes the androgen receptor in prostate cancer cells by inactivating histone deacetylase 6. *Proc Natl Acad Sci U S A,* 106**,** 16663-8.

GOEDERT, M., CUENDA, A., CRAXTON, M., JAKES, R. & COHEN, P. 1997. Activation of the novel stress-activated protein kinase SAPK4 by cytokines and cellular stresses is mediated by SKK3 (MKK6); comparison of its substrate specificity with that of other SAP kinases. *EMBO J,* 16**,** 3563-71.

GONZALEZ-TERAN, B., LOPEZ, J. A., RODRIGUEZ, E., LEIVA, L., MARTINEZ-MARTINEZ, S., BERNAL, J. A., JIMENEZ-BORREGUERO, L. J., REDONDO, J. M., VAZQUEZ, J. & SABIO, G. 2016a. p38gamma and delta promote heart hypertrophy by targeting the mTOR-inhibitory protein DEPTOR for degradation. *Nat Commun,* 7**,** 10477.

GONZALEZ-TERAN, B., MATESANZ, N., NIKOLIC, I., VERDUGO, M. A., SREERAMKUMAR, V., HERNANDEZ-COSIDO, L., MORA, A., CRAINICIUC, G., SAIZ, M. L., BERNARDO, E., LEIVA-VEGA, L., RODRIGUEZ, E., BONDIA, V., TORRES, J. L., PEREZ-SIEIRA, S., ORTEGA, L., CUENDA, A., SANCHEZ-MADRID, F., NOGUEIRAS, R., HIDALGO, A., MARCOS, M. & SABIO, G. 2016b. p38gamma and p38delta reprogram liver metabolism by modulating neutrophil infiltration. *EMBO J,* 35**,** 536-52.

GOODSON, M. L., HONG, Y., ROGERS, R., MATUNIS, M. J., PARK-SARGE, O. K. & SARGE, K. D. 2001. Sumo-1 modification regulates the DNA binding activity of heat shock transcription factor 2, a promyelocytic leukemia nuclear body associated transcription factor. *J Biol Chem,* 276**,** 18513-8.

GORMAN, A. M., SZEGEZDI, E., QUIGNEY, D. J. & SAMALI, A. 2005. Hsp27 inhibits 6-hydroxydopamine-induced cytochrome c release and apoptosis in PC12 cells. *Biochem Biophys Res Commun,* 327**,** 801-10.

GREEN, R. A., MAYERS, J. R., WANG, S., LEWELLYN, L., DESAI, A., AUDHYA, A. & OEGEMA, K. 2013. The midbody ring scaffolds the abscission machinery in the absence of midbody microtubules. *J Cell Biol,* 203**,** 505-20.

GREENBLATT, M. B., SHIM, J. H., ZOU, W., SITARA, D., SCHWEITZER, M., HU, D., LOTINUN, S., SANO, Y., BARON, R., PARK, J. M., ARTHUR, S., XIE, M., SCHNEIDER, M. D., ZHAI, B., GYGI, S., DAVIS, R. & GLIMCHER, L. H. 2010. The p38 MAPK pathway is essential for skeletogenesis and bone homeostasis in mice. *J Clin Invest,* 120**,** 2457-73.

GROVER, A., SHANDILYA, A., AGRAWAL, V., PRATIK, P., BHASME, D., BISARIA, V. S. & SUNDAR, D. 2011. Hsp90/Cdc37 chaperone/co-chaperone complex, a novel junction anticancer target elucidated by the mode of action of herbal drug Withaferin A. *BMC Bioinformatics,* 12 Suppl 1**,** S30.

GUETTOUCHE, T., BOELLMANN, F., LANE, W. S. & VOELLMY, R. 2005. Analysis of phosphorylation of human heat shock factor 1 in cells experiencing a stress. *BMC Biochem,* 6**,** 4.

GURGIS, F. M., ZIAZIARIS, W. & MUNOZ, L. 2014. Mitogen-activated protein kinase-activated protein kinase 2 in neuroinflammation, heat shock protein 27 phosphorylation, and cell cycle: role and targeting. *Mol Pharmacol,* 85**,** 345-56.

HAMILTON, K. L., MBAI, F. N., GUPTA, S. & KNOWLTON, A. A. 2004. Estrogen, heat shock proteins, and NFkappaB in human vascular endothelium. *Arterioscler Thromb Vasc Biol,* 24**,** 1628-33.

HAN, J., LEE, J. D., BIBBS, L. & ULEVITCH, R. J. 1994. A MAP kinase targeted by endotoxin and hyperosmolarity in mammalian cells. *Science,* 265**,** 808-11.

HAN, S., CHOI, J. R., SOON SHIN, K. & KANG, S. J. 2012. Resveratrol upregulated heat shock proteins and extended the survival of G93A-SOD1 mice. *Brain Res,* 1483**,** 112-7.

HANAHAN, D. & WEINBERG, R. A. 2011. Hallmarks of cancer: the next generation. *Cell,* 144**,** 646-74.

HARTEVELT, M. M., BAVINCK, J. N., KOOTTE, A. M., VERMEER, B. J. & VANDENBROUCKE, J. P. 1990. Incidence of skin cancer after renal transplantation in The Netherlands. *Transplantation,* 49**,** 506-9.

HASEGAWA, M., CUENDA, A., SPILLANTINI, M. G., THOMAS, G. M., BUEE-SCHERRER, V., COHEN, P. & GOEDERT, M. 1999. Stress-activated protein kinase-3 interacts with the PDZ domain of alpha1-syntrophin. A mechanism for specific substrate recognition. *J Biol Chem,* 274**,** 12626-31.

HASHIMOTO-TORII, K., TORII, M., FUJIMOTO, M., NAKAI, A., EL FATIMY, R., MEZGER, V., JU, M. J., ISHII, S., CHAO, S. H., BRENNAND, K. J., GAGE, F. H. & RAKIC, P. 2014. Roles of heat shock factor 1 in neuronal response to fetal environmental risks and its relevance to brain disorders. *Neuron,* 82**,** 560-72.

HATCHER, H., PLANALP, R., CHO, J., TORTI, F. M. & TORTI, S. V. 2008. Curcumin: from ancient medicine to current clinical trials. *Cell Mol Life Sci,* 65**,** 1631-52.

HAYES, J. D. & DINKOVA-KOSTOVA, A. T. 2014. The Nrf2 regulatory network provides an interface between redox and intermediary metabolism. *Trends Biochem Sci,* 39**,** 199-218.

HE, S., LIMI, S., MCGREAL, R. S., XIE, Q., BRENNAN, L. A., KANTOROW, W. L., KOKAVEC, J., MAJUMDAR, R., HOU, H., JR., EDELMANN, W., LIU, W., ASHERY-PADAN, R., ZAVADIL, J., KANTOROW, M., SKOULTCHI, A. I., STOPKA, T. & CVEKL, A. 2016. Chromatin remodeling enzyme Snf2h regulates embryonic lens differentiation and denucleation. *Development,* 143**,** 1937-47.

HECTOR, A., GRIESE, M. & HARTL, D. 2014. Oxidative stress in cystic fibrosis lung disease: an early event, but worth targeting? *Eur Respir J,* 44**,** 17-9.

HENSEN, S. M., HELDENS, L., VAN ENCKEVORT, C. M., VAN GENESEN, S. T., PRUIJN, G. J. & LUBSEN, N. H. 2013a. Activation of the antioxidant response in methionine deprived human cells results in an HSF1-independent increase in HSPA1A mRNA levels. *Biochimie,* 95**,** 1245-51.

HENSEN, S. M., HELDENS, L., VAN GENESEN, S. T., PRUIJN, G. J. & LUBSEN, N. H. 2013b. A delayed antioxidant response in heat-stressed cells expressing a non-DNA binding HSF1 mutant. *Cell Stress Chaperones,* 18**,** 455-73.

HETMAN, M., CAVANAUGH, J. E., KIMELMAN, D. & XIA, Z. 2000. Role of glycogen synthase kinase-3beta in neuronal apoptosis induced by trophic withdrawal. *J Neurosci,* 20**,** 2567-74.

HEYDARI, A. R., WU, B., TAKAHASHI, R., STRONG, R. & RICHARDSON, A. 1993. Expression of heat shock protein 70 is altered by age and diet at the level of transcription. *Mol Cell Biol,* 13**,** 2909-18.

HIERONYMUS, H., LAMB, J., ROSS, K. N., PENG, X. P., CLEMENT, C., RODINA, A., NIETO, M., DU, J., STEGMAIER, K., RAJ, S. M., MALONEY, K. N., CLARDY, J., HAHN, W. C., CHIOSIS, G. & GOLUB, T. R. 2006. Gene expression signature-based chemical genomic prediction identifies a novel class of HSP90 pathway modulators. *Cancer Cell,* 10**,** 321-30.

HIETAKANGAS, V., AHLSKOG, J. K., JAKOBSSON, A. M., HELLESUO, M., SAHLBERG, N. M., HOLMBERG, C. I., MIKHAILOV, A., PALVIMO, J. J., PIRKKALA, L. & SISTONEN, L. 2003. Phosphorylation of serine 303 is a prerequisite for the stress-inducible SUMO modification of heat shock factor 1. *Mol Cell Biol,* 23**,** 2953-68.

HIETAKANGAS, V., ANCKAR, J., BLOMSTER, H. A., FUJIMOTO, M., PALVIMO, J. J., NAKAI, A. & SISTONEN, L. 2006. PDSM, a motif for phosphorylation-dependent SUMO modification. *Proc Natl Acad Sci U S A,* 103**,** 45-50.

HILGARTH, R. S., HONG, Y., PARK-SARGE, O. K. & SARGE, K. D. 2003. Insights into the regulation of heat shock transcription factor 1 SUMO-1 modification. *Biochem Biophys Res Commun,* 303**,** 196-200.

HIROTSU, Y., KATSUOKA, F., FUNAYAMA, R., NAGASHIMA, T., NISHIDA, Y., NAKAYAMA, K., ENGEL, J. D. & YAMAMOTO, M. 2012. Nrf2-MafG heterodimers contribute globally to antioxidant and metabolic networks. *Nucleic Acids Res,* 40**,** 10228-39.

HOLMBERG, C. I., HIETAKANGAS, V., MIKHAILOV, A., RANTANEN, J. O., KALLIO, M., MEINANDER, A., HELLMAN, J., MORRICE, N., MACKINTOSH, C., MORIMOTO, R. I., ERIKSSON, J. E. & SISTONEN, L. 2001. Phosphorylation of serine 230 promotes inducible transcriptional activity of heat shock factor 1. *EMBO J,* 20**,** 3800-10.

HONDA, T., YOSHIZAWA, H., SUNDARARAJAN, C., DAVID, E., LAJOIE, M. J., FAVALORO, F. G., JR., JANOSIK, T., SU, X., HONDA, Y., ROEBUCK, B. D. & GRIBBLE, G. W. 2011. Tricyclic compounds containing nonenolizable cyano enones. A novel class of highly potent anti-inflammatory and cytoprotective agents. *J Med Chem,* 54**,** 1762-78.

HONG, Y., ROGERS, R., MATUNIS, M. J., MAYHEW, C. N., GOODSON, M. L., PARK-SARGE, O. K. & SARGE, K. D. 2001. Regulation of heat shock transcription factor 1 by stress-induced SUMO-1 modification. *J Biol Chem,* 276**,** 40263-7.

HONG, Y. H., UDDIN, M. H., JO, U., KIM, B., SONG, J., SUH, D. H., KIM, H. S. & SONG, Y. S. 2015. ROS Accumulation by PEITC Selectively Kills Ovarian Cancer Cells via UPR-Mediated Apoptosis. *Front Oncol,* 5**,** 167.

HOSHINO, T., MURAO, N., NAMBA, T., TAKEHARA, M., ADACHI, H., KATSUNO, M., SOBUE, G., MATSUSHIMA, T., SUZUKI, T. & MIZUSHIMA, T. 2011. Suppression of Alzheimer's disease-related phenotypes by expression of heat shock protein 70 in mice. *J Neurosci,* 31**,** 5225-34.

HOWITZ, K. T., BITTERMAN, K. J., COHEN, H. Y., LAMMING, D. W., LAVU, S., WOOD, J. G., ZIPKIN, R. E., CHUNG, P., KISIELEWSKI, A., ZHANG, L. L., SCHERER, B. & SINCLAIR, D. A. 2003. Small molecule activators of sirtuins extend Saccharomyces cerevisiae lifespan. *Nature,* 425**,** 191-6.

HSIEH, C. C., KURO-O, M., ROSENBLATT, K. P., BROBEY, R. & PAPACONSTANTINOU, J. 2010. The ASK1-Signalosome regulates p38 MAPK activity in response to levels of endogenous oxidative stress in the Klotho mouse models of aging. *Aging (Albany NY),* 2**,** 597-611.

HU, C. K., COUGHLIN, M. & MITCHISON, T. J. 2012. Midbody assembly and its regulation during cytokinesis. *Mol Biol Cell,* 23**,** 1024-34.

HU, L., MAGESH, S., CHEN, L., WANG, L., LEWIS, T. A., CHEN, Y., KHODIER, C., INOYAMA, D., BEAMER, L. J., EMGE, T. J., SHEN, J., KERRIGAN, J. E., KONG, A. N., DANDAPANI, S., PALMER, M., SCHREIBER, S. L. & MUNOZ, B. 2013. Discovery of a small-molecule inhibitor and cellular probe of Keap1-Nrf2 protein-protein interaction. *Bioorg Med Chem Lett,* 23**,** 3039-43.

HU, R., XU, C., SHEN, G., JAIN, M. R., KHOR, T. O., GOPALKRISHNAN, A., LIN, W., REDDY, B., CHAN, J. Y. & KONG, A. N. 2006a. Gene expression profiles induced by cancer chemopreventive isothiocyanate sulforaphane in the liver of C57BL/6J mice and C57BL/6J/Nrf2 (-/-) mice. *Cancer lett,* 243**,** 170-92.

HU, R., XU, C., SHEN, G., JAIN, M. R., KHOR, T. O., GOPALKRISHNAN, A., LIN, W., REDDY, B., CHAN, J. Y. & KONG, A. N. 2006b. Identification of Nrf2-regulated genes induced by chemopreventive isothiocyanate PEITC by oligonucleotide microarray. *Life sci,* 79**,** 1944-55.

HU, Y. & MIVECHI, N. F. 2011. Promotion of heat shock factor Hsf1 degradation via adaptor protein filamin A-interacting protein 1-like (FILIP-1L). *J Biol Chem,* 286**,** 31397-408.

HUBBARD, B. P. & SINCLAIR, D. A. 2014. Small molecule SIRT1 activators for the treatment of aging and age-related diseases. *Trends Pharmacol Sci,* 35**,** 146-54.

HUBBARD, J., ERLICHMAN, C., TOFT, D. O., QIN, R., STENSGARD, B. A., FELTEN, S., TEN EYCK, C., BATZEL, G., IVY, S. P. & HALUSKA, P. Phase I study of 17-allylamino-17 demethoxygeldanamycin, gemcitabine and/or cisplatin in patients with refractory solid tumors. *Invest New Drugs,* 29**,** 473-80.

HUTTER, M. M., SIEVERS, R. E., BARBOSA, V. & WOLFE, C. L. 1994. Heat-shock protein induction in rat hearts. A direct correlation between the amount of heat-shock protein induced and the degree of myocardial protection. *Circulation,* 89**,** 355-60.

ICHIJO, H., NISHIDA, E., IRIE, K., TEN DIJKE, P., SAITOH, M., MORIGUCHI, T., TAKAGI, M., MATSUMOTO, K., MIYAZONO, K. & GOTOH, Y. 1997. Induction of apoptosis by ASK1, a mammalian MAPKKK that activates SAPK/JNK and p38 signaling pathways. *Science,* 275**,** 90-4.

ICHIMURA, Y., WAGURI, S., SOU, Y. S., KAGEYAMA, S., HASEGAWA, J., ISHIMURA, R., SAITO, T., YANG, Y., KOUNO, T., FUKUTOMI, T., HOSHII, T., HIRAO, A., TAKAGI, K., MIZUSHIMA, T., MOTOHASHI, H., LEE, M. S., YOSHIMORI, T., TANAKA, K., YAMAMOTO, M. & KOMATSU, M. 2013. Phosphorylation of p62 activates the Keap1-Nrf2 pathway during selective autophagy. *Mol Cell,* 51**,** 618-31.

INOUYE, S., KATSUKI, K., IZU, H., FUJIMOTO, M., SUGAHARA, K., YAMADA, S., SHINKAI, Y., OKA, Y., KATOH, Y. & NAKAI, A. 2003. Activation of heat shock genes is not necessary for protection by heat shock transcription factor 1 against cell death due to a single exposure to high temperatures. *Mol Cell Biol,* 23**,** 5882-95.

ITOH, K., WAKABAYASHI, N., KATOH, Y., ISHII, T., IGARASHI, K., ENGEL, J. D. & YAMAMOTO, M. 1999. Keap1 represses nuclear activation of antioxidant responsive elements by Nrf2 through binding to the amino-terminal Neh2 domain. *Genes Dev,* 13**,** 76-86.

ITTNER, A., BLOCK, H., REICHEL, C. A., VARJOSALO, M., GEHART, H., SUMARA, G., GSTAIGER, M., KROMBACH, F., ZARBOCK, A. & RICCI, R. 2012. Regulation of PTEN activity by p38delta-PKD1 signaling in neutrophils confers inflammatory responses in the lung. *J Exp Med,* 209**,** 2229-46.

JACOBS, A. T. & MARNETT, L. J. 2007. Heat shock factor 1 attenuates 4-Hydroxynonenal-mediated apoptosis: critical role for heat shock protein 70 induction and stabilization of Bcl-XL. *J Biol Chem,* 282**,** 33412-20.

JACOBS, A. T. & MARNETT, L. J. 2010. Systems analysis of protein modification and cellular responses induced by electrophile stress. *Acc Chem Res,* 43**,** 673-83.

JACOBY, E., TRESADERN, G., BEMBENEK, S., WROBLOWSKI, B., BUYCK, C., NEEFS, J. M., RASSOKHIN, D., PONCELET, A., HUNT, J. & VAN VLIJMEN, H. 2015. Extending kinome coverage by analysis of kinase inhibitor broad profiling data. *Drug Discov Today,* 20**,** 652-8.

JAEGER, A. M., PEMBLE, C. W. T., SISTONEN, L. & THIELE, D. J. 2016. Structures of HSF2 reveal mechanisms for differential regulation of human heat-shock factors. *Nat Struct Mol Biol,* 23**,** 147-54.

JAIN, A., LAMARK, T., SJOTTEM, E., LARSEN, K. B., AWUH, J. A., OVERVATN, A., MCMAHON, M., HAYES, J. D. & JOHANSEN, T. 2010. p62/SQSTM1 is a target gene for transcription factor NRF2 and creates a positive feedback loop by inducing antioxidant response element-driven gene transcription. *J Biol Chem,* 285**,** 22576-91.

JANAKIRAM, N. B., INDRANIE, C., MALISETTY, S. V., JAGAN, P., STEELE, V. E. & RAO, C. V. 2008. Chemoprevention of colon carcinogenesis by oleanolic acid and its analog in male F344 rats and modulation of COX-2 and apoptosis in human colon HT-29 cancer cells. *Pharm Res,* 25**,** 2151-7.

JENSEN, P., MOLLER, B. & HANSEN, S. 2000. Skin cancer in kidney and heart transplant recipients and different long-term immunosuppressive therapy regimens. *J Am Acad Dermatol,* 42**,** 307.

JESUS, J. A., LAGO, J. H., LAURENTI, M. D., YAMAMOTO, E. S. & PASSERO, L. F. 2015. Antimicrobial activity of oleanolic and ursolic acids: an update. *Evid Based Complement Alternat Med,* 2015**,** 620472.

JHAVERI, K., TALDONE, T., MODI, S. & CHIOSIS, G. 2012. Advances in the clinical development of heat shock protein 90 (Hsp90) inhibitors in cancers. *Biochim Biophys Acta,* 1823**,** 742-55.

JIANG, Y. Q., WANG, X. L., CAO, X. H., YE, Z. Y., LI, L. & CAI, W. Q. 2013. Increased heat shock transcription factor 1 in the cerebellum reverses the deficiency of Purkinje cells in Alzheimer's disease. *Brain Res,* 1519**,** 105-11.

JIMENEZ-ARELLANES, A., LUNA-HERRERA, J., CORNEJO-GARRIDO, J., LOPEZ-GARCIA, S., CASTRO-MUSSOT, M. E., MECKES-FISCHER, M., MATA-ESPINOSA, D., MARQUINA, B., TORRES, J. & HERNANDEZ-PANDO, R. 2013. Ursolic and oleanolic acids as antimicrobial and immunomodulatory compounds for tuberculosis treatment. *BMC Complement Altern Med,* 13**,** 258.

JING, Y., LIU, W., CAO, H., ZHANG, D., YAO, X., ZHANG, S., XIA, H., LI, D., WANG, Y. C., YAN, J., HUI, L. & YING, H. 2015. Hepatic p38alpha regulates gluconeogenesis by suppressing AMPK. *J Hepatol,* 62**,** 1319-27.

JIYAD, Z., OLSEN, C. M., BURKE, M. T., ISBEL, N. M. & GREEN, A. C. 2016. Azathioprine and Risk of Skin Cancer in Organ Transplant Recipients: Systematic Review and Meta-analysis. *Am J Transplant*. (in press)

JOHNSON, S. A. & HUNTER, T. 2005. Kinomics: methods for deciphering the kinome. *Nat Methods,* 2**,** 17-25.

JOLLY, C. & MORIMOTO, R. I. 2000. Role of the heat shock response and molecular chaperones in oncogenesis and cell death. *J Natl Cancer Inst,* 92**,** 1564-72.

JOSEPH, J. A. & ROTH, G. S. 1992. Cholinergic systems in aging: the role of oxidative stress. *Clin Neuropharmacol,* 15 Suppl 1 Pt A**,** 508A-509A.

JUTOORU, I., GUTHRIE, A. S., CHADALAPAKA, G., PATHI, S., KIM, K., BURGHARDT, R., JIN, U. H. & SAFE, S. 2014. Mechanism of action of phenethylisothiocyanate and other reactive oxygen species-inducing anticancer agents. *Mol Cell Biol,* 34**,** 2382-95.

KALLIO, M., CHANG, Y., MANUEL, M., ALASTALO, T. P., RALLU, M., GITTON, Y., PIRKKALA, L., LOONES, M. T., PASLARU, L., LARNEY, S., HIARD, S., MORANGE, M., SISTONEN, L. & MEZGER, V. 2002. Brain abnormalities, defective meiotic chromosome synapsis and female subfertility in HSF2 null mice. *EMBO J,* 21**,** 2591-601.

KALRA, S., KNATKO, E. V., ZHANG, Y., HONDA, T., YAMAMOTO, M. & DINKOVA-KOSTOVA, A. T. 2012. Highly potent activation of Nrf2 by topical tricyclic bis(cyano enone): implications for protection against UV radiation during thiopurine therapy. *Cancer Prev Res (Phila),* 5**,** 973-81.

KANG, M. I., KOBAYASHI, A., WAKABAYASHI, N., KIM, S. G. & YAMAMOTO, M. 2004. Scaffolding of Keap1 to the actin cytoskeleton controls the function of Nrf2 as key regulator of cytoprotective phase 2 genes. *Proc Natl Acad Sci U S A,* 101**,** 2046-51.

KANITKAR, M. & BHONDE, R. R. 2008. Curcumin treatment enhances islet recovery by induction of heat shock response proteins, Hsp70 and heme oxygenase-1, during cryopreservation. *Life Sci,* 82**,** 182-9.

KANSANEN, E., JYRKKANEN, H. K., VOLGER, O. L., LEINONEN, H., KIVELA, A. M., HAKKINEN, S. K., WOODCOCK, S. R., SCHOPFER, F. J., HORREVOETS, A. J., YLA-HERTTUALA, S., FREEMAN, B. A. & LEVONEN, A. L. 2009. Nrf2-dependent and -independent responses to

nitro-fatty acids in human endothelial cells: identification of heat shock response as the major pathway activated by nitro-oleic acid. *J Biol Chem,* 284**,** 33233-41.
KARMAZYN, M., MAILER, K. & CURRIE, R. W. 1990. Acquisition and decay of heat-shock-enhanced postischemic ventricular recovery. *Am J Physiol,* 259**,** H424-31.
KARRAN, P. 2006. Thiopurines, DNA damage, DNA repair and therapy-related cancer. *Br Med Bull,* 79-80**,** 153-70.
KATO, K., ITO, H., KAMEI, K. & IWAMOTO, I. 1998. Stimulation of the stress-induced expression of stress proteins by curcumin in cultured cells and in rat tissues in vivo. *Cell Stress Chaperones,* 3**,** 152-60.
KAWAZOE, Y., TANABE, M., SASAI, N., NAGATA, K. & NAKAI, A. 1999. HSF3 is a major heat shock responsive factor duringchicken embryonic development. *Eur J Biochem,* 265**,** 688-97.
KAZEMI-ESFARJANI, P. & BENZER, S. 2000. Genetic suppression of polyglutamine toxicity in Drosophila. *Science,* 287**,** 1837-40.
KE, T., WANG, Q. K., JI, B., WANG, X., LIU, P., ZHANG, X., TANG, Z., REN, X. & LIU, M. 2006. Novel HSF4 mutation causes congenital total white cataract in a Chinese family. *Am J Ophthalmol,* 142**,** 298-303.
KENSLER, T. W., NG, D., CARMELLA, S. G., CHEN, M., JACOBSON, L. P., MUNOZ, A., EGNER, P. A., CHEN, J. G., QIAN, G. S., CHEN, T. Y., FAHEY, J. W., TALALAY, P., GROOPMAN, J. D., YUAN, J. M. & HECHT, S. S. 2012. Modulation of the metabolism of airborne pollutants by glucoraphanin-rich and sulforaphane-rich broccoli sprout beverages in Qidong, China. *Carcinogenesis,* 33**,** 101-7.
KENSLER, T. W., WAKABAYASHI, N. & BISWAL, S. 2007. Cell survival responses to environmental stresses via the Keap1-Nrf2-ARE pathway. *Annu Rev Pharmacol Toxicol,* 47**,** 89-116.
KEREN, A. & BENGAL, E. 2010. Studying MAP Kinase pathways during early development of Xenopus laevis. *Methods Mol Biol,* 661**,** 409-20.
KHAN, S. & HEIKKILA, J. J. 2011. Curcumin-induced inhibition of proteasomal activity, enhanced HSP accumulation and the acquisition of thermotolerance in Xenopus laevis A6 cells. *Comp Biochem Physiol A Mol Integr Physiol,* 158**,** 566-76.
KHOR, T. O., CHEUNG, W. K., PRAWAN, A., REDDY, B. S. & KONG, A. N. 2008. Chemoprevention of familial adenomatous polyposis in Apc(Min/+) mice by phenethyl isothiocyanate (PEITC). *Mol Carcinog,* 47**,** 321-5.
KIAEI, M., KIPIANI, K., PETRI, S., CHEN, J., CALINGASAN, N. Y. & BEAL, M. F. 2005. Celastrol blocks neuronal cell death and extends life in transgenic mouse model of amyotrophic lateral sclerosis. *Neurodegener Dis,* 2**,** 246-54.
KIM, E., WANG, B., SASTRY, N., MASLIAH, E., NELSON, P. T., CAI, H. & LIAO, F. F. 2016. NEDD4-mediated HSF1 degradation underlies alpha-synucleinopathy. *Hum Mol Genet,* 25**,** 211-22.
KIM, G., MERIIN, A. B., GABAI, V. L., CHRISTIANS, E., BENJAMIN, I., WILSON, A., WOLOZIN, B. & SHERMAN, M. Y. 2012a. The heat shock transcription factor Hsf1 is downregulated in DNA damage-associated senescence, contributing to the maintenance of senescence phenotype. *Aging Cell,* 11**,** 617-27.
KIM, K. A., LEE, J. S., PARK, H. J., KIM, J. W., KIM, C. J., SHIM, I. S., KIM, N. J., HAN, S. M. & LIM, S. 2004. Inhibition of cytochrome P450 activities by oleanolic acid and ursolic acid in human liver microsomes. *Life Sci,* 74**,** 2769-79.
KIM, K. H., JEONG, J. Y., SURH, Y. J. & KIM, K. W. 2010. Expression of stress-response ATF3 is mediated by Nrf2 in astrocytes. *Nucleic acids Res,* 38**,** 48-59.
KIM, S. & SHAH, K. 2007. Dissecting yeast Hog1 MAP kinase pathway using a chemical genetic approach. *FEBS Lett,* 581**,** 1209-16.
KIM, S. A., YOON, J. H. & AHN, S. G. 2012b. Heat shock factor 4a (HSF4a) represses HSF2 expression and HSF2-mediated transcriptional activity. *J Cell Physiol,* 227**,** 1-6.
KIM, S. A., YOON, J. H., LEE, S. H. & AHN, S. G. 2005. Polo-like kinase 1 phosphorylates heat shock transcription factor 1 and mediates its nuclear translocation during heat stress. *J Biol Chem,* 280**,** 12653-7.
KIM, S. H., HONG, J. H. & LEE, Y. C. 2014. Oleanolic acid suppresses ovalbumin-induced airway inflammation and Th2-mediated allergic asthma by modulating the transcription factors T-bet, GATA-3, RORgammat and Foxp3 in asthmatic mice. *Int Immunopharmacol,* 18**,** 311-24.
KLINE, M. P. & MORIMOTO, R. I. 1997. Repression of the heat shock factor 1 transcriptional activation domain is modulated by constitutive phosphorylation. *Mol Cell Biol,* 17**,** 2107-15.
KNATKO, E. V., IBBOTSON, S. H., ZHANG, Y., HIGGINS, M., FAHEY, J. W., TALALAY, P., DAWE, R. S., FERGUSON, J., HUANG, J. T., CLARKE, R., ZHENG, S., SAITO, A., KALRA, S., BENEDICT, A. L., HONDA, T., PROBY, C. M. & DINKOVA-KOSTOVA, A. T. 2015. Nrf2

Activation Protects against Solar-Simulated Ultraviolet Radiation in Mice and Humans. *Cancer Prev Res (Phila),* 8**,** 475-86.
KNOWLTON, A. A., KAPADIA, S., TORRE-AMIONE, G., DURAND, J. B., BIES, R., YOUNG, J. & MANN, D. L. 1998. Differential expression of heat shock proteins in normal and failing human hearts. *J Mol Cell Cardiol,* 30**,** 811-8.
KNOWLTON, A. A. & KORZICK, D. H. 2014. Estrogen and the female heart. *Mol Cell Endocrinol*, 389, 31-39
KNOWLTON, A. A. & SUN, L. 2001. Heat-shock factor-1, steroid hormones, and regulation of heat-shock protein expression in the heart. *Am J Physiol Heart Circ Physiol,* 280**,** H455-64.
KOBAYASHI, A., KANG, M. I., OKAWA, H., OHTSUJI, M., ZENKE, Y., CHIBA, T., IGARASHI, K. & YAMAMOTO, M. 2004. Oxidative stress sensor Keap1 functions as an adaptor for Cul3-based E3 ligase to regulate proteasomal degradation of Nrf2. *Mol Cell Biol,* 24**,** 7130-9.
KOMATSU, M., KUROKAWA, H., WAGURI, S., TAGUCHI, K., KOBAYASHI, A., ICHIMURA, Y., SOU, Y. S., UENO, I., SAKAMOTO, A., TONG, K. I., KIM, M., NISHITO, Y., IEMURA, S., NATSUME, T., UENO, T., KOMINAMI, E., MOTOHASHI, H., TANAKA, K. & YAMAMOTO, M. 2010. The selective autophagy substrate p62 activates the stress responsive transcription factor Nrf2 through inactivation of Keap1. *Nat Cell Biol,* 12**,** 213-23.
KOMATSU, M., KUROKAWA, H., WAGURI, S., TAGUCHI, K., KOBAYASHI, A., ICHIMURA, Y., SOU, Y. S., UENO, I., SAKAMOTO, A., TONG, K. I., KIM, M., NISHITO, Y., IEMURA, S., NATSUME, T., UENO, T., KOMINAMI, E., MOTOHASHI, H., TANAKA, K. & YAMAMOTO, M. 2010b. The selective autophagy substrate p62 activates the stress responsive transcription factor Nrf2 through inactivation of Keap1. *Nature cell biology,* 12**,** 213-23.
KOMATSU, M., WAGURI, S., UENO, T., IWATA, J., MURATA, S., TANIDA, I., EZAKI, J., MIZUSHIMA, N., OHSUMI, Y., UCHIYAMA, Y., KOMINAMI, E., TANAKA, K. & CHIBA, T. 2005. Impairment of starvation-induced and constitutive autophagy in Atg7-deficient mice. *J Cell Biol,* 169**,** 425-34.
KONDO, N., KATSUNO, M., ADACHI, H., MINAMIYAMA, M., DOI, H., MATSUMOTO, S., MIYAZAKI, Y., IIDA, M., TOHNAI, G., NAKATSUJI, H., ISHIGAKI, S., FUJIOKA, Y., WATANABE, H., TANAKA, F., NAKAI, A. & SOBUE, G. 2013. Heat shock factor-1 influences pathological lesion distribution of polyglutamine-induced neurodegeneration. *Nat Commun,* 4**,** 1405.
KOSTOV, R. V., KNATKO, E. V., MCLAUGHLIN, L. A., HENDERSON, C. J., ZHENG, S., HUANG, J. T., HONDA, T. & DINKOVA-KOSTOVA, A. T. 2015. Pharmacokinetics and pharmacodynamics of orally administered acetylenic tricyclic bis(cyanoenone), a highly potent Nrf2 activator with a reversible covalent mode of action. *Biochem Biophys Res Commun,* 465**,** 402-7.
KOURTIS, N., MOUBARAK, R. S., ARANDA-ORGILLES, B., LUI, K., AYDIN, I. T., TRIMARCHI, T., DARVISHIAN, F., SALVAGGIO, C., ZHONG, J., BHATT, K., CHEN, E. I., CELEBI, J. T., LAZARIS, C., TSIRIGOS, A., OSMAN, I., HERNANDO, E. & AIFANTIS, I. 2015. FBXW7 modulates cellular stress response and metastatic potential through HSF1 post-translational modification. *Nat Cell Biol,* 17**,** 322-32.
KUBO, M., LI, T. S., KURAZUMI, H., TAKEMOTO, Y., OHSHIMA, M., YAMAMOTO, Y., NISHIMOTO, A., MIKAMO, A., FUJIMOTO, M., NAKAI, A. & HAMANO, K. 2012. Heat shock factor 1 contributes to ischemia-induced angiogenesis by regulating the mobilization and recruitment of bone marrow stem/progenitor cells. *PLoS One,* 7**,** e37934.
KUMA, Y., SABIO, G., BAIN, J., SHPIRO, N., MARQUEZ, R. & CUENDA, A. 2005. BIRB796 inhibits all p38 MAPK isoforms in vitro and in vivo. *J Biol Chem,* 280**,** 19472-9.
KWAK, M. K., RAMOS-GOMEZ, M., WAKABAYASHI, N. & KENSLER, T. W. 2004. Chemoprevention by 1,2-dithiole-3-thiones through induction of NQO1 and other phase 2 enzymes. *Methods Enzymol,* 382**,** 414-23.
KWAK, Y. D., WANG, B., LI, J. J., WANG, R., DENG, Q., DIAO, S., CHEN, Y., XU, R., MASLIAH, E., XU, H., SUNG, J. J. & LIAO, F. F. 2012. Upregulation of the E3 ligase NEDD4-1 by oxidative stress degrades IGF-1 receptor protein in neurodegeneration. *J Neurosci,* 32**,** 10971-81.
LABBADIA, J., CUNLIFFE, H., WEISS, A., KATSYUBA, E., SATHASIVAM, K., SEREDENINA, T., WOODMAN, B., MOUSSAOUI, S., FRENTZEL, S., LUTHI-CARTER, R., PAGANETTI, P. & BATES, G. P. 2011. Altered chromatin architecture underlies progressive impairment of the heat shock response in mouse models of Huntington disease. *J Clin Invest,* 121**,** 3306-19.
LAO, C. D., RUFFIN, M. T. T., NORMOLLE, D., HEATH, D. D., MURRAY, S. I., BAILEY, J. M., BOGGS, M. E., CROWELL, J., ROCK, C. L. & BRENNER, D. E. 2006. Dose escalation of a curcuminoid formulation. *BMC Complement Altern Med,* 6**,** 10.
LARA-GONZALEZ, P., WESTHORPE, F. G. & TAYLOR, S. S. 2012. The spindle assembly checkpoint. *Curr Biol,* 22**,** R966-80.

LASSAR, A. B. 2009. The p38 MAPK family, a pushmi-pullyu of skeletal muscle differentiation. *J Cell Biol,* 187**,** 941-3.
LAU, A., WANG, X. J., ZHAO, F., VILLENEUVE, N. F., WU, T., JIANG, T., SUN, Z., WHITE, E. & ZHANG, D. D. 2010. A noncanonical mechanism of Nrf2 activation by autophagy deficiency: direct interaction between Keap1 and p62. *Mol Cell Biol,* 30**,** 3275-85.
LAWSON, S. K., DOBRIKOVA, E. Y., SHVEYGERT, M. & GROMEIER, M. 2013. p38alpha mitogen-activated protein kinase depletion and repression of signal transduction to translation machinery by miR-124 and -128 in neurons. *Mol Cell Biol,* 33**,** 127-35.
LE MASSON, F., RAZAK, Z., KAIGO, M., AUDOUARD, C., CHARRY, C., COOKE, H., WESTWOOD, J. T. & CHRISTIANS, E. S. 2011. Identification of heat shock factor 1 molecular and cellular targets during embryonic and adult female meiosis. *Mol Cell Biol,* 31**,** 3410-23.
LEE, J. C., LAYDON, J. T., MCDONNELL, P. C., GALLAGHER, T. F., KUMAR, S., GREEN, D., MCNULTY, D., BLUMENTHAL, M. J., HEYS, J. R., LANDVATTER, S. W. & ET AL. 1994. A protein kinase involved in the regulation of inflammatory cytokine biosynthesis. *Nature,* 372**,** 739-46.
LEE, J. C. & YOUNG, P. R. 1996. Role of CSB/p38/RK stress response kinase in LPS and cytokine signaling mechanisms. *J Leukoc Biol,* 59**,** 152-7.
LEE, J. M., CALKINS, M. J., CHAN, K., KAN, Y. W. & JOHNSON, J. A. 2003. Identification of the NF-E2-related factor-2-dependent genes conferring protection against oxidative stress in primary cortical astrocytes using oligonucleotide microarray analysis. *J Biol Chem,* 278**,** 12029-38.
LEE, M. J., NISHIO, H., AYAKI, H., YAMAMOTO, M. & SUMINO, K. 2002a. Upregulation of stress response mRNAs in COS-7 cells exposed to cadmium. *Toxicology,* 174**,** 109-17.
LEE, S. J., PARK, S. Y., NA, J. G. & KIM, Y. J. 2002b. Osmolarity hypersensitivity of hog1 deleted mutants is suppressed by mutation in KSS1 in budding yeast Saccharomyces cerevisiae. *FEMS Microbiol Lett,* 209**,** 9-14.
LEE, W. H., LOO, C. Y., BEBAWY, M., LUK, F., MASON, R. S. & ROHANIZADEH, R. 2013. Curcumin and its derivatives: their application in neuropharmacology and neuroscience in the 21st century. *Curr Neuropharmacol,* 11**,** 338-78.
LEE, Y. J., KIM, E. H., LEE, J. S., JEOUNG, D., BAE, S., KWON, S. H. & LEE, Y. S. 2008a. HSF1 as a mitotic regulator: phosphorylation of HSF1 by Plk1 is essential for mitotic progression. *Cancer Res,* 68**,** 7550-60.
LEE, Y. J., LEE, H. J., LEE, J. S., JEOUNG, D., KANG, C. M., BAE, S., LEE, S. J., KWON, S. H., KANG, D. & LEE, Y. S. 2008b. A novel function for HSF1-induced mitotic exit failure and genomic instability through direct interaction between HSF1 and Cdc20. *Oncogene,* 27**,** 2999-3009.
LESKO, E., GOZDZIK, J., KIJOWSKI, J., JENNER, B., WIECHA, O. & MAJKA, M. 2007. HSP90 antagonist, geldanamycin, inhibits proliferation, induces apoptosis and blocks migration of rhabdomyosarcoma cells in vitro and seeding into bone marrow in vivo. *Anticancer Drugs,* 18**,** 1173-81.
LEVONEN, A. L., LANDAR, A., RAMACHANDRAN, A., CEASER, E. K., DICKINSON, D. A., ZANONI, G., MORROW, J. D. & DARLEY-USMAR, V. M. 2004. Cellular mechanisms of redox cell signalling: role of cysteine modification in controlling antioxidant defences in response to electrophilic lipid oxidation products. *Biochem J,* 378**,** 373-82.
LI, S., MA, W., FEI, T., LOU, Q., ZHANG, Y., CUI, X., QIN, X., ZHANG, J., LIU, G., DONG, Z., MA, Y., SONG, Z. & HU, Y. 2014. Upregulation of heat shock factor 1 transcription activity is associated with hepatocellular carcinoma progression. *Mol Med Rep,* 10**,** 2313-21.
LI, X., ZHANG, D., HANNINK, M. & BEAMER, L. J. 2004. Crystal structure of the Kelch domain of human Keap1. *J Biol Chem,* 279**,** 54750-8.
LI, Y., ZHANG, T., SCHWARTZ, S. J. & SUN, D. 2011. Sulforaphane Potentiates the Efficacy of 17-Allylamino 17-Demethoxygeldanamycin Against Pancreatic Cancer Through Enhanced Abrogation of Hsp90 Chaperone Function. *Nutrition and cancer*.
LIBY, K., YORE, M. M., ROEBUCK, B. D., BAUMGARTNER, K. J., HONDA, T., SUNDARARAJAN, C., YOSHIZAWA, H., GRIBBLE, G. W., WILLIAMS, C. R., RISINGSONG, R., ROYCE, D. B., DINKOVA-KOSTOVA, A. T., STEPHENSON, K. K., EGNER, P. A., YATES, M. S., GROOPMAN, J. D., KENSLER, T. W. & SPORN, M. B. 2008. A novel acetylenic tricyclic bis-(cyano enone) potently induces phase 2 cytoprotective pathways and blocks liver carcinogenesis induced by aflatoxin. *Cancer Res,* 68**,** 6727-33.
LIN, C. H., TALLAKSEN-GREENE, S., CHIEN, W. M., CEARLEY, J. A., JACKSON, W. S., CROUSE, A. B., REN, S., LI, X. J., ALBIN, R. L. & DETLOFF, P. J. 2001. Neurological abnormalities in a knock-in mouse model of Huntington's disease. *Hum Mol Genet,* 10**,** 137-44.

LIN, P. Y., SIMON, S. M., KOH, W. K., FOLORUNSO, O., UMBAUGH, C. S. & PIERCE, A. 2013. Heat shock factor 1 over-expression protects against exposure of hydrophobic residues on mutant SOD1 and early mortality in a mouse model of amyotrophic lateral sclerosis. *Mol Neurodegener,* 8**,** 43.
LITTLEFIELD, O. & NELSON, H. C. 1999. A new use for the 'wing' of the 'winged' helix-turn-helix motif in the HSF-DNA cocrystal. *Nat Struct Biol,* 6**,** 464-70.
LIU, A. Y., LIN, Z., CHOI, H. S., SORHAGE, F. & LI, B. 1989. Attenuated induction of heat shock gene expression in aging diploid fibroblasts. *J Biol Chem,* 264**,** 12037-45.
LIU, A. Y., MATHUR, R., MEI, N., LANGHAMMER, C. G., BABIARZ, B. & FIRESTEIN, B. L. 2011. Neuroprotective drug riluzole amplifies the heat shock factor 1 (HSF1)- and glutamate transporter 1 (GLT1)-dependent cytoprotective mechanisms for neuronal survival. *J Biol Chem,* 286**,** 2785-94.
LIU, C., LI, Y., ZUO, G., XU, W., GAO, H., YANG, Y., YAMAHARA, J., WANG, J. & LI, Y. 2013. Oleanolic Acid diminishes liquid fructose-induced Fatty liver in rats: role of modulation of hepatic sterol regulatory element-binding protein-1c-mediated expression of genes responsible for de novo Fatty Acid synthesis. *Evid Based Complement Alternat Med,* 2013**,** 1045-52.
LIU, J. 1995. Pharmacology of oleanolic acid and ursolic acid. *J Ethnopharmacol,* 49**,** 57-68.
LIU, J., LIU, Y. & KLAASSEN, C. D. 1995. Protective effect of oleanolic acid against chemical-induced acute necrotic liver injury in mice. *Zhongguo Yao Li Xue Bao,* 16**,** 97-102.
LIU, P. C. & THIELE, D. J. 1999. Modulation of human heat shock factor trimerization by the linker domain. *J Biol Chem,* 274**,** 17219-25.
LIU, X., WARD, K., XAVIER, C., JANN, J., CLARK, A. F., PANG, I. H. & WU, H. 2015. The novel triterpenoid RTA 408 protects human retinal pigment epithelial cells against HO-induced cell injury via NF-E2-related factor 2 (Nrf2) activation. *Redox Biol,* 8**,** 98-109.
LO, S. C., LI, X., HENZL, M. T., BEAMER, L. J. & HANNINK, M. 2006. Structure of the Keap1:Nrf2 interface provides mechanistic insight into Nrf2 signaling. *EMBO J,* 25**,** 3605-17.
LOCKE, M. & TANGUAY, R. M. 1996. Diminished heat shock response in the aged myocardium. *Cell Stress Chaperones,* 1**,** 251-60.
LOCKE, M., TANGUAY, R. M., KLABUNDE, R. E. & IANUZZO, C. D. 1995. Enhanced postischemic myocardial recovery following exercise induction of HSP 72. *Am J Physiol,* 269**,** H320-5.
LU, H. & HALLSTROM, T. C. 2012. Sensitivity to TOP2 targeting chemotherapeutics is regulated by Oct1 and FILIP1L. *PLoS One,* 7**,** e42921.
LU, L., HACKETT, S. F., MINCEY, A., LAI, H. & CAMPOCHIARO, P. A. 2006. Effects of different types of oxidative stress in RPE cells. *J Cell Physiol,* 206**,** 119-25.
LU, M., KIM, H. E., LI, C. R., KIM, S., KWAK, I. J., LEE, Y. J., KIM, S. S., MOON, J. Y., KIM, C. H., KIM, D. K., KANG, H. S. & PARK, J. S. 2008. Two distinct disulfide bonds formed in human heat shock transcription factor 1 act in opposition to regulate its DNA binding activity. *Biochemistry,* 47**,** 6007-15.
LU, M., LEE, Y. J., PARK, S. M., KANG, H. S., KANG, S. W., KIM, S. & PARK, J. S. 2009. Aromatic-participant interactions are essential for disulfide-bond-based trimerization in human heat shock transcription factor 1. *Biochemistry,* 48**,** 3795-7.
LU, Y. F., LIU, J., WU, K. C. & KLAASSEN, C. D. 2014. Protection against phalloidin-induced liver injury by oleanolic acid involves Nrf2 activation and suppression of Oatp1b2. *Toxicol Lett,* 232**,** 326-332.
LU, Z. C. & WAN, F. H. 2008. Differential gene expression in whitefly (Bemisia tabaci) B-biotype females and males under heat-shock condition. *Comp Biochem Physiol Part D Genomics Proteomics,* 3**,** 257-62.
MABANDLA, M. V., NYOKA, M. & DANIELS, W. M. 2015. Early use of oleanolic acid provides protection against 6-hydroxydopamine induced dopamine neurodegeneration. *Brain Res,* 1622**,** 64-71.
MAHALINGAIAH, P. K., PONNUSAMY, L. & SINGH, K. P. 2015. Chronic oxidative stress causes estrogen-independent aggressive phenotype, and epigenetic inactivation of estrogen receptor alpha in MCF-7 breast cancer cells. *Breast Cancer Res Treat,* 153**,** 41-56.
MAINES, M. D. & EWING, J. F. 1996. Stress response of the rat testis: in situ hydridization and immunohistochemical analysis of heme oxygenase-1 (HSP32) induction by hyperthermia. *Biol Reprod,* 54**,** 1070-9.
MALHOTRA, D., PORTALES-CASAMAR, E., SINGH, A., SRIVASTAVA, S., ARENILLAS, D., HAPPEL, C., SHYR, C., WAKABAYASHI, N., KENSLER, T. W., WASSERMAN, W. W. & BISWAL, S. 2010. Global mapping of binding sites for Nrf2 identifies novel targets in cell survival response through ChIP-Seq profiling and network analysis. *Nucleic Acids Res,* 38**,** 5718-34.

MANGIARINI, L., SATHASIVAM, K., SELLER, M., COZENS, B., HARPER, A., HETHERINGTON, C., LAWTON, M., TROTTIER, Y., LEHRACH, H., DAVIES, S. W. & BATES, G. P. 1996. Exon 1 of the HD gene with an expanded CAG repeat is sufficient to cause a progressive neurological phenotype in transgenic mice. *Cell,* 87**,** 493-506.

MANNA, P. R. & STOCCO, D. M. 2011. The role of specific mitogen-activated protein kinase signaling cascades in the regulation of steroidogenesis. *J Signal Transduct,* 2011**,** 821615.

MARBER, M. S., MESTRIL, R., CHI, S. H., SAYEN, M. R., YELLON, D. M. & DILLMANN, W. H. 1995. Overexpression of the rat inducible 70-kD heat stress protein in a transgenic mouse increases the resistance of the heart to ischemic injury. *J Clin Invest,* 95**,** 1446-56.

MARCOTTE, D., ZENG, W., HUS, J. C., MCKENZIE, A., HESSION, C., JIN, P., BERGERON, C., LUGOVSKOY, A., ENYEDY, I., CUERVO, H., WANG, D., ATMANENE, C., ROECKLIN, D., VECCHI, M., VIVAT, V., KRAEMER, J., WINKLER, D., HONG, V., CHAO, J., LUKASHEV, M. & SILVIAN, L. 2013. Small molecules inhibit the interaction of Nrf2 and the Keap1 Kelch domain through a non-covalent mechanism. *Bioorg Med Chem,* 21**,** 4011-9.

MARTINEZ-RUIZ, A., VILLANUEVA, L., GONZALEZ DE ORDUNA, C., LOPEZ-FERRER, D., HIGUERAS, M. A., TARIN, C., RODRIGUEZ-CRESPO, I., VAZQUEZ, J. & LAMAS, S. 2005. S-nitrosylation of Hsp90 promotes the inhibition of its ATPase and endothelial nitric oxide synthase regulatory activities. *Proc Natl Acad Sci U S A,* 102**,** 8525-30.

MARUNOUCHI, T., ARAKI, M., MURATA, M., TAKAGI, N. & TANONAKA, K. 2013a. Possible involvement of HSP90-HSF1 multichaperone complex in impairment of HSP72 induction in the failing heart following myocardial infarction in rats. *J Pharmacol Sci,* 123**,** 336-46.

MARUNOUCHI, T., MURATA, M., TAKAGI, N. & TANONAKA, K. 2013b. Possible involvement of phosphorylated heat-shock factor-1 in changes in heat shock protein 72 induction in the failing rat heart following myocardial infarction. *Biol Pharm Bull,* 36**,** 1332-40.

MATTS, R. L., BRANDT, G. E., LU, Y., DIXIT, A., MOLLAPOUR, M., WANG, S., DONNELLY, A. C., NECKERS, L., VERKHIVKER, G. & BLAGG, B. S. 2011. A systematic protocol for the characterization of Hsp90 modulators. *Bioorg Med Chem,* 19**,** 684-92.

MCCANN, H., STEVENS, C. H., CARTWRIGHT, H. & HALLIDAY, G. M. 2014. alpha-Synucleinopathy phenotypes. *Parkinsonism Relat Disord,* 20 Suppl 1**,** S62-7.

MCMAHON, M., LAMONT, D. J., BEATTIE, K. A. & HAYES, J. D. 2010. Keap1 perceives stress via three sensors for the endogenous signaling molecules nitric oxide, zinc, and alkenals. *Proc Natl Acad Sci U S A,* 107**,** 18838-43.

MCMAHON, M., THOMAS, N., ITOH, K., YAMAMOTO, M. & HAYES, J. D. 2004. Redox-regulated turnover of Nrf2 is determined by at least two separate protein domains, the redox-sensitive Neh2 degron and the redox-insensitive Neh6 degron. *J Biol Chem,* 279**,** 31556-67.

MCMAHON, M., THOMAS, N., ITOH, K., YAMAMOTO, M. & HAYES, J. D. 2006. Dimerization of substrate adaptors can facilitate cullin-mediated ubiquitylation of proteins by a "tethering" mechanism: a two-site interaction model for the Nrf2-Keap1 complex. *J Biol Chem,* 281**,** 24756-68.

MEHLEN, P., HICKEY, E., WEBER, L. A. & ARRIGO, A. P. 1997. Large unphosphorylated aggregates as the active form of hsp27 which controls intracellular reactive oxygen species and glutathione levels and generates a protection against TNFalpha in NIH-3T3-ras cells. *Biochem Biophys Res Commun,* 241**,** 187-92.

MEHLEN, P., KRETZ-REMY, C., PREVILLE, X. & ARRIGO, A. P. 1996. Human hsp27, Drosophila hsp27 and human alphaB-crystallin expression-mediated increase in glutathione is essential for the protective activity of these proteins against TNFalpha-induced cell death. *EMBO J,* 15**,** 2695-706.

MEHLEN, P., PREVILLE, X., CHAREYRON, P., BRIOLAY, J., KLEMENZ, R. & ARRIGO, A. P. 1995. Constitutive expression of human hsp27, Drosophila hsp27, or human alpha B-crystallin confers resistance to TNF- and oxidative stress-induced cytotoxicity in stably transfected murine L929 fibroblasts. *J Immunol,* 154**,** 363-74.

MEHLMAN, M. A. 1992. Dangerous and cancer-causing properties of products and chemicals in the oil refining and petrochemical industry. VIII. Health effects of motor fuels: carcinogenicity of gasoline--scientific update. *Environ Res,* 59**,** 238-49.

MENDILLO, M. L., SANTAGATA, S., KOEVA, M., BELL, G. W., HU, R., TAMIMI, R. M., FRAENKEL, E., INCE, T. A., WHITESELL, L. & LINDQUIST, S. 2012. HSF1 Drives a Transcriptional Program Distinct from Heat Shock to Support Highly Malignant Human Cancers. *Cell,* 150**,** 549-62.

METCHAT, A., AKERFELT, M., BIERKAMP, C., DELSINNE, V., SISTONEN, L., ALEXANDRE, H. & CHRISTIANS, E. S. 2009. Mammalian heat shock factor 1 is essential for oocyte meiosis and directly regulates Hsp90alpha expression. *J Biol Chem,* 284**,** 9521-8.
METZLER, B., ABIA, R., AHMAD, M., WERNIG, F., PACHINGER, O., HU, Y. & XU, Q. 2003. Activation of heat shock transcription factor 1 in atherosclerosis. *Am J Pathol,* 162**,** 1669-76.
MITSUISHI, Y., TAGUCHI, K., KAWATANI, Y., SHIBATA, T., NUKIWA, T., ABURATANI, H., YAMAMOTO, M. & MOTOHASHI, H. 2012. Nrf2 redirects glucose and glutamine into anabolic pathways in metabolic reprogramming. *Cancer Cell,* 22**,** 66-79.
MIZUMURA, K., TAKEDA, K., HASHIMOTO, S., HORIE, T. & ICHIJO, H. 2006. Identification of Op18/stathmin as a potential target of ASK1-p38 MAP kinase cascade. *J Cell Physiol,* 206**,** 363-70.
MOON, Y. J., BRAZEAU, D. A. & MORRIS, M. E. 2011. Dietary phenethyl isothiocyanate alters gene expression in human breast cancer cells. *Evid Based Complement Alternat Med,* 2011.
MORIMOTO, R. I. 2011. The heat shock response: systems biology of proteotoxic stress in aging and disease. *Cold Spring Harb Symp Quant Biol,* 76**,** 91-9.
MORLEY, J. F. & MORIMOTO, R. I. 2004. Regulation of longevity in Caenorhabditis elegans by heat shock factor and molecular chaperones. *Mol Biol Cell,* 15**,** 657-64.
MOSSER, D. D., CARON, A. W., BOURGET, L., MERIIN, A. B., SHERMAN, M. Y., MORIMOTO, R. I. & MASSIE, B. 2000. The chaperone function of hsp70 is required for protection against stress-induced apoptosis. *Mol Cell Biol,* 20**,** 7146-59.
MUKUNDWA, A., LANGA, S. O., MUKARATIRWA, S. & MASOLA, B. 2016. In vivo effects of diabetes, insulin and oleanolic acid on enzymes of glycogen metabolism in the skin of streptozotocin-induced diabetic male Sprague-Dawley rats. *Biochem Biophys Res Commun,* 471**,** 315-9.
MUNTANE, J., PUIG-PARELLADA, P. & MITJAVILA, M. T. 1995. Iron metabolism and oxidative stress during acute and chronic phases of experimental inflammation: effect of iron-dextran and deferoxamine. *J Lab Clin Med,* 126**,** 435-43.
MURSHID, A., CHOU, S. D., PRINCE, T., ZHANG, Y., BHARTI, A. & CALDERWOOD, S. K. 2010. Protein kinase A binds and activates heat shock factor 1. *PLoS One,* 5**,** e13830.
MYZAK, M. C., DASHWOOD, W. M., ORNER, G. A., HO, E. & DASHWOOD, R. H. 2006a. Sulforaphane inhibits histone deacetylase in vivo and suppresses tumorigenesis in Apc-minus mice. *The FASEB J,* 20**,** 506-8.
MYZAK, M. C., HARDIN, K., WANG, R., DASHWOOD, R. H. & HO, E. 2006b. Sulforaphane inhibits histone deacetylase activity in BPH-1, LnCaP and PC-3 prostate epithelial cells. *Carcinogenesis,* 27**,** 811-9.
MYZAK, M. C., KARPLUS, P. A., CHUNG, F. L. & DASHWOOD, R. H. 2004. A novel mechanism of chemoprotection by sulforaphane: inhibition of histone deacetylase. *Cancer Res,* 64**,** 5767-74.
NACHAT, A., TUROFF-ORTMEYER, S., LIU, C. & MCCULLOCH, M. 2016. PEITC in End-Stage B-Cell Prolymphocytic Leukemia: Case Report of Possible Sensitization to Salvage R-CHOP. *Perm J,* 20**,** 74-80.
NAGAKURA, T., YASUDA, N., YAMAZAKI, K., IKUTA, H., YOSHIKAWA, S., ASANO, O. & TANAKA, I. 2001. Improved glucose tolerance via enhanced glucose-dependent insulin secretion in dipeptidyl peptidase IV-deficient Fischer rats. *Biochem Biophys Res Commun,* 284**,** 501-6.
NAKAI, A. & ISHIKAWA, T. 2000. A nuclear localization signal is essential for stress-induced dimer-to-trimer transition of heat shock transcription factor 3. *J Biol Chem,* 275**,** 34665-71.
NAKAI, A., KAWAZOE, Y., TANABE, M., NAGATA, K. & MORIMOTO, R. I. 1995. The DNA-binding properties of two heat shock factors, HSF1 and HSF3, are induced in the avian erythroblast cell line HD6. *Mol Cell Biol,* 15**,** 5268-78.
NAKAI, A., SUZUKI, M. & TANABE, M. 2000. Arrest of spermatogenesis in mice expressing an active heat shock transcription factor 1. *EMBO J,* 19**,** 1545-54.
NAKAI, A., TANABE, M., KAWAZOE, Y., INAZAWA, J., MORIMOTO, R. I. & NAGATA, K. 1997. HSF4, a new member of the human heat shock factor family which lacks properties of a transcriptional activator. *Mol Cell Biol,* 17**,** 469-81.
NARENDRA, D., TANAKA, A., SUEN, D. F. & YOULE, R. J. 2008. Parkin is recruited selectively to impaired mitochondria and promotes their autophagy. *J Cell Biol,* 183**,** 795-803.
NEEF, D. W., TURSKI, M. L. & THIELE, D. J. 2010. Modulation of heat shock transcription factor 1 as a therapeutic target for small molecule intervention in neurodegenerative disease. *PLoS Biol,* 8**,** e1000291.
NEWTON, E. M., KNAUF, U., GREEN, M. & KINGSTON, R. E. 1996. The regulatory domain of human heat shock factor 1 is sufficient to sense heat stress. *Mol Cell Biol,* 16**,** 839-46.

NIMMANAPALLI, R., O'BRYAN, E. & BHALLA, K. 2001. Geldanamycin and its analogue 17-allylamino-17-demethoxygeldanamycin lowers Bcr-Abl levels and induces apoptosis and differentiation of Bcr-Abl-positive human leukemic blasts. *Cancer Res,* 61**,** 1799-804.

NISHIZAWA, J., NAKAI, A., HIGASHI, T., TANABE, M., NOMOTO, S., MATSUDA, K., BAN, T. & NAGATA, K. 1996. Reperfusion causes significant activation of heat shock transcription factor 1 in ischemic rat heart. *Circulation,* 94**,** 2185-92.

NISHIZAWA, J., NAKAI, A., MATSUDA, K., KOMEDA, M., BAN, T. & NAGATA, K. 1999. Reactive oxygen species play an important role in the activation of heat shock factor 1 in ischemic-reperfused heart. *Circulation,* 99**,** 934-41.

NITTA, Y., ABE, K., AOKI, M., OHNO, I. & ISOYAMA, S. 1994. Diminished heat shock protein 70 mRNA induction in aged rat hearts after ischemia. *Am J Physiol,* 267**,** H1795-803.

NOGALES, E., WOLF, S. G. & DOWNING, K. H. 1998. Structure of the alpha beta tubulin dimer by electron crystallography. *Nature,* 391**,** 199-203.

OLSEN, J. V., BLAGOEV, B., GNAD, F., MACEK, B., KUMAR, C., MORTENSEN, P. & MANN, M. 2006. Global, in vivo, and site-specific phosphorylation dynamics in signaling networks. *Cell,* 127**,** 635-48.

OSTLING, P., BJORK, J. K., ROOS-MATTJUS, P., MEZGER, V. & SISTONEN, L. 2007. Heat shock factor 2 (HSF2) contributes to inducible expression of hsp genes through interplay with HSF1. *J Biol Chem,* 282**,** 7077-86.

PARIS, D., GANEY, N. J., LAPORTE, V., PATEL, N. S., BEAULIEU-ABDELAHAD, D., BACHMEIER, C., MARCH, A., AIT-GHEZALA, G. & MULLAN, M. J. 2010. Reduction of beta-amyloid pathology by celastrol in a transgenic mouse model of Alzheimer's disease. *J Neuroinflammation,* 7**,** 17.

PARKER, C. G., HUNT, J., DIENER, K., MCGINLEY, M., SORIANO, B., KEESLER, G. A., BRAY, J., YAO, Z., WANG, X. S., KOHNO, T. & LICHENSTEIN, H. S. 1998. Identification of stathmin as a novel substrate for p38 delta. *Biochem Biophys Res Commun,* 249**,** 791-6.

PATEL, S. B., CAMERON, P. M., O'KEEFE, S. J., FRANTZ-WATTLEY, B., THOMPSON, J., O'NEILL, E. A., TENNIS, T., LIU, L., BECKER, J. W. & SCAPIN, G. 2009. The three-dimensional structure of MAP kinase p38beta: different features of the ATP-binding site in p38beta compared with p38alpha. *Acta Crystallogr D Biol Crystallogr,* 65**,** 777-85.

PENG, W., ZHANG, Y., ZHENG, M., CHENG, H., ZHU, W., CAO, C. M. & XIAO, R. P. 2010. Cardioprotection by CaMKII-deltaB is mediated by phosphorylation of heat shock factor 1 and subsequent expression of inducible heat shock protein 70. *Circ Res,* 106**,** 102-10.

PENG, X., GUO, X., BORKAN, S. C., BHARTI, A., KURAMOCHI, Y., CALDERWOOD, S. & SAWYER, D. B. 2005. Heat shock protein 90 stabilization of ErbB2 expression is disrupted by ATP depletion in myocytes. *J Biol Chem,* 280**,** 13148-52.

PEREZ, F. P., BOSE, D., MALONEY, B., NHO, K., SHAH, K. & LAHIRI, D. K. 2014. Late-onset Alzheimer's disease, heating up and foxed by several proteins: pathomolecular effects of the aging process. *J Alzheimers Dis,* 40**,** 1-17.

PERISIC, O., XIAO, H. & LIS, J. T. 1989. Stable binding of Drosophila heat shock factor to head-to-head and tail-to-tail repeats of a conserved 5 bp recognition unit. *Cell,* 59**,** 797-806.

PERNG, M. D., CAIRNS, L., VAN DEN, I. P., PRESCOTT, A., HUTCHESON, A. M. & QUINLAN, R. A. 1999. Intermediate filament interactions can be altered by HSP27 and alphaB-crystallin. *J Cell Sci,* 112 (Pt 13)**,** 2099-112.

PETERANDERL, R. & NELSON, H. C. 1992. Trimerization of the heat shock transcription factor by a triple-stranded alpha-helical coiled-coil. *Biochemistry,* 31**,** 12272-6.

PICKRELL, A. M. & YOULE, R. J. 2015. The roles of PINK1, parkin, and mitochondrial fidelity in Parkinson's disease. *Neuron,* 85**,** 257-73.

PIERCE, A., PODLUTSKAYA, N., HALLORAN, J. J., HUSSONG, S. A., LIN, P. Y., BURBANK, R., HART, M. J. & GALVAN, V. 2013. Over-expression of heat shock factor 1 phenocopies the effect of chronic inhibition of TOR by rapamycin and is sufficient to ameliorate Alzheimer's-like deficits in mice modeling the disease. *J Neurochem,* 124**,** 880-93.

PIETSCH, E. C., CHAN, J. Y., TORTI, F. M. & TORTI, S. V. 2003. Nrf2 mediates the induction of ferritin H in response to xenobiotics and cancer chemopreventive dithiolethiones. *J Biol Chem,* 278**,** 2361-9.

PLEDGIE-TRACY, A., SOBOLEWSKI, M. D. & DAVIDSON, N. E. 2007. Sulforaphane induces cell type-specific apoptosis in human breast cancer cell lines. *Mol Cancer Ther,* 6**,** 1013-21.

POSAS, F., WURGLER-MURPHY, S. M., MAEDA, T., WITTEN, E. A., THAI, T. C. & SAITO, H. 1996. Yeast HOG1 MAP kinase cascade is regulated by a multistep phosphorelay mechanism in the SLN1-YPD1-SSK1 "two-component" osmosensor. *Cell,* 86**,** 865-75.

PRAKASAM, R., FUJIMOTO, M., TAKII, R., HAYASHIDA, N., TAKAKI, E., TAN, K., WU, F., INOUYE, S. & NAKAI, A. 2013. Chicken IL-6 is a heat-shock gene. *FEBS Lett,* 587**,** 3541-7.

PRAPROTNIK, D., SMITH, M. A., RICHEY, P. L., VINTERS, H. V. & PERRY, G. 1996. Plasma membrane fragility in dystrophic neurites in senile plaques of Alzheimer's disease: an index of oxidative stress. *Acta Neuropathol,* 91**,** 1-5.

PRESTERA, T., TALALAY, P., ALAM, J., AHN, Y. I., LEE, P. J. & CHOI, A. M. 1995. Parallel induction of heme oxygenase-1 and chemoprotective phase 2 enzymes by electrophiles and antioxidants: regulation by upstream antioxidant-responsive elements (ARE). *Mol Med,* 1**,** 827-37.

RABINDRAN, S. K., HAROUN, R. I., CLOS, J., WISNIEWSKI, J. & WU, C. 1993. Regulation of heat shock factor trimer formation: role of a conserved leucine zipper. *Science,* 259**,** 230-4.

RACHAKONDA, G., XIONG, Y., SEKHAR, K. R., STAMER, S. L., LIEBLER, D. C. & FREEMAN, M. L. 2008. Covalent modification at Cys151 dissociates the electrophile sensor Keap1 from the ubiquitin ligase CUL3. *Chem Res Toxicol,* 21**,** 705-10.

RAJASEKARAN, N. S., CONNELL, P., CHRISTIANS, E. S., YAN, L. J., TAYLOR, R. P., OROSZ, A., ZHANG, X. Q., STEVENSON, T. J., PESHOCK, R. M., LEOPOLD, J. A., BARRY, W. H., LOSCALZO, J., ODELBERG, S. J. & BENJAMIN, I. J. 2007. Human alpha B-crystallin mutation causes oxido-reductive stress and protein aggregation cardiomyopathy in mice. *Cell,* 130**,** 427-39.

RAJASEKARAN, N. S., FIRPO, M. A., MILASH, B. A., WEISS, R. B. & BENJAMIN, I. J. 2008. Global expression profiling identifies a novel biosignature for protein aggregation R120GCryAB cardiomyopathy in mice. *Physiol Genomics,* 35**,** 165-72.

RAJASEKARAN, N. S., VARADHARAJ, S., KHANDERAO, G. D., DAVIDSON, C. J., KANNAN, S., FIRPO, M. A., ZWEIER, J. L. & BENJAMIN, I. J. 2011. Sustained activation of nuclear erythroid 2-related factor 2/antioxidant response element signaling promotes reductive stress in the human mutant protein aggregation cardiomyopathy in mice. *Antioxid Redox Signal,* 14**,** 957-71.

RAYCHAUDHURI, S., LOEW, C., KORNER, R., PINKERT, S., THEIS, M., HAYER-HARTL, M., BUCHHOLZ, F. & HARTL, F. U. 2014. Interplay of acetyltransferase EP300 and the proteasome system in regulating heat shock transcription factor 1. *Cell,* 156**,** 975-85.

REISMAN, S. A., ALEKSUNES, L. M. & KLAASSEN, C. D. 2009. Oleanolic acid activates Nrf2 and protects from acetaminophen hepatotoxicity via Nrf2-dependent and Nrf2-independent processes. *Biochem Pharmacol,* 77**,** 1273-82.

REISMAN, S. A., GOLDSBERRY, A. R., LEE, C. Y., O'GRADY, M. L., PROKSCH, J. W., WARD, K. W. & MEYER, C. J. 2015. Topical application of RTA 408 lotion activates Nrf2 in human skin and is well-tolerated by healthy human volunteers. *BMC Dermatol,* 15**,** 10.

REISMAN, S. A., LEE, C. Y., MEYER, C. J., PROKSCH, J. W., SONIS, S. T. & WARD, K. W. 2014. Topical application of the synthetic triterpenoid RTA 408 protects mice from radiation-induced dermatitis. *Radiat Res,* 181**,** 512-20.

REMY, G., RISCO, A. M., INESTA-VAQUERA, F. A., GONZALEZ-TERAN, B., SABIO, G., DAVIS, R. J. & CUENDA, A. 2010. Differential activation of p38MAPK isoforms by MKK6 and MKK3. *Cell Signal,* 22**,** 660-7.

RETZLAFF, M., STAHL, M., EBERL, H. C., LAGLEDER, S., BECK, J., KESSLER, H. & BUCHNER, J. 2009. Hsp90 is regulated by a switch point in the C-terminal domain. *EMBO Rep,* 10**,** 1147-53.

REYNOLDS, C. H., NEBREDA, A. R., GIBB, G. M., UTTON, M. A. & ANDERTON, B. H. 1997. Reactivating kinase/p38 phosphorylates tau protein in vitro. *J Neurochem,* 69**,** 191-8.

RICHTER, K., HASLBECK, M. & BUCHNER, J. 2010. The heat shock response: life on the verge of death. *Mol Cell,* 40**,** 253-66.

RITOSSA, F. 1996. Discovery of the heat shock response. *Cell Stress Chaperones,* 1**,** 97-8.

RITOSSA, F. M. 1964. Experimental Activation of Specific Loci in Polytene Chromosomes of Drosophila. *Exp Cell Res,* 35**,** 601-7.

RITOSSA, F. M. & VONBORSTEL, R. C. 1964. Chromosome Puffs in Drosophila Induced by Ribonuclease. *Science,* 145**,** 513-4.

RODRIGUEZ-CARBALLO, E., GAMEZ, B. & VENTURA, F. 2016. p38 MAPK Signaling in Osteoblast Differentiation. *Front Cell Dev Biol,* 4**,** 40.

ROSSI, A., CIAFRE, S., BALSAMO, M., PIERIMARCHI, P. & SANTORO, M. G. 2006. Targeting the heat shock factor 1 by RNA interference: a potent tool to enhance hyperthermochemotherapy efficacy in cervical cancer. *Cancer Res,* 66**,** 7678-85.

ROSSI, A., ELIA, G. & SANTORO, M. G. 1996. 2-Cyclopenten-1-one, a new inducer of heat shock protein 70 with antiviral activity. *J Biol Chem,* 271**,** 32192-6.

ROY, S. M., GRUM-TOKARS, V. L., SCHAVOCKY, J. P., SAEED, F., STANISZEWSKI, A., TEICH, A. F., ARANCIO, O., BACHSTETTER, A. D., WEBSTER, S. J., VAN ELDIK, L. J., MINASOV, G., ANDERSON, W. F., PELLETIER, J. C. & WATTERSON, D. M. 2015. Targeting human central nervous system protein kinases: An isoform selective p38alphaMAPK inhibitor that attenuates disease progression in Alzheimer's disease mouse models. *ACS Chem Neurosci,* 6**,** 666-80.

SAHA, A. & DESHAIES, R. J. 2008. Multimodal activation of the ubiquitin ligase SCF by Nedd8 conjugation. *Mol Cell,* 32**,** 21-31.

SAITO, R., SUZUKI, T., HIRAMOTO, K., ASAMI, S., NAGANUMA, E., SUDA, H., ISO, T., YAMAMOTO, H., MORITA, M., BAIRD, L., FURUSAWA, Y., NEGISHI, T., ICHINOSE, M. & YAMAMOTO, M. 2015. Characterizations of Three Major Cysteine Sensors of Keap1 in Stress Response. *Mol Cell Biol,* 36**,** 271-84.

SAITO, T., ICHIMURA, Y., TAGUCHI, K., SUZUKI, T., MIZUSHIMA, T., TAKAGI, K., HIROSE, Y., NAGAHASHI, M., ISO, T., FUKUTOMI, T., OHISHI, M., ENDO, K., UEMURA, T., NISHITO, Y., OKUDA, S., OBATA, M., KOUNO, T., IMAMURA, R., TADA, Y., OBATA, R., YASUDA, D., TAKAHASHI, K., FUJIMURA, T., PI, J., LEE, M. S., UENO, T., OHE, T., MASHINO, T., WAKAI, T., KOJIMA, H., OKABE, T., NAGANO, T., MOTOHASHI, H., WAGURI, S., SOGA, T., YAMAMOTO, M., TANAKA, K. & KOMATSU, M. 2016. p62/Sqstm1 promotes malignancy of HCV-positive hepatocellular carcinoma through Nrf2-dependent metabolic reprogramming. *Nat Commun,* 7**,** 12030.

SAITOH, M., NISHITOH, H., FUJII, M., TAKEDA, K., TOBIUME, K., SAWADA, Y., KAWABATA, M., MIYAZONO, K. & ICHIJO, H. 1998. Mammalian thioredoxin is a direct inhibitor of apoptosis signal-regulating kinase (ASK) 1. *EMBO J,* 17**,** 2596-606.

SANDQVIST, A., BJORK, J. K., AKERFELT, M., CHITIKOVA, Z., GRICHINE, A., VOURC'H, C., JOLLY, C., SALMINEN, T. A., NYMALM, Y. & SISTONEN, L. 2009. Heterotrimerization of heat-shock factors 1 and 2 provides a transcriptional switch in response to distinct stimuli. *Mol Biol Cell,* 20**,** 1340-7.

SANGLE, G. V., ZHAO, R., MIZUNO, T. M. & SHEN, G. X. 2010. Involvement of RAGE, NADPH oxidase, and Ras/Raf-1 pathway in glycated LDL-induced expression of heat shock factor-1 and plasminogen activator inhibitor-1 in vascular endothelial cells. *Endocrinology,* 151**,** 4455-66.

SANTAGATA, S., HU, R., LIN, N. U., MENDILLO, M. L., COLLINS, L. C., HANKINSON, S. E., SCHNITT, S. J., WHITESELL, L., TAMIMI, R. M., LINDQUIST, S. & INCE, T. A. 2011. High levels of nuclear heat-shock factor 1 (HSF1) are associated with poor prognosis in breast cancer. *Proc Natl Acad Sci U S A,* 108**,** 18378-83.

SANTAGATA, S., MENDILLO, M. L., TANG, Y. C., SUBRAMANIAN, A., PERLEY, C. C., ROCHE, S. P., WONG, B., NARAYAN, R., KWON, H., KOEVA, M., AMON, A., GOLUB, T. R., PORCO, J. A., JR., WHITESELL, L. & LINDQUIST, S. 2013. Tight coordination of protein translation and HSF1 activation supports the anabolic malignant state. *Science,* 341**,** 1238303.

SANTAGATA, S., XU, Y. M., WIJERATNE, E. M., KONTNIK, R., ROONEY, C., PERLEY, C. C., KWON, H., CLARDY, J., KESARI, S., WHITESELL, L., LINDQUIST, S. & GUNATILAKA, A. A. 2012. Using the heat-shock response to discover anticancer compounds that target protein homeostasis. *ACS Chem Biol,* 7**,** 340-9.

SARGE, K. D., MURPHY, S. P. & MORIMOTO, R. I. 1993. Activation of heat shock gene transcription by heat shock factor 1 involves oligomerization, acquisition of DNA-binding activity, and nuclear localization and can occur in the absence of stress. *Mol Cell Biol,* 13**,** 1392-407.

SARIKAS, A., HARTMANN, T. & PAN, Z. Q. 2011. The cullin protein family. *Genome Biol,* 12**,** 220.

SARKAR, C., PAL, S., DAS, N. & DINDA, B. 2014. Ameliorative effects of oleanolic acid on fluoride induced metabolic and oxidative dysfunctions in rat brain: Experimental and biochemical studies. *Food Chem Toxicol,* 66**,** 224-36.

SASAKI, H., SATO, H., KURIYAMA-MATSUMURA, K., SATO, K., MAEBARA, K., WANG, H., TAMBA, M., ITOH, K., YAMAMOTO, M. & BANNAI, S. 2002. Electrophile response element-mediated induction of the cystine/glutamate exchange transporter gene expression. *J Biol Chem,* 277**,** 44765-71.

SATO, H., AMAGAI, K., SHIMIZUKAWA, R. & TAMAI, Y. 2009. Stable generation of serum- and feeder-free embryonic stem cell-derived mice with full germline-competency by using a GSK3 specific inhibitor. *Genesis,* 47**,** 414-22.

SATOH, T., REZAIE, T., SEKI, M., SUNICO, C. R., TABUCHI, T., KITAGAWA, T., YANAGITAI, M., SENZAKI, M., KOSEGAWA, C., TAIRA, H., MCKERCHER, S. R., HOFFMAN, J. K., ROTH, G. P. & LIPTON, S. A. 2011. Dual neuroprotective pathways of a pro-electrophilic compound via

HSF-1-activated heat-shock proteins and Nrf2-activated phase 2 antioxidant response enzymes. *J Neurochem*.

SAYDAM, N., STEINER, F., GEORGIEV, O. & SCHAFFNER, W. 2003. Heat and heavy metal stress synergize to mediate transcriptional hyperactivation by metal-responsive transcription factor MTF-1. *J Biol Chem,* 278**,** 31879-83.

SCHEPERS, H., GEUGIEN, M., VAN DER TOORN, M., BRYANTSEV, A. L., KAMPINGA, H. H., EGGEN, B. J. & VELLENGA, E. 2005. HSP27 protects AML cells against VP-16-induced apoptosis through modulation of p38 and c-Jun. *Exp Hematol,* 33**,** 660-70.

SCHINDLER, E. M., HINDES, A., GRIBBEN, E. L., BURNS, C. J., YIN, Y., LIN, M. H., OWEN, R. J., LONGMORE, G. D., KISSLING, G. E., ARTHUR, J. S. & EFIMOVA, T. 2009. p38delta Mitogen-activated protein kinase is essential for skin tumor development in mice. *Cancer Res,* 69**,** 4648-55.

SCHUETZ, T. J., GALLO, G. J., SHELDON, L., TEMPST, P. & KINGSTON, R. E. 1991. Isolation of a cDNA for HSF2: evidence for two heat shock factor genes in humans. *Proc Natl Acad Sci U S A,* 88**,** 6911-5.

SCHULTE, T. W., BLAGOSKLONNY, M. V., INGUI, C. & NECKERS, L. 1995. Disruption of the Raf-1-Hsp90 molecular complex results in destabilization of Raf-1 and loss of Raf-1-Ras association. *J Biol Chem,* 270**,** 24585-8.

SEO, H. R., CHUNG, D. Y., LEE, Y. J., LEE, D. H., KIM, J. I., BAE, S., CHUNG, H. Y., LEE, S. J., JEOUNG, D. & LEE, Y. S. 2006. Heat shock protein 25 or inducible heat shock protein 70 activates heat shock factor 1: dephosphorylation on serine 307 through inhibition of ERK1/2 phosphorylation. *J Biol Chem,* 281**,** 17220-7.

SEO, M., LEE, Y. I., CHO, C. H., BAE, C. D., KIM, I. H. & JUHNN, Y. S. 2002. Bi-directional regulation of UV-induced activation of p38 kinase and c-Jun N-terminal kinase by G protein beta gamma-subunits. *J Biol Chem,* 277**,** 24197-203.

SEO, M. S., OH, S. Y., PARK, M. J., KIM, S. M., KIM, M. Y., HAN, S. I., PARK, H. G. & KANG, H. S. 2005. Implication of reactive oxygen species, ERK1/2, and p38MAPK in sodium salicylate-induced heat shock protein 72 expression in C6 glioma cells. *Int J Mol Med,* 16**,** 841-9.

SHARMA, R., SHARMA, A., CHAUDHARY, P., PEARCE, V., VATSYAYAN, R., SINGH, S. V., AWASTHI, S. & AWASTHI, Y. C. 2010. Role of lipid peroxidation in cellular responses to D,L-sulforaphane, a promising cancer chemopreventive agent. *Biochemistry,* 49**,** 3191-202.

SHARROCKS, A. D., YANG, S. H. & GALANIS, A. 2000. Docking domains and substrate-specificity determination for MAP kinases. *Trends Biochem Sci,* 25**,** 448-53.

SHEN, S. Q., ZHANG, Y., XIANG, J. J. & XIONG, C. L. 2007. Protective effect of curcumin against liver warm ischemia/reperfusion injury in rat model is associated with regulation of heat shock protein and antioxidant enzymes. *World J Gastroenterol,* 13**,** 1953-61.

SHI, Y., MOSSER, D. D. & MORIMOTO, R. I. 1998. Molecular chaperones as HSF1-specific transcriptional repressors. *Genes Dev,* 12**,** 654-66.

SHINKAWA, T., TAN, K., FUJIMOTO, M., HAYASHIDA, N., YAMAMOTO, K., TAKAKI, E., TAKII, R., PRAKASAM, R., INOUYE, S., MEZGER, V. & NAKAI, A. 2011. Heat shock factor 2 is required for maintaining proteostasis against febrile-range thermal stress and polyglutamine aggregation. *Mol Biol Cell,* 22**,** 3571-83.

SIES, H. 2015. Oxidative stress: a concept in redox biology and medicine. *Redox Biol,* 4**,** 180-3.

SINGH, A., HAPPEL, C., MANNA, S. K., ACQUAAH-MENSAH, G., CARRERERO, J., KUMAR, S., NASIPURI, P., KRAUSZ, K. W., WAKABAYASHI, N., DEWI, R., BOROS, L. G., GONZALEZ, F. J., GABRIELSON, E., WONG, K. K., GIRNUN, G. & BISWAL, S. 2013. Transcription factor NRF2 regulates miR-1 and miR-206 to drive tumorigenesis. *J Clin Invest,* 123**,** 2921-34.

SINGH, G. B., SINGH, S., BANI, S., GUPTA, B. D. & BANERJEE, S. K. 1992. Anti-inflammatory activity of oleanolic acid in rats and mice. *J Pharm Pharmacol,* 44**,** 456-8.

SMAOUI, N., BELTAIEF, O., BENHAMED, S., M'RAD, R., MAAZOUL, F., OUERTANI, A., CHAABOUNI, H. & HEJTMANCIK, J. F. 2004. A homozygous splice mutation in the HSF4 gene is associated with an autosomal recessive congenital cataract. *Invest Ophthalmol Vis Sci,* 45**,** 2716-21.

SMATHERS, R. L., GALLIGAN, J. J., STEWART, B. J. & PETERSEN, D. R. 2011. Overview of lipid peroxidation products and hepatic protein modification in alcoholic liver disease. Chem. Biol. Interact*,* 192**,** 107-12.

SNYDER, G. H., CENNERAZZO, M. J., KARALIS, A. J. & FIELD, D. 1981. Electrostatic influence of local cysteine environments on disulfide exchange kinetics. *Biochemistry,* 20**,** 6509-19.

SOGA, M., MATSUZAWA, A. & ICHIJO, H. 2012. Oxidative Stress-Induced Diseases via the ASK1 Signaling Pathway. *Int J Cell Biol,* 2012**,** 439587.

SONCIN, F., ZHANG, X., CHU, B., WANG, X., ASEA, A., ANN STEVENSON, M., SACKS, D. B. & CALDERWOOD, S. K. 2003. Transcriptional activity and DNA binding of heat shock factor-1 involve phosphorylation on threonine 142 by CK2. *Biochem Biophys Res Commun,* 303**,** 700-6.

SORGER, P. K. & NELSON, H. C. 1989. Trimerization of a yeast transcriptional activator via a coiled-coil motif. *Cell,* 59**,** 807-13.

STRONACH, B. E. & PERRIMON, N. 1999. Stress signaling in Drosophila. *Oncogene,* 18**,** 6172-82.

STUHLMEIER, K. M. 2000. Activation and regulation of Hsp32 and Hsp70. *Eur J Biochem,* 267**,** 1161-7.

SULLIVAN, E. K., WEIRICH, C. S., GUYON, J. R., SIF, S. & KINGSTON, R. E. 2001. Transcriptional activation domains of human heat shock factor 1 recruit human SWI/SNF. *Mol Cell Biol,* 21**,** 5826-37.

SUMARA, G., FORMENTINI, I., COLLINS, S., SUMARA, I., WINDAK, R., BODENMILLER, B., RAMRACHEYA, R., CAILLE, D., JIANG, H., PLATT, K. A., MEDA, P., AEBERSOLD, R., RORSMAN, P. & RICCI, R. 2009. Regulation of PKD by the MAPK p38delta in insulin secretion and glucose homeostasis. *Cell,* 136**,** 235-48.

SURH, Y. J. & CHUN, K. S. 2007. Cancer chemopreventive effects of curcumin. *Adv Exp Med Biol,* 595**,** 149-72.

SUTHERLAND, C. 2011. What Are the bona fide GSK3 Substrates? *Int J Alzheimers Dis,* 2011**,** 505607.

SUZUKI, K., BOSE, P., LEONG-QUONG, R. Y., FUJITA, D. J. & RIABOWOL, K. 2010. REAP: A two minute cell fractionation method. *BMC Res Notes,* 3**,** 294.

SUZUKI, K., MURTUZA, B., SAMMUT, I. A., LATIF, N., JAYAKUMAR, J., SMOLENSKI, R. T., KANEDA, Y., SAWA, Y., MATSUDA, H. & YACOUB, M. H. 2002. Heat shock protein 72 enhances manganese superoxide dismutase activity during myocardial ischemia-reperfusion injury, associated with mitochondrial protection and apoptosis reduction. *Circulation,* 106**,** I270-6.

SUZUKI, T., MOTOHASHI, H. & YAMAMOTO, M. 2013. Toward clinical application of the Keap1-Nrf2 pathway. *Trends Pharmacol Sci,* 34**,** 340-6.

TAIPALE, M., KRYKBAEVA, I., KOEVA, M., KAYATEKIN, C., WESTOVER, K. D., KARRAS, G. I. & LINDQUIST, S. 2012. Quantitative analysis of HSP90-client interactions reveals principles of substrate recognition. *Cell,* 150**,** 987-1001.

TAKAHASHI, I., EMI, Y., HASUDA, S., KAKEJI, Y., MAEHARA, Y. & SUGIMACHI, K. 2002a. Clinical application of hyperthermia combined with anticancer drugs for the treatment of solid tumors. *Surgery,* 131**,** S78-84.

TAKAHASHI, R., TOYODA, E., AOKI, Y., SUZUKI, K. T. & GOTO, S. 2002b. Paradoxical increase of heat-shock response with age in a substrain of F344 rats: comparison between F344/DuCrj and F344/Jcl. *Mech Ageing Dev,* 123**,** 1605-15.

TAKAYA, K., SUZUKI, T., MOTOHASHI, H., ONODERA, K., SATOMI, S., KENSLER, T. W. & YAMAMOTO, M. 2012. Validation of the multiple sensor mechanism of the Keap1-Nrf2 system. *Free Radic Biol Med,* 53**,** 817-27.

TAKII, R., INOUYE, S., FUJIMOTO, M., NAKAMURA, T., SHINKAWA, T., PRAKASAM, R., TAN, K., HAYASHIDA, N., ICHIKAWA, H., HAI, T. & NAKAI, A. 2010. Heat shock transcription factor 1 inhibits expression of IL-6 through activating transcription factor 3. *J Immunol,* 184**,** 1041-8.

TANG, Z., DAI, S., HE, Y., DOTY, R. A., SHULTZ, L. D., SAMPSON, S. B. & DAI, C. 2015. MEK guards proteome stability and inhibits tumor-suppressive amyloidogenesis via HSF1. *Cell,* 160**,** 729-44.

TANONAKA, K., TOGA, W., YOSHIDA, H. & TAKEO, S. 2003. Myocardial heat shock protein changes in the failing heart following coronary artery ligation. *Heart Lung Circ,* 12**,** 60-5.

TEN HOVE, W., HOUBEN, L. A., RAAIJMAKERS, J. A., BRACKE, M. & KOENDERMAN, L. 2007. Differential regulation of TNFalpha and GM-CSF induced activation of P38 MAPK in neutrophils and eosinophils. *Mol Immunol,* 44**,** 2492-6.

TER HAAR, E., PRABHAKAR, P., LIU, X. & LEPRE, C. 2007. Crystal structure of the p38 alpha-MAPKAP kinase 2 heterodimer. *J Biol Chem,* 282**,** 9733-9.

THIMMULAPPA, R. K., MAI, K. H., SRISUMA, S., KENSLER, T. W., YAMAMOTO, M. & BISWAL, S. 2002. Identification of Nrf2-regulated genes induced by the chemopreventive agent sulforaphane by oligonucleotide microarray. *Cancer Res,* 62**,** 5196-203.

THOMPSON, C. A. & BURCHAM, P. C. 2008. Genome-wide transcriptional responses to acrolein. *Chem Res Toxicol,* 21**,** 2245-56.

TISSIERES, A., MITCHELL, H. K. & TRACY, U. M. 1974. Protein synthesis in salivary glands of Drosophila melanogaster: relation to chromosome puffs. *J Mol Biol,* 84**,** 389-98.
TIWARI, S. K., AGARWAL, S., SETH, B., YADAV, A., NAIR, S., BHATNAGAR, P., KARMAKAR, M., KUMARI, M., CHAUHAN, L. K., PATEL, D. K., SRIVASTAVA, V., SINGH, D., GUPTA, S. K., TRIPATHI, A., CHATURVEDI, R. K. & GUPTA, K. C. 2014. Curcumin-loaded nanoparticles potently induce adult neurogenesis and reverse cognitive deficits in Alzheimer's disease model via canonical Wnt/beta-catenin pathway. *ACS Nano,* 8**,** 76-103.
TOBIUME, K., MATSUZAWA, A., TAKAHASHI, T., NISHITOH, H., MORITA, K., TAKEDA, K., MINOWA, O., MIYAZONO, K., NODA, T. & ICHIJO, H. 2001. ASK1 is required for sustained activations of JNK/p38 MAP kinases and apoptosis. *EMBO Rep,* 2**,** 222-8.
TONG, K. I., KATOH, Y., KUSUNOKI, H., ITOH, K., TANAKA, T. & YAMAMOTO, M. 2006. Keap1 recruits Neh2 through binding to ETGE and DLG motifs: characterization of the two-site molecular recognition model. *Mol Cell Biol,* 2**6,** 2887-900.
TONG, K. I., PADMANABHAN, B., KOBAYASHI, A., SHANG, C., HIROTSU, Y., YOKOYAMA, S. & YAMAMOTO, M. 2007. Different electrostatic potentials define ETGE and DLG motifs as hinge and latch in oxidative stress response. *Mol Cell Biol,* 2**7,** 7511-21.
TORMOS, A. M., ARDUINI, A., TALENS-VISCONTI, R., DEL BARCO BARRANTES, I., NEBREDA, A. R. & SASTRE, J. 2013. Liver-specific p38alpha deficiency causes reduced cell growth and cytokinesis failure during chronic biliary cirrhosis in mice. *Hepatology,* 57**,** 1950-61.
TREMPOLEC, N., DAVE-COLL, N. & NEBREDA, A. R. 2013. SnapShot: p38 MAPK signaling. *Cell,* 152**,** 656-656 e1.
TRINKLEIN, N. D., MURRAY, J. I., HARTMAN, S. J., BOTSTEIN, D. & MYERS, R. M. 2004. The role of heat shock transcription factor 1 in the genome-wide regulation of the mammalian heat shock response. *Mol Biol Cell,* 15**,** 1254-61.
TROST, S. U., OMENS, J. H., KARLON, W. J., MEYER, M., MESTRIL, R., COVELL, J. W. & DILLMANN, W. H. 1998. Protection against myocardial dysfunction after a brief ischemic period in transgenic mice expressing inducible heat shock protein 70. *J Clin Invest,* 101**,** 855-62.
TROTT, A., WEST, J. D., KLAIC, L., WESTERHEIDE, S. D., SILVERMAN, R. B., MORIMOTO, R. I. & MORANO, K. A. 2008. Activation of heat shock and antioxidant responses by the natural product celastrol: transcriptional signatures of a thiol-targeted molecule. *Mol Biol Cell,* 19**,** 1104-12.
TUSZYNSKI, J. A., CARPENTER, E. J., HUZIL, J. T., MALINSKI, W., LUCHKO, T. & LUDUENA, R. F. 2006. The evolution of the structure of tubulin and its potential consequences for the role and function of microtubules in cells and embryos. *Int J Dev Biol,* 50**,** 341-58.
UBERSAX, J. A. & FERRELL, J. E., JR. 2007. Mechanisms of specificity in protein phosphorylation. *Nat Rev Mol Cell Biol,* 8**,** 530-41.
UCHIYAMA, T., ATSUTA, H., UTSUGI, T., OGURI, M., HASEGAWA, A., NAKAMURA, T., NAKAI, A., NAKATA, M., MARUYAMA, I., TOMURA, H., OKAJIMA, F., TOMONO, S., KAWAZU, S., NAGAI, R. & KURABAYASHI, M. 2007. HSF1 and constitutively active HSF1 improve vascular endothelial function (heat shock proteins improve vascular endothelial function). *Atherosclerosis,* 190**,** 321-9.
VAN OOSTEN-HAWLE, P., PORTER, R. S. & MORIMOTO, R. I. 2013. Regulation of organismal proteostasis by transcellular chaperone signaling. *Cell,* 153**,** 1366-78.
VASUDEVAN, S. A., SKOKO, J., WANG, K., BURLINGAME, S. M., PATEL, P. N., LAZO, J. S., NUCHTERN, J. G. & YANG, J. 2005. MKP-8, a novel MAPK phosphatase that inhibits p38 kinase. *Biochem Biophys Res Commun,* 330**,** 511-8.
VEDAM, K., NISHIJIMA, Y., DRUHAN, L. J., KHAN, M., MOLDOVAN, N. I., ZWEIER, J. L. & ILANGOVAN, G. 2010. Role of heat shock factor-1 activation in the doxorubicin-induced heart failure in mice. *Am J Physiol Heart Circ Physiol,* 298**,** H1832-41.
VERMA, M., SHARMA, A., NAIDU, S., BHADRA, A. K., KUKRETI, R. & TANEJA, V. 2012. Curcumin prevents formation of polyglutamine aggregates by inhibiting Vps36, a component of the ESCRT-II complex. *PLoS One,* 7**,** e42923.
VERMA, P., PFISTER, J. A., MALLICK, S. & D'MELLO, S. R. 2014. HSF1 protects neurons through a novel trimerization- and HSP-independent mechanism. *J Neurosci,* 34**,** 1599-612.
VIHERVAARA, A., SERGELIUS, C., VASARA, J., BLOM, M. A., ELSING, A. N., ROOS-MATTJUS, P. & SISTONEN, L. 2013. Transcriptional response to stress in the dynamic chromatin environment of cycling and mitotic cells. *Proc Natl Acad Sci U S A,* 110**,** E3388-97.
VILA, A., TALLMAN, K. A., JACOBS, A. T., LIEBLER, D. C., PORTER, N. A. & MARNETT, L. J. 2008. Identification of protein targets of 4-hydroxynonenal using click chemistry for ex vivo biotinylation of azido and alkynyl derivatives. *Chem Res Toxicol,* 21**,** 432-44.

WANG, G., YING, Z., JIN, X., TU, N., ZHANG, Y., PHILLIPS, M., MOSKOPHIDIS, D. & MIVECHI, N. F. 2004a. Essential requirement for both hsf1 and hsf2 transcriptional activity in spermatogenesis and male fertility. *Genesis,* 38**,** 66-80.
WANG, H., LIU, K., GENG, M., GAO, P., WU, X., HAI, Y., LI, Y., LI, Y., LUO, L., HAYES, J. D., WANG, X. J. & TANG, X. 2013a. RXRalpha inhibits the NRF2-ARE signaling pathway through a direct interaction with the Neh7 domain of NRF2. *Cancer Res,* 73**,** 3097-108.
WANG, H., YANG, H., SHIVALILA, C. S., DAWLATY, M. M., CHENG, A. W., ZHANG, F. & JAENISCH, R. 2013b. One-step generation of mice carrying mutations in multiple genes by CRISPR/Cas-mediated genome engineering. *Cell,* 153**,** 910-8.
WANG, X., CHEN, Y., ABDELKADER, D., HASSAN, W., SUN, H. & LIU, J. 2015. Combination therapy with oleanolic acid and metformin as a synergistic treatment for diabetes. *J Diabetes Res,* 2015**,** 973287.
WANG, X., KHALEQUE, M. A., ZHAO, M. J., ZHONG, R., GAESTEL, M. & CALDERWOOD, S. K. 2006. Phosphorylation of HSF1 by MAPK-activated protein kinase 2 on serine 121, inhibits transcriptional activity and promotes HSP90 binding. *J Biol Chem,* 281**,** 782-91.
WANG, X., YE, X. L., LIU, R., CHEN, H. L., BAI, H., LIANG, X., ZHANG, X. D., WANG, Z., LI, W. L. & HAI, C. X. 2010. Antioxidant activities of oleanolic acid in vitro: possible role of Nrf2 and MAP kinases. *Chem Biol Interact,* 184**,** 328-37.
WANG, Y., GIBNEY, P. A., WEST, J. D. & MORANO, K. A. 2012. The yeast Hsp70 Ssa1 is a sensor for activation of the heat shock response by thiol-reactive compounds. *Mol Biol Cell,* 23**,** 3290-8.
WANG, Y., THERIAULT, J. R., HE, H., GONG, J. & CALDERWOOD, S. K. 2004b. Expression of a dominant negative heat shock factor-1 construct inhibits aneuploidy in prostate carcinoma cells. *J Biol Chem,* 279**,** 32651-9.
WARRICK, J. M., CHAN, H. Y., GRAY-BOARD, G. L., CHAI, Y., PAULSON, H. L. & BONINI, N. M. 1999. Suppression of polyglutamine-mediated neurodegeneration in Drosophila by the molecular chaperone HSP70. *Nat Genet,* 23**,** 425-8.
WELCKER, M. & CLURMAN, B. E. 2008. FBW7 ubiquitin ligase: a tumour suppressor at the crossroads of cell division, growth and differentiation. *Nat Rev Cancer,* 8**,** 83-93.
WESTERHEIDE, S. D., ANCKAR, J., STEVENS, S. M., JR., SISTONEN, L. & MORIMOTO, R. I. 2009. Stress-inducible regulation of heat shock factor 1 by the deacetylase SIRT1. *Science,* 323**,** 1063-6.
WESTERHEIDE, S. D., BOSMAN, J. D., MBADUGHA, B. N., KAWAHARA, T. L., MATSUMOTO, G., KIM, S., GU, W., DEVLIN, J. P., SILVERMAN, R. B. & MORIMOTO, R. I. 2004a. Celastrols as inducers of the heat shock response and cytoprotection. *J Biol Chem,* 279**,** 56053-60.
WESTERHEIDE, S. D., BOSMAN, J. D., MBADUGHA, B. N., KAWAHARA, T. L., MATSUMOTO, G., KIM, S., GU, W., DEVLIN, J. P., SILVERMAN, R. B. & MORIMOTO, R. I. 2004b. Celastrols as inducers of the heat shock response and cytoprotection. *J Biol Chem,* 279**,** 56053-60.
WHITMARSH, A. J. & DAVIS, R. J. 2007. Role of mitogen-activated protein kinase kinase 4 in cancer. *Oncogene,* 26**,** 3172-84.
WILD, A. C. & MULCAHY, R. T. 2000. Regulation of gamma-glutamylcysteine synthetase subunit gene expression: insights into transcriptional control of antioxidant defenses. *Free Radical Res,* 32**,** 281-301.
WILSON, K. P., FITZGIBBON, M. J., CARON, P. R., GRIFFITH, J. P., CHEN, W., MCCAFFREY, P. G., CHAMBERS, S. P. & SU, M. S. 1996. Crystal structure of p38 mitogen-activated protein kinase. *J Biol Chem,* 271**,** 27696-700.
WINKEL, A. F., ENGEL, C. K., MARGERIE, D., KANNT, A., SZILLAT, H., GLOMBIK, H., KALLUS, C., RUF, S., GUSSREGEN, S., RIEDEL, J., HERLING, A. W., VON KNETHEN, A., WEIGERT, A., BRUNE, B. & SCHMOLL, D. 2015. Characterization of RA839, a Noncovalent Small Molecule Binder to Keap1 and Selective Activator of Nrf2 Signaling. *J Biol Chem,* 290**,** 28446-55.
WINKLER, A., ARKIND, C., MATTISON, C. P., BURKHOLDER, A., KNOCHE, K. & OTA, I. 2002. Heat stress activates the yeast high-osmolarity glycerol mitogen-activated protein kinase pathway, and protein tyrosine phosphatases are essential under heat stress. *Eukaryot Cell,* 1**,** 163-73.
WOODMAN, B., BUTLER, R., LANDLES, C., LUPTON, M. K., TSE, J., HOCKLY, E., MOFFITT, H., SATHASIVAM, K. & BATES, G. P. 2007. The Hdh(Q150/Q150) knock-in mouse model of HD and the R6/2 exon 1 model develop comparable and widespread molecular phenotypes. *Brain Res Bull,* 72**,** 83-97.
WU, J. H., MIAO, W., HU, L. G. & BATIST, G. 2010. Identification and characterization of novel Nrf2 inducers designed to target the intervening region of Keap1. *Chem Biol Drug Des,* 75**,** 475-80.

WU, K. C., CUI, J. Y. & KLAASSEN, C. D. 2011. Beneficial role of nrf2 in regulating NADPH generation and consumption. *Toxicol Sci,* 123**,** 590-600.
WU, L., HU, C., HUANG, M., JIANG, M., LU, L. & TANG, J. 2013. Heat shock transcription factor 1 attenuates TNFalpha-induced cardiomyocyte death through suppression of NFkappaB pathway. *Gene,* 527**,** 89-94.
WU, L. X., XU, J. H., HUANG, X. W., ZHANG, K. Z., WEN, C. X. & CHEN, Y. Z. 2006. Down-regulation of p210(bcr/abl) by curcumin involves disrupting molecular chaperone functions of Hsp90. *Acta Pharmacol Sin,* 27**,** 694-9.
WUST, P., HILDEBRANDT, B., SREENIVASA, G., RAU, B., GELLERMANN, J., RIESS, H., FELIX, R. & SCHLAG, P. M. 2002. Hyperthermia in combined treatment of cancer. *Lancet Oncol,* 3**,** 487-97.
XAVIER, I. J., MERCIER, P. A., MCLOUGHLIN, C. M., ALI, A., WOODGETT, J. R. & OVSENEK, N. 2000. Glycogen synthase kinase 3beta negatively regulates both DNA-binding and transcriptional activities of heat shock factor 1. *J Biol Chem,* 275**,** 29147-52.
XIA, W. & VOELLMY, R. 1997. Hyperphosphorylation of heat shock transcription factor 1 is correlated with transcriptional competence and slow dissociation of active factor trimers. *J Biol Chem,* 272**,** 4094-102.
XIAO, D., POWOLNY, A. A., MOURA, M. B., KELLEY, E. E., BOMMAREDDY, A., KIM, S. H., HAHM, E. R., NORMOLLE, D., VAN HOUTEN, B. & SINGH, S. V. 2010. Phenethyl isothiocyanate inhibits oxidative phosphorylation to trigger reactive oxygen species-mediated death of human prostate cancer cells. *J Biol Chem,* 285**,** 26558-69.
XIAO, X., ZUO, X., DAVIS, A. A., MCMILLAN, D. R., CURRY, B. B., RICHARDSON, J. A. & BENJAMIN, I. J. 1999. HSF1 is required for extra-embryonic development, postnatal growth and protection during inflammatory responses in mice. *EMBO J,* 18**,** 5943-52.
XIAO, Z., MI, L., CHUNG, F. L. & VEENSTRA, T. D. 2012. Proteomic analysis of covalent modifications of tubulins by isothiocyanates. *J Nutr,* 142**,** 1377S-81S.
XIE, H. B., CAMMARATO, A., RAJASEKARAN, N. S., ZHANG, H., SUGGS, J. A., LIN, H. C., BERNSTEIN, S. I., BENJAMIN, I. J. & GOLIC, K. G. 2013. The NADPH metabolic network regulates human alphaB-crystallin cardiomyopathy and reductive stress in Drosophila melanogaster. *PLoS Genet,* 9**,** e1003544.
XING, J., KORNHAUSER, J. M., XIA, Z., THIELE, E. A. & GREENBERG, M. E. 1998. Nerve growth factor activates extracellular signal-regulated kinase and p38 mitogen-activated protein kinase pathways to stimulate CREB serine 133 phosphorylation. *Mol Cell Biol,* 18**,** 1946-55.
XU, D., ZALMAS, L. P. & LA THANGUE, N. B. 2008. A transcription cofactor required for the heat-shock response. *EMBO Rep,* 9**,** 662-9.
XU, Q., HU, Y., KLEINDIENST, R. & WICK, G. 1997. Nitric oxide induces heat-shock protein 70 expression in vascular smooth muscle cells via activation of heat shock factor 1. *J Clin Invest,* 100**,** 1089-97.
XU, Y. M., HUANG, D. Y., CHIU, J. F. & LAU, A. T. 2012. Post-translational modification of human heat shock factors and their functions: a recent update by proteomic approach. *J Proteome Res,* 11**,** 2625-34.
YAN, L. J., CHRISTIANS, E. S., LIU, L., XIAO, X., SOHAL, R. S. & BENJAMIN, I. J. 2002. Mouse heat shock transcription factor 1 deficiency alters cardiac redox homeostasis and increases mitochondrial oxidative damage. *EMBO J,* 21**,** 5164-72.
YANG, J., BRIDGES, K., CHEN, K. Y. & LIU, A. Y. 2008. Riluzole increases the amount of latent HSF1 for an amplified heat shock response and cytoprotection. *PLoS One,* 3**,** e2864.
YERBURY, J. J., GOWER, D., VANAGS, L., ROBERTS, K., LEE, J. A. & ECROYD, H. 2013. The small heat shock proteins alphaB-crystallin and Hsp27 suppress SOD1 aggregation in vitro. *Cell Stress Chaperones,* 18**,** 251-7.
YIH, L. H., HSU, N. C., KUO, H. H. & WU, Y. C. 2012. Inhibition of the heat shock response by PI103 enhances the cytotoxicity of arsenic trioxide. *Toxicol Sci,* 128**,** 126-36.
YIN, N., QI, X., TSAI, S., LU, Y., BASIR, Z., OSHIMA, K., THOMAS, J. P., MYERS, C. R., STONER, G. & CHEN, G. 2016. p38gamma MAPK is required for inflammation-associated colon tumorigenesis. *Oncogene,* 35**,** 1039-48.
YIN, P., KAWAMURA, T., HE, M., VANAJA, D. K. & YOUNG, C. Y. 2009. Phenethyl isothiocyanate induces cell cycle arrest and reduction of alpha- and beta-tubulin isotypes in human prostate cancer cells. *Cell Biol Int,* 33**,** 57-64.
YOSHIMA, T., YURA, T. & YANAGI, H. 1998. Function of the C-terminal transactivation domain of human heat shock factor 2 is modulated by the adjacent negative regulatory segment. *Nucleic Acids Res,* 26**,** 2580-5.

YOUNG, P. R. 2013. Perspective on the discovery and scientific impact of p38 MAP kinase. *J Biomol Screen,* 18**,** 1156-63.
YU, Y., HAMZA, A., ZHANG, T., GU, M., ZOU, P., NEWMAN, B., LI, Y., GUNATILAKA, A. A., ZHAN, C. G. & SUN, D. 2010. Withaferin A targets heat shock protein 90 in pancreatic cancer cells. *Biochem Pharmacol,* 79**,** 542-51.
YUAN, J. M., MURPHY, S. E., STEPANOV, I., WANG, R., CARMELLA, S. G., NELSON, H. H., HATSUKAMI, D. & HECHT, S. S. 2016. 2-Phenethyl Isothiocyanate, Glutathione S-transferase M1 and T1 Polymorphisms, and Detoxification of Volatile Organic Carcinogens and Toxicants in Tobacco Smoke. *Cancer Prev Res (Phila),* 9**,** 598-606.
ZARUBIN, T. & HAN, J. 2005. Activation and signaling of the p38 MAP kinase pathway. *Cell Res,* 15**,** 11-8.
ZARZOV, P., BOUCHERIE, H. & MANN, C. 1997. A yeast heat shock transcription factor (Hsf1) mutant is defective in both Hsc82/Hsp82 synthesis and spindle pole body duplication. *J Cell Sci,* 110 (Pt 16)**,** 1879-91.
ZHANG, B., AU, Q., YOON, I. S., TREMBLAY, M. H., YIP, G., ZHOU, Y., BARBER, J. R. & NG, S. C. 2009a. Identification of small-molecule HSF1 amplifiers by high content screening in protection of cells from stress induced injury. *Biochem Biophys Res Commun,* 390**,** 925-30.
ZHANG, D. D. & HANNINK, M. 2003. Distinct cysteine residues in Keap1 are required for Keap1-dependent ubiquitination of Nrf2 and for stabilization of Nrf2 by chemopreventive agents and oxidative stress. *Mol Cell Biol,* 23**,** 8137-51.
ZHANG, D. D., LO, S. C., SUN, Z., HABIB, G. M., LIEBERMAN, M. W. & HANNINK, M. 2005. Ubiquitination of Keap1, a BTB-Kelch substrate adaptor protein for Cul3, targets Keap1 for degradation by a proteasome-independent pathway. *J Biol Chem,* 280**,** 30091-9.
ZHANG, Q. & ZHANG, G. 2002. Activation and autophosphorylation of apoptosis signal-regulating kinase 1 (ASK1) following cerebral ischemia in rat hippocampus. *Neurosci Lett,* 329**,** 232-6.
ZHANG, Q. S., MADDOCK, D. A., CHEN, J. P., HEO, S., CHIU, C., LAI, D., SOUZA, K., MEHTA, S. & WAN, Y. S. 2001. Cytokine-induced p38 activation feedback regulates the prolonged activation of AKT cell survival pathway initiated by reactive oxygen species in response to UV irradiation in human keratinocytes. *Int J Oncol,* 19**,** 1057-61.
ZHANG, T., HAMZA, A., CAO, X., WANG, B., YU, S., ZHAN, C. G. & SUN, D. 2008. A novel Hsp90 inhibitor to disrupt Hsp90/Cdc37 complex against pancreatic cancer cells. *Mol Cancer Ther,* 7**,** 162-70.
ZHANG, T., LI, Y., YU, Y., ZOU, P., JIANG, Y. & SUN, D. 2009b. Characterization of celastrol to inhibit hsp90 and cdc37 interaction. *J Biol Chem,* 284**,** 35381-9.
ZHANG, T., LIU, H., ZHU, C., BRIGGS, K., KANG, Y., FLEMING, J. A. & CURLEY, S. A. 2012. Silencing thioredoxin induces liver cancer cell senescence under hypoxia. *Hepatol Res,* 42**,** 706-13.
ZHANG, X., JEFFS, G., REN, X., O'DONOVAN, P., MONTANER, B., PERRETT, C. M., KARRAN, P. & XU, Y. Z. 2007. Novel DNA lesions generated by the interaction between therapeutic thiopurines and UVA light. *DNA Repair (Amst),* 6**,** 344-54.
ZHANG, Y., AHN, Y. H., BENJAMIN, I. J., HONDA, T., HICKS, R. J., CALABRESE, V., COLE, P. A. & DINKOVA-KOSTOVA, A. T. 2011. HSF1-dependent upregulation of Hsp70 by sulfhydryl-reactive inducers of the KEAP1/NRF2/ARE pathway. *Chem Biol,* 18**,** 1355-61.
ZHANG, Y., DAYALAN NAIDU, S., SAMARASINGHE, K., VAN HECKE, G. C., PHEELY, A., BORONINA, T. N., COLE, R. N., BENJAMIN, I. J., COLE, P. A., AHN, Y. H. & DINKOVA-KOSTOVA, A. T. 2014. Sulphoxythiocarbamates modify cysteine residues in HSP90 causing degradation of client proteins and inhibition of cancer cell proliferation. *Br J Cancer,* 110**,** 71-82.
ZHANG, Y., WADE, K. L., PRESTERA, T. & TALALAY, P. 1996. Quantitative determination of isothiocyanates, dithiocarbamates, carbon disulfide, and related thiocarbonyl compounds by cyclocondensation with 1,2-benzenedithiol. *Anal Biochem,* 239**,** 160-7.
ZHANG, Y. Q. & SARGE, K. D. 2007. Celastrol inhibits polyglutamine aggregation and toxicity though induction of the heat shock response. *J Mol Med (Berl),* 85**,** 1421-8.
ZHAO, R., MA, X. & SHEN, G. X. 2008. Transcriptional regulation of plasminogen activator inhibitor-1 in vascular endothelial cells induced by oxidized very low density lipoproteins. *Mol Cell Biochem,* 317**,** 197-204.
ZHAO, R., MA, X., XIE, X. & SHEN, G. X. 2009. Involvement of NADPH oxidase in oxidized LDL-induced upregulation of heat shock factor-1 and plasminogen activator inhibitor-1 in vascular endothelial cells. *Am J Physiol Endocrinol Metab,* 297**,** E104-11.
ZHAO, R., MOGHADASIAN, M. H. & SHEN, G. X. 2011. Involvement of NADPH oxidase in up-regulation of plasminogen activator inhibitor-1 and heat shock factor-1 in mouse embryo

fibroblasts induced by oxidized LDL and in apolipoprotein E-deficient mice. *Free Radic Res,* 45**,** 1013-23.

ZHAO, R. & SHEN, G. X. 2007. Involvement of heat shock factor-1 in glycated LDL-induced upregulation of plasminogen activator inhibitor-1 in vascular endothelial cells. *Diabetes,* 56**,** 1436-44.

ZHENG, C., LIN, Z., ZHAO, Z. J., YANG, Y., NIU, H. & SHEN, X. 2006. MAPK-activated protein kinase-2 (MK2)-mediated formation and phosphorylation-regulated dissociation of the signal complex consisting of p38, MK2, Akt, and Hsp27. *J Biol Chem,* 281**,** 37215-26.

ZHENG, S., SANTOSH LAXMI, Y. R., DAVID, E., DINKOVA-KOSTOVA, A. T., SHIAVONI, K. H., REN, Y., ZHENG, Y., TREVINO, I., BUMEISTER, R., OJIMA, I., WIGLEY, W. C., BLISKA, J. B., MIERKE, D. F. & HONDA, T. 2012. Synthesis, chemical reactivity as Michael acceptors, and biological potency of monocyclic cyanoenones, novel and highly potent anti-inflammatory and cytoprotective agents. *J Med Chem,* 55**,** 4837-46.

ZHU, B. T. & CONNEY, A. H. 1998. Functional role of estrogen metabolism in target cells: review and perspectives. *Carcinogenesis,* 19**,** 1-27.

ZHU, X., ROTTKAMP, C. A., BOUX, H., TAKEDA, A., PERRY, G. & SMITH, M. A. 2000. Activation of p38 kinase links tau phosphorylation, oxidative stress, and cell cycle-related events in Alzheimer disease. *J Neuropathol Exp Neurol,* 59**,** 880-8.

ZINGARELLI, B., HAKE, P. W., O'CONNOR, M., DENENBERG, A., WONG, H. R., KONG, S. & ARONOW, B. J. 2004. Differential regulation of activator protein-1 and heat shock factor-1 in myocardial ischemia and reperfusion injury: role of poly(ADP-ribose) polymerase-1. *Am J Physiol Heart Circ Physiol,* 286**,** H1408-15.

ZIPPER, L. M. & MULCAHY, R. T. 2002. The Keap1 BTB/POZ dimerization function is required to sequester Nrf2 in cytoplasm. *J Biol Chem,* 277**,** 36544-52.

ZOU, J., GUO, Y., GUETTOUCHE, T., SMITH, D. F. & VOELLMY, R. 1998. Repression of heat shock transcription factor HSF1 activation by HSP90 (HSP90 complex) that forms a stress-sensitive complex with HSF1. *Cell,* 94**,** 471-80.

ZOU, Y., LI, J., MA, H., JIANG, H., YUAN, J., GONG, H., LIANG, Y., GUAN, A., WU, J., LI, L., ZHOU, N., NIU, Y., SUN, A., NAKAI, A., WANG, P., TAKANO, H., KOMURO, I. & GE, J. 2011. Heat shock transcription factor 1 protects heart after pressure overload through promoting myocardial angiogenesis in male mice. *J Mol Cell Cardiol,* 51**,** 821-9.

ZOU, Y., ZHU, W., SAKAMOTO, M., QIN, Y., AKAZAWA, H., TOKO, H., MIZUKAMI, M., TAKEDA, N., MINAMINO, T., TAKANO, H., NAGAI, T., NAKAI, A. & KOMURO, I. 2003. Heat shock transcription factor 1 protects cardiomyocytes from ischemia/reperfusion injury. *Circulation,* 108**,** 3024-30.

ZUR, R., GARCIA-IBANEZ, L., NUNEZ-BUIZA, A., APARICIO, N., LIAPPAS, G., ESCOS, A., RISCO, A., PAGE, A., SAIZ-LADERA, C., ALSINA-BEAUCHAMP, D., MONTANS, J., PARAMIO, J. M. & CUENDA, A. 2015. Combined deletion of p38gamma and p38delta reduces skin inflammation and protects from carcinogenesis. *Oncotarget,* 6**,** 12920-35.

APPENDIX FIGURE 5.1A

A

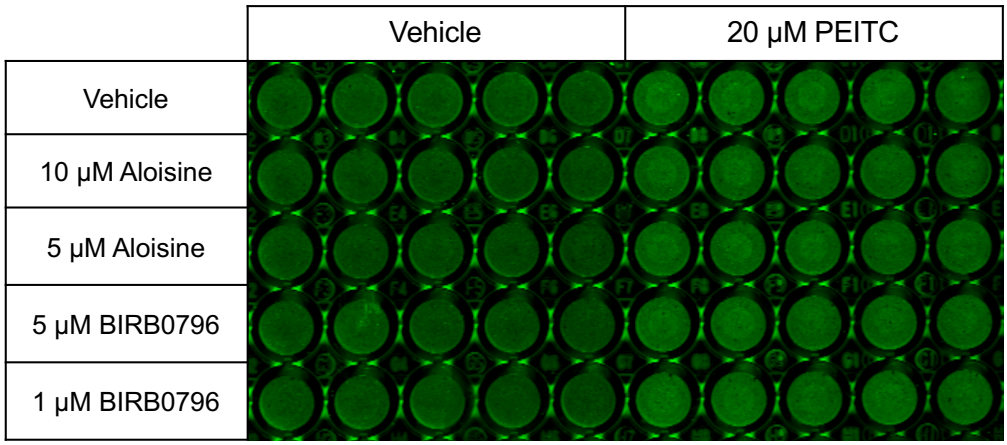

B

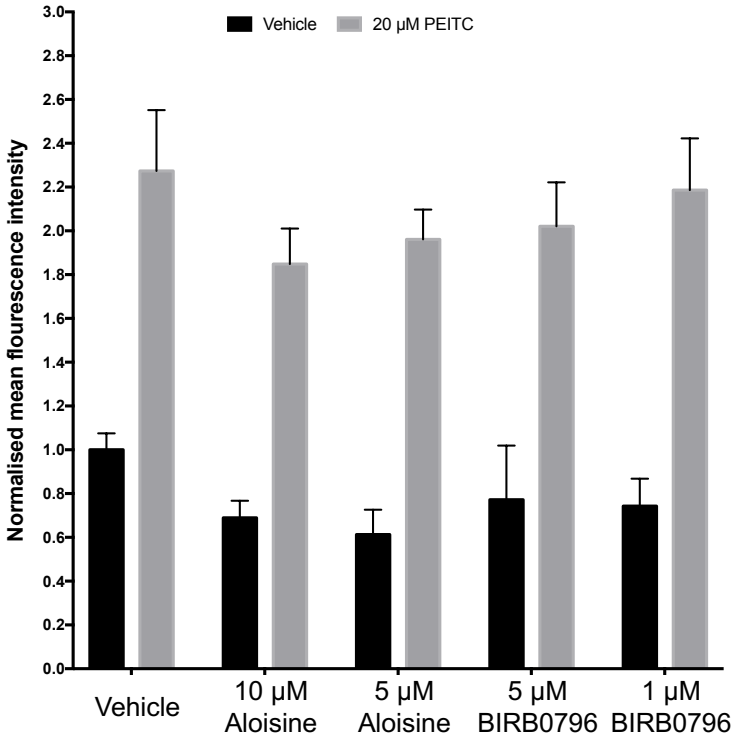

Appendix Fig. 5.1A. In-cell western kinase inhibitor screen. MCF7 cells (1 x 10^4) were seeded in each well of a 96-well plate, and 16 h after seeding, the cells were pre-treated with either the vehicle (0.1% DMSO) or the kinase inhibitors (Aloisine or BIRB0796) dissolved in conditioned media for 1 h. Subsequently, the cells were treated with either the vehicle or 20 μM PEITC dissolved in conditioned media for a further 3 h and fixed immediately after treatment. The cells were subjected to the in cell western technique. The fixed cells were incubated with HSF1 pS326 primary antibody. Following primary antibody incubation, the cells were incubated with secondary goat anti-rabbit IRDye 680 nm (LiCOR) antibody. Subsequently, the 96-well plate was scanned and quantified using the LI-COR® Odyssey® Infrared Imaging system. The background values were obtained from wells which contained cells that were not incubated with the primary antibody but were only incubated with the secondary antibody.

APPENDIX FIGURE 5.1B

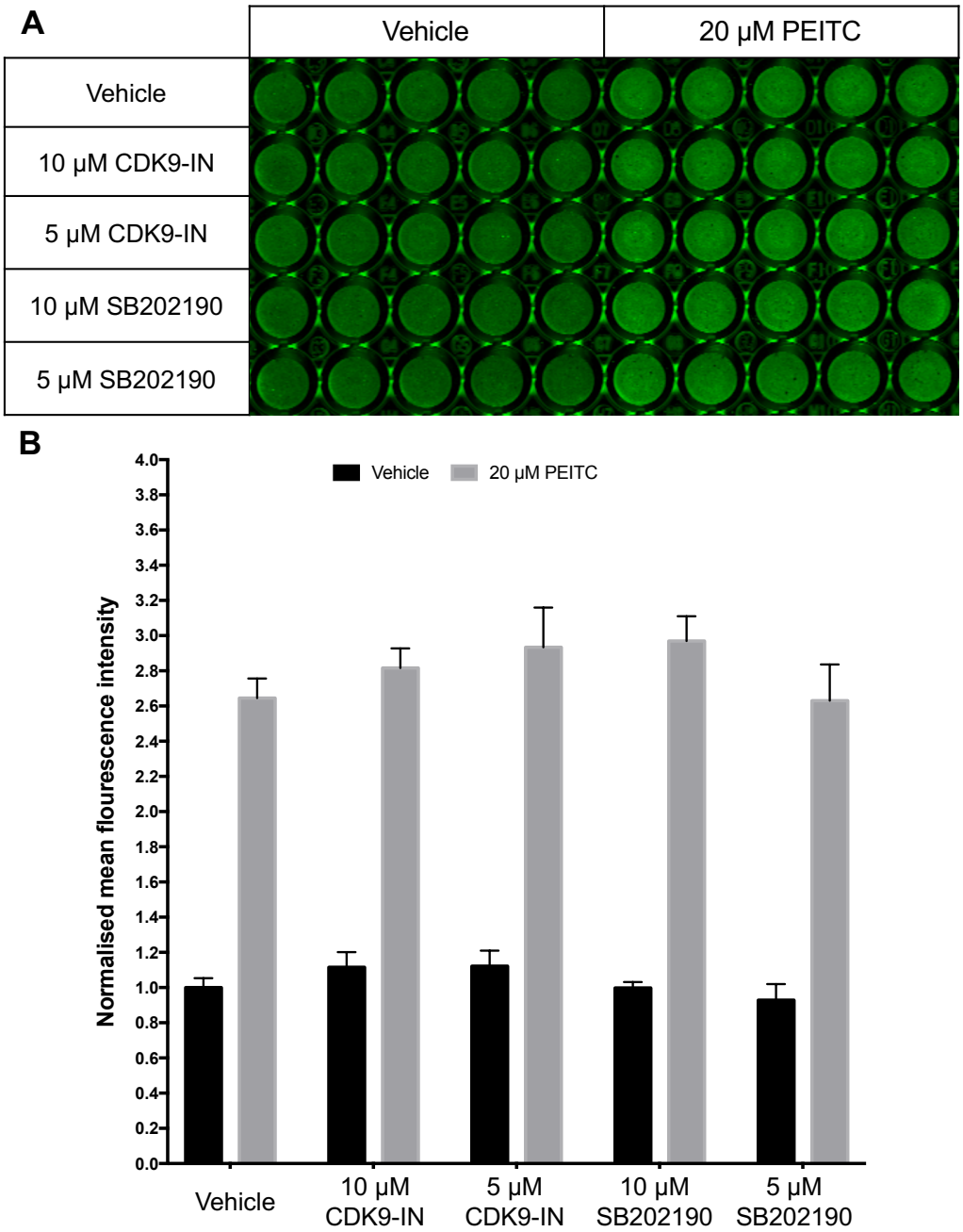

Appendix Fig. 5.1B. In-cell western kinase inhibitor screen. MCF7 cells (1 x 10^4) were seeded in each well of a 96-well plate, and 16 h after seeding, the cells were pre-treated with either the vehicle (0.1% DMSO) or the kinase inhibitors (CDK9-In or SB202190) dissolved in conditioned media for 1 h. Subsequently, the cells were treated with either the vehicle or 20 μM PEITC dissolved in conditioned media for a further 3 h and fixed immediately after treatment. The cells were subjected to the in cell western technique. The fixed cells were incubated with HSF1 pS326 primary antibody. Following primary antibody incubation, the cells were incubated with secondary goat anti-rabbit IRDye 680 nm (LiCOR) antibody. Subsequently, the 96-well plate was scanned and quantified using the LI-COR® Odyssey® Infrared Imaging system. The background values were obtained from wells which contained cells that were not incubated with the primary antibody but were only incubated with the secondary antibody.

APPENDIX FIGURE 5.1C

A

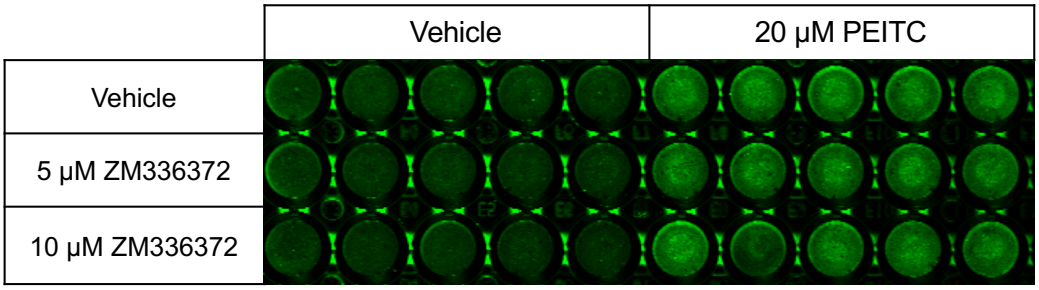

B

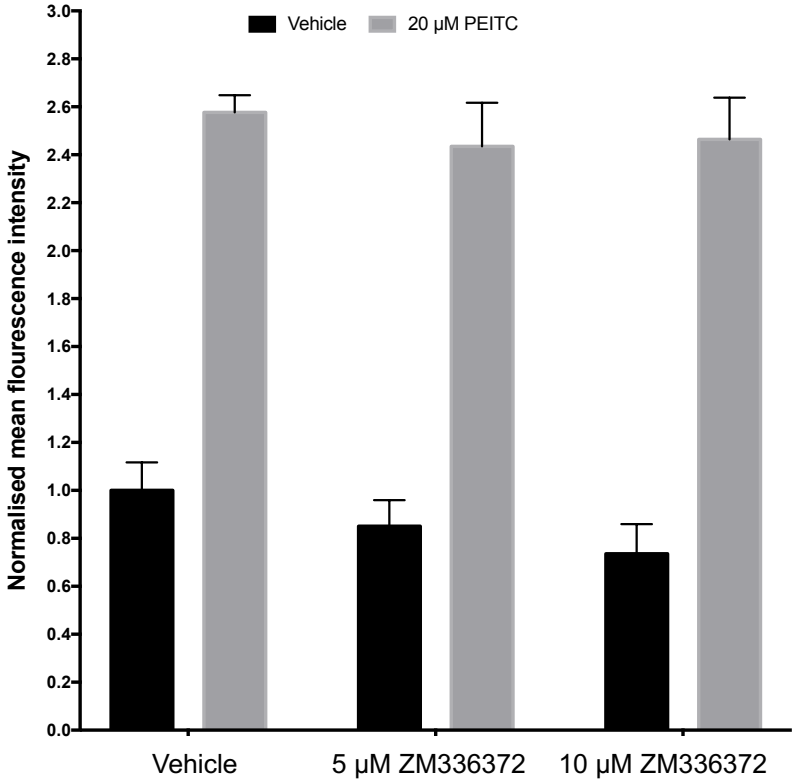

Appendix Fig. 5.1C. In-cell western kinase inhibitor screen. MCF7 cells (1 x 10^4) were seeded in each well of a 96-well plate, and 16 h after seeding, the cells were pre-treated with either the vehicle (0.1% DMSO) or the p38 kinase inhibitor ZM336372 dissolved in conditioned media for 1 h. Subsequently, the cells were treated with either the vehicle or 20 μM PEITC dissolved in conditioned media for a further 3 h and fixed immediately after treatment. The cells were subjected to the in cell western technique. The fixed cells were incubated with HSF1 pS326 primary antibody. Following primary antibody incubation, the cells were incubated with secondary goat anti-rabbit IRDye 680 nm (LiCOR) antibody. Subsequently, the 96-well plate was scanned and quantified using the LI-COR® Odyssey® Infrared Imaging system. The background values were obtained from wells which contained cells that were not incubated with the primary antibody but were only incubated with the secondary antibody.

APPENDIX FIGURE 5.2

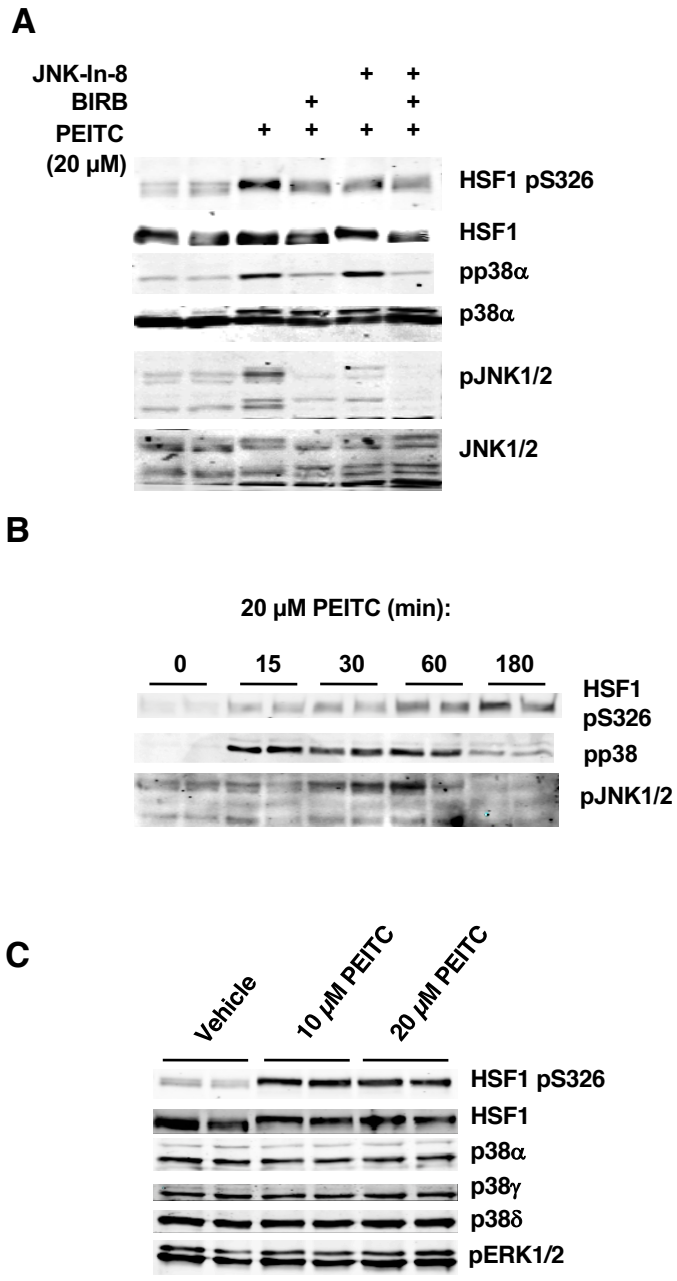

Appendix Fig. 5.2. PEITC activates p38 and JNK1/2 MAPK. MDA-MB-231 cells (2.5 x 10^5 per well) growing in 6-well plates were treated with vehicle (0.1% acetonitrile) or PEITC for either 24 h (**A)** or for the indicated periods of time (**B**) and 3 h (**C**). The levels of HSF1, pS326 HSF1 Hsp70, the p38 isoforms α, β, ɣ, and δ, phosphorylated p38 (pp38), phosphorylated p38α (pp38α), JNK1/2, and phosphorylated JNK1/2 (JNK1/2), were detected by western blot analysis. Experiment performed by Dr. Ana Risco and Dr. Ana Cuenda.